Université de Montréal

Pro-fibrotic role of ERK3-MK5 during pressure-overload induced cardiac hypertrophy

par
Dharmendra Dingar
Département de Biochimie
Faculté de Médecine

Thèse présentée à la Faculté des études supérieures
en vue de l'obtention du grade de
Philosophiae Doctor (Ph.D.)
en biochimie

22 December 2010

Université de Montréal
Faculté des études supérieures

Cette thèse intitulée:

Pro-fibrotic role of ERK3-MK5 during pressure-overload induced cardiac hypertrophy

présentée par:
Dharmendra Dingar

a été évalué par un jury composé des personnes suivantes:

Dr. Nikolaus Heveker
président-rapporteur

Dr. Bruce Gordon Allen
directeur de recherche

Dr. Marc Servant
membre du jury

Dr. Howard A. Rockman
examinateur externe

Dr. Christian Deschepper
représentant du doyen

ABSTRACT

There are 4 isoforms of p38 MAP kinase: α, β, γ, and δ. p38 signaling has been implicated in fibrosis and apoptosis during cardiac hypertrophy. MK5, originally identified as a p38 Regulated/Activated Protein Kinase (PRAK), is known to be downstream of p38 mitogen activated protein kinase (MAPK). Although highly expressed in the heart, the physiological roles of MK5 remain unknown. To determine if MK5 plays a role in mediating detrimental effects downstream of p38, we studied the effect of transverse aortic constriction (TAC)-induced chronic pressure overload in mice heterozygous for a knockout of MK5 ($MK5^{+/-}$). Moreover, as MK5 is also activated by the atypical MAPKs, ERK3 and ERK4, the effects of TAC were also studied in $ERK3^{+/-}$ mice. Wild-type ($MK5^{+/+}$; $ERK3^{+/+}$) littermates were used as controls.

Two wks post-TAC, heart weight/body weight ratios were significantly and similarly increased in both $MK5^{+/-}$ and $MK5^{+/+}$ hearts. Trans-thoracic echocardiography revealed that pressure overload impaired left ventricular diastolic function in $MK5^{+/+}$, but not in $MK5^{+/-}$ hearts. In addition, less collagen deposition, assessed by Masson trichrome staining, was observed in $MK5^{+/-}$ hearts 2 and 3 wks post-TAC. Furthermore, TAC-induced increases in collagen alpha1 type1 mRNA levels were significantly lower in $MK5^{+/-}$ hearts at both 2 and 3 wks post-TAC. Immunoprecipitation of MK5 resulted in co-immunoprecipitation of ERK3 but not ERK4 or p38α in either acute or chronic sham-operated and TAC hearts. In contrast, exogenous GST-MK5 pulled down endogenous ERK4 and p38α, but not ERK3, from mouse heart lysates. Neither exogenous GST-ERK3 nor GST-p38α pulled down MK5. These results suggest that MK5 associates with, and is regulated by ERK3, but not ERK4 or p38α in heart. At physiological expressional levels, all MK5 was bound to ERK3 and hence not available to bind exogenous protein. Along similar lines, mice heterozygous for an ERK3 knockout ($ERK3^{+/-}$) also showed reduced or absent collagen deposition and lower collagen alpha1 type1 mRNA levels 3 wks post-TAC. This data suggests an important pro-fibrotic role of MK5-ERK3 signaling during chronic pressure overload.

We also demonstrated the existence of 5 splice variants of (MK5.1-5), including the originally published form (MK5.1). MK5.2 and MK5.5 had a 6 base pair deletion in exon 12: MK5.3 lacked exon 12: and MK5.4 and MK5.5 lacked exons 2-6. Subsequently, expression of the splice variants at the mRNA level was quantified by real time qPCR. Although ubiquitously expressed, the relative abundance of each variant was tissue-specific (heart, kidney, pancreas, skeletal muscle, lung, liver, and brain). Additionally, the relative abundance of MK5 splice variants changed in the heart during pressure overload and post-natal development. Furthermore, immunofluorescence revealed MK5.1-5.3 localized to the nucleus and MK5.4-5.5 to the cytoplasm in unstimulated HEK 293 cells. Upon stimulation with anisomycin, which activates p38 MAPK, MK5.1-5.3 translocated from the nucleus to the cytoplasm and small amounts of MK5.4-5.5 relocated to the nucleus. These splice variants may further diversify MK5-ERK3 signaling in the heart, but their exact role awaits further investigation.

With the exception of p38δ, all p38 isoforms are expressed in the heart and α is considered to be the prominent isoform in this tissue. qPCR and western blot analysis revealed p38α and p38γ to be the predominant isoforms and p38β and p38δ are expressed at comparable levels in the adult heart. Confocal immunofluorescence studies revealed p38α and p38γ in both the cytoplasm and nucleus. However, in response to TAC, p38γ accumulated in the nucleus whereas the distribution of p38α remained unaffected. The high abundance of p38γ and its nuclear accumulation during chronic pressure overload suggest that this isoform may play a role in gene expression during pathological cardiac remodeling.

In conclusion, we have shown for the first time a pro-fibrotic role for MK5-ERK3 signaling during chronic pressure overload. Moreover, comparable expression levels of p38γ with p38α, and differential localization of p38γ during acute or chronic pressure overload, suggest these isoforms play different roles during cardiac remodeling.

RÉSUMÉ

Il y a 4 isoforme de p38 : α, β, δ, and γ. MK5, à l'origine identifié comme étant un régulateur de PRAK (Regulated/Activated Protein Kinase), est maintenant connu pour être activée par la protéine kinase p38 (qui est un mitogène activé par la protéine kinase, MAPK). Cette dernière est impliquée dans les mécanismes de fibrose et d'apoptose pendant l'hypertrophie cardiaque. De plus, MK5 est également activée par les MAPKs atypiques; ERK3 et ERK4. Bien qu'elles soient fortement exprimées dans le cœur, le rôle physiologique de MK5 et ERK3 demeure inconnu. Par conséquent, nous avons étudié l'effet de la constriction aortique transversale (TAC) – induisant un surcharge chronique de pression chez les souris hétèrozygotes *knockout* pour MK5 ($MK5^{+/-}$) ou ERK3 ($ERK3^{+/-}$) et pour leurs types sauvages ($MK5^{+/+}$ et $ERK3^{+/+}$).

Deux sem post-TAC; le ratio de poids du cœur/poids corporel a été augmenté chez les 2 souris $MK5^{+/-}$ et $MK5^{+/+}$. L'échocardiographie de la trans-thoracique démontre que la surcharge de pression a altéré la fonction diastolique du ventricule gauche chez MK5+/+, mais pas chez la souris $MK5^{+/-}$. De plus, nous avons observé moins de dépôt de collagène, évalué par une coloration au trichrome de Masson, 2 et 3 sem post-TAC chez les souris $MK5^{+/-}$. Parallèlement, le niveau de l'ARNm de collagène type1 alpha-1 a été significativement diminué dans les cœurs des souris $MK5^{+/-}$, 2 et 3 sem post-TAC. De même, ERK3, mais pas ERK5 ni p38α, co-IP avec MK5 dans les 2 modèles des cœurs TAC; aigus ou chroniques. En revanche, l'ajout exogénique de GST-MK5 a abaissé ERK4 et p38α, mais pas ERK3 dans les lysâtes de cœur de souris. Par contre, GST-ERK3 et GST-p38α ne démontrent aucune co-IP avec MK5. Ces données suggèrent que dans le cœur seul ERK3, et non ERK4 ou p38α, est capable d'interagir avec, et réguler MK5. A niveau physiologique MK5 interagit entièrement avec ERK3 et par conséquent MK5 n'est pas disponible pour lier les protéines exogéniques. Les souris hétérozygotes pour ERK3 ($ERK3^{+/-}$) ont également démontré une réduction ou une absence de collagène et une faible expression d'ARNm du collagène type1 alpha1, 3 sem post-TAC. Ces résultats démontrent un important rôle pro-fibrotique de la signalisation MK5-ERK3 pendant une surcharge chronique de pression.

Nous avons également démontré 5 variant d'épissage de (MK5.1-5), y compris la forme originale (MK5.1). MK5.2 et MK5.5 subissent une délétion de 6 paires de base dans l'exon 12 : MK5.3 manque l'exon 12 : MK5.4 et MK5.5 manquent les exons 2-6. L'expression des ARNm des différents variant d'épissage a été vérifiée par PCR en temps réel (qPCR). Bien que l'expression est ubiquitaire, l'abondance relative de chaque variant était tissu-spécifique (cœur, rein, pancréas, muscle squelettique, poumon, foie, et cerveau). En plus, l'abondance relative des variant d'épissage varie pendant la surcharge de pression et le développement postnatal du cœur. En outre, l'immunofluorescence a indiqué que MK5.1-5.3 se localise au noyau alors que MK5.4-5.5 est situé au niveau cytoplasmic dans les cellules HEK 293 non stimulées. Suite à une stimulation avec l'anisomycin, un activateur de p38 MAPK, MK5.1-5.3 se translocalise du noyau au cytoplasme alors qu'une petite fraction de MK5.4-5.5 translocalise vers le noyau. Ces variant d'épissage peuvent diversifier la signalisation de MK5-ERK3 dans cœur, mais leur rôle exact oblige des recherches supplémentaires.

Excepté l'isoforme δ, toutes les isoformes de p38 sont exprimées dans le cœur et la forme α est considérée comme étant l'isoforme dominante. L'analyse par qPCR et immunobuvardage de type western ont démontré que p38α et p38γ sont les deux isoformes prédominantes alors que p38β et p38δ sont exprimées aux mêmes niveaux dans le cœur de rat adulte. L'immunofluorescence a démontré que p38α et p38γ se trouvent dans le cytoplasme et le noyau. Cependant, suite à la surcharge par TAC, p38γ s'est accumulé dans noyau tandis que la distribution de p38α est demeurée inchangée. Ainsi, l'abondance de p38γ et sa translocalisation nucléaire suite à la surcharge de pression indique un rôle potentiel dans l'expression génique pendant le remodelage cardiaque.

En conclusion, nous avons mis en évidence pour la première fois un rôle pro-fibrotique pour la signalisation MK5-ERK3 pendant une surcharge chronique de pression. D'ailleurs, les niveaux comparables d'expression de p38γ avec p38α, et la localisation différentielle de p38γ pendant la surcharge aiguë ou chronique de pression suggèrent différents rôles possibles pour ces isoformes pendant le remodelage hypertrophique cardiaque.

TABLE OF CONTENTS

LIST OF TABLES

Table Page

LIST OF FIGURES

LIST OF ABBREVIATIONS

%EF	Percentage ejection fraction
%FS	Percentage fractional shortening
ANP	Atrial natriuretic peptide
AS	Anti-sense
BW	Body weight
COL1 α1	Collagen type 1 alpha 1
DMSO	Dimethylsulfoxide
DNA	Deoxyribonucleic acid
DTT	Dithiothreitol
E	Early mitral filling E-wave velocity
Em	Early mitral annular velocity
ERK1/2	Extracellular signal-regulated kinase 1/2
ERK3	Extra-cellular regulated kinase 3
ERK4	Extra-cellular regulated kinase 4
ERK5	Extra-cellular regulated kinase 5
FPLC	Fast protein liquid chromatography
GAPDH	Glyceraldehyde 3-phosphate dehydrogenase
GPCR	G protein coupled-receptor
GSK-3β	glycogen synthase kinase-3β
GST	Glutathione S-transferase
HEK293	Human embryonic kidney 293
IGF-2	Insulin like growth factor-2
IP	Immunoprecipitation
IVRT	Isovolumic relaxation time
IVRTc	Heart rate corrected IVRT
JNK	c-jun amino-terminal kinase
LV	Left ventricle
MAPK	Mitogen-activated protein kinase

MAPKAPK5	MAP kinase-activated protein kinase 5
MBP	Myelin basic protein
MK	MAPK-activated protein kinase
MK2	MAP kinase-activated protein kinase-2
MK3	MAP kinase-activated protein kinase-3
MK5	MAP kinase-activated protein kinase-5
MPI	Myocardial performance index
mRNA	Messenger RNA
NES	Nuclear export signal
NLS	Nuclear localization signal
PAGE	Polyacrylamide gel electrophoresis
PKI	Cyclic AMP-dependent protein kinase inhibitory peptide
PMSF	Phenylmethylsulfonyl fluoride
PRAK	p38 Regulated/Activated Protein Kinase
qPCR	Quantitative polymer chain reaction
RNA	Ribonucleic acid
S	Sense
TAC	Transverse aortic constriction
TGF-β1	Transforming growth factor beta 1
TGF-β3	Transforming growth factor beta 3
TRAF6	TNF receptor associated factor 6
TTE	Transthorasic echocardiogram
TX-100	Triton X-100
β-MHC	β-myosin heavy chain

ACKNOWLEDGEMENTS

I express my gratitude to my PhD supervisor Dr. Bruce Allen, without him it would have been not possible to complete this task. He has provided good support and guidance throughout my doctoral work. Under his guidance, I learned a lot about signaling mechanisms in the heart during both normal and pathological conditions. Working with Dr. Allen equipped me with various scientific techniques and taught how to ask the right questions and how to address those questions using the correct scientific tools. I would also like to thanks members of thesis committee; Dr. Sylvain Meloche and Dr. Benoit Coulombe, for their valuable research input.

I also wish to thanks Dr. Matthias Gaestel and Dr. Sylvain Meloche for providing us with MK5 and ERK3 knockout mice as well as Dr. Jean-Claude Tardif and Dr. Yanfen Shi for echocardiography support.

I acknowledge technical help from Mr. Marc-Antoine Gillis, Mr. Louis R. Villeneuve, Ms. Karine Bouthillier, and Ms. Maya Mamarbachi.

I also would like to thanks Canadian Institutes of Health Research (CIHR) for providing funds to do my research project as well as to those mice who sacrificed their life for the greater cause of science and betterment of human health.

Finally, I appreciate all the help I got during my doctoral work from my colleagues; George Vaniotis, Nadege Moise, Nada Farhat, Dr. Clemence Merlen, Dr. Maya Khairallah, and Catherine Lavoie.

DEDICATION

To my mother and late father.

INTRODUCTION

I) Cardiac hypertrophy

Hypertrophy of an organ is described as an increase in the size of its cells. The central characteristics of cardiac hypertrophy are an increase in cardiomyocyte size, increased organisation of the sarcomere, and enhanced protein synthesis. This can generate different architectural patterns, which are generally described as being either eccentric or concentric hypertrophy. In *eccentric hypertrophy*, there is an increase in cardiac mass and chamber volume while relative wall thickness may be unchanged, decreased, or increased. *Concentric hypertrophy* refers to an increase in cardiac mass and relative wall thickness with reduced or unchanged chamber volume (Fig. 1). During eccentric hypertrophy heart enlargement is the result of the addition of new sarcomeres in series, to lengthen the cardiomyocyte. During concentric hypertrophy, the reduction in chamber volume is the result of the addition of new sarcomeres in parallel, to increase the width of cardiomyocytes. Hypertrophy can be further classified as: 1) developmental hypertrophy, which is linked to the normal post-natal growth of the heart, 2) pathological hypertrophy, which is linked to disease-inducing stimuli such as pressure or volume overload, and 3) physiological hypertrophy, often seen in athletes and is linked to exercise or pregnancy. Physiological and developmental hypertrophy are characterised by a uniform profile of ventricular wall and septal growth that is matched by an increase in chamber dimension, while pathological cardiac hypertrophy is characterised by a thickened ventricular wall and septum with a net change in ventricular chamber dimensions [1, 2].

Pathologic cardiac hypertrophy is a compensatory response to stress and occurs when the heart is continuously exposed to increased external stimuli such as stretch, hemodynamic overload and/or increased neurohormonal factors. These stimuli are associated with the release of hormones, cytokines, chemokines, and peptide growth factors [1]. The mechanisms where biomechanical signals are transmitted across the plasma membrane remains unclear, although they probably involve stretch-sensitive ion channels, integrins, and other structural proteins in a complex network that links the

extracellular matrix, cytoskeleton, sarcomere, Ca^{2+}-handling proteins, and nucleus [3]. The general understanding of hypertensive heart disease is development of concentric left ventricular hypertrophy with diastolic dysfunction, which is followed by ventricular dilatation with impaired contractility.

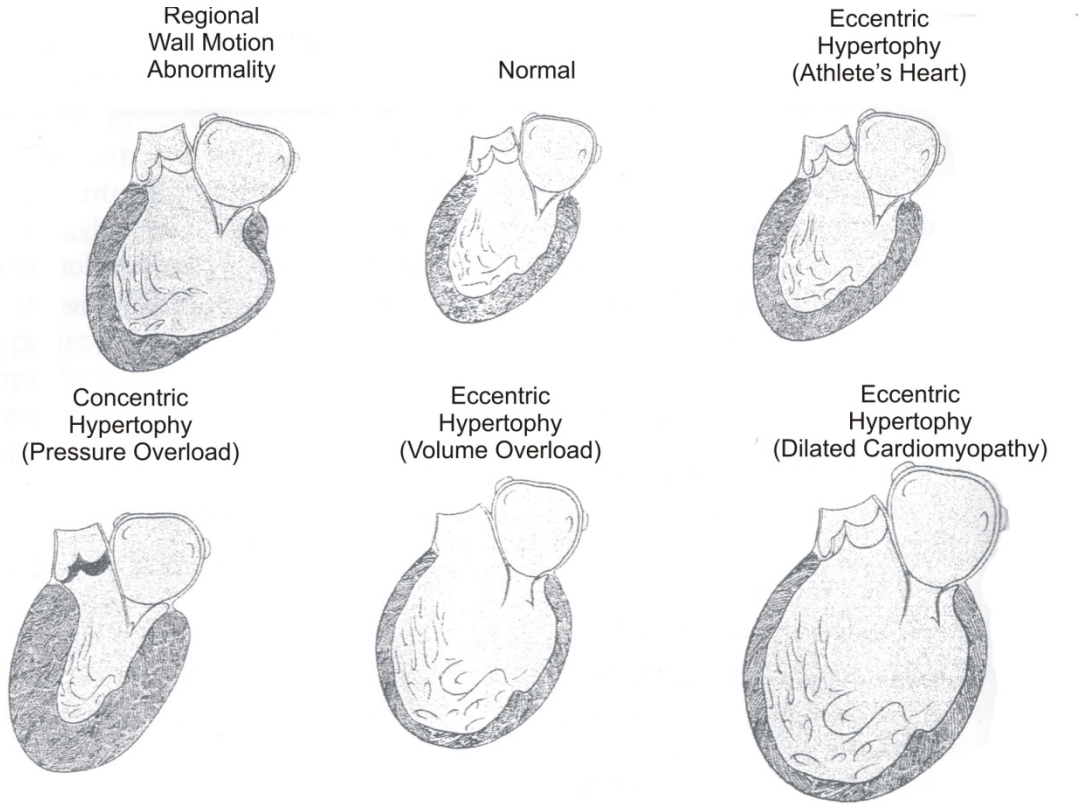

Fig. 1. Architectural patterns of cardiac hypertrophy. After myocardial infarction, eccentric hypertrophy in the non-infarcted region cause regional wall motion abnormalities. Ejection fraction is decreased in dilated cardiomyopathy and increased in volume overload-induced eccentric hypertrophy. In the case of pressure overload-induced hypertrophy, diastolic function is reduced due to increased stiffness of the ventricle (taken from [2]).

II) Physiological and pathological remodelling of the heart

Apart from the differences in morphology observed in physiological and pathological hypertrophy, there are also differences at the molecular level. In physiological hypertrophy cardiac function remains normal or is enhanced whereas in pathological hypertrophy cardiac function is reduced over time. In addition, physiological hypertrophy is generally reversible whereas pathological hypertrophy is not [4]. Furthermore, hypertrophy induced by exercise is usually not accompanied by interstitial collagen deposition [5] while hypertrophy induced by pressure- or volume-overload has collagen deposition [6]. In addition, contrary to physiological hypertrophy, pathological hypertrophy is associated with the re-expression of fetal genes such as atrial natriuretic peptide (ANP), B-type natriuretic peptide (BNP) and the fetal isoforms of contractile proteins such as α-actin and β-myosin heavy chain (β-MHC), as well as the down-regulation of α-MHC and sarcoplasmic reticulum Ca^{2+}-ATPase expression [4]. Furthermore, differential regulation in α-MHC and β-MHC is observed in hypertrophy induced by exercise versus pressure overload [7]. The shift in expression of myosin heavy chain isoform (exchange "low" and "high") that accompanies a reversion to the fetal phenotype weakens the heart by reducing shortening velocity while at the same time helping the heart adapt to the greater energy requirements associated with increased wall stress, as β-MHC (low ATPase activity) develops tension with greater efficiency than α-MHC (high ATPase activity). Another important consequence of the reversion to the fetal phenotype is the reduction of expression of sarco (endo) plasmic reticulum calcium pump ATPase (SERCA) that contributes to arrhythmias and sudden death as seen in end stage heart failure. SERCA participate in intracellular calcium cycle by transporting Ca^{2+} back into the SR in order to allow the myocardium to relax after each contraction [2]. Remodelling caused by hypertension is a major risk factor for heart failure. The stiffening of the heart, caused by excessive collagen accumulation, together with the loss of contractility, as a result of myocyte apoptosis or necrosis, are major undesirable consequences of pathological remodelling [8]. From this point onward the term cardiac hypertrophy or hypertrophy is used to describe pathological hypertrophy.

III) Cardiac cells and the extracellular matrix

Cardiac myocytes make up the majority of the heart's mass, however numerically-speaking approximately 70% of the cells in the heart are smaller non-myocytes. The heart is made up of myocytes, vascular smooth muscle cells, endothelial cells, and fibroblasts. The fibroblast secretes extracellular matrix proteins (connective tissue) that contributes to heart's tensile strength and stiffness. The extracellular matrix (ECM) consists mainly of fibrillar and network collagens, elastic fibres formed by elastin, hydrated proteoglycans and adhesive proteins such as fibronectin and laminin, which couple myocytes to the collagen networks. The ECM provides a scaffold for both myocytes and non-myocytes and hence distributes mechanical forces throughout the myocardium, and transmits mechanical signals to individual cells via surface receptors [9, 10]. Furthermore, the cells' cell surface or adhesion proteins connect its actin microfilaments to extracellular matrix proteins, which include the dystrophin glycoprotein complex and integrins. Dystroglycans bind to many ECM proteins including fibronectin and laminin, while integrins bind to fibronectin, laminin, and vitronectin, which along with heparans and other proteoglycans link the integrins to collagen. Integrins lack enzymatic activity but they do allow mechanical stresses to activate a number of signal transduction pathways by modifying the activity of small G-proteins such as Rho, Rac, and Ras; focal adhesion associated kinases (FAKs); and a variety of protein kinases including Akt, Raf, MEK, and ERK [2]. The ECM's connections to the intracellular cytoskeletal and signaling proteins through cell surface proteins are shown in Figure 2.

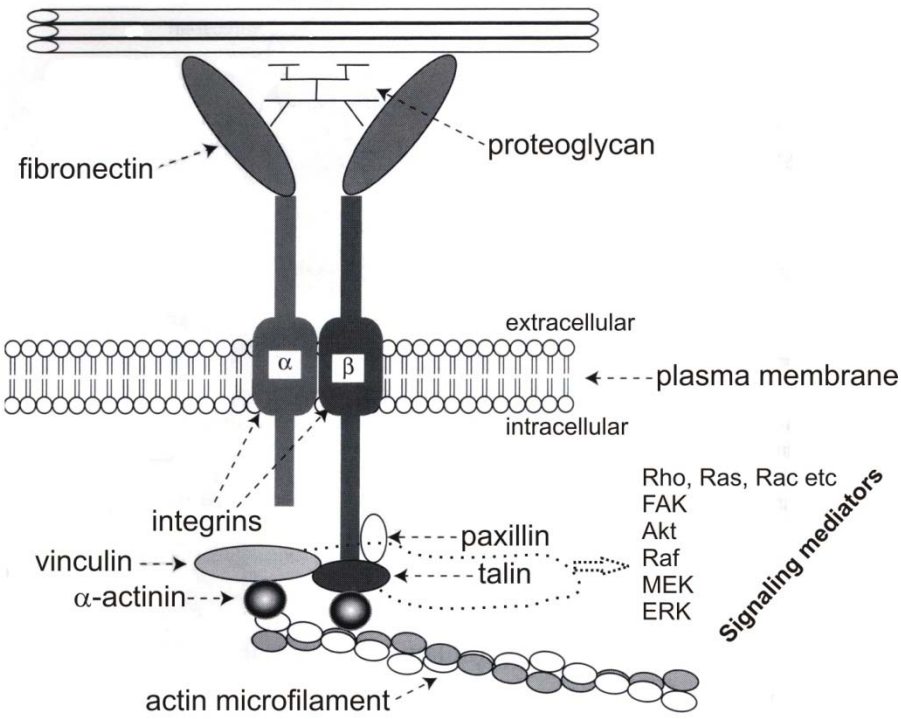

Fig. 2. Integrins' interaction with the extracellular matrix and a number of intracellular signaling pathways. See explanation in the text (modified from [2]).

The connective tissue within the myocardium or the network of fibrillar collagen based on morphology are divided into: 1) *endomysium*, which surrounds individual cardiomyocytes and function as the sites for connections to cardiomyocyte cytoskeletal proteins across the plasma membrane, 2) *perimycium,* which supports groups of myocytes or surrounds muscle fibres, and 3) *epimycium,* which encases the entire muscle [2]. The endomycium is also the source of ECM scaffolding for blood vessels. Pathological cardiac remodelling's fundamental characteristic is myocardial stiffness, which is associated with fibrosis, systolic and diastolic dysfunction, and changes in cardiac cellularity. An increase in collagen (fibrosis or accumulated perimycium) during hypertrophy is coupled with diastolic heart failure, whereas the degradation of collagen (endomysial and perimysial) is associated with ventricular dilatation and systolic heart failure [6]. Therefore, the right proportion of ECM is critical for the heart's normal

physiological function and any anomaly in synthesis or degradation can have devastating consequences.

IV) Cellular signaling

Cardiomyocyte function is influenced by interactions with the ECM, autocrine and paracrine secreted molecules, and circulating hormones. Therefore, it is important to understand cellular events at the molecular level. Membrane receptors and/or mechanical sensors permit cardiomyocytes to sense stress caused by pressure- or volume-overload. This is then transmitted through numerous signaling cascades, which results in alteration in gene expression and subsequently changes in physiology of the heart.

a) Sensing biomechanical signaling

In cardiomyocyte, the cytoskeletal proteins transmit tension developed by the contractile proteins from one sarcomere to another and to the cell surface. Interactions of these proteins are shown in figure 3. Apart from participating in this mechanical function, many cytoskeletal proteins also participate in signaling. Therefore, cardiomyocytes can directly sense deformation or stretch through an internal sensory apparatus, which includes integrins and MLPs (muscle LIM protein), and translate it into internal biochemical changes. Melusin, which interacts with the integrin beta 1 cytoplasmic domain, senses pressure-overload stress in cardiomyocytes and, in turn, regulates the inhibitory phosphorylation of glycogen synthase kinase-3β (GSK-3β). Melusin knockout mice develop dilated cardiomyopathy and contractile dysfunction in response to chronic pressure overload; however, they respond similarly to wild type mice when treated with angiotensin II and phenylephrine [11]. Additionally, cardiac-selective inactivation of integrin or integrin effector molecules, such as focal adhesion kinase (FAK), in mice leads to dilated cardiomyopathy [12]. Another stretch-sensing apparatus is the sarcomere's Z-disc, specifically the MLP, which is anchored at the Z disc, to telethonin (T-cap), a titin-interacting protein (Fig. 3). MLP is considered to

sense stretch through a complex of transducing proteins and then signal through the calcineurin-NFAT pathway [13, 14].

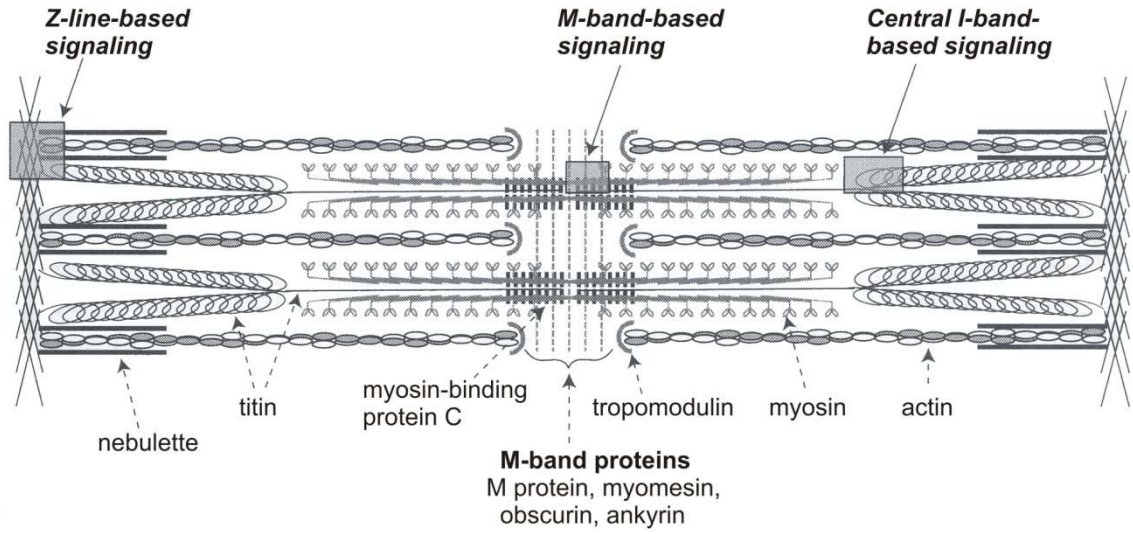

Fig. 3. Cytoskeletal proteins of sarcomere. Titin, a huge protein of molecular weight 3,000,000, and t-cap (telethonin) both link Z lines to the thick filament. On the thick filament titin is connected to myosin by myosin-binding protein C. Sarcomere's signal transduction active regions are labeled as Z-line base signaling, M-band base signaling, and central I-band-based signaling (adopted from [2]).

Angiotensin II type 1 (AT1) receptors have been well characterized for mediating angiotensin II signaling during cardiac hypertrophy. Zou et al show that AT1 receptors sense stretch and activate downstream signaling in an angiotensin II (Ang II) independent manner. Angiotensin knock out mice develop hypertrophy after the aortic banding [15]. This peculiar signaling was later shown as an emerging phenomenon, now know as biased agonism, wherein ligands are able to induce conformational change of receptor that preferentially activate specific downstream signaling pathways. Stretch activates AT1 receptor-β-arrestin signaling which is independent of the classical paradigm of Ang II-mediated G-protein activation [16].

b) Sensing secreted molecules at the cell surface by receptors

When the heart is subjected to hemodynamic stress, the body responds by producing endogenous signals, which can be systemic or local and can lead to a variety of changes in the heart. The cell's cytosol and extracellular space are separated by the plasma membrane, which act a as barrier, but also allows signal transduction through cell-surface receptor proteins. There are three known classes of cell-surface receptor proteins: ion channel-linked, G protein-linked, and enzyme-linked [17]. Ion channel-linked receptors are transiently opened or closed by ligands, briefly changing the ion permeability of the plasma membrane. G protein-coupled receptors (GPCRs) belong to a large superfamily of homologous, seven transmembrane proteins that regulate the activity of separate plasma membrane-bound proteins (enzyme or ion channel) through trimeric GTP-binding regulatory proteins (G protein). Enzyme-linked receptors, most of which are single transmembrane proteins, when activated, either function directly as enzymes or are associated with enzymes [17]. In the heart, GPCRs are the most widely studied, and include catecholamines signaling through α-/β-adrenergic receptors, endothelin acting on the ET_A and ET_B receptors, Ang II signaling through AT_1 and AT_2 receptors, adenosine signaling through A_1 and A_2 receptors, and acetylcholine signaling through muscarinic receptors [18]. Ang II and endothelin 1 (ET-1), which binds to GPCRs associated with $G_{\alpha q}$ and $G_{\alpha 11}$, and β-adrenergic stimulation, which binds to GPCRs associated with Gs, cause cardiac hypertrophy and fibrosis, as well as cardiomyocyte apoptosis [8]. There is more interest in signaling mediated by $G_{\alpha q}/G_{\alpha 11}$, which are required for the development of pathological hypertrophy. Double knockout of $G_{\alpha q}/G_{\alpha 11}$ showed no detectable hypertrophy, but showed myocardial fibrosis and apoptosis post-transverse aortic constriction [19]. Over expression of the activated or wild type form of $G_{\alpha q}$ resulted in development of cardiac hypertrophy that lead into progression towards apoptosis and heart failure [20, 21]. These receptors regulate several different intracellular signaling cascades. Here we will focus more specifically on the MAPK signaling cascades.

MAPK signaling in the heart

Five distinct MAPK pathways have been identified in mammals: the extracellular signal-regulated kinases (ERKs) ERK1/2, ERK3/4, ERK5, c-jun amino-terminal kinases (JNKs) (1-3), and p38 MAPKs (α, β, γ, and δ) [22]. Each pathway, except for ERK3/4, displays a characteristic hierarchical organization wherein MAPK kinase kinases (MAPKKK) phosphorylate and activate MAPK kinases (MAPKK), which in turn activate their respective MAPKs. In the cardiac myocyte MAPK signaling is initiated by GPCRs, receptor serine/threonine kinases (e.g., transforming growth factor- β (TGFβ)), receptor tyrosine kinases (e.g., IGF-1 and fibroblast growth factor receptors), cardiotrophin-1 (gp130 receptor), and by mechanical stress such as stretch (Fig. 4) [1].

i) ERK1/2

The ERK1/2 module consists of MAPKKKs, A-Raf, B-Raf, and Raf-1, the MAPKKs MEK1 and MEK2, and MAPKs ERK1 and ERK2. MEK1 and MEK2 catalyze a dual phosphorylation (T-E-Y) within the activation loop of ERK1/2, resulting in a conformational change that removes steric blocking of the activation loop, which in turn facilitates substrate binding [23]. In the heart, MEK1-ERK1/2 activation is required for hypertrophic growth. Cardiac specific over-expression of activated MEK1 results in the development of concentric hypertrophy without any signs of cardiomyopathy or interstitial fibrosis [24]. In contrast, cardiac-specific over-expression of an activated form of Ras, an upstream kinase of Raf, promoted a cardiomyopathy that was characterized by pathological cardiac remodeling and premature death [25]. In contrast, mice having cardiac-specific expression of dominant negative Raf showed marked resistance to hypertrophy along with inhibition of ERK, but not p38 or JNK, activation following pressure overload [26]. These data suggest that ERK1/2 activity is required for growth and is beneficial whereas upstream Ras regulates multiple downstream signaling targets which are both beneficial and detrimental to the heart. Recent evidence suggests that ERK1/2 may specifically be required for concentric hypertrophy. ERK1/2 knock out mice develop eccentric hypertrophy whereas mice

having myocyte-targeted expression of constitutively active MEK1 develop concentric hypertrophy after pathological insult [27]. This shows the importance of ERK1/2 in directing the heart towards concentric versus eccentric growth.

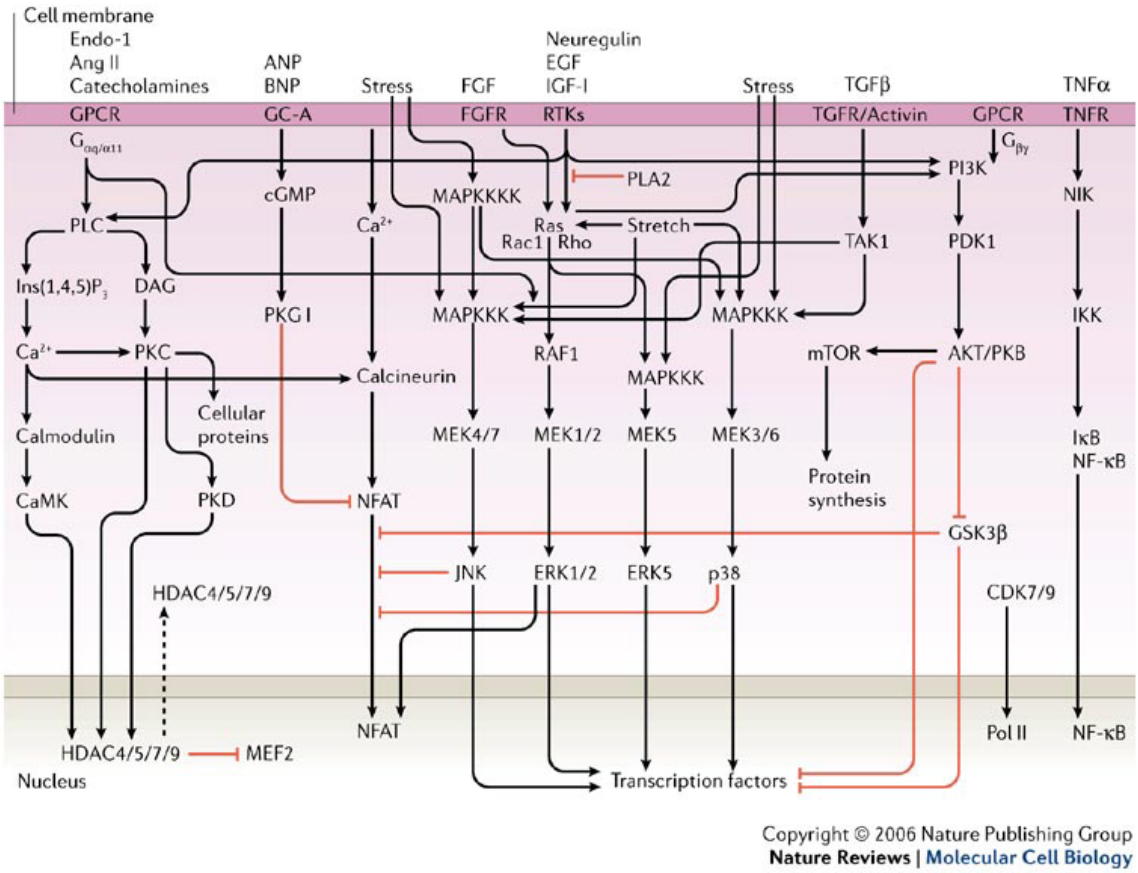

Fig. 4. MAPK and other signaling pathways involved in cardiac hypertrophic reposne (taken from [1])

ii) p38 MAPK

The p38 MAPK module consists of MAPKKKs MEKKs 1-4, MLK-2 and -3, DLK, ASK-1, Cot (Tpl2), and Tak1, the MAPKKs MKK3 and MKK6, and four known p38 isoforms (p38α, p38β, p38γ, and p38δ) [23]. MKK3 and MKK6 phosphorylate the dual phosphorylation site (T-G-Y) in the activation loop of p38 MAPKs. p38α and p38β are ubiquitously expressed, while p38γ is primarily expressed in striated muscle and

p38δ is expressed in lung, kidney, testis, pancreas, and small intestine [28, 29]. To date, except for p38δ, all isoforms (p38α, p38β, and p38γ) have been detected in the heart [30]. All four p38 isoforms have been knocked out in mice: p38α-deficient mice show embryonic lethality due to placental defects, while p38β-, p38γ-, and p38δ-null mice appear to have normal phenotypes [31].

To determine if p38 MAPK plays a role in pathologic cardiac remodeling, transgenic mice over-expressing dominant negative forms of p38α (DN-p38α) or p38β (DN-p38β) were examined [32, 33]. Transgenic mice expressing DN-p38α or DN-p38β developed cardiac hypertrophy but were resistant to cardiac fibrosis after transverse aortic constriction [32]. In another study, Wang et al. dissected the functions of the p38α and p38β isoforms in neonatal cardiomyocytes infected with adenoviral vectors expressing activated mutants of upstream activators of the p38 kinases, MAP kinase kinase 3b(E) (MKK3bE) and MAP kinase kinase 6b(E) (MKK6bE). Infected cardiomyocytes showed a hypertrophic response including enhanced sarcomeric organization, increased cell size, and increased ANP expression. MKK3bE-expressing cells were more apoptotic. The hypertrophic response was suppressed upon co-expression of DN-p38β. The apoptotic effect of MKK3bE was suppressed upon co-expression of DN-p38α [33]. This study demonstrated that p38α is pro-apoptotic and p38β is pro-hypertrophic in neonatal myocytes. Additionally, in transgenic mice with myocyte-specific expression of MKK3bE or MKK6bE, both MKK3bE and MKK6bE transgenic hearts exhibited a marked increase in interstitial fibrosis, increased fetal gene expression, but no significant signs of hypertrophy. These mice also died at 7-9 weeks of age [34]. These studies suggest a detrimental effect of MKK3/6 and p38 activation; however, other studies have shown somewhat contradictory observations. For example, cardiac specific transgenic mice expressing DN-p38α, DN-MKK3, or DN-MKK6 developed enhanced hypertrophy at baseline as well as during pressure overload, or infusion of Ang II, isoproterenol, or phenylephrine. Enhancement of hypertrophy was attributed to the ability of DN-p38α to promote the nuclear localization of the transcription factor nuclear factor of activated T cells (NFAT) and hence increase the expression of NFAT-regulated genes. In addition to promoting a hypertrophic response

in the absence additional causative factors, DN-p38α and DN-MKK3 also produced an increase in interstitial fibrosis [35]. Mice having a cardiac-specific p38α knockout appear to possess a normal cardiac phenotype. However, after TAC, $p38\alpha^{-/-}$ hearts became hypertrophic similar to wild type, but display more extensive interstitial fibrosis in addition to cardiomyocyte apoptosis [36].

Although the results from various studies seem contradictory, they do appear to indicate that p38 activation is detrimental in the heart. Recently, it has been shown that inducing the expression of constitutively active MKK3 (CA-MKK3) in the adult heart leads to cardiac hypertrophy, ECM remodeling, contractile dysfunction, fetal gene expression (ANP and β-MHC), and lethal bradycardic heart failure within 8 days. However, removal of MK2, a well characterized downstream target of p38, in a CA-MKK3 background rescued some aspects of the above pathological response [37]. Moreover, reduced apoptotic cell death in cultured myocytes and intact heart upon pressure overload or ischemia/reperfusion was observed upon pharmacological inhibition of p38α/β activity using a specific inhibitor, SB203580 [38, 39]. Along the same lines, inhibition of p38α/β during ischemia/reperfusion injury or myocardial infarction improved cardiac function and reduced remodeling [40, 41]. TAK1 (TGF-β-activated kinase-1) is an MAPKKK that activates MKK3 and MKK6 [42], and is known to interact with type II TGFβ receptors (TBR II) and TRAF6 in cardiomyocytes [43]. Like TGFβ, TAK1 is activated by pro-inflammatory cytokines such as TNFα and IL-1 [44]. In the heart, TAK1 is implicated in pathological remodeling. Zhang et al generated a line of transgenic mice with cardiac-specific expression of activated TAK1. These mice revealed that constitutive activation of TAK1 was sufficient to induce cardiac hypertrophy, which was accompanied by fibrosis, apoptosis, severe myocardial dysfunction, fetal gene reactivation, and early lethality [45]. Hence, from a therapeutic point of view, there is great interest in the inhibition of p38α/β kinase activity in the diseased heart. For this reason p38α/β inhibitors have advanced to phase I clinical trials [46].

In addition to canonical phosphorylation by upstream kinases MKK3/6, p38α also undergoes autophosphorylation. In HEK 293 cells in response to TNFα treatment,

TRAF6-TAB1-p38α form a complex in which TAB1 (transforming growth factor-β-activated protein kinase 1 (TAK1)-binding protein 1) facilitates p38α autophosphorylation [47]. This TAB1 dependent autophosphorylation of p38α, which is independent of MKK3/6, has been implicated in p38 mediated ischemic/reperfusion injury in the heart [48]. Li et al. further showed the requirement of AMP-activated protein kinase (AMPK) for the TAB1 mediated autophosphorylation of p38 in AMPK knockout ischemic heart [49]. Moreover, ZAP70 (zeta-chain associated protein kinase, 70 kDa) has been shown to induce p38 autophosphorylation in T cells. ZAP70 is a tyrosine kinase that, upon activation by a T-cell receptor, phosphorylates p38 on Tyr-323, which then causes p38 autophosphorylation at residues Thr-180 and Tyr-182 in its activation loop [50].

TAB1 mediated non-canonical autophosphorylation of p38 is negatively regulated. In cardiomyocytes and other cells, p38α autophosphorylation was negatively regulated by the Hsp70-Cdc37 chaperone complex via direct binding of p38 with Cdc37. The Hsp70-Cdc37 complex inhibited both basal and TAB1 mediated p38α autophosphorylation whereas it does not inhibit the phosphorylation of p38 by canonical upstream kinase MKK3 [51] . Furthermore, inhibition of Hsp70 activity increased p38 autophosphorylation and apoptosis in myocytes [51]. In addition, p38 phosphorylates TAB1 at three different sites and causes the inhibition of TAK1 activation in response to pro-inflammatory cytokines or osmotic stress, resulting in feed-back inhibition of p38 signaling as well as suggesting the importance of p38 in the regulation of TAK1 downstream signaling such as JNK or IKK [52]. Canonical p38 phosphorylation is also negatively regulated by protein phosphatases, which interact with phosphorylated p38 but not the non-phosphorylated form of p38 [53]. Mitogen-activated protein kinase phosphatase (MKPs) are dual-specificity phosphatases (DUSP) involved in the dephosphorylation, and hence inactivation of ERK1/2, JNK, and p38. There are ten proteins in this subgroup and they all show varying degrees of substrate specificity [54]. p38 is also negatively regulated by serine threonine phosphatase PP2Cα [53],

p38 regulates number of transcription factors, either directly or through different MKs as discussed below. GATA4 is an important transcription factor in heart required

for cardiac development and differentiation as well as cardiac survival and hypertrophy [55]. GATA4's transcriptional activity is controlled through its Ser105 phosphorylation by ERK1/2 and p38 [56, 57]. p38 also phosphorylates NFAT (Fig. 4) and hence regulates its nuclear entry and transcriptional activity [35].

iii) Atypical MAPKs: ERK3/ERK4

ERK3 is a 720 amino acid protein of molecular mass 100 kDa and ERK4 is a 587 amino acid protein with molecular mass 70 kDa. Both proteins share 73% sequence homology within their kinase domains. Atypical MAPKs are distinct in two aspects from conventional MAP kinases: first, conventional MAP kinases have dual phospho-acceptor site (T-X-Y) while atypical MAPKs have a single phospho-acceptor site (S-E-G) in their activation loop. Second, subdomain VIII in the kinase domain of conventional MAP kinases has the sequence A-P-E while all the ERK3 and ERK4 orthologs have S-P-R. Having an arginine at this position makes ERK3/ERK4 unique within the human kinome. Subdomain VIII lies in the C-terminal lobe of the kinase domain and mutation of a glutamic acid residue within subdomain VIII of protein kinase A slightly reduces its affinity for substrates. Moreover, ERK3 and ERK4 also have C-terminal extensions, downstream of an N-terminal kinase domain, that are 50% identical in the first 150 amino acids while the remaining C-terminus is divergent. In contrast to the conventional MAP kinases, ERK3 and ERK4 are only found in vertebrates (reviewed in [58]).

Coulombe et al. showed that unlike other MAPKs, ERK3 is a highly unstable protein, that is continually degraded in proliferating cells with a half life of only 30 min. Given that inhibition of the proteosome with inhibitors like MG-132 or lactacystin increased the half life of ERK3 from 30 min to over 2 hours, ERK3 degradation is likely mediated by the proteosome. Inactivation of the ubiquitin-activating enzyme E1, but not a phosphorylation-site mutation, kinase dead mutant, or truncation of the C-terminal extension, results in accumulation of ERK3 protein [59]. This suggests that proteolysis of ERK3 is dependent on its polyubiquitination and not on the phosphorylation of its activation loop, its kinase activity, or its C-terminal extension. Generally an internal

lysine residue is ubiquitinated by the ubiquitin-proteosome pathway. However, this is not the case with ERK3, as a lysine-less mutant of ERK3 is still ubiquitinated and degraded. In fact, ERK3 has a unique mode of ubiquitination. Mass spectrometry has shown that ERK3 is conjugated to ubiquitin via its free NH_2 terminus and this observation was further reinforced by increasing the size of the N-terminal sequence tag leading to increased stability of the protein [60]. Along with post-translational regulation, ERK3 is also regulated at the transcriptional level. Inhibition of the proteosome activates p38 MAPK, possibly by regulating expression or stability of protein upstream of MKK3/6, which leads to an increase in ERK3 transcription and translation. Increased ERK3 expression reduced the anti-proliferative effect induced by proteosome inhibition, which might suggest an intracellular rescue mechanism against cell stress and damage induced by proteosome inhibition [61]. Additionally, ERK3 is also regulated at the level of protein stability during cell differentiation. For example, ERK3 protein accumulates during the differentiation of C2C12 myoblasts into muscle cells [59]. Unlike ERK3, ERK4 is a far more stable protein [62, 63].

ERK3 has been implicated in insulin secretion by islet β-cells induced by glucose and phorbol-12-myristate-13-acetate (PMA). In this pathway ERK3 associates with microtubule-associated protein 2 (MAP2) and increases MAP2 serine phosphorylation [64]. It has been shown that along with MAP2 phosphorylation there is an increase in serine phosphorylation of ERK3 upon activation of PKC by PMA, although the identity of this ERK3 serine residue is not known. In other studies there was no change in the phosphorylation of ERK3 at Ser-189 in HEK293 cells following PMA treatment, mitogenic or stress stimuli. However there are other serine residues in ERK3 that are phosphorylated. MK5 phosphorylates Ser-386 [65]. In addition, Ser-684, Ser-688, and Ser-705 are phosphorylated by cyclin B-Cdk1 [66]. Hence, the identity of the serine phosphorylation in β-cells needs to be determined using ERK3 phosphorylation-site specific antibodies or site-directed mutagenesis. Furthermore, ERK3 may also been involved in cancer. The great majority of tissue and peripheral blood samples from patients with oral cancer have increased levels of ERK3 [67]. Along similar lines, ERK3 levels are reduced in cells where PCNA (proliferating cell nuclear

antigen) expression has been down regulated by siRNA. PCNA has been shown to be up-regulated in a number of chronic myologenous leukemia (CML) patients [68]. These observations suggest that ERK3 may also play a role in carcinogenesis, although a direct link between ERK3 activation and the development or prevention of cancer has not yet been demonstrated.

In certain cell types, overexpression of ERK3 inhibits cell cycle progression [69]. In NIH 3T3 fibroblasts over-expression of ERK3 causes G_1 arrest [59] and this inhibition of entry into S phase requires the nucleocytoplasmic shuttling of ERK3, as exclusively nuclear (ERK3-NES) or cytoplasmic (ERK3-NLS) ERK3 fusion proteins were less effective for cell cycle arrest than the wild type kinase [70]. Moreover, mutation of Ser-189 to either a non-phosphorylatable alanine residue or a phosphomimetic glutamic acid residue does not change the subcellular localization of ERK3 in NIH 3T3 fibroblasts [70]. These observations suggest that factors responsible for nuclear-cytoplasmic shuttling of ERK3, not the upstream kinase of ERK3, might be deciding the fate of ERK3 function in cell cycle G_1 arrest. On similar lines it has been suggested that the phosphatase hCdc14A might be keeping the signaling complex comprising ERK3/4, MK5, and cyclin D3 in the cytoplasm, resulting in G_1 cell cycle arrest [71], but this still requires direct experimental proof.

As mentioned above, hCdc14A dephosphorylates ERK3 at sites phosphorylated by Cdk [71]. ERK3 is phosphorylated within its C-terminal extension at Ser-684, Ser-688, Thr-698, and Ser-705 by cyclin B-Cdk1 during mitosis and dephosphorylated by hCdc14A and hCdc14B at the end of mitosis [66]. Each of these sites is followed by a proline residue, conserved in mammals, and lies within a minimal Cdk consensus phosphorylation site. This hyperphosphorylation of ERK3 reduces its mobility on SDS-PAGE. Moreover, phosphorylation of these four residues increases the stability of ERK3 during mitosis [66]. Cyclin B-Cdk-1 activity is at its peak during mitosis and is required for the G_2/M transition and cell cycle progression [72]. Cdc14 is a proline-directed phosphatase that opposes the actions of Cdk and hence plays a role in regulating a cells exit from mitosis [73]. This understanding of the regulation of ERK3 by cyclin B-Cdk1 and hCdc14 during cell cycle and the stabilization of ERK3 by

phosphorylation provides important insights into the function of this kinase. It would be interesting to know about the purpose of increased ERK3 stability during mitosis as this may help to reveal the role of this kinase in other cellular functions.

Klinger et al. recently generated a line of ERK3 knockout mice in a C57BL/6 background. These mice lack the 2^{nd}, 3^{rd}, and 4^{th} exons in ERK3 and, because of a stop codon insertion in the gene, results in a null allele. $ERK3^{-/-}$ mice are born with normal Mendelian frequency but all neonates die within 24h due to acute respiratory failure. Loss of ERK3 leads to reduced lung cell proliferation (pulmonary hypoplasia) and abnormal maturation of the distal lung epithelium from an early stage in pulmonary development. Additionally, loss of ERK3 leads to a 10-15% reduction in fetal growth, along with a 25-40% reduction in the absolute weight of the lung, liver, and heart of E18.5 embryos. Also, serum levels of insulin like growth factor 2 (IGF-2) are reduced in $ERK3^{-/-}$ mice [74]. Like ERK3, IGF-2 has been implicated in fetal growth. IGF-2 knockout mice show a 40% reduction in body weight compared to wild type littermates and this growth retardation begins in the embryonic period [75]. Evidence of intrauterine growth restriction (IUGR) in $ERK3^{-/-}$ mice, similar to other animal models and human population, puts ERK3 knockout mice at a higher risk for diabetes, hypertension and coronary heart disease later in life [74]. In humans, IUGR is defined as birth weight at or below 2 standard deviations for gestational age or approximating $<10^{th}$% gestational-age adjusted birth weight. So it would be interesting to follow cardiovascular function in these mice as they age.

iv) *JNK*

Mice deficient in JNK1, JNK2, or JNK3 as well as double knockout of JNK1/JNK3 or JNK2/JNK3 survive normally, with the exception of JNK1/JNK2 double knockout mice, which are embryonic lethal and show dysregulation of apoptosis in the brain. During early brain development, JNK1 and JNK2 regulate region-specific apoptosis [76]. In the heart JNK1/2 regulates pro-apoptotic signaling during ischemia-reperfusion. After ischemia-reperfusion injury in JNK1 or JNK2 knock-out mice as well as in mice expressing cardiac specific dominant negative JNK1/2, there was less injury

and apoptosis in the heart [77]. In contrast, JNK1 is cardiac protective during episodes of acute hemodynamic stress. JNK1 knockout, but not JNK2 or JNK3, mice showed increased apoptosis upon acute pressure overload. During periods of longer hemodynamic stress, function recovered in JNK1 knockout hearts, which could be due to a redundant function of JNK2 [78]. Similarly, an upstream activator of JNK, MEKK1, shows a cardiac protective role during periods of acute hemodynamic stress. In addition, in MEKK1 knockout mice the activation of JNK is abolished and cell death is increased in response to pressure overload [79]. Taken together, the studies described above suggest that the JNKs' pro- and anti-apoptotic signaling is dependent on cell type as well as the nature and duration of the stress stimuli.

NFAT is localized in the cytoplasm and moves into the nucleus upon dephosphorylation by calcineurin, which is activated in response to an increase in cytoplasmic Ca^{2+} concentration, where it activates gene expression [80]. JNK negatively regulates hypertrophy by phosphorylating NFAT and hence preventing its nuclear import. JNK1/2 knockout and cardiac specific dominant negative JNK1/2 mice show increased myocardial growth with age and following hemodynamic stress as a result of pressure overload due to decreased NFAT phosphorylation. Additionally, the increase in pressure overload-induced hypertrophy observed in JNK-deficient mice was diminished in a calcineurin-deficient background [81].

v) ERK5/big MAPK (BMK) 1

ERK5 knockout mice show embryonic lethality associated with defective blood vessel and cardiac development [82]. Myocyte enhancer factor 2 (MEF2)-A, -C, and -D transcriptional activity is regulated by ERK5 and they are all well characterized substrates of ERK5 [83, 84]. Cardiomyocyte-specific ERK5 knockout mice are viable and show no apparent defects [85]. In the heart, ERK5 is pro-hypertrophic, pro-fibrotic and anti-apoptotic. Cardiac-specific ERK5 knockout mice show less hypertrophic growth and fibrosis, with increased apoptosis, following hypertrophic stimuli. The reduction in the hypertrophic growth in ERK5 knockout hearts is due to the reduced MEF-2 transcriptional activity [86]. A deficiency in MEK5, the upstream kinase of

ERK5, is also embryonic lethal and results in cardiovascular defects with increased apoptosis in the heart, head and dorsal region of the embryo [83]. These studies in knock-out mice demonstrate the importance of ERK5 in cardiac development and function.

MAPK downstream signaling

Downstream of MAPKs are several MAPK-activated protein kinases (MAPKAPKs or MKs) such as MK2, MK3, and MK5. All MKs have a single kinase domain and have a similar consensus phosphorylation site within their activation loop (Ser or Thr followed by proline residue) for phosphorylation by proline-directed kinases such as p38α and p38β but not p38γ or p38δ. Based on homology within the kinase catalytic domain, all MKs belong to the calcium/calmodulin-dependent protein kinase (CaMK) superfamily. MAPKs specifically interacts with their substrates through docking domains. All MKs have a similar D domain, a stretch of positively charged residues flanked by hydrophobic residues, where p38 binds through its CD motif, negatively charged residues flanked by hydrophobic residues [23].

(a) *MK5/MAPKAPK5/PRAK*

To date MK5 has been shown to be regulated by p38, PKA and ERK3/ERK4.

(i) Regulation of MK5 by p38

New et al. and Ni et al. simultaneously identified MK5 and named it PRAK (p38-regulated/activated kinase) and MAPKAPK5 (MAPK-activated protein kinase 5), respectively [87, 88]. From this point forward, this kinase will be referred to as MK5. The *mapkapk5* gene codes for a 473 aa protein kinase in humans and mice. Its orthologues are present in most of vertebrates but do not appear to be present in *C. elegans* or *Drosophila*. MK5 is expressed in the heart, brain, placenta, lung, liver, skeletal muscle, kidney, and pancreas, and shows a 33% amino acid sequence homology with MK2 and MK3. As found in other MKs, MK5 contains a conserved LXTP motif where threonine is the single phospho acceptor site. MK5 is phosphorylated at residue

Thr-182 by both p38α and p38β *in vitro* and *in vivo.* Upon stimulation of HeLa cells with pro-inflammatory cytokines or stress such as TNFα, PMA, or arsenite, activated MK5 phosphorylates Hsp27, in manner which is sensitive to the p38α/β specific inhibitor, SB203580, suggesting p38 specific activation [88]. In different cell lines (COS-1, HEK293, NIH 3T3, and HeLa cells) over-expressing MK5, Seternes et al. have shown that MK5 is primarily localized in the nuclear compartment, and shuttles between the nucleus and the cytoplasm. MK5 physically interacts with p38α/β and upon stimulation with arsenite or sorbitol it translocates into the cytoplasm, and this nuclear export is sensitive to SB203580, suggesting a p38 dependent nuclear export. For p38 mediated nuclear export of MK5, its Thr-182 phosphorylation, but not its kinase activity, is required, as generation of a kinase dead mutant of MK5, where lysine-51 is mutated to a glutamic acid, has no impact on MK5's ability to move to the cytoplasm. Lys-51 is required for ATP binding. Furthermore, MK5 has both a nuclear localization signal (NLS) and a nuclear export signal (NES) in its C-terminal. The NLS and D domain (p38 binding site) sequences overlap, hence binding of phospho p38 to D domain (NLS) of MK5 it may block the binding of importin to the NLS and therefore cause nuclear export of MK5 [89, 90]. The subcellular distribution of MK5 in resting cells and stimulated cells is shown in Figure 5.

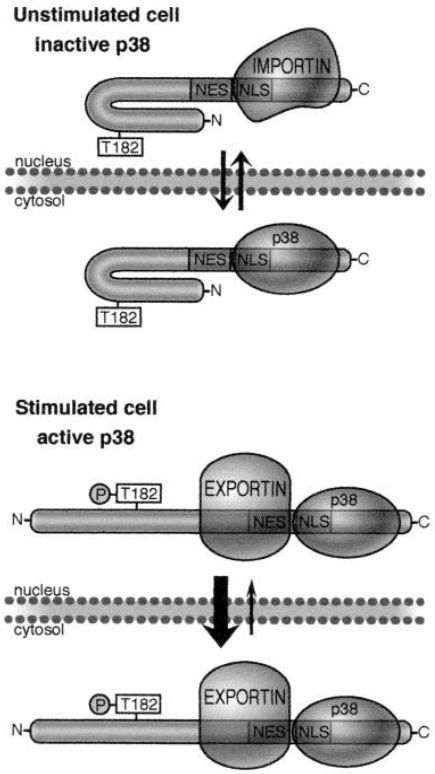

Fig. 5. Model for the regulation of MK5's subcellular distribution. The top panel shows unstimulated cells where the NLS on MK5 is in an open conformation and hence both p38 and importin may compete for interaction. The lower panel shows stimulated cells, where binding of phospho p38 to D domain (NLS) may block the NLS binding to importin and moreover, phosphorylation of Thr-182 may cause conformational changes, which may lead to activation or unmasking of the NES (adopted from [89])

Li et al. further dissected the regulation of MK5's subcellular localization by p38α and p38β and its effect on proliferation of NIH3T3 cells. p38α and p38β lack an NLS and an NES and localize to both the nucleus and the cytoplasm. MK5 alone is localized in the nucleus, however when co-expressed with p38α, the p38α-MK5 complex showed solely nuclear localization while the p38β-MK5 complex was solely localized in the cytoplasm. The distinct subcelluar localization of these two complexes is determined by two amino acid residues in of p38α/β: Asp-145 and Leu-156 in p38α, and Gly-145 and Val-156 in p38β [91]. Based on the crystal structure of p38α and its

complex with MK2 [92, 93], models of the p38α-MK5 and p38β-MK5 complexes show that Leu-156 in p38α and Val-156 in p38β differently affect the conformation of the MK5 NLS, and therefore its interaction with p38β, but not with p38α, may interfere with the binding of importin α with the MK5 NLS and prevent its nuclear import. Moreover, nuclear localization of MK5 by p38α reduces the proliferation of NIH3T3 cells and this inhibition is removed with the cytosolic localization of MK5 by p38β [91]. This study has shown the importance of MK5's cellular localization for its physiological function and suggests that phosphorylation of MK5 at Thr-182 causes its nuclear export thus removing its ability to inhibit cellular proliferation.

A greater understanding of the physiologic role of MK5 in mice came from studies by Sun et al. who developed a line of mice that did not express MK5 [94]. MK5-null mice revealed the requirement for MK5 in *ras-p38* induced senescence and tumor suppression. MK5-null mice on a mixed 129 X C57BL/6 genetic background are viable, fertile and show no apparent health or behavioral problems. These null mice are, however, more vulnerable to dimethylbenzanthracene (DMBA) induced carcinogenesis. DMBA is a well characterized skin carcinogenic mutagen, and after its administration to $MK5^{+/+}$, $MK5^{+/-}$, and $MK5^{-/-}$ mice, the $MK5^{+/-}$ (40%) and $MK5^{-/-}$ (62%) mice developed skin papillomas. More than 90% of DMBA induced skin tumors contain activated *Ha-ras* and p38 is shown to play a major role in *ras*-induced senescence [94]. Other studies have shown that oncogene-induced senescence is a major barrier to tumorigenesis [95]. Given that MK5 is downstream of p38, this implies a possible role for MK5 in oncogene-induced senescence. Western blot and immunohistochemical analysis of tumors obtained from $MK5^{+/-}$ and $MK5^{-/-}$ mice were negative for the senescence-associated β-galactosidase (SA-β-gal), and showed reduced levels of $p16^{INK4A}$, DcR2, and Dec1 senescence markers, which suggests deletion of MK5 abolishes DMBA-induced senescence and hence promotes the development of tumors. Additionally, evidence for MK5's role in senescence was further strengthened by gain of function studies, as $MK5^{-/-}$ primary mouse fibroblasts show expression of senescence markers after transduction with an activated *ras* allele along with the wild-type MK5, but not with activated *ras* and kinase dead mutant of MK5 (Lys-51-Met). Further understanding

of the signaling cascade was elucidated following assessment of MK5 activity, which was increased in *ras* and MKK3/6E transfected MEF cells and was inhibited by SB203580, an inhibitor for p38α/β, suggesting that MK5 activity was mediated by p38. Furthermore, MK5 regulates oncogene-induced senescence through p53 by phosphorylating Ser-37. In addition, reduced p53 activity in MK5-deficient cells was correlated with reduced $p21^{WAF1}$ expression, which was previously shown to increase in *ras*-induced senescence. Moreover, the involvement of MK5 was specific to cancer causing conditions in which *ras* was involved and not in other signaling cascades that mediate tumor suppression through p53, as MK5 was not required for DNA-damage-induced-G1 arrest regulated by p53-p21 signaling [94].

Similarly, MK5 is implicated in replicative senescence that is associated with increased MKK4 abundance. MK5 Ser-93 and p38 phosphorylation were increased in senescent human diploid fibroblasts. This was shown to be due to an increase in the expression of MKK4, an upstream kinase of p38 and JNK. Conversely, p38 and MK5 phosphorylation were decreased following over-expression of microRNAs miR-15b, miR-24, miR-25, and miR-141, which suppresses MKK4 translation [96]. This data further supports the notion that MK5 is involved in senescence. Unfortunately, MK5 Ser-93 phosphorylation, has never been characterized and is not the site phosphorylated by p38, PKA, or ERK3/ERK4 (explained in the following text). These results suggest the existence of yet another kinase capable of phosphorylating MK5; however, phosphorylation of Ser-93 needs to be validated by site directed mutagenesis.

(ii) Regulation of MK5 by PKA

cAMP-dependent protein kinase (PKA) is a tetrameric holoenzyme, which consists of two catalytic (C) and two regulatory (R) subunits. cAMP binds to the regulatory subunits and causes them to dissociate from the catalytic subunits, leaving the catalytic subunits free to phosphorylate its substrates. Cyclic AMP (cAMP) functions as an intracellular second messenger to transmit extracellular signals [97]. Gerits et al. have shown that PKA mediates microfilament rearrangement in PC12 cells through phosphorylation and nuclear export of MK5. Endogenous or exogenously expressed

MK5 showed cytoplasmic translocalization upon treatment with forskolin or co-expression of the catalytic subunit of PKA tagged with a nuclear localization signal (Cα-NLS) [98]. Forskolin is a diterpene obtained from an Indian plant, *Coleus forskohlii*, which directly activates adenylate cyclase, and increases cAMP levels that leads to the activation of PKA [99]. Over-expressed MK5 and the Cα subunit of PKA physically interact, allowing PKA to phosphorylate MK5 and increase its activity, while similar interaction between MK2 and PKA was not observed [98]. In contrast to a previous study where the nuclear export of MK5 mediated by p38 was dependent on Thr-182 phosphorylation and not on its activity (MK5 Lys-51-Glu mutant) [89, 90], PKA-mediated MK5 nuclear export requires both Thr-182 phosphorylation and kinase activity [98], suggesting differential requirements for nuclear export in signaling mediated by p38 and PKA. Dependence on MK5 kinase activity for PKA mediated nuclear export suggests the involvement of an MK5 substrate in nuclear export, which would require the identification of MK5's substrate(s) and their possible role(s). Additionally, siRNA-induced knockdown of MK5 inhibited the PKA mediated F-actin remodeling, suggesting MK5 is essential for this microfilament rearrangement [98]. Recently Kostenko et al. further elaborated the above findings in a similar cell line, showing that PKA-MK5 mediated F-actin rearrangement requires Hsp27 phosphorylation by MK5 [100]. It is well known that the non-phosphorylated form of Hsp27 binds to the barbed, growing ends of actin filaments, which stabilizes them and inhibits further polymerization. Upon phosphorylation, Hsp27 no longer binds to actin, thus allowing F-actin remodeling [101]. Numerous stimuli activate F-actin remodeling through p38/MK2 mediated Hsp27 phosphorylation [102]. However, p38 MAPK and MK2 were not activated following forskolin treatment, where PKA-MK5-Hsp27 mediates F-actin rearrangement [100], suggesting the possible existence of different mechanisms for regulation of microfilament rearrangement depending on the stimuli. In contrast, PKA has been shown to phosphorylate MK5 at Ser-115, causing it to translocate to the cytoplasm, and induce Hsp27 phosphorylation-dependent cytoskeletal remodeling. This process is independent of Thr-182 phosphorylation and MK5 kinase activity [103], which was shown to be required, by the same group, in PKA mediated nuclear export

[98]. Two different models have been proposed to explain this ambiguity. The first model implies that, Ser-115 might be inaccessible for PKA following Thr-182-Ala and Lys-51-Glu mutation because of conformational changes, while the second model suggests Ser-115 might be phosphorylated by PKA, but because of conformational changes induced by these mutations, NES exposure is prevented and MK5 remains within the nucleus. Moreover, nuclear export of MK5 mediated by p38, ERK3, and ERK4 do not require Ser-115 phosphorylation [103]. This makes Ser-115 a unique phosphorylation site, which is only regulated by PKA and not by other MK5 kinases. But again this was done in an over-expressed cellular environment and needs to be confirmed under more physiological conditions, which may reveal a role of MK5 in beta adrenergic signaling in the heart.

14-3-3 proteins are acidic dimeric proteins that recognize phosphorylated or non-phosphorylated Ser/Thr motifs in a sequence-specific manner and are involved in regulation of numerous signaling pathways. 14-3-3ε has been shown to negatively regulate the F-actin remodeling mediated by MK5. HeLa cells over-expressing MK5 show increased cell migration due to Hsp27 phosphorylation and F-actin polymerization, which was prevented when MK5 was co-expressed with 14-3-3ε. MK5 dependent phosphorylation of Hsp27 was inhibited by 14-3-3ε. Both endogenous and exogenously, expressed MK5 and 14-3-3ε interact physically, and this interaction inhibits MK5's kinase activity. Conversely, the increase in cell migration observed upon transfection with MK5 was further augmented when 14-3-3ε expression was knocked down using siRNA [104]. The interaction of MK5 with 14-3-3ε represents an important mechanism for the negative regulation of MK5 activity.

Gerits et al. analyzed the MK5 promoter region in mouse, rat, and human and observed a number of consensus binding sites for transcription factors, but only cAMP-responsive element (CRE) and heat shock factors were functional in PC12 cells. Treatment of cells with forskolin, which increases activity of CRE binding protein (CREB), or heat-shock increased MK5 mRNA without any change at protein levels, and the increased mRNA levels were not due to change in mRNA stability. Moreover,

reduction in CREB levels by siRNA reduced the mRNA levels of MK5, suggesting that CREB controls the basal level of MK5 expression [105].

(iii) Regulation of MK5 by ERK3/ERK4

Shi et al. have generated a line of MK5 knockout mice by homologous recombination [106]. In this line of mice, exon 6, which codes for part of the kinase domain, was removed and hence these mice express a catalytically inactive form of MK5. Moreover, this deletion makes MK5 less stable, likely due to protein misfolding. The MK5 functional knockout mice described by Shi et al. and the MK5 null mice discussed above [94] are in a similar mixed 129 X C57BL/6 genetic background. Both the MK5 functional knockout and MK5-null mice are viable, fertile, and show no abnormalities in behavior, tissue morphology, or health. However, after back-crossing 129 X C57BL/6 MK5 functional knockout mice onto a C57BL/6 genetic background, MK5 functional knockout mice showed embryonic lethality and were under represented after E12 [107]. Hence, depending on genetic background, the absence of MK5 activity may be embryonic lethal. As MK2 and MK5 are both downstream of p38 and have been shown to phosphorylate Hsp25 (mouse homologue of Hsp27), Shi et al. compared the phenotype of $MK5^{-/-}$ and $MK2^{-/-}$ mice. Unlike deletion of MK2, the absence of MK5 activity had no effect on 1) lipopolysaccharide (LPS)-induced biosynthesis of cytokines such as tumor necrosis factor (TNF), interleukin-6 (IL-6), and gamma interferon (IFN-γ), 2) cell migration, and 3) p38 stability. Moreover, when over-expressed MK5, unlike MK2, fails to physically interact with endogenous p38 in HEK 293 cells. Furthermore, the ability of arsenite to induce Hsp25 phosphorylation was abrogated in MEF cells deficient with MK2 but not MK5 [106]. This study has shown the differential functional properties of MK2 and MK5, and raised serious doubts regarding MK5's role in downstream p38 signaling and its ability to phosphorylate Hsp25 *in vivo*.

The studies of Seternes and Kant et al. were a major breakthrough in our understanding of MK5 as well as ERK3/ERK4 signaling. These authors showed that MK5 is regulated by atypical MAPKs ERK3/ERK4 [63, 108]. Using a yeast two-hybrid assay, Seternes et al. found that MK5 interacts with ERK3. They have also shown that a

physical interaction with MK5 is required to maintain endogenous ERK3 protein levels and that ERK3 is able to phosphorylate and activate of MK5. Further experiments in RAW 264.7 cells showed a direct interaction between ERK3 and MK5, whereas no such interaction was observed between endogenous MK5 and p38. On the other hand ERK3 fails to interact with MK2, MK3, MSK1 or MNK1, which are structurally related to MK5. Heterologously expressed ERK3 was localized in both the nuclear and cytoplasmic compartments while MK5 was mainly nuclear. However, when co-expressed, MK5 and ERK3 both co-localized to the cytoplasm, and this change in localization did not require the kinase activity of either ERK3 or MK5, or MK5 Thr-182 phosphorylation [108], which was shown to be essential for p38-mediated nuclear export [89, 90]. Additionally, ERK3 binds to the C-terminal of MK5, downstream of its NLS where p38 binds [108]. This suggests different regulation of MK5 by p38 and ERK3 in terms of both their physical interaction and cellular redistribution. Similar to p38, ERK3 has been shown to phosphorylate MK5 on Thr-182 and increase its activation. Primary MEF cells derived from ERK3 knock-out mice showed a 25% reduction in MK5 activity in $ERK3^{+/-}$ and a 50% reduction in $ERK3^{-/-}$ cells compared to $ERK3^{+/+}$ cells, without any change in protein levels [108]. This suggests that *in vivo* MK5 is regulated by ERK3. The 50% of MK5 activity that remained in the absence of ERK3 raises the possibility that other kinases are also involved. In addition, as mentioned above, the physical presence of MK5 is required for the stabilization of ERK3. Reducing MK5 expression using siRNA dramatically reduced the endogenous level of ERK3, and this was overcome by transfecting with MK5. Furthermore, a constitutively active mutant of MK5 phosphorylated ERK3 [108], suggesting that ERK3 is a substrate as well as kinase for MK5.

Concurrently, Schumacher et al. also showed an interaction between MK5 and ERK3; however, they observed a cytoplasmic localization of ERK3 when expressed in HEK293 cells. They further showed that the site in ERK3 phosphorylated by MK5 is not Ser-189, the known phosphorylation site in the ERK3 S-E-G motif. ERK3 and MK5 interact through their C-terminal amino acids 301-358 (ERK3) and 369-473 (MK5). Moreover, $MK5^{-/-}$ MEF cells had reduced levels of ERK3 [107], showing requirement

of MK5 for stabilization of ERK3. The catalytic activity of MK5 is required for its Thr-182 phosphorylation, suggesting that ERK3 binding promotes the autophosphorylation of MK5 [107].

During embryogenesis ERK3 mRNA expression peaks at day E11 and a similar pattern of expression was observed for MK5 mRNA, reinforcing the concept that a direct interaction with MK5 is required for ERK3 stability [107]. Other studies have shown that ERK3 accumulates during cell differentiation and that augmented ERK3 levels inhibit cellular proliferation by inducing G1 arrest [59]. These observations suggest a possible role for ERK3-MK5 signaling during mouse development.

Similar to ERK3, MK5 interacts with and is regulated by another atypical kinase, ERK4 [63, 108]. When expressed in HEK 293 cells, ERK4 localizes to the cytoplasm and upon co-expression with MK5, which mainly localizes in the nucleus, led to the export of MK5 from the nucleus. The kinase activity of ERK4 is essential for MK5 activation but not for its translocation. Similar to ERK3, ERK4 is phosphorylated by activated MK5 and binds at the same amino acid residues (e.g., 369-473) in the C-terminus of MK5. However, in contrast to ERK3, the phosphorylated form of ERK4 migrates slower on SDS-PAGE than the non-phosphorylated form [63]. Ablation of ERK3 by homologous recombination or siRNA-mediated knock down resulted in a 50% reduction in MK5 activity [108], and a similar reduction in MK5 activity was observed in siRNA mediated knock down of ERK4. Moreover, a combined siRNA-mediated knock down of both ERK3 and ERK4 resulted in a 80% reduction in MK5 activity [63], suggesting that both ERK3 and ERK4 are physiological regulators of MK5 activity. Unlike ERK3 [108], ERK4 is a stable protein and does not require the chaperoning activity of MK5 [63]. Over-expressed ERK4 forms a complex with ERK3. At endogenous levels, ERK4 interacts with MK5 in an ERK3-deficient background, as does ERK3 in an ERK4-deficient background [62, 63]. These observations suggest that MK5 interacts independently with either ERK4 or ERK3. It remains to be determined whether 1) MK5 exists in two separate complexes (e.g., ERK3-MK5, ERK4-MK5), 2) that MK5, ERK3, and ERK4 can form a single complex, or 3) if there is a pool of ERK3-ERK4 complexes without MK5.

The typical MAP kinases (ERK1/2, p38, JNK) are activated by dual phosphorylation within a T-X-Y motif in the activation loop. Atypical MAPKs ERK3 and ERK4 contain an S-E-G motif and have a single phospho-acceptor site, Ser-189 in ERK3 and Ser-186 in ERK4, within their activation loop. Independent of ERK4 or MK5 kinase activity, over-expressed ERK4 is phosphorylated on Ser-186, suggesting the existence of an ERK4 kinase. Furthermore, this phosphorylation does not change following cellular treatment with extracellular stimuli such as PDGF, newborn calf serum (NCS), PMA, arsenite, H_2O_2, or UV-C, which activate the classical MAPKs [109]. Phosphorylated ERK4's reduced electrophoric mobility [63] is not the result of Ser-186 phosphorylation, but is due to MK5-mediated phosphorylation at another site [109]. Moreover, co-expression of MK5 and ERK4 increased the phosphorylation of ERK4 at Ser-186; however, this phosphorylation does not require catalytically active MK5 [109]. This could be a result of MK5 protecting the site from dephosphorylation or, alternatively, the binding of MK5 to ERK4 might assist in the recruitment or activation of ERK4 Ser-186 kinase. Phosphorylation of ERK4 at Ser-186 is required for it to act as a substrate, for cytoplasmic anchoring, and activation of MK5. ERK4 and MK5 form a weak complex that is stabilized following Ser-186 phosphorylation *in vivo* and results in the phosphorylation and activation of MK5, which in turn phosphorylates ERK4 (site other than Ser-186), and results in a mobility shift [109].

Concurrently Deleris et al. showed that ERK3 and ERK4 are phosphorylated on their S-E-G motif (Ser-189 for ERK3 and Ser-186 for ERK4) in resting cells and this phosphorylation is required for binding, activation and translocation of MK5 [65]. Similar to ERK4 [109], ERK3 phosphorylation of Ser-189 does not change following treatment with extracellular mitogenic or stress stimuli. A combination of phosphopeptide mapping and tandem mass spectrometric analysis showed the Ser-386 phosphorylation site in ERK3/ERK4, which is conserved and could be the site for MK5 mediated phosphorylation, lies in a putative MK5 consensus sequence, but this still needs more direct evidence [65].

Aberg et al. identified specific interaction sites in MK5 as well as in ERK3/ERK4 and gave detailed (molecular) insight into the MK5-ERK3 and MK5-

ERK4 interaction [110]. Two separate C-terminal regions, encompassing residues 383-393 and 460-465 in MK5 are required for it to interact with ERK3 and ERK4. Co-expression of a deletion mutant of ERK3 or ERK4 in either of these regions prevents the translocation of MK5. Unlike p38, the ERK3 and ERK4 CD and ED domains do not participate in the interaction with MK5. Peptide overlay assays have identified the MK5 interaction motif (FRIEDE) in ERK3 (332-337) and ERK4 (328-333), which is in the L16 extension loop lying C-terminal to the CD domain [110]. The L16 loop of MAPKs has been proposed to be a protein-protein interaction motif required for homodimerization [111, 112]; however, the findings of Aberg et al. suggest it is involved in binding with its substrate. The substitution of isoleucine to lysine in the FRIEDE motif of ERK3 or ERK4 completely abrogates binding, activation, and translocation of MK5. Molecular modeling using the crystal structure of phosphorylated and unphosphorylated ERK2 suggests that phosphorylation of the ERK4 S-E-G motif results in a conformational change of the protein and exposure of Ile-330, concealed by the αC helix in unphosphorylated ERK4, so that it is free to interact with MK5. The requirement of phosphorylation within the activation loop (S-E-G) and the resulting accessibility of the interaction motif (FRIEDE) suggests a switch mechanism whereby phosphorylation of the activation loop of ERK3/ERK4 regulates its interaction with MK5 [110]. The model for the activation of the ERK3/ERK4-MK5 complexes is shown in the Figure 6.

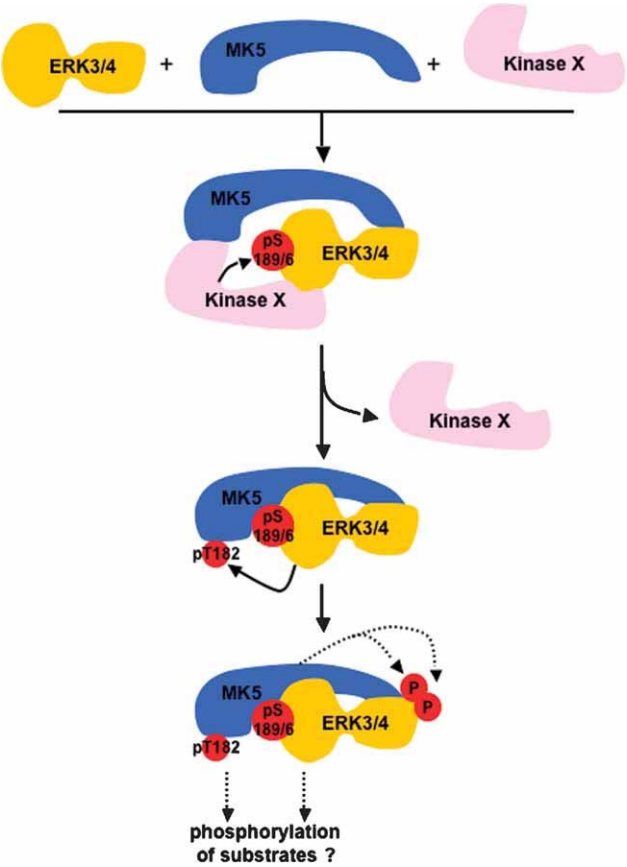

Fig. 6. A model of the activation of ERK3/ERK4-MK5 complexes. MK5 binds weakly to ERK3/ERK4, which helps to recruit a Ser-189/Ser-186 phosphorylating kinase. Alternatively, interaction with an ERK3/ERK4-kinase results in phosphorylation at Ser-189/Ser-186 phosphorylation, exposure of the interaction motif (FRIEDE), and subsequent recruitment of MK5. Activated ERK3/ERK4 phosphorylates Thr-182 on MK5, which fully activates MK5 and induces the phosphorylation of ERK3/ERK4 probably on Ser-386 (acquired from [65]).

Hansen et al. recently demonstrated an interaction between Cdc14A and ERK3, which affects the subcellular localization of MK5 [71]. Cdc14 is a serine/threonine phosphoprotein phosphatase. In humans cdc14 exists as two homologues, hCdc14A and hCdc14B, which differ within their C-terminal domain but have around 50% sequence identity within their catalytic domains. hCdc14A plays a role in the centrosome cycle,

mitosis, and cytokinesis and is selective for Cdk substrates [113]. Concerning ERK3 and hCdc14A, they form a complex when over-expressed in human U2-OS osteosarcoma cells and formation of this complex is independent of the phosphatase activity of hCdc14A. When over-expressed, both ERK3 and hCdc14A co-localized in interphase cells centrosome. hCdc14A dephosphorylates Cdk-mediated phosphorylation of ERK3 within the region 316-721 [71], and hence does not alter phosphorylation at Ser-189. Furthermore, like ERK3/ERK4, the binding of hCdc14A to MK5 is independent of its catalytic (phosphatase) activity and results in the accumulation of MK5 in the cytoplasm. To date, it remains unclear whether hCdc14A interacts directly with MK5 or indirectly via binding to ERK3 [71].

(iv) Pharmacological inhibitors of MK5

Recently, several new MK5 inhibitors have been discovered such as noroxoaconitine, flavokavain A, epigallocatechin gallate (EGCG), GLPG0259, PF-3644022[(10*R*)-10-methyl-3-(6-methylpyridin-3-yl)-9,10,11,12-tetrahydro-8*H*-[1,4] diazepino[5',6':4,5]thieno[3,2-*f*]quinolin-8-one] and 2-(2-quinolin-3-ylpyridin-4-yl)-1,5,6,7-tetrahydro-4*H*-pyrrolo[3,2-*c*]pyridine-4-one, which may help stimulate further research and lead to therapies involving diseases where MK5 activity is implicated. The diterpenoid alkaloid noroxoaconitine inhibits MK5 activity (IC_{50}=37.5μM) against PRAKtide (MK5 substrate peptide) or Hsp27 and inhibits PKA-induced cytoplasmic localization. This compound also inhibits MK3 but not MK2 activity [114]. Similar to noroxoaconitine, flavokavain A (IC_{50}=10 μM) from kava inhibits MK5 and MK3 activity but not MK2 [115]. Epigallocatechin gallate, derived from green tea, also inhibits MK5 activity (IC_{50}< 10 μM) but its effect on MK2 and MK3 was not tested [116]. The potent MK2 inhibitor, 2-(2-quinolin-3-ylpyridin-4-yl)-1,5,6,7-tetrahydro-4*H*-pyrrolo[3,2-*c*]pyridine-4-one (IC_{50}=8.5 nM) is also able to inhibit MK5 (IC_{50}=81 nM) more potently than the MK3 (IC_{50}=210 nM) [117]. Similarly, PF-3644022 inhibit MK2 and MK5 (IC_{50}=5 nM) more potently than the MK3 (IC_{50}=53 nM) [118]. Recently, Galapagos pharmaceutical have developed MK5 inhibitor GLPG0259 for use in the treatment of rheumatoid arthritis (RA). This compound has shown a good safety profile

in phase I studies and full results of phase-II clinical trials are expected in end of 2011 (http://www.glpg.com/pharmaceuticals/ra.htm).

(v) MK5 in the heart

Apart from its expression at mRNA and protein level [63, 88, 105] nothing is currently known about the role of MK5 in the heart.

(b) MK2/MAPKAPK2

MK2 is considered to be a major downstream effector of p38 MAPK and it controls p38-mediated inflammatory regulation in immune cells. MK2 knockout ($MK2^{-/-}$) mice made by homologous recombination showed no apparent abnormalities in behavior, and they were viable and fertile, although they were resistant to LPS induced endotoxic shock. The increased resistance to stress was due to decreased production of cytokines such as tumor necrosis factor (TNF)-α and interleukin (IL)-6. Following treatment with LPS, $MK2^{-/-}$ mice showed no increase in Hsp25 phosphorylation in the heart, suggesting that MK2 is the major kinase for Hsp25 *in vivo* [119]. MK2 controls the stability of IL-6 mRNA and inhibits the translation of TNF mRNA through the AU-rich element (ARE) in the 3'untranslated region (3'UTR) of these cytokines' mRNA [120]. MK2 is able to control the stability of these mRNAs through the phosphorylation of RNA-binding proteins such as tristetraprolin (TTP). TTP binds to the ARE in the 3'UTR of mRNA and directs their degradation. Upon phosphorylation by MK2, TTP binds to a 14-3-3 protein and hence is unable to bind to and destabilize mRNA [102]. Along with TNFα and IL-6, MK2 also controls the stability of IL-8, urokinase plasminogen activator (uPA), and cyclooxygenase-2 [121, 122].

In addition to regulating the stability and translation of mRNA as mentioned above, MK2 also controls gene transcription through the phosphorylation of transcription factors such as serum response factor (SRF), CREB, and activating transcription factor (ATF). In fibroblasts derived from MK2 knockout mice, upon treatment with arsenite, there was no phosphorylation of SRF, suggesting MK2 mediated regulation of SRF [123]. SRF also controls serum response element (SRE)

containing promoter activity of immediate early genes such as *c-fos* [124]. In addition to MK2, SRF phosphorylation is also under the control of ribosomal S6 kinase p90rsk, which is activated by serum via ERK, and CaM kinase II and IV, which are activated by increases in intracellular calcium concentration [125, 126]. Moreover, CREB and ATF-1 transcriptional activity is controlled by MK2 phosphorylation in response to fibroblast growth factor (FGF) or stress [127]. MK2 and p38α mutually stabilize each other, as the protein level of p38α was significantly reduced in an MK2-deficient background, and similarly MK2 protein levels were reduced in p38α-deficient embryonic fibroblasts [128, 129].

Streicher et al. demonstrated the importance of MK2 in MKK3-p38 signaling in the heart. These authors selectively induced the expression of activated MKK3 in the heart, which activated p38. These studies were performed in both $MK2^{+/+}$ and $MK2^{-/-}$ mice. Induction of activated MKK3 led to cardiac hypertrophy, extracellular matrix remodeling, contractile dysfunction, activation of hypertrophic gene markers (ANP and β-MHC), and lethal bradycardic heart failure within 8 days. However, removal of MK2 in an activated MKK3 background rescued some aspects of the above pathological response, such as partially ameliorated hypertrophy and contractile dysfunction, and prevention of early lethality due to lethal bradycardic heart failure. Hence some of the pathological responses of p38 signaling are mediated by MK2. Additionally, these authors also noted that MK2 is involved in the regulation of COX-2 protein synthesis without having any effect on mRNA levels [37]. Inhibition of p38α/β activity by SB203580 reduces apoptotic cell death in cultured myocytes and in intact heart upon exposure to pressure overload or ischemia/reperfusion [38, 39]. $MK2^{-/-}$ hearts have been shown to be resistant to myocardial ischemic reperfusion injury in terms of reduced myocardial infarct size, low number of apoptotic cardiomyocytes, and hence higher recovery of post-ischemic ventricular performance [130]. These observations further indicate that MK2 mediates some of the detrimental downstream effects of p38 activation in the heart.

(c) MK3/3pK/MAPKAPK3

MK3 and MK2 are both serine/threonine protein kinases, share 75% sequence identity and have extensive similarity in terms of structure, substrate specificity, and regulation by upstream kinases [102]. Additionally, *in vivo* MK3 shows redundant functions to MK2. Ronkina et al generated MK3 knockout mice, which were viable and showed no apparent abnormal tissue morphology [131]. Unlike MK2 knockout mice [132], MK3 knockout mice did not show reduced levels of TNF, p38, or tristetraprolin, although double knockout of MK2 and MK3, showed further reduction in p38 stability, and in TNF, or tristetraprolin expression compared to MK2 knockout mice. Moreover, over-expression of MK3 in MK2 knockout MEF cells rescued Hsp25 phosphorylation upon stress, and prevented p38 breakdown [133]. The observed lack of a robust effect in MK3 knockout mice similar to MK2 knockout mice could be because of lower cellular MK3 expression levels and activity compared to MK2 [134].

V) Extracellular matrix (ECM) regulation during cardiac hypertrophy

The quantity and quality of collagen in terms of its synthesis, cross-linking, and degradation are highly important for filling and ejection properties and the overall function of the heart. Fibrosis impairs both systolic and diastolic cardiac function. During hypertrophy, diastolic heart failure is coupled with an increase in collagen, whereas ventricular dilatation and systolic heart failure are coupled with degradation of collagen [6].

a) ECM synthesis during cardiac hypertrophy

In the hypertensive heart, reactive and reparative fibrosis occur because of the expansion of the ECM [135]. In the normal heart, fibroblasts synthesize the ECM proteins. However, in pathological conditions, morphologically distinct cells, myofibroblasts, appear. These cells have specific characteristics: they are fibroblast-like in term of their expression of ECM proteins and smooth muscle-like in terms of migration and expression of α-SMA. Fibroblast-to-myofibroblast differentiation and myofibroblast-mediated collagen turnover is regulated by autocrine and paracrine

factors produced in the myocardium as well as endocrine hormones from the circulation [6, 136]. The alteration in myocardial diastolic function because of increased stiffness during hypertension results from both an increase in myocardial total collagen content [137] and an increase in the amount of the collagen subtype with high tensile strength, type I, relative to other major subtype, type III [138]. The tensile strength of type I collagen, and its ability to withstand tensile stress, approximate that of steel [139]. Moreover, the increase in myocardial stiffness is also associated with an increase in collagen cross-linking [140].

Transforming growth factor-β (TGF-β) has a major influence on fibroblast proliferation, their phenotypic conversion to myofibroblasts, and synthesis and secretion of ECM proteins including collagen, fibronectin, and proteoglycans [141]. TGF-β at the same time reduces the degradation of ECM by inhibiting the expression of matrix metalloproteinase (MMP) and by inducing synthesis of protease inhibitors, such as Plasminogen Activator Inhibitor-1 (PAI-1) and Tissue Inhibitors of Metalloproteinases (TIMPs) [142]. There are three TGFβ isoforms, TGF-β1, TGF-β2, and TGF-β3, which are secreted by cells in their inactive form. The activity of mature TGF-β is masked by non-covalent interaction with a dimer of its N-terminal pro-peptide, called latency associated protein (LAP), which is often linked with latent TGF-β binding protein (LTBP) by a disulphide bond. Formation of this complex increases the stability of TGF-β and targets it to the ECM and the cell surface. The inactive TGF-β complex is activated by its proteolytic cleavage by plasmin or thrombospondin-1 (tsp-1) [143, 144]. Once activated, TGF-β1 mediates its signaling through the activation of its receptor (TGF-β receptor type 1 and type 2), which phosphorylate Smad 2 and 3. Co-Smad (Smad 4) binds to phospho Smad 2/3 and translocates to the nucleus where it acts as a transcription factor. Smad's transcriptional control depends on its interaction with co-repressors or co-activators. Inhibitory Smads, Smad6 and/or Smad 7, compete for binding of Smad 2 and 3 to the type 1 receptor and prevent its activation as well as increase receptor degradation (reviewed in [145]). TGF-β1 deficient mice show a marked reduction in collagen deposition and TGF-β1 itself is insufficient to produce persistent fibrotic responses *in vivo* or *in vitro*. Synergy between TGF-β and other

extracellular ligands, such as connective tissue growth factor (CTGF) and endothelin-1 (ET-1), is required to induce and increase in interstitial fibrosis [146].

The lack of complete prevention of bleomycin-induced pulmonary fibrosis, an animal model of idiopathic pulmonary fibrosis (IPF), by a TGF-β antagonist, led Oga et al to discover TGF-β independent regulation of IPF by prostaglandins in prostaglandin F (PGF) receptor (FP) knockout mice. They observed an attenuation of pulmonary fibrosis in FP knockout mice compared to wild type mice, where TGF-β activity and downstream Smad phosphorylation were unaltered. Interestingly, FP deficiency and the TGF-β receptor I kinase inhibitor SD-208 show additive effects with respect to reducing fibrosis, suggesting independent regulation of pulmonary fibrosis by these pathways. Moreover, the regulation of collagen expression by $PGF_{2\alpha}$-FP involved Rho kinase-ROCK (Rho-associated kinase) activity [147]. The regulation of fibrosis in other organs such as kidney, heart, liver, and skin are the same as in the lung [148], so extrapolation of these studies in the cardiac fibrosis requires further study.

b) ECM degradation during cardiac hypertrophy

ECM degradation is carried out by different matrix metalloproteinases (MMPs). The heart contains MMP1, MMP8, and MMP13. MMP13 initiates the process of ECM degradation by cleaving the α-chain of type I and type II collagen. MMP2 and MMP9, then further process the collagen fragments [149]. MMPs are synthesized and secreted into the extracellular space as inactive pro-enzymes (pro-MMPs), that bind to specific extracellular proteins and stay inactive until their pro-peptide domain is cleaved by serine proteases, secreted MMPs, or the highly related membrane-type MMPs. MMPs are also regulated at the transcriptional level by hormones, cytokines, growth factors, and mechanical strain. Moreover, active MMPs are inhibited by TIMPs, which bind to the catalytic domain of MMPs and thus block substrate binding. There are four species of TIMPs, TIMP1-4, and they are regulated at the transcriptional level (reviewed in [9]). A growing number of studies show an increase in fibrosis causes diastolic heart failure with preserved systolic function, whereas degradation of collagen scaffolding by altered ratio of MMPs/TIMPs causes ventricular dilatation and reduced ejection fraction or

systolic heart failure. Laviades et al. detected increased levels of circulating TIMP1 and reduced levels of circulating MMP1 and collagen type 1 telopeptide (a product of collagen degradation) in patients with left ventricular hypertrophy [150]. In contrast, the MMP1:TIMP1 ratio was increased in tissue and serum samples of patients diagnosed with systolic heart failure and MMP1 levels were higher in patients with systolic heart failure compared to those with diastolic heart failure [151].

c) Regulation of ECM by microRNA

MicroRNAs (miRNAs) are small ribonucleic acid molecules of approximately 22 nucleotides in length that act as gene silencers by inhibiting mRNA translation or promoting mRNA degradation. Many miRNAs are expressed in a cell- and tissue-specific manner and there is currently estimated to be more than 1000 miRNAs encoded by the human genome [152]. In the heart, several miRNAs have been implicated in the regulation of fibrosis, such as mir-21, -29, -30, and -133. Thum et al. have shown that mir-21 regulates fibrosis and hypertrophy, and implicated in regulation of ERK1/2. Mir-21 levels are increased in fibroblasts of failing hearts. Mir-21 increases ERK1/2 activity through expression inhibition of Sprouty homolog 1 (Spry 1), a negative regulator of the ERK1/2 pathway. This results in fibroblast proliferation and fibrosis. Conversely, specific antagomir-mediated silencing of mir-21 in pressure overload-induced hypertrophy results in reduction of ERK1/2 activity, inhibition of interstitial fibrosis, and attenuation of cardiac dysfunction. Interestingly, mir-21 not only attenuates the hypertrophy and fibrosis induced by pressure overload, but actually reverses stress-induced cardiac remodelling [153]. Moreover, mir-30 and mir-133 have been shown to regulate the expression of CTGF, a key pro-fibrotic factor. Mir-133 is expressed solely in cardiomyocytes while mir-30 is expressed in both cardiac fibroblasts and cardiomyocytes. CTGF expression is increased in mir-30 and mir-133 knock-down cardiomyocytes and fibroblast. Conversely, over-expression of these miRNAs decreased both CTGF and collagen expression. Additionally, in humans the expression of CTGF and mir-30 and mir-133 is inversely related in the extent of left ventricular hypertrophy [154]. Furthermore, to add to the growing number of miRNAs implicated in cardiac

disease, van Rooij et al. have shown the involvement of mir-29 in the expression of multiple ECM proteins, including collagens, fibrillins, and elastin. The mir-29 family of miRNAs are down regulated in regions adjacent to an infarct and down-regulation of mir-29 with anti-mirs *in vitro* and *in vivo* induces collagen expression. In contrast, over expression of mir-29 in fibroblasts reduces collagen expression [155]. Taken together, these studies provide an interesting insight into the regulation of cardiac remodelling by miRNAs, which can be exploited by manipulating miRNA levels for therapeutic purposes in pathological cardiac remodelling and heart failure.

MATERIALS AND METHODS

I) Materials

Membrane grade (reduced) Triton X-100 (TX-100), leupeptin, and PMSF were from Roche Molecular Biochemicals, SDS-Polyacrylamide gel electrophoresis reagents, nitrocellulose, and Bradford protein assay reagents were from Bio-Rad Laboratories. The cAMP-dependent protein kinase inhibitor peptide (PKI, amino acid sequence TTYADFIASGRTGRRNAIHD) was from the University of Calgary Peptide Synthesis Core Facility. Canine hsp27, cloned into the pET24a expression vector [156], was a gift from Dr. William Gerthoffer (Reno, NV). His6-ERK3-GST, cloned into the pHGST.1 expression vector was a gift from Dr. Sylvain Meloche [157]. Anti-GST from GE health care (27-4577-01), anti-EGFP was from BD Biosciences (# 8371-1), anti-MK5 (PRAK A-7) was from Santa Cruz Biotechnology (sc-46667), anti-V5 was from Invitrogen (R960-25), anti-Hsp27 was gift from Dr. William Gerthoffer (Reno, NV), anti-p38α was from Santa Cruz Biotechnology (sc-535), anti-p38γ was from upstate (#07-474), anti p38δ was from cell signaling (#2308), anti-p38β was a gift from Dr. Jacques Landry, anti phopho-p38 MAPK was from cell signaling (#2911S), anti phospho-Hsp27 (S-82) was from cell signaling (#2401S), anti-phospho Hsp27 (S-15) was from Stressgen (SPA-525), anti-ERK3 (D-23) was from Santa Cruz Biotechnology (sc-155), anti-ERK4 (N-20) was from Santa Cruz Biotechnology (sc-68169), anti-GAPDH was from Ambion (#4300), alexa fluor secondary antibodies were from invitrogen, primers were synthesized from Invitrogen. HRP-conjugated secondary antibodies were from Jackson ImmunoResearch Laboratories. All other reagents were of analytical grade or best grade available. Plasmids were transformed to *E. coli* competent strain BL21 (DE3) and expression induced by the addition of 1 mM isopropyl-β-D-thiogalactopyranoside (IPTG). GST fusion proteins were purified by affinity chromatography on glutathione Sepharose.

II) Methods

1) Total RNA isolation from mouse heart

Mice were anesthetized with intraperitoneal injection of sodium pentobarbital (0.55 mg/ kg body weight). Hearts were then quickly dissected, trimmed, and ventricular blood removed after gently pressing the heart on tissue paper. Hearts were frozen in liquid nitrogen and total cellular RNA was isolated with RNeasy® Mini kit (Qiagen Inc. #74104) with minor modifications. Briefly, tissue was pulverized in mortar pestle in presence of liquid nitrogen and then homogenized in 2 ml of TRIzol reagent (Sigma) using a Polytron at 10,000 RPM (2 x 15 s). Samples were incubated for 5 min room at temperature (RT), 0.4 ml chloroform was added, vortexed and incubated again at RT for 2-3 min. Following centrifugation for 15 min at 18,300 x g and 4 °C to promote phase separation, the aqueous (upper) phase was collected (1.3 ml). For simplification, the aqueous phase was divided into two 1.5 micro centrifuge tubes. From this point onward all manipulation were done at RT. RNA was precipitated by addition of an equal volume of 70% ethanol, immediately applied to Qiagen columns, and centrifuged for 15 sec at 18,300 x g. Two columns were used for each heart homogenate. Columns were washed with 350 µl RW1 buffer, centrifuged for 15 sec at 18,300 x g and then incubated with RNase-free DNase (27.27 Kunitz units) plus RDD buffer (70 µl) for 15 minute. Columns were washed again with 350 µl RW1 buffer and centrifuged (15 sec, 18,300 x g). Column collection tubes were changed and the columns washed twice with 500 µl RPE buffer twice and centrifuged (15 sec, 18,300 x g). Columns were centrifuged for 1 min to remove excess RPE buffer. To elute the RNA, collection tubes were changed, RNase free water (45 µl) added, and the columns incubated at RT for 1 min, and then centrifuged at 18,300 x g for 1 min. The purified RNA from two different columns, corresponding to RNA isolated from the same heart, were pooled and kept on ice. RNA was quantified by determining absorbance (A) at 260 and 280 nm and only samples having an A260/A280 ratio greater than 1.8 were used in subsequent studies. RNA quality and DNA contamination was assessed by resolving 1 µg of each RNA sample on 0.8% agarose gels. A portion of the isolated RNA was used for cDNA synthesis and

the remainder was stored at -80 °C. RNA isolations were done as rapidly as possible, with no interruptions prior to cDNA synthesis or transfer to storage.

2) Total RNA isolation from heart tissue sections

After surgery mouse hearts were frozen in liquid nitrogen-chilled 2-methyl butane. Hearts were embedded in Tissue-Tek O.C.T. compound (Sakura Finetek USA, inc.), longitudinal cryosections (14 µm) of the ventricles were prepared, sections transferred to 2 ml cryovials wth screw caps and O-rings, and frozen in liquid nitrogen. Total cellular RNA was isolated from cryosections using RNeasy® Micro kits (Qiagen Inc. #74004) with minor modifications. Total RNA was extracted by vortexing tissue section in 300 µl TRIzol reagent (Sigma) and 66.7 pg/µl carrier RNA for 30 sec, and incubated at RT for 5 min. Chloroform (60 µl) was added, and tubes were vortexed and incubated at room temperature for 2-3 min. Phase separation was promoted by centrifugation for 15 min at 18,300 x g and 4 °C. After this stage all subsequent manipulations were done at RT. The upper (aqueous, 165 µl) phase was collected, RNA was precipitated after addition of an equal volume of 70% ethanol, immediately applied onto Qiagen columns, and the columns centrifuged for 15 sec at 18,300 x g. Columns were washed with 350 µl RW1 buffer and centrifuged. Columns were incubated with RNase-free DNase I (10 µl) plus RDD buffer (70 µl) for 15 min. Columns were washed again with 350 µl RW1 buffer and centrifuged. The column collection tube was changed and the columns washed twice with 500 µl RPE buffer and centrifuged. Columns were the washed with 500 µl 80% ethanol and centrifuged at 18,300 x g for 2 min. The collection tubes ware changed and the columns centrifuged at 18,300 x g for 5 min with opened lids to facilitate the removal of the ethanol. The collection tubes were changed, 14 µl RNase-free water was added, and the columns were centrifuged at 18,300 x g for 1 min to elute the RNA. As the RNA yeild was small, it was not feasible to quantify total RNA. Hence, cDNA synthesis was performed in a 20 µl reaction volume containing 10.9 µl total RNA as described in the following section.

3) cDNA synthesis

First strand cDNA synthesis was performed in a 20 µl reaction volume containing 1 µg of total RNA, 100 ng of random primers, 1X First Strand buffer (50 mM tris-HCl pH 8.3, 75 mM KCl, 3 mM $MgCl_2$), 0.5 mM dNTP, 10 mM DTT, 40 U RNaseOUT recombinant ribonuclease inhibitor, and 200 U of M-MLV reverse transcriptase (Invitrogen #28025-013) according to the manufacturer's protocol. Total RNA (1 µg) was added to microcentrifuge tubes containing 1 µl 10 mM dNTP and 0.1 µl (1µg/µl) random primers (Invitrogen #48190-011) and the final volume adjusted to 12 µl by the addition of distilled water. Reaction tubes were heated to 65 °C for 5 min and then chilled on ice. Next, 4 µl 5X first-strand buffer, 2 µl 0.1 M DTT, and 1 µl RNaseOUT Recombinant Ribonuclease Inhibitor (40 units/µl) were added and the tubes incubated at 37 °C for 2 min. Finally, 1 µl (200 units) of M-MLV RT was added, tubes were mixed gently, and centrifuged to return the reaction mixture to the bottom of the tubes. cDNA synthesis was done in a PCR thermocycler with incubations at 25 ^{o}C for 10 min, 37 ^{o}C for 50 min, and 70 ^{o}C for 15 min.

4) Quantitative real-time PCR (qPCR)

qPCR was performed using a MX3000P QPCR system (Stratagene). Each amplification reaction mixture (25 µl) contained 6.25 ng cDNA equivalent to reverse transcribed RNA, 300 nM forward and reverse primers, 30 nM ROX, 12.5 µl platinum SYBR green mix (2X) (Invitrogen # 11733-046). qPCR reaction conditions were: 1 cycle at 95 °C for 10 min, 40 cycles at 95 °C for 30 s, 55 °C for 30 s (temp. and time vary as per primer pair; see Table 1), and 1 cycle at 72 °C for 1 min. SYBR green fluorescence was measured at the end of the annealing and extension phases of each cycle. The specificity of each primer pair for a single amplicon was verified by analyzing the dissociation curve. In addition, to verify that the intended sequences were being amplified, amplicons were gel-purified and sequenced. The amplification efficiency for each primer pair was determined from a standard curve of 50-3.25 ng reverse-transcribed RNA isolated from the heart after two-fold serial dilutions. The efficiency for each primer pair was between 90-110%. Glyceraldehyde-3-phosphate

dehydrogenase (GAPDH) was employed as an internal control. Hence, all samples were normalized to GAPDH, which was amplified in parallel in the same run, with MxPro software (Stratagene).

Primers specific for each mRNA of interest were designed using Clone Manager 6 (Sci Ed Software, USA) and based on the cDNA sequences in the NCBI database: p38α (NM_011951), p38β (NM_011161), p38γ (NM_013871), and p38δ (NM_011950), MK5 (NM_ 010765), GAPDH (NM_008084), ANP (AK147180), BNP (NM_008726), β-MHC (AY056464), COL1A1 (NM_007742), TGF-β1 (NM_011577), and TGF-β3 (NM_009368). The forward and reverse primers used are shown in Table 1.

5) DH5α chemical competent cells

DYT media (Tryptone 1.6%, Yeast extract 1%, NaCl 0.5%, pH 7.0) was innoculated with DH5α cells and incubated overnight at 37 °C with constant shaking. The next day, flasks containing 40 ml DYT media were innoculated with 1ml of bacterial culture and incubated 37 °C with constant shaking until the optical density at 600 nm had reached 0.6. Cultures were then transferred to centrifuge tubes, incubated on ice for 15 min, 1 ml of $CaCl_2$ (50 mM) was added, after 2 min. 19 ml of 50 mM $CaCl_2$ was again added, and the bacteria incubated on ice for 2 hrs. The bacterial suspension was centrifuged, the pellet suspended in 1 ml 50 mM $CaCl_2$, and then diluted with an additional 3 ml 50 mM $CaCl_2$ after a few min. After incubation onernight on ice, 150 µl aliquots of transformed DH5α were prepared in microcentrifuge tubes and frozen using an ethanol/dry ice slurry. Aliquots were then stored at -80 °C.

6) Transformation of BL-21 or DH5α competent cells

An aliquot (25 µl) of frozen *E. coli* competent strain BL21 (DE3) bacteria (Novagen) was thawed on ice for 15 min, 1 µl of construct was added, and the cells were incubated on ice for an additional 30 min. Bacteria were then incubated for 45 s in a 42^{o}C water bath and then placed on ice for 2 min. SOC media (500 µl) was then added and the cells were incubated for 60 min at 37^{o}C with constant shaking. Cells were spread onto two DYT agar plates (DYT media + 1.5% agar) containing ampicillin (100

μg/ml). The choice of antibiotic depends upon antibiotic resistance gene within the actual construct. Cells were incubated overnight at 37°C, an antibiotic-resistant colony was picked, transferred to a tube containing 10 ml of DYT media plus ampicillin (100 μg/ml), and grown for 6 h at 37 °C.

Competent BL-21 cells were used for expression of fusion protein while DH5α cells were used for construct amplification. Transformation of competent DH5α cells was as described for BL-21 cells except incubations were at 37 °C, instead of 42 °C. Moreover, when the construct contained a chloramphenicol resistant gene, 25 μg/ml of chloramphenicol was included in the culture media.

7) Cloning of p38 MAPK isoforms

Human cDNA for p38α was purchased in pOTB7 vector (Open Biosystem), p38β was in a pCMV-SPORT6 vector (Open Biosystem), p38γ (a gift from Dr. Jiahuai Han) was in a pET 14b vector and, and p38δ was in a pOTB7 vector (ATCC). Full-length inserts of each p38 isoform were subcloned into a modified pGEX-6P vector (GE Healthcare) in phase with, and located 3' to, a GST-6His coding sequence as described in the following section.

i) Cloning of p38α

E. coli competent strain DH5α was transformed with p38α-pOTB7 and the plasmid amplified by growing the cells overnight at 37 °C in DYT media contained chloramphenicol (25 μg/ml). The plasmid was extracted and purified using QIAprep spin miniprep kits (Qiagen) as per manufacturer's protocol. PCR was employed to amplify a fragment of p38α, extending from the 5' terminus to the HindIII site, in a reaction containing 0.5 μg of p38α-pOTB7 template, 400 nM forward and reverse primers BA108 and BA105 (Table-1), 60 mM Tris-SO_4 (pH 9.1), 18 mM $(NH_4)_2SO_4$, 1.8 mM M_gSO_4, and 1 μl Elongase enzyme mix (Invitrogen). PCR cycles were: 1 cycle at 94 °C for 30 s, 25 cycles at 94 °C for 30 s, 55 °C for 30 s, 68 °C for 30 s and 1 cycle at 72 °C for 10 min. In parallel, primer BA106 (Table-1) was used as a template to amplify a construct encoding 6 His amino acid residues and BamHI restriction site in a

reaction (50 µl) containing 400 nM forward and reverse primers BA103 and BA104 (Table-1), and other reagents as mentioned above. PCR products from both the reactions (51 bp DNA from BA 106 and 393 bp DNA from p38α-pOTB7) were separated on an agarose gel and purified using a QIAquick gel extraction kit (Qiagen). These two purified DNAs were mixed together and a PCR carried out using forward and reverse primers BA104 and BA105 (Table-1) as described above. The final PCR product (421 bp DNA) was separated on an agarose gel and purified using a QIAquick gel extraction kit. This 421 bp DNA and p38α-pOTB7 vector were digested separately with 60 units HindIII restriction enzyme, 10 mM Tris-HCl (pH 7.9), 50 mM NaCl, 10 mM $MgCl_2$, 1 mM DTT, 100 µg/ml BSA at 37 °C for 5-6 h and then the restriction enzyme was inactivated by heating at 65 °C for 20 min. The HindIII digestion buffer was removed from both reactions using Centricon YM-30 centrifugal filtration units (Millipore). Both products were then digested with 60 units BamH1 restriction enzyme for 5-6 h at 37 °C in a buffer that contained 50 mM Tris-HCl (pH 7.9), 100 mM NaCl, 10 mM $MgCl_2$, 1 mM DTT, 100 µg/ml BSA. The p38α-pOTB7 BamH1 digest was then incubated with 10 units alkaline phosphatase for 1 h at 37 °C. Both the 2539 bp phosphatase-treated p38α-pOTB7 BamH1 and the 315 bp 6His-p38α 5' fragment were separated on agarose gel, extracted, and purified using a QIAquick gel extraction kit. Purified 2539 bp DNA vector and 315 bp DNA insert were mixed with a 1:7 ratio and incubated overnight at 16 °C with 400 units of T4 DNA ligase in 50 mM Tris-HCl (pH 7.5), 10 mM $MgCl_2$, 1 mM ATP, and 10 mM DTT. The final ligated vector was transformed into DH5α competent cells, spread on DYT agar contained 25 µg/ml chloramphenicol, and grown overnight at 37 °C. Several antibiotic resistant colonies were picked and used to inoculate DYT media contained chloramphenicol. Cultures were grown overnight at 37 °C. Vector was then extracted and purified using QIAprep spin miniprep kits (Qiagen). In addition, the orientation of the insert within the vector (6His-p38α-pOTB7) was confirmed both by BamHI and HindIII restriction enzyme digestion and by DNA sequencing.

The 6His-p38α insert was transfered from pOTB7 into pGEX-6P as described in following text. 6His-p38α-pOTB7 and pGEX-6P vectors were digested with BamHI as described above, separated on agarose gel, and purified using a QIAquick gel extraction

kit. Both the vectors were then digested for 5-6 h at at 37 °C with XhoI in 10 mM Tris-HCl (pH 7.9), 50 mM NaCl, 10 mM $MgCl_2$, 1 mM DTT, 100 μg/ml BSA. pGEX-6P was then dephosphoryulated with 10 U alkaline phosphatase (1 h, 37 °C). DNA from both the reactions were separated on an agarose gel and purified using a QIAquick gel extraction kit. The digested and dephosphorylated pGEX-6P vector and digested 6His-p38α DNA (insert) were ligated (1:3 ratio) as described above using T4 DNA ligase. The final ligated product (6His-p38α-pGEX-6p) was transformed into DH5α, the cells grown in DYT media contained 100 μg/ml ampicillin, and then the plasmid extracted and purified using a QIAprep spin miniprep kit. The orientation and sequence of the 6His-p38α-pGEX-6p insert were confirmed by DNA sequencing.

ii) Cloning of p38β

Human p38β cDNA was excised from pCMV-SPORT6 and inserted in phase, 3' to GST-6His in pGEX-6P bacterial expression vector by cloning as described follows.

DH5α were transformed with p38β-pCMV and grown overnight at 37 °C in DYT media containing 100 μg/ml ampicillin., p38β-pCMV was extracted and purified using a QIAprep spin miniprep kit (Qiagen) as per the manufacturer's protocol. A fragment of p38β between the 5' terminus and the BamHI restriction site was amplified by PCR using 0.5 μg p38α-pOTB7 as a template and 400 nM forward and reverse primers (BA 109 and 114 (Table-1)) as described above. In parallel, primer BA112 was used as a template to amplify a construct encoding a 6 His sequence plus an EcoRI restriction site in a PCR reaction mixture (50 μl) that contained 400 nM forward and reverse primers (BA107 and 110 (Table-1)). PCR products (52 bp DNA from BA 112 and 506 bp DNA from p38β-pCMV) were separated on an agarose gel and purified using QIAquick gel extraction kits (Qiagen). The two purified DNAs were mixed together along with forward and reverse primer BA110 and BA109 (Table-1) and amplified by PCR as described above. The resulting PCR product (534 bp DNA) was separated on agarose gel and purified using a QIAquick gel extraction kit. The 534 bp DNA fragment and p38β-pCMV vector were separately digested for 5-6 h at 37 °C with 60 units EcoRI restriction enzyme, 10 mM Tris-HCl (pH 7.9), 50 mM NaCl, 10 mM $MgCl_2$, 1 mM

DTT, and 100 μg/ml BSA. The PRC reactions were then incubated at 65 °C for 20 min to inactivate the EcoRI. The EcoRI digestion buffer was removed from both reactions using Centricon YM-30 centrifugal filtration units (Millipore) and both fragments were digested with 60 units BamH1 for 5-6 h at 37 °C in a buffer containing 50 mM Tris-HCl (pH 7.9), 100 mM NaCl, 10 mM $MgCl_2$, 1 mM DTT, 100 μg/ml BSA. The p38β-pCMV fragment was dephosphorylated by incubating at 37 °C for 1 h with 10 U of alkaline phosphatase. The 6592 bp fragment from p38β-pCMV and 516 bp 6His-5'-p38β fragment were separated on an agarose gel, purified using an QIAquick gel extraction kit, combined in a 1:7 ratio (vector:insert), and ligated by incubating with 400 U T4 DNA ligase in 50 mM Tris-HCl (pH 7.5), 10 mM $MgCl_2$, 1 mM ATP, 10 mM DTT at 16 °C overnight. The ligated vector was transformed into DH5α competent cells and spread on DYT agar contained 100μg/ml ampicillin and grown overnight at 37 °C. Antibiotic resistant colonies were picked and used to inoculate DYT media contained ampicillin 100 μg/ml. Transformants were grown overnight at 37 °C and the plasmids isolated and purified using QIAprep spin miniprep kits (Qiagen). Finally, ligation of the insert in to the vector (6His-p38β-pCMV) was verified both by PCR using 400 nM of forward and reverse primer (BA109 and 110 (Table-1)) for the expected 534 bp DNA amplicon and also by DNA sequencing.

Following text explains the transfer of 6His-p38β DNA from pCMV vector in to pGEX-6p vector. 6His-p38β-pCMV and pGEX-6p vectors were digested separately with EcoRI as described above and the digested DNAs were separated on agarose gel and purified using a QIAquick gel extraction kit. Both vectors were then digested (5-6 h, 37 °C) with NotI in a buffer that contained 50 mM Tris-HCl (pH 7.9), 100 mM NaCl, 10 mM $MgCl_2$, 1 mM DTT, and 100 μg/ml BSA. The pGEX-6P vector was dephosphorylated using alkaline phosphatase as described above. Both DNAs were separated on agarose gel and purified uisng a QIAquick gel extraction kit. pGEX-6P vector digested 6His-p38β (insert) were ligated (2:1 ratio) as described above. Ligated product (6His-p38β-pGEX-6p) was transformed into DH5α and amplified by growing the transformants in DYT media containing 100 μg/ml ampicillin. The vector was

purified uisng a QIAprep spin miniprep kit and the orientation and sequence of the insert was confirmed by DNA sequencing.

iii) Cloning of p38δ

Human p38δ cDNA excised from pOTB7 and inserted in phase 3' of GST-6His in pGEX-6P as described below.

p38δ-pOTB7 was transformted into DH5α and the transformed cells grown in DYT media contained 25 μg/ml chloramphenicol. The plasmid extracted and purified using a plasmid maxiprep kit (Sigma) as directed by the manufacturer. Following purification, p38γ-pOTB7 was concentrated by addition of 0.1 volume 3.0 M sodium acetate buffer (pH 5.2) and 0.7 volume isopropyl alcohol. The insert was confirmed to be human p38δ by DNA sequencing using primer BA94 (Table-1) and alignment with the appropriate NCBI cDNA sequence (AF092535). The p38δ cDNA was amplified by PCR using 0.5 μg of p38δ-pOTB7 as a template along with 400 nM forward and reverse primers (BA95 and 96 (Table-1)) as described above. The PCR product was separated on a 2% agarose gel, extracted, and purified using a QIAquick gel extraction kit (Qiagen). The resulting purified DNA (12 μg) was ligated with pCR2.1-TOPO vector following the manufacture's protocol (Invitrogen), ligated vector was transformed into bacteria, and transformants grown on DYT agar plate containing ampicillin (100 μg/ml) and X-Gal. Numerous white (positive) clones were picked, used to inoculate DYT media containing ampicillin (100 μg/ml), and grown overnight at 37 °C. hp38δ-pCR2.1 was extracted from the bacteria and purified using a QIAprep spin miniprep kit. The insert's orientation and sequence were confirmed by both digestion with EcoR1 and DNA sequencing. Subsequently, 3 μg p38δ-pOTB7 and 15 μg hp38δ-pCR2.1 were digested for 5-6 h at 37 °C with 60 units BamH1 in 50 mM Tris-HCl (pH 7.9), 100 mM NaCl, 10 mM $MgCl_2$, 1 mM DTT, 100 μg/ml BSA, the digestion products separated on agarose gels, extracted, and purified using QIAquick gel extraction kits. Both the digested and purified hp38δ-pOTB7 and hp38δ-pCR2.1 were again digested with 15 units of BbsI in 10 mM Tris-HCl (pH 7.9), 50 mM NaCl, 10 mM $MgCl_2$, 1 mM DTT, 100 μg/ml BSA at 37 °C for 5-6 h. The hp38δ-pOTB7 was then dephosphorylation

using alkaline phosphatase as described above. Both digestion reactions were separated on agarose gels, the 3241 bp DNA from hp38δ-pOTB7, and 269 bp DNA from hp38δ-pCR2.1 were purified using QIAquick gel extraction kits, and then incubated at a ration of 3:1 (insert:vector) with T4 DNA ligase as described above. The ligated vector was transformed in DH5α competent cells, plated on DYT agar contained 25μg/ml chloramphenicol, and incubated overnight at 37 °C. Antibiotic resistant colonies were picked, used to inoculate DYT media contained chloramphenicol, and cells grown overnight at 37 °C. The plasmid was then purified using a QIAprep spin miniprep kit (Qiagen). Correct insertion into pOTB7 was confirmed by digesting with NdeI and EcoRI.

p38δ cDNA was excised from pOTB7 and inserted into a pGEX-6P-6His vector which was prepared previously. The insertion was done by digesting both p38δ- pOTB7 and pGEX-6P-6His with NdeI and XhoI digestion. pGEX-6p-6His was dephosphoryated with alkaline phosphatase, and then resulting DNAs ligated using T4 DNA ligase enzyme as described above. Ligated pGEX-6p-6His-p38δ was transformed into DH5α competent bacteria, amplified, and then purified using a QIAprep spin miniprep kit (Qiagen). The orientation and integrity of the p38δ insert were confirmed by DNA sequencing.

8) Coomassie Brilliant Blue (R250) staining and destaining

Acrylamide gels were stained for 30 min or overnight in closed container in 0.1 % w/v Coomassie Brilliant Blue R250 in H_20:methanol:acetic acid, 45:45:10 under constant shaking. Gels were destained in H_20:methanol:acetic acid, 75:20:5 as required.

9) Expression and purification of GST-fusion proteins

E. coli competent strain BL21 was transformed with the expression vectors described above and the transformate grown as mentioned in *transformation of BL-21 or DH5α competent cells subsection*. The 6 h culture (10 ml) was used to inoculate 0.3 l of DYT media contained antibiotic. Once the optical density at 600 nm reached 0.6, expression of the GST-fusion protein was induced by the addition of 1 mM IPTG.

Following induction, bacteria were incubated at 37 °C with shaking (200 rpm) for 6-7 h or overnight. The bacterial suspension was centrifuged at 12,000 x g for 10 min in Sorval SLA-8000 rotor, the pellet was re-suspended with saline, and centrifuged at 12,000 x g for 10 min. The bacterial pellet was suspended in cold phosphate buffer saline (PBS pH 7.5) containing 1% TX-100, 10 mM benzamidine, and 2 mM PMSF. Bacteria were lysed on ice by sonication 4 times at 35% amplitude (Sonics and Materials inc. Vibra-Cell) for one minute with 15 s intervals, and then incubated for 30 min at 4 °C with stirring. Bacterial lysates were centrifuged for 1 h at 125,000 x g and 4 °C in Beckman type 45Ti rotor. Cleared lysates were loaded onto GST-Trap columns using an FPLC system with the following program: wash column with 5 column volumes of TBSE (pH 7.3 at 4 °C) at 0.5 ml/min, load lysate at 0.2 ml/min, wash with 10 column volumes of TBSE at 0.5 ml/min, and elute GST-fusion protein 3 column volumes of 10 mM glutathione in TBSE (pH 8.0 at 4 °C) at 0.5 ml/min. Fractions of 1.0 ml were collected and absorbance at 260 nm (A260) was monitored. Fractions corresponding the the peak of A260 nm were pooled and dialyzed against TBSE at 4 °C to remove the glutathione, and then dialyzed once against storage buffer comprising 50% glycerol, 50 mM Tris (pH 7.5 at 5 °C), 150 mM NaCl, 0.1 mM EGTA, 0.03% Brij 35, 1 mM benzamidine, 0.2 mM PMSF, and 0.1% β-mercaptoethanol. Finally, protein concentrations were determined by Bradford protein assay, aliquots were prepared, snap-frozen using liquid nitrogen, and stored at -80 °C.

10) Immunocytofluorescence

The subcellular localization of each MK5 variant was determined by confocal fluorescence microscopy. A total of 3 x 10^5 HEK293 cells were seeded onto laminin (15 μg/ml for 20 min)-coated glass coverslips in 12 well culture plates with Dulbecco's Modified Eagle Medium (DMEM) containing 10% fetal calf serum, and allowed to adhere for 24 h. Cells were then rinsed once with DMEM and transfected with 1.6 μg of the indicated pIRES-EGFP-MK5-V5 variant construct using OptiMEM II (Gibco) and Lipofectamine 2000 (Invitrogen) as per the manufacturers' protocols. After 5-6 h of transfection, the medium was replaced with DMEM containing 10% fetal bovine serum

and the cells incubated for an additional 24 h. At the end of this 24 h period, cells were serum starved for 6 h, treated with or without agonist, rinsed with ice-cold PBS, and fixed for 20 min in ice-cold PBS containing 2% paraformaldehyde (pH 7.2). The fixative was removed by washing three times with ice-cold PBS. Cells were blocked and permeabilized by incubating for 30 min in PBS containing 2% donkey serum and 0.1% (w/v) TX-100. Coverslips were rinsed once with ice-cold PBS and incubated overnight in a humidified chamber with anti-MK5 antibody diluted (1:100) in PBS containing 1% donkey serum and 0.05% (w/v) TX-100. To remove excess primary antibody, cover slips were washed three times with ice-cold PBS. Coverslips were then incubated for 1 h in PBS containing 1% donkey serum, 0.05% (w/v) TX-100, Alexa fluor 555-conjugated donkey anti-mouse IgG antibody (1:600) and 1.5 μM TO-PRO 3. Finally, coverslips were rinsed three times with ice-cold PBS, drained, and mounted onto glass slides using 15 μl of DABCO/glycerol medium. Excess DABCO/glycerol medium was drained and coverslips were sealed with nail polish. The intracellular localization of MK5, TO-PRO 3, and EGFP were visualized using a LSM 510 confocal fluorescence microscope.

11) Detection of p38α and p38γ subcellular localization by confocal microscopy

Cryosections (14 μm) were prepared from mouse heart ventricles as described above. Three sections per heart were placed on precleaned microscope slides (Fisher Scientific) and fixed for 20 min using ice-cold 4% paraformaldehyde in PBS (pH 7.2). After fixation, cells were washed three times with ice-cold PBS (5 min) and then blocked and permeabilized for 60 min in a solution containing 2% donkey serum and 0.5% Triton X-100 in PBS. The slides were rinsed once with ice-cold PBS and incubated for overnight with primary antibody (1:100 for p38α and 1.200 for p38γ) diluted in PBS containing 1% donkey serum, 0.1% TX-100 at 4 °C in closed humidified chamber. The next day, the sections were rinsed three times with ice-cold PBS and incubated for 1 h with Alexa fluor 488-labelled donkey anti-rabbit IgG (1:600) and 1.5 μM TO-PRO 3 iodide in PBS containing 1% donkey serum and 0.1% TX-100. Finally, slides were rinsed three times with ice-cold PBS, drained, and coverslips were mounted onto glass slides using 15 μl of DABCO/glycerol medium. Excess DABCO/glycerol

medium was removed and the coverslips sealed with nail polish. The intracellular localization of p38α, p38γ, and TO-PRO 3 (nuclear marker) were revealled using a scanning confocal fluorescence microscope (LSM 510 Carl Zeiss, Oberkochen, Germany).

12) Preparation of murine cardiac lysates

Mouse hearts were pulverized under nitrogen as described above. The powdered tissue was resuspended using a 2 ml Potter-Elvehjem tissue grinder (25-30 passes) in 1.2 ml of ice-cold lysis buffer comprising 50 mM Tris (pH 7.5 at 4°C), 20 mM β-glycerophosphate, 20 mM NaF, 5 mM EDTA, 10 mM EGTA, 1.0% TX-100, 1 mM Na_3VO_4, 1 μM microcystin LR, 5 mM DTT, 10 μg/ml leupeptin, 0.5 mM PMSF, and 10 mM benzamidine. Homogenates were then cleared of cellular debris by centrifugation for 60 min at 100,000 x g (48,000 RPM) and 4°C in a Beckman TLA-100.3 rotor. Finally, supernatants were collected, protein concentration determined by the Bradford method, aliquoted, snap-frozen using liquid nitrogen, and stored at -80°C.

13) Immunoprecipitation of endogenous MK5

Heart lysates were prepared as described above. Protein A/G$^+$-Agarose beads (50 μl of a 25% slurry; Santa Cruz Biotechnology) were washed once with lysis buffer (400 μl) and centrifuged at 1 min at 2300 x g, and 4 °C. Anti-MK5 antibodies (2 μg) were diluted to 200 μl with lysis buffer and precoupled to Protein A/G$^+$-Agarose beads by incubating for 5 h at 4 °C with constant mixing. To remove any uncoupled primary antibody, antibody-coated beads were washed three times with lysis buffer prior to immunoprecipitation reactions. Heart lysates (2 mg) were added to the antibody-coated beads and IP reactions were incubated overnight at 4°C with constant mixing. Beads were washed five times with lysis buffer (500 μl), the bead pellets suspended in 20 μl of 2X SDS sample buffer, and heated at 70 °C for 90 s. The beads were pelleted by a brief centrifugation and the supernatants loaded immediately onto 10-20% acrylamide-gradient SDS-PAGE gels.

14) GST-pull down assay

HEK293 cells were seeded (6 x 10^5/35 mm dish) in DMEM containing 10% fetal bovine serum and allowed to adhere for 24 h. Cells were then rinsed once with DMEM and transfected with 3.2 µg of the indicated pIRES-EGFP-MK5-V5 variant construct using OptiMEM II (Gibco) and Lipofectamine 2000 (Invitrogen) as per the manufacturer's protocol. After 5-6 h of transfection, the OptiMEM II media was replaced with DMEM containing 10% fetal bovine and the cells incubated for and additional 24 h. At the end of this 24 h period, cells were rinsed with ice-cold PBS, lysed in 200 µl lysis buffer (see above) on ice, scraped, transferred to 1.5 ml microcentrifuge tubes, and passed 30-40 times through a 21-gauge needle. Cell lysates were then cleared of cellular debris by centrifugation for 30 min at 100,000 x g and 4 °C in a Beckman TLA-100.3 rotor. The supernatants were aliquoted, snap-frozen using liquid nitrogen, and stored at -80 °C until use. His-ERK3-GST or GST (1 µg) alone was mixed with 150 ug cell lysate and incubated for 1 h at 4 °C with constant mixing. Next, 20 µl of a 50% slurry of glutathione Sepharose beads, washed once with lysis buffer and centrifuged for 1 min, at 2300 x g, and 4 °C, was added and samples incubated for 30 min at 4°C with constant mixing. Pull downs were washed three times with lysis buffer and twice with 50 mM Tris (pH 7.5 at 4 °C). The bead pellet was suspended in 20 µl of SDS sample buffer and heated at 70 °C for 90 s. The beads were removed by a brief centrifugation and the supernatants loaded immediately onto 10-20% acrylamide-gradient SDS-PAGE gels.

15) Genotyping

Genotyping was by PCR using mouse tail DNA. Mouse tail biopsies were frozen at -20 °C untill use. Samples were lysed for 2-3 h at 55 °C in 50 mM Tris (pH 8.0 at RT), 150 mM NaCl, 25 mM EDTA, 0.25% SDS, and 400 µg/ml proteinase K. The volume of lysis buffer was 50-100 µl, but it varied according to the length of each individual tail biopsy sample. During lysis, samples were vortexed at hourly intervals. Lysates were centrifuged for 15 s at 14,600 x g and RT, vortexed, and centrifuged again for 10 min. An aliquot (1 µl) of each supernatant was diluted 200-fold with water, a few

mg of chelex-100 resin (Bio-Rad) was added, vortexed, centrifuged for 15 s, and heated at 95 °C for 10 min to inactivate the proteinase K. Samples were mixed, centrifuged, and PCR was done in a 25 µl reaction volume comprising 10 µl sample, 400 nM primers (5'-CGTAACACTAGCCACA GTTGTAACTGA-3',5'-CATATACTTGTAAGCACAG CTCTGAGTT-3'), 750 mM Tris-HCl (pH 8.8 at 25 °C), 200 mM $(NH_4)_2SO_4$, 0.1% (v/v) Tween 20, 1.5 mM $MgCl_2$, 200 µM dNTPs, and 1.25 U Taq DNA polymerase. PCR conditions were: 1 cycle at 94 °C for 10 min, 40 cycles at 94 °C for 30 s, 58 °C for 45 s, 72 °C for 1 min, and 1 cycle at 72 °C for 10 min. 6X sample buffer was added to each PCR reaction, tubes were vortexed, and each sample loaded onto 2% agarose gels contained ethidium bromide. Electrophoresis was at 80 V for 30-45 min.

16) Activation of p38 MAPK and determining its specific activity

Purified GST-p38 isoforms were activated by incubating in the presence of constitutively active His6-MKK6(EE) as described previously [158]. To separate phosphorylated GST-p38 from His6-MKK6(EE), reaction mixtures were incubated with glutathione Sepharose beads for 2-3 h at 4 °C on a clinical rotor, centrifuged for 2 min at 5,000 rpm and 4 °C, washed thrice with TBS containing 1 mM EDTA (TBSE), and bound GST-p38 eluted with reduced glutathione. Purified, activated p38 was then dialyzed against TBSE buffer followed by a storage buffer comprising 50% (v/v) glycerol, 50 mM Tris (pH 7.5 at 5 °C), 150 mM NaCl, 0.1 mM EGTA, 0.03% Brij 35, 1 mM benzamidine, 0.2 mM PMSF, and 0.1% β-mercaptoethanol. Protein concentrations for each isoform were determined following SDS-PAGE using BSA as a standard. Briefly, proteins were separated on 10-20% acrylamide-gradient gels and stained with Coomassie Brilliant Blue R250. Gels were scanned using a VersaDoc 4000 imaging system and GST-p38 and BSA band densities determined using Quantity One software (Bio-Rad Laboratories, Inc) and the quantity of p38 protein determined from the BSA standard curve by linear regression using GraphPad Prism version 4. The specific activity of each phosphorylated GST-p38 isoform was determined by incubating activated GST-p38 (20 ng) with 0.33 mg/ml MBP, 100 µM [γ^{32}P]-ATP (10 µCi), 1 mM EGTA, 10 mM $MgCl_2$, 10 mM DTT, 10 µg/ml leupeptin, 1 mM Na_3VO_4, and 1 µM

microcystin LR at 30 °C for 2, 5, 8, and 10 min. Reactions were terminated with SDS-PAGE sample buffer and separated on 10-20% SDS-PAGE, stained with Coomassie blue, the bands corresponding to MBP xcised from the gel, and ^{32}P incorporation into MBP measured by liquid scintillation counting.

17) In vitro protein kinase assay

Rat heart cytosol and nuclear fractions were prepared as described previously [159]. Cytosolic or nuclear proteins (50 μg) were incubated with GST-MK5 (1 mU), 10 μM [$\gamma^{32}P$]ATP (10 μCi), 25 mM Tris-HCl (pH 7.5 at 4 °C), 1 mM EGTA, 10 mM $MgCl_2$, 10 mM DTT, 1 mM Na_3VO_4, 1 μM microcystin LR, 10 μg/ml leupeptin, and 1 μM PKI for 60 min at 30 °C. Reactions were terminated using 4X SDS-PAGE sample buffer and proteins separated on 10-20% SDS-PAGE. Gels were stained with Coomassie Brilliant blue R250, dried and exposed to Kodak BioMax MS film. For 2D gels, following phosphorylation, proteins were precipitated and the resuspended in rehydration buffer (see below). Briefly, 1 μl 2% sodium deoxycholate was added to the phosphorylation assay and the tubes placed on ice. After 20 min., 10 μl 100% trichloroacetic acid was added, samples were vortexed, incubated on ice for 60 min, and then centrifuged for 15 min at 18,300 x g and 4 °C. The protein pellet was washed twice with cold acetone and dried in SpeedVac for 5 min. The dried, precipitated proteins were dissolved in rehydration buffer (8 M Urea, 2% CHAPS, 25 mM DTT, 0.2% Bio-Lyte 3/10 ampholyte, bromophenol blue for faint color). Samples were resolved on 7 cm pH 3-10 IPG strips (Bio-Rad), under mineral oil, using a Bio-Rad Protean IEF cell with the following protocol: active rehydration at 50 V for 12 h, 250 V for 15 min, a linear gradient of 250-to-10,000 V over 3 h, 10,000 V for 4 h, followed by 500 V until the samples were removed from the IEF cell. After the run, the excess mineral oil was removed by gently touching the IPG strips to tissue paper. The strips were incubated in equilibration buffer I (0.375 M Tris pH 8.8, 6 M urea, 2% SDS, 20% glycerol, and 130 mM DTT) and then equilibration buffer II (0.375 M Tris pH 8.8, 6 M urea, 2% SDS, 20% glycerol, and 135 mM iodoacetamide) for 10 min each with continuous, gentle shaking. Strips were rinsed free of excess equilibration buffer by dipping 3-4 times in

SDS-PAGE running buffer. For the second dimension, proteins were resolved on 10-20% acrylamide-gradient SDS-PAGE. Briefly, strips were put on top of the acrylamide gel, without trapping air bubbles between strips and gel, then strips were covered with 0.5% agarose prepared in running buffer containing a small amount of bromophenol, top and bottom reservoirs filled with running buffer, and electrophoresed for 6-7 h at constant current (25 mA/gel) and 15 °C. Gels were stained, dried, and exposed to film as described above.

18) Miscellaneous methods

Protein concentrations were determined by the Bradford method using bovine serum albumin (BSA) as a standard.

19) Immunoblotting

SDS-PAGE and immunoblotting were performed as described previously [159]. Following the transfer, nitrocellulose membranes were rinsed in PBS and fixed with glutaraldehyde [160].

20) Statistical Analysis

Quantitative analysis was performed by a single observer in a blinded manner. One-way ANOVA followed by Newman-Keuls post tests were performed using Graphpad Prism version 4 for Mac. Values were shown ± S.E. ***, $p < 0.001$: **, $p < 0.01$: *, $p < 0.05$.

Table 1. Primers used during cloning

Name	**Primers**
BA 94	5'- ATG ACT GGC TAC GTG GTG ACC -3'
BA 95	5'- AGG GCA TCA CCA GGT AGA AGT CAT A -3'
BA 96	5'- GGA TCC CAT ATG AGC CTC ATC CGG AAA AAG GGC TTC -3'
BA 103	5'- AAC GTG GGC CTC TCC TGA GAC ATG T -3'
BA 104	5'- CTC AGG ATC CCA TCA TCA TCA TCA TC -3'
BA 105	5'- GAT AAG GAA CTG AAC ATG GTC -3'
BA 106	5'- CAT CAT CAT CAT CAT CAC ATG TCT CAG G -3'
BA 107	5'- GAA GCC GGC GCG AGG GCC CGA CAT G -3'
BA 108	5'- ATG TCT CAG GAG AGG CCC ACG TT -3'
BA 109	5'- AAA TCC AGG ATC CTG AGC TCA CAG -3'
BA 110	5'- TCT AGG AAT TCA TCA TCA TCA TC -3'
BA 112	5'- TCA TCA TCA TCA TCA CAT GTC GGG CCC TC -3'
BA 114	5'- ATG TCG GGC CCT CGC GCC GGC TTC -3'

HYPOTHESIS AND OBJECTIVES

Hypothesis

In the heart, p38 MAP kinase has been implicated in the regulation of apoptosis (p38α), hypertrophy (p38β), and fibrosis. The means whereby this cascade modulates these distinct responses and the involvement of other isoforms (p38γ, p38δ) is still unknown, but must involve specific downstream signaling components of the p38 MAP kinase cascade. Downstream targets of p38 MAP kinase include transcription factors as well as MAP kinase activated protein kinases (MKs). The known MKs regulated by p38 MAP kinase are MK2, MK3, and MK5. Little is known about p38 isoform-selective activation of the MKs or the substrates of the individual MK subtypes, in particular MK5. Additionally, MK5 is also known to be phosphorylated by atypical MAPKs ERK3 and ERK4. Thus far, the physiological role of MK5 as well as ERK3/ERK4 remains unknown. **The hypothesis of the current study is: in the heart, MK5 is involved in the detrimental effects associated with p38 activation and given that MK5 activity is also regulated by ERK3 and ERK4, they may also play some role.**

Objectives

The specific objectives to test the above hypothesis were;

- To study the involvement of MK5, downstream of p38, in regards to regulation of any of the physiological effects induced by chronic pressure overload in mice heterozygous for a functional knockout of MK5 ($MK5^{+/-}$).
- To determine whether MK5 signaling in the heart is mediated by p38, ERK3, ERK4, or any combination of the three.
- To determine involvement of ERK3 or ERK4, potential upstream regulators of MK5, in the regulation of any of the physiological effects of MK5 during hypertrophy using $ERK3^{+/-}$ and $ERK4^{-/-}$ mice.

- To identify substrates of MK5 and p38 isoforms *in vitro* using subcellular fractions (e.g. cytosol, cytoskeleton, nuclear membrane, and nucleoplasm) obtained from ventricular myocytes.
- To characterize the expression and cellular distribution of all p38 isoforms the heart and determine the effects on chronic pressure overload..

ARTICLE-1

Dingar D, Benoit MJ, Mamarbachi AM, Villeneuve LR, Gillis MA, Grandy S, Gaestel M, Fiset C, and Allen BG. “Characterization of the expression and regulation of MK5 in the murine ventricular myocardium.” Cell Signal. 2010 22(7):1063-1075.

Characterization of the expression and regulation of MK5 in the murine ventricular myocardium

Dharmendra Dingar[a,b], Marie-Josée Benoit[a,b], Aida M. Mamarbachi[a], Louis R. Villeneuve[a], Marc-Antoine Gillis[a], Scott Grandy[a,d], Matthias Gaestel[e], Celine Fiset[a,d], Bruce G. Allen [a,b,c,f,*]

[a] Montreal Heart Institute, 5000 Belanger St., Montréal, Québec, Canada H1T 1C8

[b] Department of Biochemistry, Université de Montréal, Montréal, Québec, Canada H3C 3J7

[c] Department of Medicine, Université de Montréal, Montréal, Québec, Canada H3C 3J7

[d] Faculty of Pharmacy, Université de Montréal, Montréal, Québec, Canada H3C 3J7

[e] Institute of Biochemistry, Hannover Medical School, Carle-Neuberg-Strasse 1, 30625 Hannover, Germany

[f] Department of Pharmacology and Therapeutics, McGill University, Montréal, Québec, Canada H3G 1Y6

[*] Corresponding author. Montreal Heart Institute, 5000 Belanger St., Montréal, Québec, Canada H1T 1C8. Tel.: +1 514 376 3330x3591; fax: +1 514 376 1355.

Keywords: MK5/PRAK; p38 MAP kinase; ERK3; ERK4; Alternative splicing; Heart; Hypertrophy

ABSTRACT

MK5, a member of the MAPK-activated protein kinase family, is highly expressed in the heart. Whereas MK2 and MK3 are activated by p38 MAPK, MK5 has also been shown to be activated by ERK3 and ERK4. We studied the regulation of MK5 in mouse heart. mRNA for 5 splice variants (MK5.1–5.5), including the original form (MK5.1), was detected. MK5 comprises 14 exons: exon 12 splicing was modified in MK5.2, MK5.3, and MK5.5. MK5.2 and MK5.5 lacked 6 bases at the 3′-end of exon 12, whereas MK5.3 lacked exon 12, resulting in a frame shift and premature termination of translation at codon 3 of exon 13. MK5.4 and MK5.5 lacked exons 2–6, encoding kinase subdomains I–VI, and were kinase-dead. All 5 MK5 variants were detected at the mRNA level in all mouse tissues examined; however, their relative abundance was tissue-specific. Furthermore, the relative abundance of variant mRNA was altered both during hypertrophy and postnatal cardiac development, suggesting that the generation or the stability of MK5 variant mRNAs is subject to regulation. When expressed in HEK293 cells, MK5.1, MK5.2 and MK5.3 were nuclear whereas MK5.4 and MK5.5 were cytoplasmic. A p38 MAPK activator, anisomycin, induced the redistribution of each variant. In contrast, MK5 co-immunoprecipitated ERK3, but not ERK4 or p38α, in control and hypertrophying hearts. GST pull-down assays revealed unbound ERK4 and p38α but no free MK5 or ERK3 in heart lysates. Hence, 1) in heart MK5 complexes with ERK3 and 2) MK5 splice variants may mediate distinct effects thus increasing the functional diversity of ERK3–MK5 signaling.

1. Introduction

Mitogen-activated protein kinases (MAPKs) are protein serine/threonine kinases that respond to extracellular stimuli and regulate a broad range of essential cellular activities, including mitosis, metabolism, motility, survival, apoptosis, and differentiation. Five distinct MAPK pathways have been identified in mammals: extracellular signal-regulated kinases (ERKs) 1/2, ERK3/4, ERK5, c-jun amino-terminal kinases (JNKs) (1–3), and p38 MAPKs (α, β, γ, and δ) [1]. Each pathway displays a characteristic hierarchical organization wherein MAPK kinase kinases (MAPKKK) phosphorylate and activate MAPK kinases (MAPKK), which in turn activate their respective MAPKs. Downstream of certain MAPKs lies an additional tier of protein kinases, the MAP kinase-activated protein kinases (MAPKAPKs): these include MK2, MK3 and MK5 (also known as PRAK) [2].

MK2 is a major target for stress-activated p38α and p38β MAPKs. MK2-deficient mice show resistance to endotoxic shock due to impaired production of pro-inflammatory cytokines such as interleukin-6 and tumor necrosis factor-alpha (TNFα) [3]. MK2 and MK3 show 75% identity at the amino acid level [4]. However, although MK2 and MK3 show similarity in their consensus phosphorylation sites [5], not all MK2 substrates have been identified as substrates for MK3. Recent studies in MK2/MK3 double knock-out mice show that MK3 further reduces TNF production, expression of p38α, and tristetraprolin (TTP), compared to $MK2^{-/-}$ mice [6], suggesting that MK3 and MK2 have overlapping function. MK5, originally identified as a p38 regulated and activated protein kinase (PRAK) [7] and [8], was shown to mediate senescence in response to induction of oncogenic *ras* and upon activation by p38 [9]. Unlike $MK2^{-/-}$ and $MK3^{-/-}$ mice, MK5-deficient mice show no destabilization of p38α [6]. Furthermore, atypical MAPKs ERK3 and ERK4 are binding partners of MK5 [10], [11] and [12]. ERK3 and ERK4 show 50% homology with ERK1/2 within the kinase domain but have an S-E-G rather than a T-E-Y motif within the activation loop and contain a unique C-terminal extension [13]. Increased expression of ERK3 retains MK5 in cytoplasm and facilitates the activation of MK5 by cis-autophosphorylation [11]. In contrast, ERK4 directly phosphorylates MK5 [14]. Hence, p38, ERK3 and ERK4 may

all be involved in regulating MK5 activity *in vivo*. Little is known about the downstream effectors or physiological function of MK5.

Our present study demonstrates 4 novel splice variants of MK5, referred to herein as MK5.2–MK5.5, in murine cardiac ventricular myocardium. These variants result from both exon skipping and alternative splice site activation during pre-mRNA processing. MK5.4 and MK5.5 lacked a significant part of the kinase catalytic domain whereas MK5.3 lacked the putative ERK3/ERK4 binding domain. When expressed in HEK293 cells, MK5.1, MK5.2, and MK5.3 localized to the nucleus. In contrast, despite retaining NLS and NES sequences, MK5.4 and MK5.5 localized to the cytoplasm in resting cells. Furthermore, the relative abundance of MK5.3 mRNA decreased whereas MK5.4 + MK5.5 mRNA increased during cardiac hypertrophy. Finally, we demonstrate that MK5 co-immunoprecipitated ERK3, but not ERK4 or p38α, in both control hearts and those exposed to pressure overload resulting from 3 d of transverse aortic constriction (TAC). Hence, in heart, MK5 may lie downstream of ERK3, rather than p38 or ERK4, and the novel MK5 splice variants may mediate distinct effects downstream of ERK3, thus increasing the functional diversity of the ERK3–MK5 signaling pathway.

2. Materials and methods

2.1. Materials

Membrane grade (reduced) Triton X-100 (TX-100), leupeptin, and PMSF were from Roche Molecular Biochemicals. SDS-polyacrylamide gel electrophoresis reagents, nitrocellulose, and Bradford protein assay reagents were from Bio-Rad Laboratories. The cAMP-dependent protein kinase inhibitor peptide (PKI) was from the University of Calgary Peptide Synthesis Core Facility. Canine hsp27, cloned into the pET24a expression vector [15], was a gift from Dr. William Gerthoffer (Reno, NV). His6-ERK3-GST, cloned into the pHGST.1 expression vector was a gift from Dr. Sylvain Meloche [16]. Anti-EGFP antibodies were from BD Biosciences. Anti-MK5 antibodies (PRAK A-7) were from Santa Cruz Biotechnology and anti-V5 antibodies were from Invitrogen. HRP-conjugated secondary antibodies were from Jackson ImmunoResearch Laboratories. All other reagents were of analytical grade or best grade available. Plasmids were transformed to *E. coli* competent strain BL21 (DE3) and expression induced by the addition of 1 mM isopropyl-β-d-thiogalactopyranoside (IPTG). GST-fusion proteins were purified by affinity chromatography on glutathione Sepharose.

2.2. Cloning and purification of fusion proteins

Total cellular RNA was isolated using RNeasy® Mini kits (Qiagen Inc.) with minor modifications. Briefly, tissue was homogenized in 2 ml of TRIzol reagent (Sigma) using a Polytron at 10,000 rpm (2 × 15 s), 0.4 ml chloroform added and phase separation induced by centrifugation for 15 min at 18,300 *g* and 4 °C. The aqueous phase was reserved and RNA was precipitated by addition of an equal volume of 70% ethanol, and then purified on Qiagen columns according to the manufacturer's instructions. RNA was quantified by determining absorbance (A) at 260 nm and only samples having an A260/A280 ratio greater than 1.8 were used. First strand cDNA synthesis was performed in a 20 µl reaction volume containing 1 µg of total RNA, 100 ng of random primers, 1× First Strand buffer (50 mM Tris–HCl pH 8.3, 75 mM KCl, 3 mM $MgCl_2$), 0.5 mM dNTP, 10 mM DTT, 40 U RNaseOUT recombinant ribonuclease inhibitor, and 200 U of M-MLV reverse transcriptase (Invitrogen),

according to the manufacturer's protocol. For PCR amplification of MK5, 2 µl aliquots of cDNA were amplified in 50 µl reactions comprising 60 mM Tris-SO_4 (pH 9.1), 18 mM $(NH_4)_2SO_4$, 1.8 mM $MgSO_4$, 200 µM dNTP, 1 µl Elongase (Invitrogen), and 400 nM primers (FWD: ***CGT GGA TCC ATG TCG GAG GAC AGC GAC ATG GAG***; REV: ***ACG AAT TCC TAC TGG GGC TCG TGG GGA AGG GTC***). PCR reactions were: 1 cycle at 94 °C for 30 s, 25 cycles at 94 °C for 30 s, 58 °C for 30 s, 68 °C for 2 min, and 1 cycle at 72 °C for 10 min. The forward and reverse primers used for PCR amplification of MK5 were designed according to the mouse MK5 cDNA sequence in the NCBI database (NM_010765). PCR products appeared as a diffuse band when electrophoresed on 1% agarose gels. The bands were excised, extracted using QIAquick Gel Extraction Kits (Qiagen), ligated into the pCR®2.1-TOPO® (Invitrogen) plasmid vector, and transformed into TOP10 competent cells. Several independent clones were sequenced. RT-PCR and cloning were performed 3 times using RNA prepared independently from 3 different animals. In total, 5 distinct mRNAs were obtained. Full length inserts of MK5.1, MK5.2, MK5.3, MK5.4, and MK5.5, in addition to MK5.1-T182A, were subcloned in phase 3′ to the GST coding sequence in pGEX-2T vector (GE Healthcare). Each pGEX-2T-MK5 variant construct was transformed into *E. coli* competent strain BL21. Transformed *E. coli* were then selected on DYT agar media contained 100 µg/ml ampicillin. The transformed bacteria were grown in DYT media contained 100 µg/ml ampicillin to an optical density of 0.6 at 600 nm and then expression of the GST-fusion protein was induced by addition of 1 mM IPTG. Following induction, bacteria were maintained at 37 °C with shaking (200 rpm) for 6–7 h. Each GST-MK5 variant was purified by affinity chromatography on GST-Trap columns (GE Healthcare). The integrity and purity of each fusion protein was determined by SDS-PAGE.

2.3. RNA analysis

Total RNA was isolated from mouse cardiac ventricles and ventricular myocytes using RNeasy® Mini kits (Qiagen Inc.) with minor modifications. Total cellular RNA was extracted by homogenizing tissue in TRIzol reagent and then purified on RNeasy

mini kit columns as per the manufacturer's protocol. Synthesis of cDNA was as described above. Quantitative real-time PCR (qPCR) was performed using a MX3000P QPCR system (Stratagene). Each amplification reaction mixture (25 µl) contained 6.25 ng cDNA equivalent to reverse transcribed RNA, 300 nM forward and reverse primers, 30 nM ROX, 12.5 µl platinum SYBR green mix (2×) (Invitrogen). qPCR reactions were: 1 cycle at 95 °C for 10 min, 40 cycles at 95 °C for 30 s, 55 °C (68 °C for MK5.4 + MK5.5) for 30 s, and 1 cycle at 72 °C for 1 min. SYBR green fluorescence was measured at the end of the annealing and extension phases of each cycle. The specificity of each primer pair for the amplicon of interest was verified using the dissociation curve. In addition, amplicons were gel purified and sequenced. The amplification efficiency for each primer pair was determined from a standard curve of 50–3.25 ng reverse transcribed RNA isolated from the heart after two-fold serial dilutions. The efficiency for each primer pair was between 90 and 110%. Glyceraldehyde-3-phosphate dehydrogenase (GAPDH) was employed as an internal control. Hence, all samples were normalized to GAPDH, which was amplified in parallel in the same run, with MxPro software (Stratagene). Primers specific for MK5 splice variants were designed using Clone Manager 6 (Sci Ed Software, USA) and based upon the sequence of murine MK5 cDNA (NM_010765). The forward and reverse primers used are shown in Table 1.

2.4. Immunocytofluorescence

The subcellular localization of each MK5 variant was determined by confocal fluorescence microscopy. AgeI–BSRgI inserts from pCR2.1-TOPO were ligated to AgeI–BSRgI digested pIRES-V5-EGFP vector. A total of 3×10^5 HEK293 cells were seeded onto laminin-coated glass coverslips in 12-well culture plates with Dulbecco's Modified Eagle Medium (DMEM) containing 10% fetal bovine serum and allowed to adhere for 24 h. Cells were then rinsed once with DMEM and transfected with 1.6 µg of the indicated pIRES-MK5-V5-EGFP variant construct using OptiMEM II (Gibco) and Lipofectamine 2000 (Invitrogen) as per manufacturer's protocol. After 5–6 h of transfection, the medium was replaced with DMEM containing 10% fetal bovine serum

for 24 h. At the end of this 24 h period, cells were serum starved for 6 h, treated with or without agonist, rinsed with ice-cold PBS, and fixed for 20 min in ice-cold PBS containing 2% paraformaldehyde (pH 7.2). The fixative was removed by washing three times with ice-cold PBS. Cells were blocked and permeabilized by incubating for 30 min in PBS containing 2% donkey serum and 0.1% (w/v) TX-100. Coverslips were rinsed once with PBS and incubated overnight in a humidified chamber with anti-MK5 antibody diluted (1:100) in PBS containing 1% donkey serum and 0.05% (w/v) TX-100. To remove excess primary antibody, cover slips were washed three times with ice-cold PBS. Coverslips were then incubated for 1 h in PBS containing 1% donkey serum, 0.05% (w/v) TX-100, Alexa fluor 555-conjugated donkey anti-mouse IgG antibody (1:400) and 1.5 μM TO-PRO 3. Finally, coverslips were rinsed three times with ice-cold PBS, drained, and mounted onto glass slides using 15 μl of DABCO/glycerol medium. The intracellular localization of MK5, TO-PRO 3, and EGFP were visualized using an LSM 510 confocal fluorescence microscope (Carl Zeiss, Oberkochen, Germany) as described previously [17], [18] and [19].

2.5. Immunoprecipitation of endogenous MK5

Mice were sedated with pentobarbital and then sacrificed. Hearts were rapidly removed, snap-frozen in liquid nitrogen, and pulverized under liquid nitrogen. The powdered tissue was resuspended in 1.2 ml of ice-cold lysis buffer (50 mM Tris–Cl (pH 7.5 at 4 °C), 20 mM β-glycerophosphate, 20 mM NaF, 5 mM EDTA, 10 mM EGTA, 1.0% (w/v) TX-100, 1 mM Na_3VO_4, 1 μM microcystin LR, 5 mM DTT, 10 μg/ml leupeptin, 0.5 mM PMSF, and 10 mM benzamidine) using a 2 ml Potter-Elvehjem tissue grinder (15 passes, on ice). Homogenates were then cleared of cellular debris by centrifugation for 30 min at 100,000 *g* and 4 °C in a Beckman TLA-100.3 rotor. The supernatants were aliquoted, snap-frozen using liquid nitrogen, and stored at − 80 °C until use. Prior to immunoprecipitation, 2 μg of anti-MK5 antibody was precoupled to 50 μl of a 25% slurry of protein A/G^+-Agarose beads (Santa Cruz Biotechnology) by incubating overnight at 4 °C with constant mixing. To remove uncoupled primary antibody, antibody-coated beads were washed three times with lysis buffer prior to

immunoprecipitation reactions. Supernatants (2 mg) were added to the antibody-coated beads and incubated overnight at 4 °C with constant mixing. Immunoprecipitations were washed three times with lysis buffer and twice with 50 mM Tris–Cl (pH 7.5 at 4 °C). The bead pellet was suspended in 20 µl of 2× SDS sample buffer and heated at 70 °C for 90 s. The beads were pelleted by a brief centrifugation and the supernatants loaded immediately onto 10–20% acrylamide-gradient SDS-PAGE gels.

2.6. GST-pull-down assay

HEK293 cells (6×10^5/35 mm dish) were seeded in DMEM containing 10% fetal bovine serum and allowed to adhere for 24 h. Cells were then rinsed once with DMEM and transfected with 3.2 µg of the indicated pIRES-MK5-V5-EGFP construct using OptiMEM II (Gibco) and Lipofectamine 2000 (Invitrogen) as per the manufacturer's protocol. After 5–6 h of transfection, the OptiMEM II media was replaced with DMEM containing 10% fetal bovine serum for 24 h. At the end of this 24 h period, cells were rinsed with ice-cold PBS, lysed in 200 µl lysis buffer (see above) on ice, scraped, transferred to 1.5 ml microcentrifuge tubes, and passed 30–40 times through a 21-gauge needle. Cell lysates were then cleared of cellular debris by centrifugation for 30 min at 100,000 *g* and 4 °C in a Beckman TLA-100.3 rotor. The supernatants were aliquoted, snap-frozen using liquid nitrogen, and stored at − 80 °C until use. His-ERK3-GST or GST alone (1 µg) was mixed with 150 µg cell lysate and incubated for 1 h at 4 °C with constant mixing. Next, 20 µl of a 50% slurry of glutathione Sepharose beads was added and samples incubated for 30 min at 4 °C with constant mixing. Pull-downs were washed three times with lysis buffer and twice with 50 mM Tris–Cl (pH 7.5 at 4 °C). The bead pellet was suspended in 20 µl of 2× SDS sample buffer and heated at 70 °C for 90 s. The beads were removed by a brief centrifugation and the supernatants loaded immediately onto 10–20% acrylamide-gradient SDS-PAGE gels.

2.7. Immunoblotting

SDS-PAGE and immunoblotting were performed as described previously [17].

2.8. Transverse aortic constriction

Pressure overload hypertrophy was induced by transverse aortic constriction (TAC) in 10–12-wk old male C57BL/6 mice (20–30 g body weight; Charles River), as previously described [20]. Sham-operated mice underwent identical interventions except for the constriction of the aorta. All animal experiments were performed according to the guidelines of the Canadian Council on Animal Care.

2.9. Miscellaneous

Protein concentrations were determined by the Bradford method [21] using bovine serum albumin (BSA) as a standard.

The sequences for the new murine MK5 splice variants shown in Supplementary Fig. 1 have been deposited in GeneBank under the accession number; MK5.2 (AY533679), MK5.3 (AY533680), MK5.4 (AY533681), and MK5.5 (AY533682).

3. Results

3.1. Molecular cloning and sequencing of murine MK5 splice variants

MK5 was cloned from cDNA prepared from murine heart total RNA. Forward and reverse primers were based upon the sequence of murine MK5 cDNA in the NCBI database (NM_010765). PCR products were cloned and sequenced, revealing 5 different products: the form of MK5 originally found in the database and 4 others. An mRNA-to-genomic sequence (MGI:1333110) alignment (http://www.ncbi.nlm.nih.gov/IEB/Research/Ostell/Spidey/) suggested the four products resulted from alternative splicing during RNA maturation. On the basis of their relative size, we refer to the form encoding full-length MK5 as MK5.1 and the novel shorter forms as MK5.2 (AY533679), MK5.3 (AY533680), MK5.4 (AY533681), and MK5.5 (AY533682). Supplementary Fig. 1 shows alignments of the putative splice sites in MK5.1–MK5.5 with the mouse genomic sequence. MK5.1 comprises 14 exons. MK5.4 and MK5.5 lack exons 2, 3, 4, 5, and 6 (Supplementary Fig. 1a,b). As shown in Supplementary Fig. 1c, MK5.2 and 5.5 lack 6 bases at the 3′-end of exon 12, presumably due to the use of an alternative 3′ splice site within this exon. MK5.3 lacks exon 12 (Supplementary Fig. 1c), resulting in a frame shift in translating exon 13 and an in-frame stop codon in the third position. MK5.1 has a 1422 base open reading frame (ORF) and is predicted to encode a 473 amino acid protein (Fig. 1) whereas MK5.2 has a 1416 base ORF and encodes a 471 amino acid protein. MK5.3 has an ORF of 1300 bases, and encodes a 369 amino acid protein. MK5.4 has a 975 base ORF, encoding a 324 amino acid protein. MK5.5 has an ORF of 969 bases and encodes a 322 amino acid protein. Aligning the predicted primary amino acid sequences for all 5 variants revealed that MK5.3 lacks the binding domain for ERK3 [11], and ERK4 [10] whereas MK5.4 and MK5.5 lack conserved protein kinase domains I, II, III, IV, V, VIa, and VIb (Fig. 1, Supplementary Fig. 2). In each case, both the nuclear localization sequence (NLS) and nuclear export sequence (NES) remain intact. Furthermore, each variant retained a threonine residue corresponding to Thr-182, the p38/ERK3/ERK4 MAPK phosphorylation site in MK5.1.

3.2. *In vivo* expression of MK5 splice variants in different tissue and MK2 deficient mice

We next wanted to determine the relative quantity of each MK5 variant in heart. Expression of MK5 variants *in vivo* at the mRNA level was quantified by real-time quantitative PCR (qPCR). Primers (Fig. 2A, Table 1) were designed to specifically amplify amplicons of equal size from total MK5 (e.g., all 5 variants), MK5.2 + MK5.5, MK5.3, and MK5.4 + MK5.5. MK5.2 + MK5.5 and MK5.4 + MK5.5 were quantified together as they shared common deletions, thus precluding selective quantification. A forward primer complementary to sequence in exon 10 and reverse primer in exon 11, which are present in all variants, were employed to quantify total MK5 mRNA. Both MK5.2 and MK5.5 have a 6 base deletion at the exon 12/13 junction. Hence, to quantify mRNA for MK5.2 + MK5.5, the forward primer was designed to be selective for the exon 12/13 junction but with a 6-base deletion, whereas the reverse primer was complementary to a region in exon 14. For MK5.3, which lacked exon 12, a forward primer in exon 11 and reverse primer spanning the exon 11/13 junction were employed. MK5.4 and MK5.5 both lack exons 2–6, inclusively, and hence were quantified using a forward primer to the exon 1/7 junction and reverse primer to the exon 8/9 junction. Amplicons for each variant were confirmed by sequencing. In addition, the specificity of each primer was validated by assessing their ability to amplify a product from MK5.1 cDNA in a pGEX-2T plasmid. With the exception of the 'total' MK5 primers, none of the primer pairs could amplify products from MK5.1 (results not shown). Using these variant-specific primers, the relative abundance of splice variant mRNAs was measured in mouse heart and isolated ventricular myocytes and expressed relative to the total abundance of MK5 transcripts (Fig. 2B). The variants MK5.2 + MK5.5 represented about 10% of total MK5 mRNA, MK5.3 was 1%, and MK5.4 + MK5.5 was 0.4%. Hence, in both mouse heart and isolated ventricular myocytes, the most abundant MK5 variant, following MK5.1, was MK5.2.

Liver, kidney, skeletal muscle, brain, pancreas, and lung express high levels of MK5 [22]. Hence, we sought to determine if MK5 splicing was tissue-specific.

Alternatively spliced variants of MK5 were observed in all tissue examined. However, the abundance of total MK5 mRNA (Fig. 2C), as well as the relative abundance of each splice variant, was tissue-specific (Fig. 2D–F). In all tissues studied, the most abundant variant, following MK5.1, was MK5.2 (Fig. 2D). Interestingly, in murine heart, the relative abundance of MK5.3 and MK5.4 + MK5.5 mRNA was greater in comparison to other tissues examined (Fig. 2E,F), although the expression of total MK5 was lower (Fig. 2C).

MK5 shows a 42% amino acid sequence similarity with MK2 and both are substrates for p38 MAPK. Furthermore, in certain tissues, including the heart, an MK2-deficiency results in reduction in p38α protein levels [4]. Hence we examined the possibility that there may be compensatory changes in expression MK5 in MK2-deficient mice. However, no changes were detected in either MK5 splicing or total MK5 mRNA in hearts from $MK2^{-/-}$ mice (Fig. 2G). This is consistent with previous results showing no change in MK5 expression in MEFs from MK2-deficient mice [23].

3.3. Expression and characterization of recombinant MK5 variants

We then sought to characterize the individual MK5 variants at the protein level. cDNAs for all MK5 variants were cloned into the bacterial expression vector pGEX-2T to generate fusion proteins with GST at the N-terminus, expressed in *E. coli*, and purified by affinity chromatography on glutathione Sepharose. Following purification, SDS-PAGE revealed GST-MK5.1, GST-MK5.2, GST-MK5.3, GST-MK5.4, GST-MK5.5, and GST-MK5.1-T182A fusion proteins of approximately 80-kDa, 80-kDa, 68-kDa, 63-kDa, 63-kDa, and 80-kDa, respectively (Fig. 3A). The identity of each band was confirmed by immunoblotting with both anti-GST and anti-MK5 antibodies (Fig. 3B). Purified preparations of GST-MK5.4 and GST-MK5.5 contained several proteins of lower molecular weight (e.g., 30–35-kDa; Fig. 3A) that were recognized by anti-GST but not by a C-terminal directed anti-MK5 antibody (Fig. 3B). Since the molecular weight of the GST moiety itself is 28-kDa, this suggests that GST-MK5.4 and GST-MK5.5 were expressed as full-length protein in *E. coli*, but were subsequently partially degraded. Similarly, when pIRES-MK5.4-V5-EGFP and pIRES-MK5.5-V5-

EGFP were expressed in HEK293 cells, immunoblotting for the V5 epitope tag or MK5 in the lysates of HEK293 cells revealed decreases in band intensity for MK5.4-V5 and MK5.5-V5 (Fig. 3C), whereas EGFP expression was not decreased. Taken together, these results suggest that, although all 5 variants were translated, MK5.4 and MK5.5 may be less stable proteins than the other variants. A similar reduced stability was observed in MK5 exon 6-deficient macrophages [23].To determine the ability of each MK5 variant to support catalytic activity, we incubated each purified recombinant MK5 with phosphorylated, active p38α, p38β, p38δ, or p38γ plus purified recombinant hsp27 (Fig. 3D). Whereas p38α and p38β phosphorylated each MK5 variant, p38γ and p38δ were much less able to do so. p38-mediated phosphorylation of MK5.1 was virtually absent when Thr-182, the site phosphorylated by p38, was replaced with Alanine. As MK5.4 and MK5.5 lack protein kinase domains I–VI, they were predicted to be catalytically inactive. This was confirmed by *in vitro* phosphorylation assay where it was observed that, whereas MK5.1, MK5.2, and MK5.3, catalyzed the incorporation of $^{32}PO_4$ into hsp27, MK5.4 and MK5.5 showed no kinase activity (Fig. 3D).

Returning to Fig. 1, an alignment of the primary amino acid sequences of all 5 variants of MK5 reveals that MK5.3 lacks the binding domain for ERK3 [11] and ERK4 [10]. GST-ERK3 pull-down assays confirmed that all MK5 variants except MK5.3 bound to GST-ERK3 (Fig. 3E). These results also suggested that the apparent lability of MK5.4 and MK5.5 was likely not a result of these variants' inability to adopt a native conformation.

3.4. Subcellular localization of exogenously expressed MK5 variants

A crucial determinant of the relevance of the MK5 variants *in vivo* is that they be translated, whereas subcellular localization is a determinant of function. Hence, each MK5 variant was transiently expressed in HEK293 cells. Previous studies have shown that MK5 localizes to the nucleus and is exported to the cytoplasm upon activation of p38 MAPK [12], [22] and [24]. First we studied the time-dependence of p38 activation by sorbitol and anisomycin and p38-dependent nuclear export of MK5 by confocal immunofluorescence microscopy. As shown by the increased levels of phospho-p38, the

p38 pathway was activated by sorbitol (Fig. 4A) and anisomycin (Fig. 4B) within 30 min and phospho-p38 levels remained elevated for at least 2 h. Hence, HEK293 cells were used to study the p38-dependent changes in the subcellular localization of endogenous MK5. In unstimulated HEK293 cells, endogenous MK5 localized to the nucleus. Following a 2 h stimulation with either sorbitol or anisomycin, MK5 immunoreactivity had translocated into the cytosol (Fig. 4C). As this prolonged stimulation was not associated with breakdown of heterologously expressed MK5.1-V5 (Fig. 4A,B) and induced translocation of endogenous MK5 (Fig. 4C), 2 h stimulations were employed in our subsequent studies of the localization and translocation of each MK5 variant. As with endogenous MK5, heterologously expressed MK5.1-V5 localized to the nucleus in unstimulated cells and was translocated to the cytoplasm upon activation of p38 MAPK with anisomycin (Fig. 5A). Thus, endogenous MK5 and exogenously expressed MK5-V5 behaved in the same manner in HEK293 cells. MK5.1-T182A localized to nucleus and did not translocate to the cytoplasm upon activation of p38 (Fig. 5F), which is consistent with previous results [22] showing that phosphorylation at Thr-182 by p38 is required for export of nuclear MK5. Furthermore, nuclear export of MK5.1-V5 was prevented by preincubation with a p38α/β inhibitor, SB203580 (Fig. 5A). Similar cellular localization and p38α/β-dependent nuclear export were observed for MK5.2-V5 and MK5.3-V5 (Fig. 5B,C). Interestingly, although each of the MK5 variants possessed both nuclear localization sequence (NLS) and nuclear export sequence (NES; Fig. 1, Supplementary Fig. 2), MK5.4-V5 and MK5.5-V5 were retained in the cytoplasm in unstimulated cells whereas small amounts of MK5.4-V5 and MK5.5-V5 immunoreactivity was detected within the nucleus following p38 activation (Fig. 5D,E). Leptomycin B, which blocks CRM1 (chromosome region maintenance 1)-dependent nuclear export, and prevents the activation-dependent translocation of both MK2 [25] and MK5.1 [24], did not alter the localization of either MK5.4-V5 or MK5.5-V5, suggesting that their cytoplasmic localization in unstimulated cells was not due to enhanced nuclear export (Fig. 5D,E).

3.5. Effect of cardiac hypertrophy and postnatal development on the expression and splicing of MK5

The relative abundance of the MK5 variants differed in a tissue-specific manner (Fig. 2). This suggested that the splicing of MK5 may be subject to regulation. Hence, to determine if cardiomyopathy altered MK5 expression and/or splicing, we examined the effect of cardiac hypertrophy induced by 1 wk of TAC. Hypertrophy is associated with a reexpression of fetal genes, including atrial and B-type natriuretic peptides (ANP, BNP), β-myosin heavy chain (β-MHC) and α-skeletal actin (α-SKA) [26]. The establishment of a hypertrophic response induced by 1-wk TAC was confirmed by the increased expression of atrial natriuretic peptide and β-myosin heavy chain (Fig. 6E,F). After 1 wk of TAC, there was no significant change in total MK5 mRNA (Fig. 6A); however, the abundance of MK5.3 mRNA had decreased whereas that of MK5.4 and MK5.5 had increased (Fig. 6C,D) relative to sham-operated mice. These results demonstrate that the pattern of MK5 splicing was altered during left ventricular hypertrophy, however this change was limited to the lowest abundance variants.We next investigated whether the expression and/or splicing of MK5 was altered in murine heart during postnatal development. Total MK5 mRNA decreased within the first 7 d, but returned to a level similar to that of the neonatal heart by 8 wk (Fig. 7A). The relative abundance of MK5.2 + MK5.5 did not change in young mice, but was significantly lower in the adult, indicating that when total MK5 mRNA increased, the generation of MK5.2 + MK5.5 did not rise proportionately (Fig. 7B). A comparison of the data shown in Fig. 7B and D indicates that the variant changing in Fig. 7B, and accounting for up to 8–9% of the total MK5 mRNA, was MK5.2. Interestingly, while the abundance of total MK5 mRNA decreased during the first weeks of life, that of MK5.3 actually increased several-fold during this period (Fig. 7C). However, even at its peak of abundance, the actual amounts of MK5.3 mRNA were low in comparison to the total quantity of MK5 mRNA. A significant 2-fold increase in the abundance of MK5.4 + MK5.5 mRNA was also noted during postnatal development, but, as with MK5.3, the actual amount of MK5.4 + MK5.5 mRNA remained comparatively low (Fig. 7D).

3.6. MK5 signaling heart

In further experiments, we sought to determine the expression of MK5 splice variants in mouse heart and mouse cardiac ventricular myocytes at the protein level. However, none of the currently available commercial antibodies was able to detect MK5 immunoreactivity in heart lysates or cytosolic extracts (data not shown). Furthermore, attempts to raise a rabbit polyclonal antibody against intact MK5.1 did not result in antisera that was useful in heart. Given that all MK5 variants retained the p38 and, with the exception of MK5.3, ERK3/ERK4 binding sites (Fig. 3E), we decided to investigate endogenous expression of MK5 variants in heart after pull-down with either GST-ERK3 or GST-p38α. Surprisingly, none of endogenous MK5 variants was pulled down with either exogenously added GST-ERK3 or GST-p38α (Fig. 8A). The band detected at 50-kDa in the input lane was also present in controls where the primary antibody was omitted (data not shown) and hence represents a non-specific interaction with the anti-mouse secondary antibody. One plausible explanation for the lack of MK5 binding to exogenous GST-ERK3 or GST-p38α is that endogenous MK5 is bound in a manner such that the docking motifs are occluded and unable to interact with exogenous ERK3 or p38α. This was further studied by adding 1 μg of exogenous MK5.1 (treated with thrombin to remove the GST moiety) to heart lysates (2 mg) prior to the pull-down assay. In this case, MK5 immunoreactivity was detected in the both GST-ERK3 and GST-p38α pull-down assays, with GST-ERK3 being more efficient, suggesting higher affinity binding (Fig. 8B). These data suggest that MK5 is expressed at the protein level in mouse heart, but that it is present in complexes and, hence, unavailable to interact with exogenously added ERK3 or p38α. To determine if endogenous MK5 was complexed with ERK3, ERK4, or p38α, MK5 was immunoprecipitated and the immune complexes probed with anti-ERK3, anti-ERK4, or anti-p38α antisera. ERK3 immunoreactivity was present in MK5 immunoprecipitates, but not the pre-immune serum control (Fig. 8C). In contrast, ERK4 and p38α immunoreactivity was not detected in MK5 immunoprecipitates. We then sought to determine if endogenous ERK3, ERK4, or p38α were free to interact with exogenous GST-MK5. Exogenously added GST-MK5.1 was able to pull-down ERK4 and p38α but not ERK3 (Fig. 8D). The slower

migrating band observed in the MK5 pull-down is consistent with the hyperphosphorylated form of ERK4 showing higher affinity for MK5 [27] and [28]. Based upon our results showing a stable interaction between ERK3 and MK5 in heart, we attempted to demonstrate the expression of MK5 splice variants at the protein level by immunoprecipitating ERK3 and then doing an MK5 immunoblot on the immune complexes; however, the ERK3 antibody was unsuitable for immunoprecipitating endogenous MK5 from heart lysates (data not shown).

The results shown in Fig. 8A–D were obtained in lysates prepared from unstressed hearts. TAC-induced pressure overload results in activation of p38 MAPK that peaks after 3 d of TAC and induces cardiac hypertrophy within 2 wk (Dingar et al., in preparation). Hence, to determine if MK5 dissociates from ERK3 and associates with p38 upon activation of the p38 MAPK pathway, we assessed if ERK3, ERK4 or p38α co-immunoprecipitated with MK5 in lysates from 3-d TAC hearts. In both TAC- and sham-operated hearts, ERK3 co-immunoprecipitated with MK5 whereas p38α immunoreactivity was not detected (Fig. 8E). Similarly, no association of MK5 with ERK4 was observed in stressed hearts. Immunoblotting using an anti-phospho-p38 antibody confirmed activation of the p38 pathway following 3 d of TAC (Fig. 8E).

ERK3 is an unstable protein and down-regulation of MK5 expression results in reduction of ERK3 protein levels [11] and [12]. Hence, if ERK3 were to be displaced from MK5 upon activation of the p38 pathway, one may expect to detect a decrease in ERK3 immunoreactivity. However, following 3-d TAC, no change in ERK3 levels was detected by immunoblotting (Fig. 8F). ERK4 expression was also unaffected (Fig. 8F). These data suggest that in heart, most or all endogenous ERK3 and MK5 were in complexes, whereas at least some of the endogenous pool of ERK4 and p38α was available to interact with the exogenous GST-MK5.1. Furthermore, MK5 complexes included ERK3 but not ERK4 or p38α, and this was independent of the activation status of the p38 MAPK pathway, indicating that, in heart, MK5 is regulated by ERK3 and not ERK4 or p38.

4. Discussion

Mapkapk5, the gene encoding MK5, lies on the negative strand of murine chromosome 5 and comprises 14 exons and 13 introns (Fig. 2A). We have demonstrated 4 novel variants of MK5, which we named MK5.2, MK5.3, MK5.4, and MK5.5. These variants appear to have resulted from a combination of exon skipping and activation of alternative splice sites during RNA maturation. MK5.2 had a 6 base deletion at the 3′-end of exon 12, perhaps arising from the selection of an alternative splice site. In MK5.3, exon 12 was totally absent. The deletion of exon 12 in MK5.3 produced a shift in reading frame in exon 13 resulting in an in-frame stop codon rather than an amino acid in position 3 of exon 13. Thus, the predicted amino acid sequence indicates that MK5.3 lacks C-terminal amino acids 370 through 473. MK5.4 resulted from skipping of exons 2 through 6, inclusively. Finally, MK5.5 lacked both exons 2–6 as well as the 6 bases at the 3′-end of exon 12 also absent from MK5.2. As a result of the deletion of exons 2–6, MK5.4 and MK5.5 lack kinase subdomains I–VIb. All MK5 variants retained both a nuclear export sequence (NES) and a nuclear localization sequence (NLS) within the C-terminus. The NLS overlaps with the p38 docking site (D-domain) [29] and p38-mediated nuclear export requires both phosphorylation of Thr-182 and masking of the NLS [22]. The predicted amino acid sequence suggests that all MK5 variants possess the D-domain that interacts with the CD domain in p38 (Fig. 1). MK5 also interacts with atypical MAPKs ERK3 and ERK4. However, while the D-domain in MK5 does not interact with the CD domains in ERK3 and ERK4, it does interact with last 50 amino acids of their C-termini [12] and [14]. Hence, with the exception of MK5.3, which lacks 106 amino acids in its C-terminus, all MK5 variants retain the binding site for ERK3 and ERK4 (Fig. 2E).

Although, as discussed above, one possible explanation for the 6 base deletion found in MK5.2 and MK5.5 is the activation of an alternative splice site at the 3′-end of exon 12, a search of the NCBI murine database revealed a predicted ORF that appears to encode MK5.2. This predicted ORF has been named "*similar to MK5 type 2*" (XM_001479242, gene ID 100047833) and lies 96.5-Mbp 3′ to *Mapkapk5* on the negative strand of chromosome 5. Hence, an alternative explanation would be that there

are only 2 splice variants, which are derived from *Mapkapk5* and *similar to MK5 type 2* primary RNA transcripts. MK5.3, which lacks exon 12, may arise from both gene transcripts, as the 6 bases missing in the *similar to MK5 type 2* ORF are found at the 3′-end of exon 12. MK5.4, which lacks exons 2–6, might result from alternative splicing of the *Mapkapk5* transcript whereas MK5.5, which lacks exons 2–6 along with the 3′-end 6 bases in exon 12, would be derived from the *similar to MK5 type 2* transcript. As both *Mapkapk5* and *similar to MK5 type 2* have the same intron/exon structure, with the exception of a 6 base deletion at the 3′-end of exon 12 in *similar to MK5 type 2*, and both are located on chromosome 5, this would be difficult to prove experimentally.

MK5 is expressed in heart, brain, placenta, lung, liver, skeletal muscle, kidney and pancreas [7]. Analysis by qPCR revealed the presence of mRNA for five MK5 variants in each of the above tissues; however, the abundance of each variant relative to the level of total MK5 was tissue-specific. In each of the tissues examined, the most abundant variant after MK5.1 was MK5.2. The relative expression of MK5.3, which lacks the ERK3 and ERK4 binding domain, was highest in the heart compared to the other tissues examined (Fig. 2C–F). MK2 and MK3 show 42% amino acid sequence homology with MK5 and all are substrates for p38 MAPK. Furthermore, in certain tissues, including the heart, an MK2-deficiency results in reduction in p38α protein levels [4]. Therefore, we examined the possibility that a deficiency in MK2 may induce compensatory changes in the expression and/or splicing of MK5. However, no changes in the abundance of MK5 splice variants were detected (Fig. 2G). These results are consistent with previous results suggesting that there is no functional overlap between MK5 and MK2 [23], despite the structural similarity [8] and evolutionary relatedness [30]. In the heart, the p38 cascade is activated by pro-hypertrophic stimuli including endothelin-1, phenylephrine, angiotensin II, mechanical stretch and pressure overload [31] and [32]. The role of MK5 in heart, as well as its substrates, remains to be elucidated. Interestingly, the relative abundance of MK5.3 mRNA was reduced after 1 wk of TAC. Further work is needed to understand the mechanism(s) regulating MK5 splicing during hypertrophic cardiomyopathy and the functional role of MK5 in the myocardium.

MK5 has been shown to localize to the nucleus when inactive and to translocate to the cytosol upon overexpression or activation of p38 [7], [22] and [24]. All MK5 variants carry both NLS and NES. When exogenously expressed in HEK293 cells, MK5.1–MK5.3 localized to the nucleus and translocated to the cytoplasm upon p38 activation. Translocation was blocked by SB203580, an inhibitor of p38α/β activity. Hence, the deletion of 2 amino acids in MK5.2 and 106 amino acids in the C-terminus of MK5.3 had no effect on their ability to form a stable interaction with p38 and undergo phosphorylation at Thr-182. Unexpectedly, MK5.4 and MK5.5 remained in the cytoplasm in unstimulated cells and a small amount of immunoreactivity was observed within the nucleus upon p38 activation. The translocation of MK5.4 and MK5.5 into the nucleus was not blocked by SB203580. Furthermore, their cytosolic localization was not altered by leptomycin B, suggesting that this altered localization was due to an inability to enter the nucleus rather than enhanced nuclear export. One possible explanation for the appearance of immunoreactivity within the nucleus following activation of p38 is that cytoplasmic MK5.4 and MK5.5 interact with p38 and enter the nucleus as heterodimers with activated p38.

The mechanisms regulating the activation and subcellular localization of MK5 are currently controversial. Both p38 and atypical MAPKs ERK3 and ERK4 have been implicated. MK5 was originally identified in HeLa cells where it was shown to be activated by p38α and p38β in response to stress, including anisomycin, or overexpression of a constitutively activated form of MKK6 [7]. As with MK2 and MK3, MK5 is primarily in the nucleus in non-stressed cells and relocalizes to the cytosol upon activation of p38. However, nuclear export of MK2 in response to arsenite or sorbitol treatment is more rapid than that of MK5, suggesting differences in regulation [24]. In addition, although stress-induced translocation of MK5 involves activation of p38, expression of kinase-dead p38α or p38β [24] as well as non-activatable p38α [22] also cause nuclear export of MK5, suggesting that the binding of p38 to MK5 may be sufficient to induce translocation. However, whereas p38 stability and stress-induced hsp27-kinase activity are reduced in MK2-deficient mice, no such effects are observed in an MK5 knock-out model [3] and [23]. Furthermore, no change in the

phosphorylation of endogenous hsp25 (the mouse homolog of hsp27) following treatment with arsenite was observed in $MK5^{-/-}$ MEFs [23]. Finally, immune complex assays fail to show activation of MK5 following treatment of $MK5^{+/+}$ MEFs with either arsenite or sorbitol [23]. These results suggest MK5 activation may not be regulated by p38 *in vivo*.

Further understanding of the regulation of MK5 activity came with the studies of atypical MAPKs ERK3 and ERK4, which bind MK5 [10], [11] and [12]. Increased expression of ERK3 retains MK5 in cytoplasm and facilitates the activation of MK5 by cis-autophosphorylation [11]. In contrast, ERK4 directly phosphorylates MK5 [14]. As ERK3 expression increases in terminally differentiated cells and growth-arrested cells [33], perhaps both ERK3/4 and p38 regulate MK5 activity depending upon the differentiation status and nature of the cell system being studied. As adult cardiac ventricular myocytes are terminally differentiated cells, one would predict that ERK3 regulation of MK5 would predominate in these cells whereas p38 may play a significant role in regulating MK5 activation in other cellular systems. In the present study, in HEK cells, translocation of both endogenous and heterologously expressed MK5 was induced by anisomycin and prevented by the p38α/β inhibitor SB203580. In contrast, in heart, under conditions where p38 activity was minimal, no association of MK5 with p38α was observed. Activation of p38 by TAC-induced pressure overload did not alter this association. Furthermore, no free MK5 was detected and at least some of the endogenous MK5 was associated with ERK3. In both $ERK3^{-/-}$ fibroblasts and HeLa cells following an siRNA-mediated knock-down of ERK3, 40–60% of the endogenous MK5 activity remained [12] and this was shown to be due to the interaction of MK5 with ERK4 [14]. Similarly, in HeLa cells, a knock-down of ERK4 reduces endogenous MK5 activity by 50% whereas simultaneous targeting of both ERK3 and ERK4 reduces MK5 activity by 80% [14]. In contrast, no interaction of MK5 with ERK4 was detected in heart. The presence of MK5-ERK3 complexes in heart raises questions concerning the regulation of MK5 activity. Current literature indicates that ERK3 must be phosphorylated within its activation loop in order to bind MK5 and this binding results in activation and cytosolic relocalization of MK5 [27]. In the present study we were

unable to determine the subcellular localization of MK5 in heart due to a lack of suitable antibodies.

The regulation, substrate specificity, and physiological functions of ERK3 and ERK4 are currently poorly understood. Neither is regulated by extracellular stimuli that activate the classical MAPKs ERK1/2, p38s, and JNKs but are constitutively phosphorylated within the S-E-G motif in their activation loop [27] and [28]. ERK3 activity appears to be regulated both at the level of expression and protein stability: it is an unstable protein that is constitutively degraded by the ubiquitin–proteosome pathway [33], [34] and [35]. The ERK3 that is expressed in excess of the abundance of certain ERK3 binding partners appears to be degraded. To date, the only protein known to stabilize ERK3 *in vivo* is MK5 and deletion of MK5 results in a reduction in ERK3 protein levels [11]. In contrast to ERK3, ERK4 is a more stable protein [10] and [14]. Furthermore, whereas ERK3 is detected in both the nucleus and the cytosol, ERK4 is strictly detected in the cytosol [14]. The differences in protein stability and subcellular localization suggest different mechanisms regulate the activity of ERK3–MK5 and ERK4–MK5 complexes. Whereas activation of MK5 by ERK4 is absolutely dependent upon ERK4 being catalytically active, catalytically inactive ERK3 is able to phosphorylate and activate MK5, albeit to a lesser extent that wild-type ERK3 [10] and [14]. The implication based upon studies in cell expression systems is that ERK3–MK5 signaling would be constitutively active. It is possible that following overexpression, conditions are created where the abundance of the ERK3–MK5 complex exceeds the cellular content of other proteins that would normally bind to, and regulate the activity of, the ERK3–MK5 complex, resulting in apparent constitutive activation. Along these lines, it was recently shown that the phosphoprotein phosphatase Cdc14A both interacts with ERK3 and MK5 and dephosphorylates a C-terminal fragment of ERK3 following phosphorylation by Cdk1 kinase [36]. It remains to be determined if Cdc14A dephosphorylates ERK3 *in vivo* or at sites other than those phosphorylated by Cdk1 kinase; however, association with a phosphatase could conceivably provide a means whereby the activation of ERK3–MK5 complexes could be regulated in response to physiological stimuli.

5. Conclusion

We have cloned and expressed 4 novel splice variants of MK5, named MK5.2–MK5.5. These variants were phosphorylated by p38α and p38β *in vitro* and when exogenously expressed in HEK293 cells each variant was translated and translocated upon activation of endogenous p38 MAPK. The relative abundance of the MK5 variant mRNAs was altered in the ventricular myocardium during pressure-induced hypertrophy and postnatal cardiac development. We demonstrated for the first time that MK5 associates with ERK3, but not ERK4 or p38, in both control hearts and those exposed to pressure overload resulting from 3 d of TAC. Hence, in heart, MK5 may be downstream of ERK3 signaling, rather than p38 or ERK4. MK5 splice variants may mediate distinct effects downstream of ERK3, thus increasing the functional diversity of the ERK3–MK5 signaling pathway. The physiological significance of ERK3–MK5 signaling in heart remains to be determined.

Abbreviations

DMSO, dimethylsulfoxide; DTT, dithiothreitol; ERK, extracellular signal-regulated kinase; FPLC, fast protein liquid chromatography; GST, glutathione Stransferase; MAP kinase, mitogen-activated protein kinase; MK2, MAP kinase-activated protein kinase-2; MK3, MAP kinase-activated protein kinase-3; MK5, MAP kinaseactivated protein kinase-5; MBP, myelin basic protein; NES, nuclear export signal; NLS, nuclear localization signal; PKI, cyclic AMP-dependent protein kinase inhibitory peptide; PAGE, polyacrylamide gel electrophoresis; PMSF, phenylmethylsulfonyl fluoride; TAC, transverse aortic constriction; TX-100, Triton X-100.

Acknowledgments

We thank Ms. Nadège Moïse for technical assistance and Dr. Maya Khairallah for her thoughtful discussion and critical reading of the manuscript. This work was supported by grants from the Canadian Institutes of Health Research [MOP-77791] and the Fonds de l'Institut de Cardiologie de Montréal (FICM). BGA and CF were Senior Scholars of the Fondation de la Recherche en Santé du Québec (FRSQ).

Appendix A. Supplementary data

Supplementary data associated with this article can be found, in the online version, at doi:10.1016/j.cellsig.2010.02.009.

References

[1] Z. Chen, T.B. Gibson, F. Robinson, L. Silvestro, G. Pearson, B. Xu, A. Wright, C. Vanderbilt, M.H. Cobb, Chem. Rev. 101 (8) (2001) 2449–2476.

[2] P.P. Roux, J. Blenis, Microbiol. Mol. Biol. Rev. 68 (2) (2004) 320–344.

[3] A. Kotlyarov, A. Neininger, C. Schubert, R. Eckert, C. Birchmeier, H.-D. Volk, M. Gaestel, Nat. Cell Biol. 1 (1999) 94–97.

[4] M. Gaestel, Nat. Rev. Mol. Cell Biol. 7 (2) (2006) 120–130.

[5] S. Ludwig, K. Engel, A. Hoffmeyer, G. Sithanandam, B. Neufeld, D. Palm, M. Gaestel, U.R. Rapp, Mol. Cell. Biol. 16 (12) (1996) 6687–6697.

[6] N. Ronkina, A. Kotlyarov, O. Dittrich-Breiholz, M. Kracht, E. Hitti, K. Milarski, R. Askew, S. Marusic, M. Gaestel, L.L. Lin, J.B. Telliez, Mol. Cell. Biol. 27 (1) (2007) 170–181.

[7] L. New, Y. Jiang, M. Zhao, K. Liu, W. Zhu, L.J. Flood, Y. Kato, G.C.N. Parry, J. Han, EMBO J. 17 (12) (1998) 3372–3384.

[8] H. Ni, X.S. Wang, K. Diener, Z. Yao, Biochem. Biophys. Res. Commun. 243 (1998) 492–496.

[9] P. Sun, N. Yoshizuka, L. New, B.A. Moser, Y. Li, R. Liao, C. Xie, J. Chen, Q. Deng, M. Yamout, M.Q. Dong, C.G. Frangou, J.R. Yates III, P.E. Wright, J. Han, Cell 128 (2) (2007) 295–308.

[10] S. Kant, S. Schumacher, M.K. Singh, A. Kispert, A. Kotlyarov, M. Gaestel, J. Biol. Chem. 281 (46) (2006) 35511–35519.

[11] S. Schumacher, K. Laass, S. Kant, Y. Shi, A. Visel, A.D. Gruber, A. Kotlyarov, M. Gaestel, EMBO J. 23 (24) (2004) 4770–4779.

[12] O.M. Seternes, T. Mikalsen, B. Johansen, E. Michaelsen, C.G. Armstrong, N.A. Morrice, B. Turgeon, S. Meloche, U. Moens, S.M. Keyse, EMBO J. 23 (24) (2004) 4780–4791.

[13] P. Coulombe, S. Meloche, Biochim. Biophys. Acta 1773 (8) (2007) 1376–1387.

[14] E. Aberg, M. Perander, B. Johansen, C. Julien, S. Meloche, S.M. Keyse, O.M. Seternes, J. Biol. Chem. 281 (46) (2006) 35499–35510.

[15] J.K. Larsen, W.T. Gerthoffer, E. Hickey, L.A. Weber, Gene 161 (2) (1995) 305–306.

[16] P. Coulombe, S. Meloche, Anal. Biochem. 310 (2) (2002) 219–222.

[17] B. Boivin, D. Chevalier, L.R. Villeneuve, E. Rousseau, B.G. Allen, J. Biol. Chem. 278 (2003) 29153–29163.

[18] B. Boivin, C. Lavoie, G. Vaniotis, A. Baragli, L.R. Villeneuve, N. Ethier, P. Trieu, B.G.Allen, T.E. Hébert, Cardiovasc. Res. 71 (1) (2006) 69–78.

[19] B. Boivin, L.R. Villeneuve, N. Farhat, D. Chevalier, B.G. Allen, J. Mol. Cell. Cardiol. 38 (2005) 665–676.

[20] H.A. Rockman, R.S. Ross, A.N. Harris, K.U. Knowlton, M.E. Steinhelper, L.J. Field, J.Ross Jr., K.R. Chien, Proc. Natl. Acad. Sci. U.S.A. 88 (18) (1991) 8277–8281.

[21] M.M. Bradford, Anal. Biochem. 72 (1976) 248–254.

[22] L. New, Y. Jiang, J. Han, Mol. Biol. Cell 14 (2003) 2603–2616.

[23] Y. Shi, A. Kotlyarov, K. Laaβ, A.D. Gruber, E. Butt, K. Marcus, H.E. Meyer, A. Friedrich, H.D. Volk, M. Gaestel, Mol. Cell. Biol. 23 (21) (2003) 7732–7741.

[24] O.M. Seternes, B. Johansen, B. Hegge, M. Johannessen, S.M. Keyse, U. Moens, Mol.Cell. Biol. 22 (20) (2002) 6931–6945.

[25] K. Engel, A. Kotlyarov, M. Gaestel, EMBO J. 17 (12) (1998) 3363–3371.

[26] X.J. Du, Br. J. Pharmacol. 152 (2) (2007) 169–171.

[27] P. Deleris, J. Rousseau, P. Coulombe, G. Rodier, P.L. Tanguay, S. Meloche, J. Cell. Physiol. 217 (3) (2008) 778–788.

[28] M. Perander, E. Aberg, B. Johansen, B. Dreyer, I.J. Guldvik, H. Outzen, S.M. Keyse, O.M.Seternes, Biochem. J. 411 (3) (2008) 613–622.

[29] T. Tanoue, R. Maeda, M. Adachi, E. Nishida, EMBO J. 20 (3) (2001) 466–479.

[30] G. Manning, D.B. Whyte, R. Martinez, T. Hunter, S. Sudarsanam, Science 298 (5600) (2002) 1912–1934.

[31] A. Clerk, A. Michael, P.H. Sugden, J. Cell Biol. 142 (1998) 523–535.

[32] T.A. Fischer, S. Ludwig, E. Flory, S. Gambaryan, K. Singh, P. Finn, M.A. Pfeffer, R.A.Kelly, J.M. Pfeffer, Hypertension 37 (5) (2001) 1222–1228.

[33] P. Coulombe, G. Rodier, S. Pelletier, J. Pellerin, S. Meloche, Mol. Cell. Biol. 23 (13) (2003) 4542–4558.

[34] P. Coulombe, G. Rodier, E. Bonneil, P. Thibault, S. Meloche, Mol. Cell. Biol. 24 (14) (2004) 6140–6150.

[35] J. Zimmermann, N. Lamerant, R. Grossenbacher, P. Furst, J. Biol. Chem. 276 (14) (2001) 10759–10766.

[36] C.A. Hansen, J. Bartek, S. Jensen, Cell Cycle 7 (3) (2008) 325–334.

Figure Legends

Fig. 1. Sequence comparison of murine MK5 splice variants. Figure shows the predicted amino acid sequences. Roman numerals above sequence refer to subdomains (I–IX) conserved in all protein kinases. The catalytic domain (residues 22–304) is indicated by a solid line above the sequence. The consensus nuclear export sequence (NES) is underlined with a solid line and the nuclear localization sequence (NES) is in bold letters. Thr-182, the site of phosphorylation by p38 MAPK is indicated by an asterisk. The ERK3/4 binding site is indicated. Dashes represent gaps.

Fig. 2. Detection of MK5 variants in murine tissues. (A) Schematic representation of the intron–exon structure of MK5 showing the location of the primers used for quantification of MK5 variant mRNAs. (B) The relative abundance of spliced MK5 mRNAs was measured in total RNA isolated from murine heart and cardiac ventricular myocytes by qPCR. (C) The relative abundance of total MK5 in various murine tissues. Abundance of (D) MK5.2 + MK5.5, (E) MK5.3, and (F) MK5.4 + MK5.5 mRNA expressed as percentage of total MK5. (G) Detection of MK5 variants in hearts from 12-wk old $MK2^{-/-}$ versus $MK2^{+/+}$ littermate mice. Shown are the mean ± S.E. (n = 3).

Fig. 3. Expression of recombinant MK5 splice variants. GST-MK5 fusion proteins were expressed in *E. coli* and purified by chromatography on glutathione Sepharose. Aliquots of purified protein were separated on 10–20% acrylamide-gradient SDS-PAGE and either (A) visualized using Coomassie Brilliant blue R250 stain or (B) transferred to nitrocellulose and probed with anti-GST (left) or anti-MK5 (right) antibodies. (C) HEK293 cells were transfected with the indicated pIRES-MK5-V5-EGFP construct. After 24 h, lysates were prepared, separated on 10–20% acrylamide-gradient SDS-PAGE, transferred to nitrocellulose, and probed with an anti-MK5 (top), anti-V5 (middle), or anti-EGFP (bottom) antibodies. (D) Activated p38 was incubated along with purified GST-MK5, hsp27, and radiolabeled [γ^{32}P]ATP. Proteins were separated on 10–20% SDS-PAGE and ^{32}P incorporation was detected by autoradiography. (E) GST pull-down assays were performed on lysates from HEK293 cells transfected with the indicated expression vectors using either recombinant ERK3-

GST or GST alone. Bound MK5 was detected by immunoblotting using an anti-V5 antibody. Equal expression of the MK5 variants was verified by loading 10% total cell lysate input. Numbers at the left indicate the positions of the molecular mass marker proteins (in kDa).

Fig. 4. Activation of p38 MAPK induces translocation of endogenous MK5 in HEK293 cells. HEK293 cells were transfected with pIRES-MK5.1-V5-EGFP. After 24 h cells were serum starved for 6 h and then treated with or without sorbitol (0.3 M) (A) or anisomycin (15 μg/ml) (B) for the indicated times and then lysates were prepared. Activation of p38 was detected by immunoblotting using an anti-phospho p38 antibody. The stability of exogenous MK5 and endogenous p38α during prolonged stress was verified by immunoblotting using anti-V5 and anti-p38α antibodies. (C) Untransfected HEK293 cells were grown for 48 h, serum starved for 6 h, and then treated with or without sorbitol (0.3 M) or anisomycin (15 μg/ml) for 2 h. Cells were then fixed and MK5 was visualized by staining with an anti-MK5 antibody and an Alexa 555-coupled secondary (anti-mouse) antibody. The upper panels are the fluorescence images whereas the lower panels contain differential interference contrast images of the same cells. Images were acquired using a 63×/1.4 plan-apochromat oil DIC objective lens.

Fig. 5. p38 MAPK activation alters the subcellular localization of MK5-V5 variants. HEK293 cells were transfected with (A) pIRES-MK5.1-V5-EGFP, (B) pIRES-MK5.2-V5-EGFP, (C) pIRES-MK5.3-V5-EGFP, (D) pIRES-MK5.4-V5-EGFP, (E) pIRES-MK5.5-V5-EGFP, or (F) pIRES-MK5.1-T182A-V5-EGFP. After 24 h of transfection cells were serum starved for 6 h and then treated with or without anisomycin (15 μg/ml, 2 h), SB203580 (20 μM), or LMB (3 ng/ml, 10 min). Where indicated, cells were preincubated with SB203580 for 10 min prior to the addition of anisomycin. Following treatment, cells were fixed and MK5 was visualized by staining with an anti-V5 antibody and Alexa 555-coupled secondary (anti-mouse) antibody (upper panels). Nuclei were visualized by TO-PRO 3 iodide (1.5 μM) staining (lower panels). Several fields of cells were examined and representative images are shown.

Fig. 6. Pressure overload-induced hypertrophy alters MK5 splicing. Pressure overload hypertrophy was induced in mice by transverse aortic constriction (TAC). Sham animals underwent the identical surgical procedure, however the aortae were not constricted. After 1 wk of TAC, mice were sacrificed, the hearts were removed, and total RNA was isolated. MK5 variants were quantified at the mRNA level by qPCR. GAPDH mRNA was employed as an internal control and the abundance of total MK5 mRNA (A) is expressed relative to 1 randomly chosen sham sample. The abundance of MK5.2 + MK5.5 (B), MK5.3 (C), and MK5.4 + MK5.5 (D) mRNAs is expressed as a percentage of total MK5 mRNA. Expression of cardiac fetal genes atrial natriuretic peptide (ANP) (E) and β-myosin heavy chain (β-MHC) (F) are expressed relative to GAPDH. Shown are the mean ± S.E. ($n = 6$). ***, $p < 0.001$: **, $p < 0.01$: *, $p < 0.05$: one-way ANOVA with Newman–Keuls post-hoc analysis.

Fig. 7. Regulation of MK5 splicing in heart during postnatal maturation. Mice were sacrificed at birth, 7 d, 20 d, or 8 wk (adult) of age and mRNA levels of MK5 variants were quantified by qPCR. The abundance of total MK5 mRNA (A) is normalized to GAPDH and expressed relative to 1 randomly chosen neonatal sample. The abundance of MK5.2 + MK5.5 (B), MK5.3 (C), and MK5.4 + MK5.5 (D) mRNAs is expressed as a percentage of total MK5 mRNA. Shown are the mean ± S.E. ($n = 3$). ***, $p < 0.001$: **, $p < 0.01$: one-way ANOVA with Newman–Keuls post-hoc analysis.

Fig. 8. MK5 interacts with ERK3 in heart. (A) GST pull-down assays were performed on murine ventricular myocardium lysates (2 mg) using either GST-p38α, ERK3-GST, or GST alone. Bound MK5 was detected by immunoblotting using an anti-MK5 monoclonal antibody. As a control, 50 μg lysate (input) was loaded in lane 1. (B) To validate the GST-pull-down assay, lysates (2 mg) were 'spiked' with 1 μg of thrombin-cleaved MK5.1 prior to performing the pull-down assay using either GST-p38α, ERK3-GST, or GST alone. Bound MK5 was detected by immunoblotting using an anti-MK5 monoclonal antibody. As a positive control, 10 ng of MK5.1 was loaded onto the gel. (C) Murine ventricular myocardium lysates were prepared and MK5 was immunoprecipitated. Purified rabbit IgG was employed in control immunoprecipitations. Co-immunoprecipitated ERK3, ERK4, or p38α was detected by immunoblotting. (D)

GST pull-down assays were performed on murine ventricular myocardium lysates (2 mg) using either GST-MK5.1 or GST alone. Bound ERK3, ERK4, or p38α was detected by immunoblotting. As a control, 50 µg of lysate (input) was loaded in lane 1. (E) Pressure overload hypertrophy was induced in mice by transverse aortic constriction (TAC). Sham animals underwent the identical surgical procedure, however the aortae were not constricted. After 3 d of TAC, mice were sacrificed, the ventricular myocardium was isolated, lysates were prepared, and MK5 was immunoprecipitated. Purified rabbit IgG was employed in control immunoprecipitations. Co-immunoprecipitated ERK3, ERK4, p38α, phospho p38, and GAPDH were detected by immunoblotting. Aliquots (50 µg) of lysate from TAC and sham hearts were included as controls (Input). Results shown are representative of 3 animals in each group. (F) Lysates (50 µg) from 3-d TAC and sham hearts were analyzed by SDS-PAGE and immunoblotting using an anti-ERK3 or anti-ERK4 antibodies. Shown are the mean ± S.E. (n = 3).

Fig. S1. Genomic alignment of cDNA sequence of MK5 variants cloned from murine heart. Panels a and b show that the 5′ deletion in MK5.4 and 5.5 corresponds to the skipping of exons 2 through 6. Panel c shows that the 6 base deletion in MK5.2 and MK5.5 corresponds to skipping of the last 6 bases of exon 12 when removing intron 12. This results in the absence of 2 amino acids, Lys and Gly. This panel also shows that MK5.3 results from skipping of exon 12, resulting in a shift in reading frame in exon 13, generating an in-frame stop codon in the third intact codon in exon 13 (bold). This variant is not the product of altered splicing at the 3′ intron/exon boundary of exon 11 as the sequence in MK5.3 does not correspond the sequence in the 5′ region of intron 11 (bold italics) or exon 12 (not shown), but aligns with the sequence in exon 13. In-frame codons flanking the sites of intron excision are underlined. NLS, nuclear localization signal; NES, nuclear export signal. Dashes represent gaps.

Fig. S2. Schematic representation of MK5 variants. NLS, nuclear localization signal; NES, nuclear export signal.

Figure 1

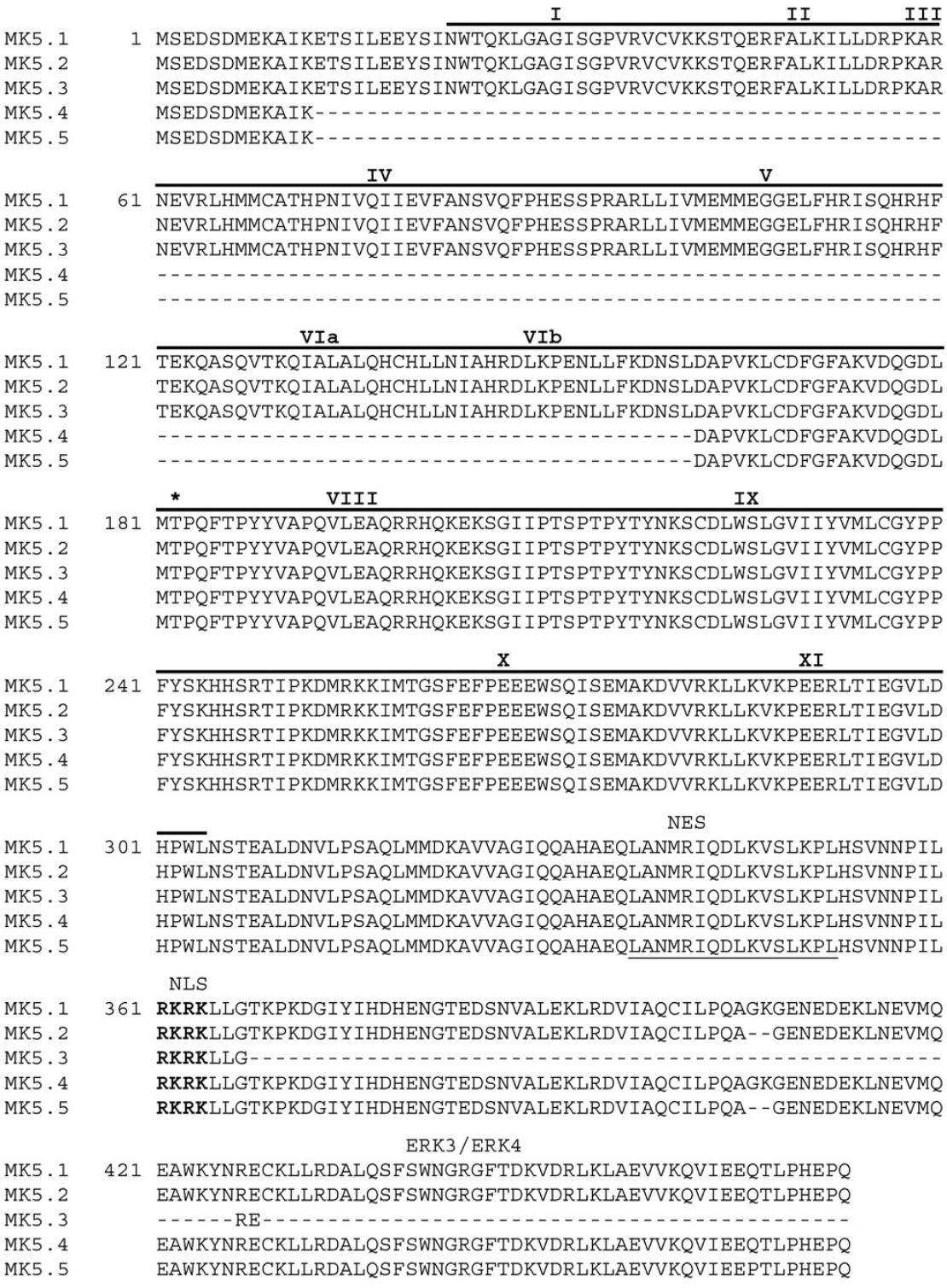
I II III
MK5.1 1 MSEDSDMEKAIKETSILEEYSINWTQKLGAGISGPVRVCVKKSTQERFALKILLDRPKAR
MK5.2 MSEDSDMEKAIKETSILEEYSINWTQKLGAGISGPVRVCVKKSTQERFALKILLDRPKAR
MK5.3 MSEDSDMEKAIKETSILEEYSINWTQKLGAGISGPVRVCVKKSTQERFALKILLDRPKAR
MK5.4 MSEDSDMEKAIK----------
MK5.5 MSEDSDMEKAIK----------
IV V
MK5.1 61 NEVRLHMMCATHPNIVQIIEVFANSVQFPHESSPRARLLIVMEMMEGGELFHRISQHRHF
MK5.2 NEVRLHMMCATHPNIVQIIEVFANSVQFPHESSPRARLLIVMEMMEGGELFHRISQHRHF
MK5.3 NEVRLHMMCATHPNIVQIIEVFANSVQFPHESSPRARLLIVMEMMEGGELFHRISQHRHF
MK5.4 ----------
MK5.5 ----------
VIa VIb
MK5.1 121 TEKQASQVTKQIALALQHCHLLNIAHRDLKPENLLFKDNSLDAPVKLCDFGFAKVDQGDL
MK5.2 TEKQASQVTKQIALALQHCHLLNIAHRDLKPENLLFKDNSLDAPVKLCDFGFAKVDQGDL
MK5.3 TEKQASQVTKQIALALQHCHLLNIAHRDLKPENLLFKDNSLDAPVKLCDFGFAKVDQGDL
MK5.4 ----------DAPVKLCDFGFAKVDQGDL
MK5.5 ----------DAPVKLCDFGFAKVDQGDL
* VIII IX
MK5.1 181 MTPQFTPYYVAPQVLEAQRRHQKEKSGIIPTSPTPYTYNKSCDLWSLGVIIYVMLCGYPP
MK5.2 MTPQFTPYYVAPQVLEAQRRHQKEKSGIIPTSPTPYTYNKSCDLWSLGVIIYVMLCGYPP
MK5.3 MTPQFTPYYVAPQVLEAQRRHQKEKSGIIPTSPTPYTYNKSCDLWSLGVIIYVMLCGYPP
MK5.4 MTPQFTPYYVAPQVLEAQRRHQKEKSGIIPTSPTPYTYNKSCDLWSLGVIIYVMLCGYPP
MK5.5 MTPQFTPYYVAPQVLEAQRRHQKEKSGIIPTSPTPYTYNKSCDLWSLGVIIYVMLCGYPP
X XI
MK5.1 241 FYSKHHSRTIPKDMRKKIMTGSFEFPEEEWSQISEMAKDVVRKLLKVKPEERLTIEGVLD
MK5.2 FYSKHHSRTIPKDMRKKIMTGSFEFPEEEWSQISEMAKDVVRKLLKVKPEERLTIEGVLD
MK5.3 FYSKHHSRTIPKDMRKKIMTGSFEFPEEEWSQISEMAKDVVRKLLKVKPEERLTIEGVLD
MK5.4 FYSKHHSRTIPKDMRKKIMTGSFEFPEEEWSQISEMAKDVVRKLLKVKPEERLTIEGVLD
MK5.5 FYSKHHSRTIPKDMRKKIMTGSFEFPEEEWSQISEMAKDVVRKLLKVKPEERLTIEGVLD
NES
MK5.1 301 HPWLNSTEALDNVLPSAQLMMDKAVVAGIQQAHAEQLANMRIQDLKVSLKPLHSVNNPIL
MK5.2 HPWLNSTEALDNVLPSAQLMMDKAVVAGIQQAHAEQLANMRIQDLKVSLKPLHSVNNPIL
MK5.3 HPWLNSTEALDNVLPSAQLMMDKAVVAGIQQAHAEQLANMRIQDLKVSLKPLHSVNNPIL
MK5.4 HPWLNSTEALDNVLPSAQLMMDKAVVAGIQQAHAEQLANMRIQDLKVSLKPLHSVNNPIL
MK5.5 HPWLNSTEALDNVLPSAQLMMDKAVVAGIQQAHAEQLANMRIQDLKVSLKPLHSVNNPIL
NLS
MK5.1 361 RKRKLLGTKPKDGIYIHDHENGTEDSNVALEKLRDVIAQCILPQAGKGENEDEKLNEVMQ
MK5.2 RKRKLLGTKPKDGIYIHDHENGTEDSNVALEKLRDVIAQCILPQA--GENEDEKLNEVMQ
MK5.3 RKRKLLG----------
MK5.4 RKRKLLGTKPKDGIYIHDHENGTEDSNVALEKLRDVIAQCILPQAGKGENEDEKLNEVMQ
MK5.5 RKRKLLGTKPKDGIYIHDHENGTEDSNVALEKLRDVIAQCILPQA--GENEDEKLNEVMQ
ERK3/ERK4
MK5.1 421 EAWKYNRECKLLRDALQSFSWNGRGFTDKVDRLKLAEVVKQVIEEQTLPHEPQ
MK5.2 EAWKYNRECKLLRDALQSFSWNGRGFTDKVDRLKLAEVVKQVIEEQTLPHEPQ
MK5.3 ------RE----------
MK5.4 EAWKYNRECKLLRDALQSFSWNGRGFTDKVDRLKLAEVVKQVIEEQTLPHEPQ
MK5.5 EAWKYNRECKLLRDALQSFSWNGRGFTDKVDRLKLAEVVKQVIEEPTLPHEPQ

Figure 2

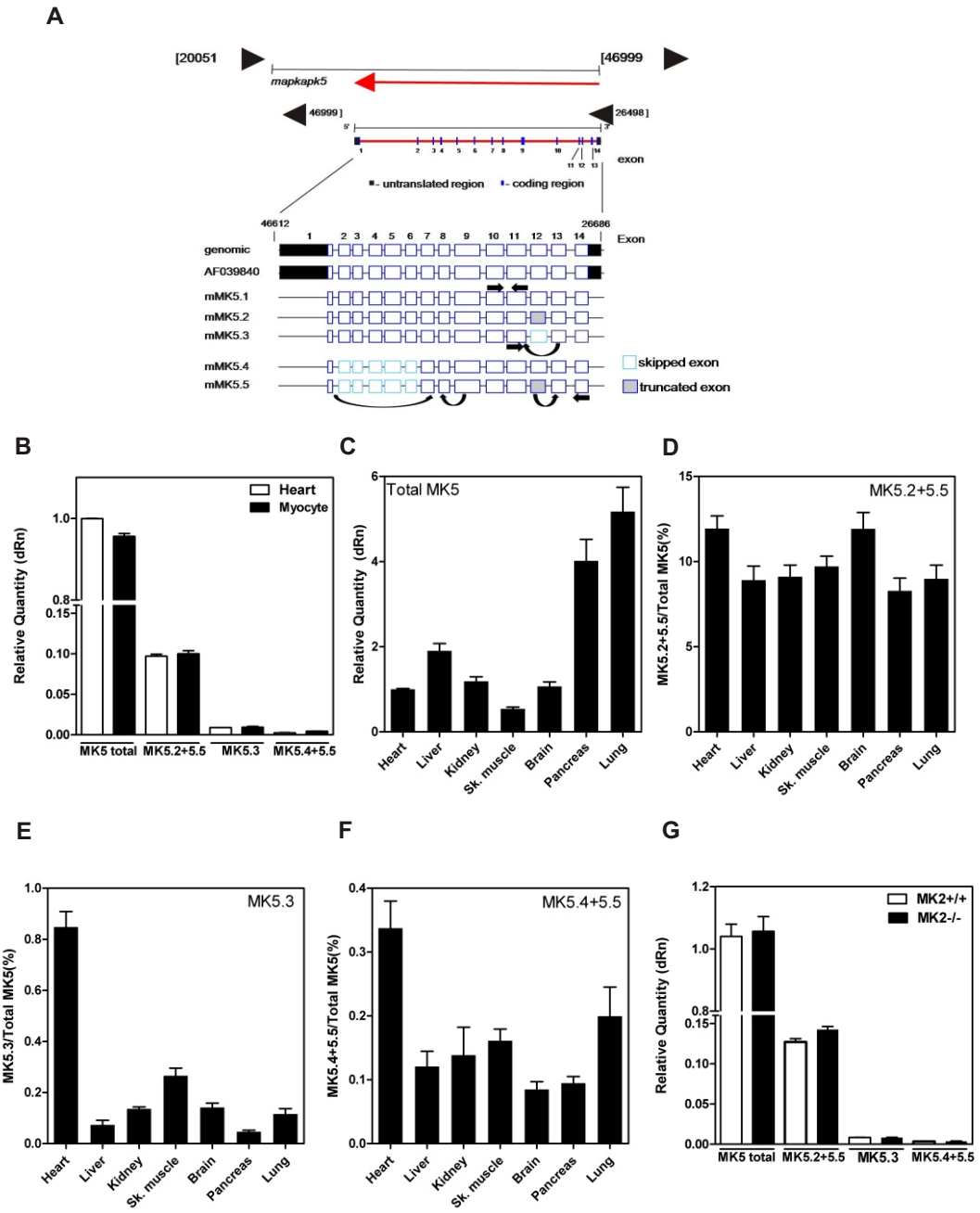
A
[20051
[46999
mapkapk5
46999]
26498]
exon
untranslated region
coding region
46612
26686
Exon
genomic
AF039840
mMK5.1
mMK5.2
mMK5.3
mMK5.4
mMK5.5
skipped exon
truncated exon
B
Heart
Myocyte
Relative Quantity (dRn)
MK5 total
MK5.2+5.5
MK5.3
MK5.4+5.5
C
Total MK5
Relative Quantity (dRn)
Heart
Liver
Kidney
Sk. muscle
Brain
Pancreas
Lung
D
MK5.2+5.5
MK5.2+5.5/Total MK5(%)
E
MK5.3
MK5.3/Total MK5(%)
F
MK5.4+5.5
MK5.4+5.5/Total MK5(%)
G
MK2+/+
MK2-/-
Relative Quantity (dRn)

Figure 3

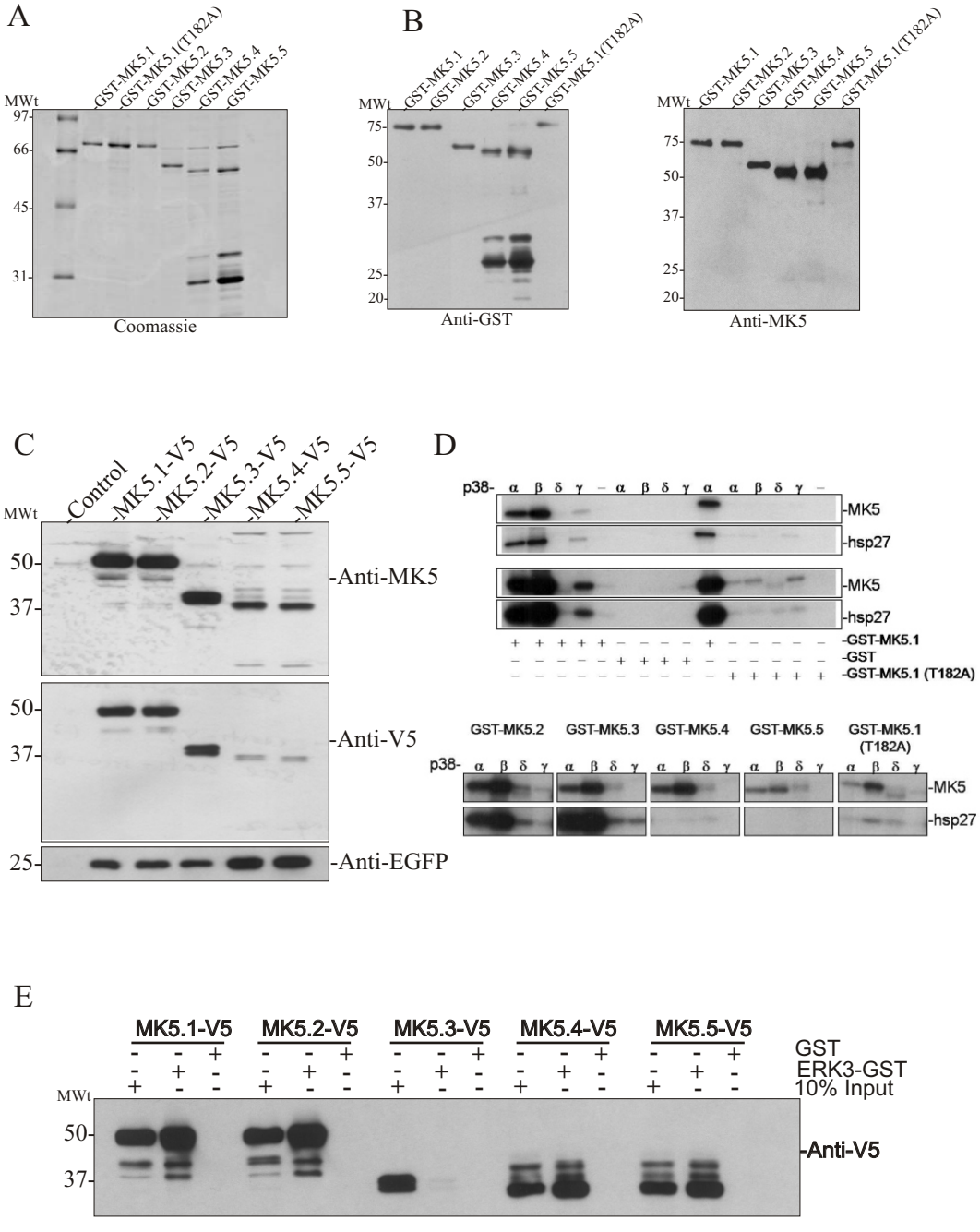
A
MWt
GST-MK5.1
GST-MK5.1(T182A)
GST-MK5.2
GST-MK5.3
GST-MK5.4
GST-MK5.5
97
66
45
31
Coomassie
B
MWt
GST-MK5.1
GST-MK5.2
GST-MK5.3
GST-MK5.4
GST-MK5.5
GST-MK5.1(T182A)
75
50
37
25
20
Anti-GST
MWt
GST-MK5.1
GST-MK5.2
GST-MK5.3
GST-MK5.4
GST-MK5.5
GST-MK5.1(T182A)
75
50
37
25
20
Anti-MK5
C
MWt
Control
MK5.1-V5
MK5.2-V5
MK5.3-V5
MK5.4-V5
MK5.5-V5
50
37
Anti-MK5
50
37
Anti-V5
25
Anti-EGFP
D
p38-
α β δ γ – α β δ γ α α β δ γ –
MK5
hsp27
MK5
hsp27
GST-MK5.1
GST
GST-MK5.1 (T182A)
GST-MK5.2
GST-MK5.3
GST-MK5.4
GST-MK5.5
GST-MK5.1 (T182A)
p38-
α β δ γ α β δ γ α β δ γ α β δ γ α β δ γ
MK5
hsp27
E
MK5.1-V5
MK5.2-V5
MK5.3-V5
MK5.4-V5
MK5.5-V5
GST
ERK3-GST
10% Input
MWt
50
37
Anti-V5

Figure 4

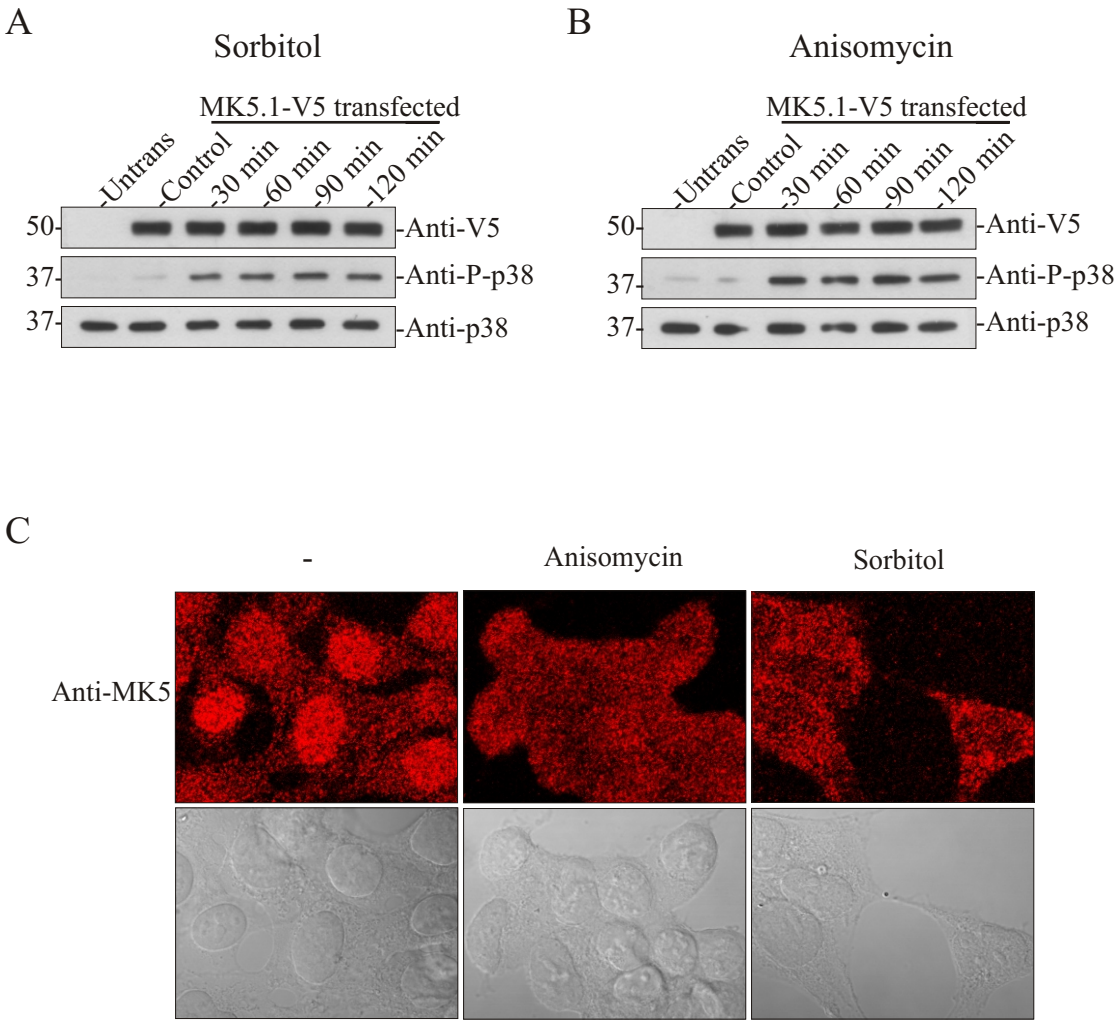
A
Sorbitol
MK5.1-V5 transfected
-Untrans
-Control
-30 min
-60 min
-90 min
-120 min
50-
-Anti-V5
37-
-Anti-P-p38
37-
-Anti-p38
B
Anisomycin
MK5.1-V5 transfected
-Untrans
-Control
-30 min
-60 min
-90 min
-120 min
50-
-Anti-V5
37-
-Anti-P-p38
37-
-Anti-p38
C
-
Anisomycin
Sorbitol
Anti-MK5

Figure 5

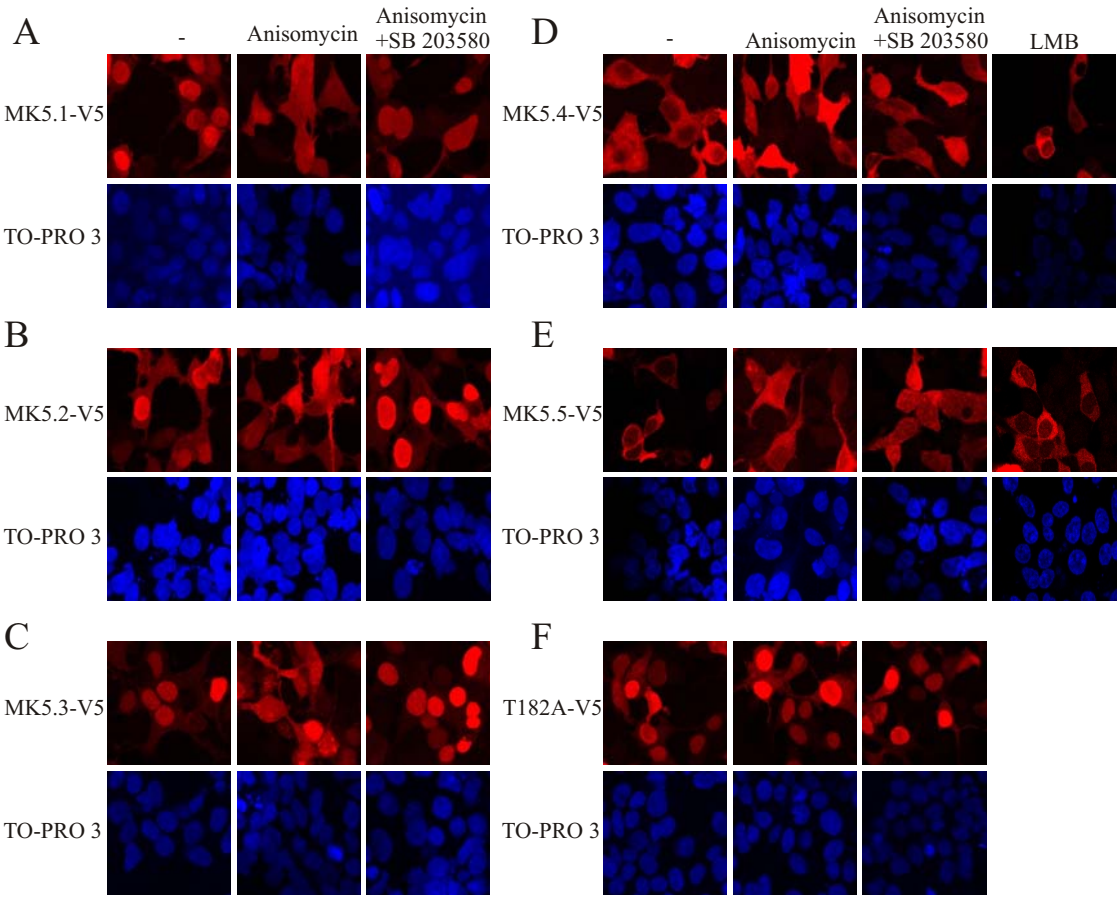
A
-
Anisomycin
Anisomycin +SB 203580
MK5.1-V5
TO-PRO 3
B
MK5.2-V5
TO-PRO 3
C
MK5.3-V5
TO-PRO 3
D
-
Anisomycin
Anisomycin +SB 203580
LMB
MK5.4-V5
TO-PRO 3
E
MK5.5-V5
TO-PRO 3
F
T182A-V5
TO-PRO 3

Figure 6

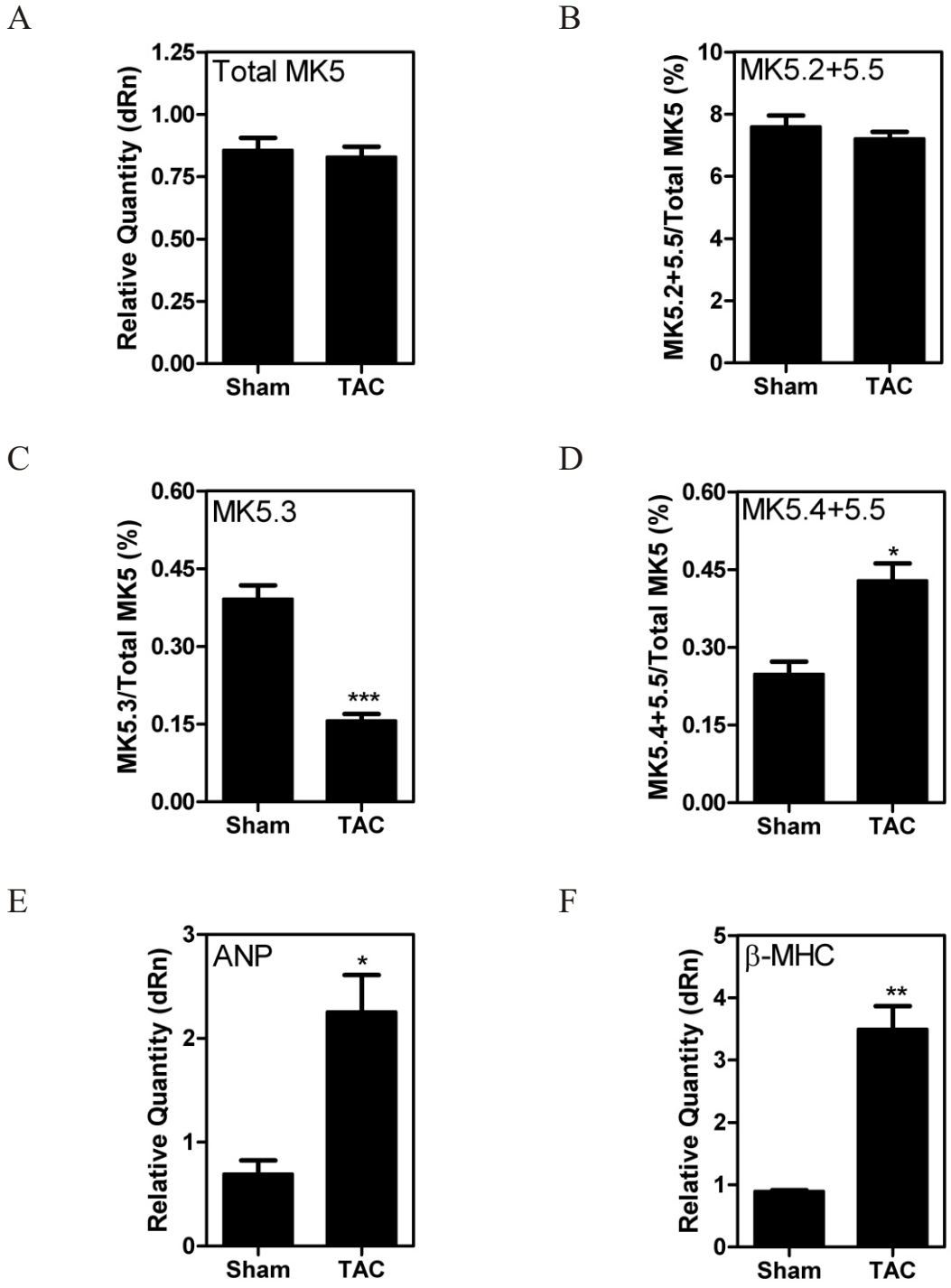
A
Total MK5
Relative Quantity (dRn)
1.25
1.00
0.75
0.50
0.25
0.00
Sham
TAC
B
MK5.2+5.5
MK5.2+5.5/Total MK5 (%)
10
8
6
4
2
0
Sham
TAC
C
MK5.3
MK5.3/Total MK5 (%)
0.60
0.45
0.30
0.15
0.00
***
Sham
TAC
D
MK5.4+5.5
MK5.4+5.5/Total MK5 (%)
0.60
0.45
0.30
0.15
0.00
*
Sham
TAC
E
ANP
Relative Quantity (dRn)
3
2
1
0
*
Sham
TAC
F
β-MHC
Relative Quantity (dRn)
5
4
3
2
1
0
**
Sham
TAC

Figure 7

A

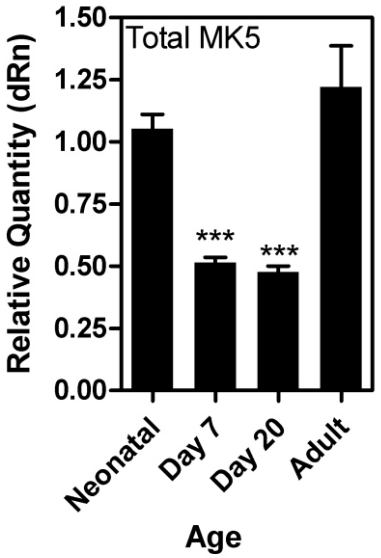

B

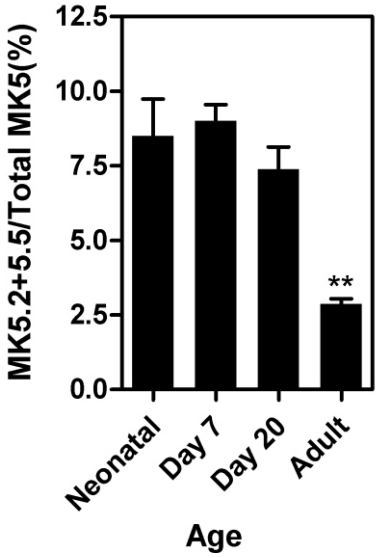

C

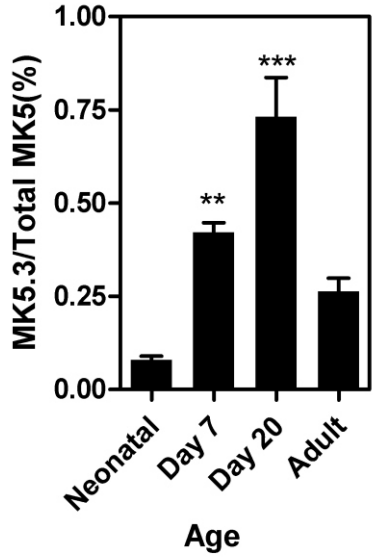

D

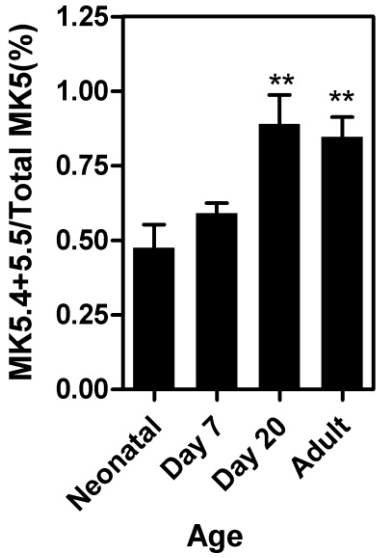

Figure 8

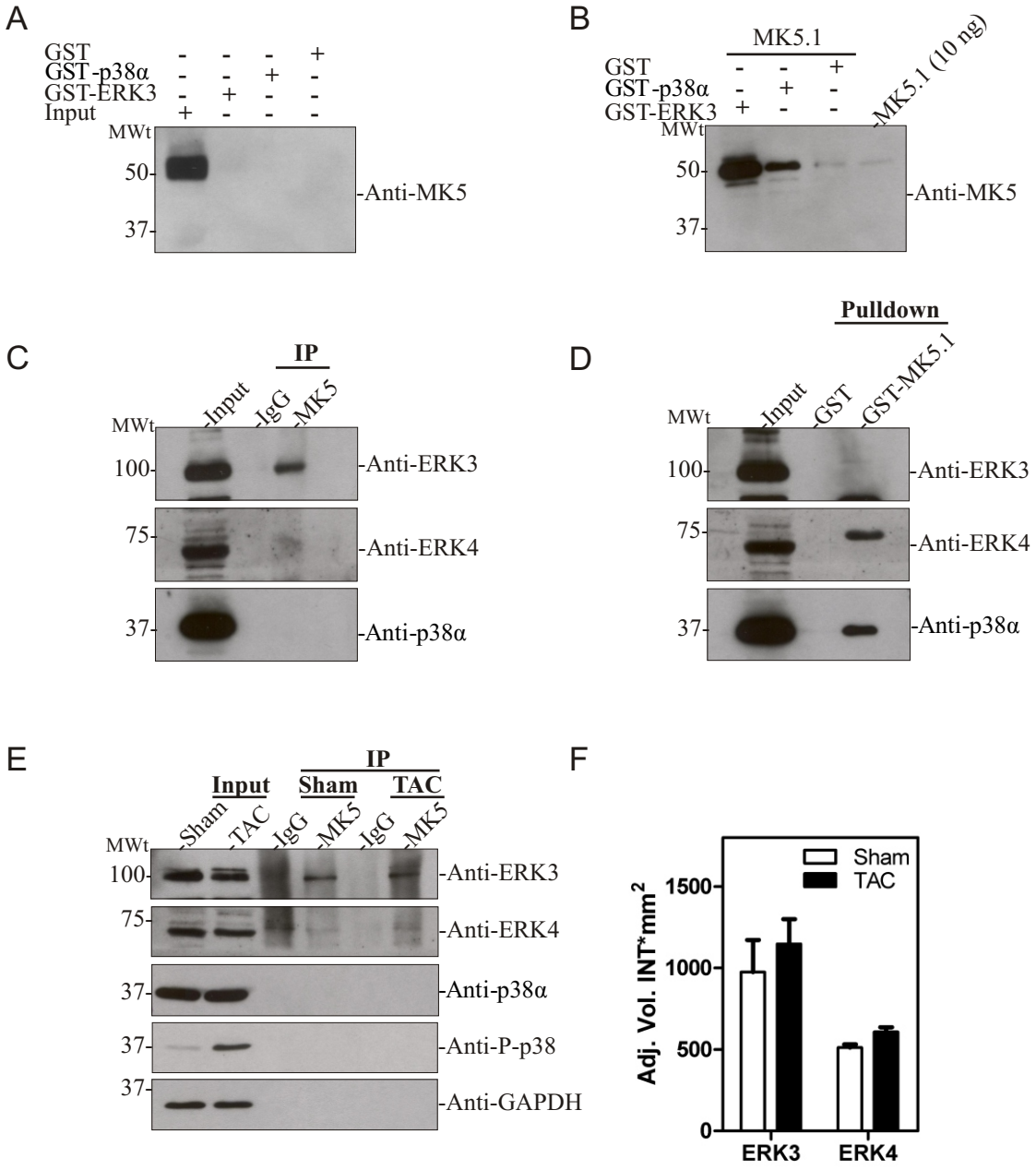
A
GST
GST-p38α
GST-ERK3
Input
MWt
50
37
-Anti-MK5
B
MK5.1
GST
GST-p38α
GST-ERK3
MK5.1 (10 ng)
MWt
50
37
-Anti-MK5
C
IP
Input
IgG
MK5
MWt
100
75
37
-Anti-ERK3
-Anti-ERK4
-Anti-p38α
D
Pulldown
Input
GST
GST-MK5.1
MWt
100
75
37
-Anti-ERK3
-Anti-ERK4
-Anti-p38α
E
Input
IP
Sham
TAC
Sham
TAC
IgG
MK5
IgG
MK5
MWt
100
75
37
37
37
-Anti-ERK3
-Anti-ERK4
-Anti-p38α
-Anti-P-p38
-Anti-GAPDH
F
Sham
TAC
Adj. Vol. INT*mm2
1500
1000
500
0
ERK3
ERK4

Supplemental Figure 1

a. Exon 1/2 junction:

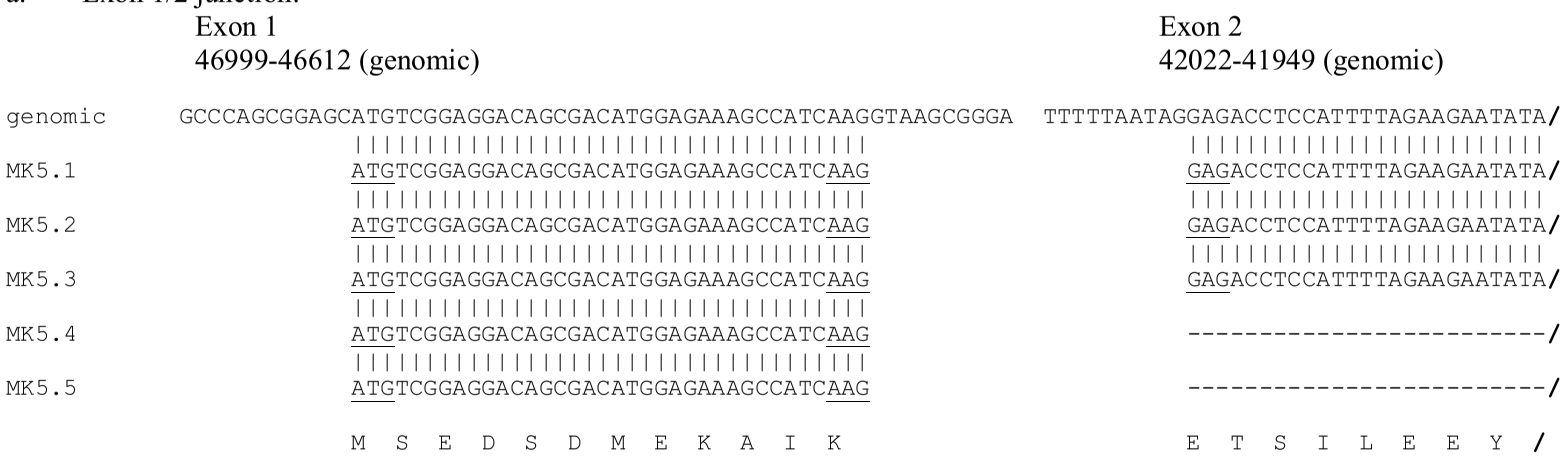

b. Exon 6/7 junction:

c. Exon 11/12/13 junction:

	Exon 11 28668-28538 (genomic)	Exon 12 28307-28186	Exon 13 27214-27110
genomic	/CTGCTGGGGTGAGTGAGCGCATTTCTTT	ATTTGTAAAGCACCAAGCC//CAGGCTGGTAAAGGTCATGCCAC	TTGCCCACAGGAGAGAATGAA/
MK5.1	/CTGCTGGG---------	CACCAAGCC//CAGGCTGGTAAAG	GAGAGAATGAA/
MK5.2	/CTGCTGGG---------	CACCAAGCC//CAGGCTG------	GAGAGAATGAA/
MK5.3	/CTGCTGGG***GAGAGAATGA***	---------//----------	GAGAGAA**TGA**A/
MK5.4	/CTGCTGGG---------	CACCAAGCC//CAGGCTGGTAAAG	GAGAGAATGAA/
MK5.5	/CTGCTGGG---------	CACCAAGCC//CAGGCTG------	GAGAGAATGAA/
	/L L G	T K P //Q A G K G	E N E / R E *

Supplemental Figure 2

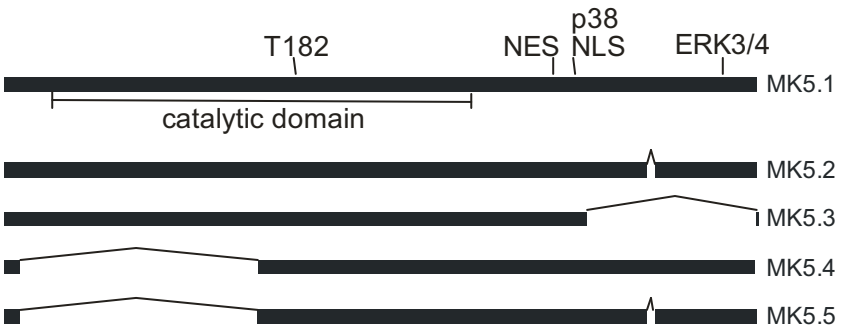

Tables

Table 1. Primers used during real-time qPCR

Target	Primers
Total MK5 S	5'-GAC AGA GGC CCT GGA TAA TGT GC-3'
Total MK5 AS	5'-GAG TGC AGG GGT TTG AGG CTG-3'
MK5.2+5.5 S	5'-TAT CCT CCC CCA GGC TGG AG-3'
MK5.2+5.5 AS	5'-CTT CGA TCA CCT GCT TTA CCA CC-3'
MK5.3 S	5'-GCG GGG ATC CAG CAG GCG CAC GCC GAG-3'
MK5.3 AS	5'-CTT CTC ATC TTC ATT CTC TCC CCA-3'
MK5.4+5.5 S	5'-AGA AAG CCA TCA AGG ACG CCC-3'
MK5.5+5.5 AS	5'-CCA CAA GTC ACA GCT CTT GTT G-3'
ANP S	5'-GTG CGG TGT CCA ACA CAG A-3'
ANP AS	5'-TTC TAC CGG CAT CTT CTC CTC-3'
β-MHC S	5'-AGG GTG GCA AAG TCA CTG CT-3'
β-MHC AS	5'-CAT CAC CTG GTC CTC CTT CA-3'
GAPDH S	5'-CTG CAC CAC CAA CTG CTT AGC-3'
GAPDH AS	5'-ACT GTG GTC ATG AGC CCT TCC A-3'

S, sense; AS, anti-sense; GAPDH, Glyceraldehyde 3-phosphate dehydrogenase; MK, MAPK-activated protein kinase; qPCR, quantitative polymer chain reaction; ANP, atrial natriuretic peptide; β-MHC, β-myosin heavy chain

ARTICLE-2

Dingar D, Merlen C, Grandy S, Gillis MA, Villeneuve LR, Mamarbachi AM, Fiset C, and Allen BG. “Effect of pressure overload-induced hypertrophy on the expression and localization of p38 MAP kinase isoforms in the mouse heart.” Cell Signal. 2010 22(11):1634-1644.

Effect of pressure overload-induced hypertrophy on the expression and localization of p38 MAP kinase isoforms in the mouse heart

Dharmendra Dingar[a, b], Clémence Merlen[a, b], Scott Grandy[a, d], Marc-Antoine Gillis[a], Louis R. Villeneuve[a], Aida M. Mamarbachi[a], Céline Fiset[a, d] and Bruce G. Allen[a, b, c, e,]

[a] Montreal Heart Institute, 5000 Belanger St., Montréal, Québec, Canada H1T 1C8

[b] Department of Biochemistry, Université de Montréal, Montréal, Québec, Canada H3C 3J7

[c] Department of Medicine, Université de Montréal, Montréal, Québec, Canada H3C 3J7

[d] Faculty of Pharmacy, Université de Montréal, Montréal, Québec, Canada H3C 3J7

[e] Department of Pharmacology and Therapeutics, McGill University, Montréal, Québec, Canada H3G 1Y6

Corresponding author. Montreal Heart Institute, 5000 Belanger St., Montréal, Québec, Canada H1T 1C8. Tel.: + 1 514 376 3330x3591; fax: + 1 514 376 1355.

Keywords: p38 MAPK; Isoforms; mRNA; Protein; Heart; Hypertrophy; Chronic pressure overload

ABSTRACT

p38 mitogen-activated protein kinases (MAPKs) are serine/threonine specific protein kinases that respond to cellular stress and regulate a broad range of cellular activities. There are four major isoforms of p38 MAPK: α, β, γ, and δ. To date, the prominent isoform in heart has been thought to be p38α. We examined the expression of each p38 isoform at both the mRNA and protein level in murine heart. mRNA for all four p38 isoforms was detected. p38γ and p38δ were expressed at protein levels comparable to p38α and 38β, respectively. In the early phase of pressure-overload hypertrophy (1–7 days after constriction of the transverse aorta), the abundance of p38β, p38γ and p38δ mRNA increased; however, no corresponding changes were detected at the protein level. Confocal immunofluorescence studies revealed p38α and p38γ in both the cytoplasm and nucleus. In the established phase of hypertrophy induced by chronic pressure overload (7–28 days after constriction of the transverse aorta), p38γ immunoreactivity accumulated in the nucleus whereas the distribution of p38α remained unaffected. Hence, both p38α and p38γ are prominent p38 isoforms in heart and p38γ may play a role in mediating the changes in gene expression associated with cardiac remodeling during pressure-overload hypertrophy.

1. Introduction

Five distinct mitogen-activated protein kinase (MAPK) pathways have been classified in mammalian cells: c-jun amino-terminal kinases (JNKs) 1, 2, and 3; p38 MAP kinases α, β, γ, and δ; extracellular signal-regulated kinases (ERKs) 1, 2; ERK3/4; and ERK5 [1]. The principle MAPKs investigated in cardiac myocytes are ERK1/2, which are activated by hypertrophic stimuli, and JNK and p38 MAPK, which are activated by cellular stress [2]. p38α and p38β are ubiquitously expressed, while p38γ is expressed in striated muscle and p38δ is expressed in lung, kidney, testis, pancreas, and small intestine [3] and [4]. To date p38α, p38β, and p38γ have been detected in heart [3] and [5].

p38 MAPK is activated by phosphorylation of the TGY motif within the activation loop by upstream kinases MKK3, MKK6, and MKK4. In addition, there exists at least 3 means whereby p38 activation is independent of MKK activity. Interactions with TAB1 or ZAP-70 [6] and [7] induce autophosphorylation of p38 within the activation loop whereas interactions with Hsp90-Cdc37 supressed this autophosphorylation [8]. Although the exact role of each p38 isoform remains to be determined, each p38 isoform has been independently knocked out in mice: p38α-deficient mice show embryonic lethality due to placental defects, whereas p38β-, p38γ-, and p38δ-null mice appear to have normal phenotypes [9]. Transgenic mice expressing dominant negative forms of p38α and p38β are resistance to cardiac fibrosis during pressure overload [10].

Due to the availability of pharmacological inhibitors, p38α and p38β have been far more extensively studied than p38γ and p38δ. Inhibition of p38α/β activity reduces apoptotic cell death in cultured myocytes and intact heart upon pressure overload or ischemia/reperfusion [11] and [12]. Additionally, improved cardiac function and reduced remodeling is observed upon inhibition of p38α/β during ischemia/reperfusion injury or myocardial infarction [13] and [14]. p38γ is the only MAPK containing a PDZ binding domain sequence (KETXL) within its carboxyl-terminus [15], which makes it unique in the MAPK family. In addition, p38γ expression is induced during muscle

differentiation [16] and it localizes in cytoplasm whereas p38α and p38β are present in the cytoplasm and nucleus in isolated cardiac myocytes [3].

p38 isoforms are currently thought to serve non-redundant functions. We have studied the expression of each p38 isoform in mouse heart to determine their presence and relative abundance. In addition, we examined the effect of pressure overload-induced cardiac hypertrophy on their expression and subcellular localization.

2. Materials and methods

2.1. Materials

SDS-polyacrylamide gel electrophoresis reagents, nitrocellulose, and Bradford protein assay reagents were from Bio-Rad Laboratories. Membrane grade (reduced) Triton X-100 (TX-100), leupeptin, and PMSF were from Roche Molecular Biochemicals. Anti-HSP27 was gift from Dr. William Gerthoffer (Reno, NV). Anti-p38α was from Santa Cruz Biotechnology (sc-535). Anti-p38γ was from Upstate Biotechnology (#07-474), anti-p38β was a gift from Dr. Jacques Landry, anti-p38δ (#2308), anti-phospho p38 MAPK (#2911S) and anti-phospho HSP27 (S-82) were from Cell Signaling Technology. Anti-phospho HSP27 (S-15) was from StressGen Biotechnologies Co. (SPA-525). Mouse anti-GAPDH was from Ambion Inc. (#4300). ALEXA fluor 488-conjugated donkey anti-rabbit secondary antibody was from Invitrogen. HRP-conjugated secondary antibodies were from Jackson ImmunoResearch Laboratories. All other reagents were of analytical grade or best grade available. Primers for PCR and qPCR were from Invitrogen. GST fusion proteins were purified by affinity chromatography on glutathione Sepharose (GE Healthcare).

2.2. Preparation of murine cardiac lysates

Mice were sacrificed after sedation with pentobarbital. Hearts were rapidly removed, snap frozen in, and pulverized under, liquid nitrogen. Heart powders were divided into two and used for both RNA extraction and protein extraction. To prepare lysates, powdered tissue was resuspended using a 2 ml Potter-Elvehjem tissue grinder (25–30 passes) in 1.2 ml of ice-cold lysis buffer comprising 50 mM Tris (pH 7.5 at 4 °C), 20 mM β-glycerophosphate, 20 mM NaF, 5 mM EDTA, 10 mM EGTA, 1.0% TX-100, 1 mM Na_3VO_4, 1 μM microcystin LR, 5 mM DTT, 10 μg/ml leupeptin, 0.5 mM PMSF, and 10 mM benzamidine. Homogenates were then cleared of cellular debris by centrifugation for 30 min at 100,000 × *g* (48,000 rpm) and 4 °C in a Beckman TLA-100.3 rotor. Finally, supernatants were collected, aliquoted, snap-frozen using liquid nitrogen, and stored at −80 °C.

2.3. Cloning and purification of fusion proteins

Human cDNA for p38α was purchased in the pOTB7 vector (Open Biosystems), p38β was in pCMV-SPORT6 (Open Biosystems), p38γ was in pET 14b (a gift from Dr. Jiahuai Han), and p38δ was in pOTB7 (ATCC). Full length inserts for each p38 isoform was then subcloned into pGEX-6P (GE Healthcare) in phase 3′ to a GST-6His coding sequence. Insertion of cDNA in to pGEX-6P was confirmed by electrophoresis on agarose gels and sequencing. Each pGEX-6P p38 construct was transformed into *E. coli* competent strain BL21 (DE3) (Novagen). Transformed *E. coli* were then selected on DYT agar media containing 100 μg/ml ampicillin. The transformed bacteria were inoculated in DYT media contained 100 μg/ml ampicillin, grown to an optical density of 0.6 at 600 nm, and then expression of the GST-fusion protein induced by addition of 1 mM isopropyl-β-D-thiogalactoside for 6–7 h at 37 °C with constant shaking. p38-fusion proteins were purified by affinity chromatography on glutathione Sepharose (GE Healthcare). The integrity and purity of each fusion protein was determined by SDS-PAGE.

2.4. RNA analysis

Mouse heart total RNA was isolated using RNeasy® Mini kits (Qiagen Inc.) with minor modifications. Briefly, total RNA was extracted by homogenizing tissue powders in 2 ml of TRIzol reagent (Sigma) using a Polytron at 10,000 rpm (2 × 15 s). Chloroform (0.4 ml) was added (for phase separation) and then samples were mixed and centrifuged for 15 min at 18,300 × *g* and 4 °C. The upper aqueous phase was collected, diluted with an equal volume of 70% ethanol, loaded onto Qiagen columns, and purified according to the manufacturer's instructions. Total RNA concentrations were determined by measuring the optical density and only samples having an 260/280 ratio between 1.8–2.1 were used. cDNA synthesis was performed in a 20 μl reaction volume containing 1 μg of total RNA, 100 ng of random primers, 1× First Strand buffer (50 mM tris–HCl pH 8.3, 75 mM KCl, 3 mM $MgCl_2$), 0.5 mM dNTP, 10 mM DTT, 40 U RNaseOUT recombinant ribonuclease inhibitor, and 200 U of M-MLV reverse transcriptase (Invitrogen), according to the manufacturer's protocol. Real-time qPCR was performed

using a MX3000P QPCR system (Stratagene). Each amplification reaction mixture (25 μl) contained 12.5 ng cDNA equivalent to reverse transcribed RNA, 300 nM forward and reverse primers, 30 nM ROX passive reference, 12.5 μl platinum SYBR green mix (2×) (Invitrogen). PCR parameters were 95 °C for 10 min, and 40 cycles of 95 °C for 30 s, 55 °C for 30 s, and 72 °C for 1 min. SYBR green fluorescence was measured at the end of the annealing and extension phases of each cycle. p38 isoform-specific primers were designed using Clone Manager 6 (Sci Ed Software, USA) and were based on the cDNA sequences in the NCBI database (p38α, NM_011951; p38β, NM_011161; p38γ, NM_013871; p38δ, NM_011950). The forward and reverse primers used are shown in Table 1. The ability of each primer pair to selectively amplify a single target sequence was verified by analyzing the dissociation curve. In addition, amplicons were gel purified and sequenced to assure amplification of the correct target sequence. The amplification efficiency for each primer pair, determined from a standard curve of 50–3.25 ng reverse transcribed RNA isolated from the murine heart after two-fold serial dilution, was found to be between 90–110%. All samples were normalized to GAPDH, which was amplified in parallel.

2.5. Subcellular localization of p38α and p38γ

Following surgical removal, mouse hearts were frozen in 2-methyl butane chilled with liquid nitrogen. Tissue was embedded in Tissue-Tek O.C.T. compound (Sakura Finetek USA, Inc.). After trimming, 14 μm transverse ventricular cryosections were prepared and stored at −80 °C prior to further use. Three sections per heart were fixed for 20 min in ice-cold 4% paraformaldehyde in PBS (pH 7.2). After fixation, sections were washed three times with ice-cold PBS (5 min), blocked and permeabilized in a PBS solution containing 2% donkey serum and 0.5% TX-100 for 60 min. Slides were rinsed once with ice-cold PBS and incubated with primary antibody diluted (1:100 for p38α and phospho p38; 1:200 for p38γ) in PBS containing 1% donkey serum and 0.1% TX-100 overnight at 4 °C in a closed humidified chamber. The next day, slides were rinsed three times with ice-cold PBS and incubated for 1 h with ALEXA fluor 488-labeled donkey anti-rabbit IgG antibody (1:600) and 1.5 μM TO-PRO 3 iodide in PBS

containing 1% donkey serum and 0.1% TX-100. Finally, slides were rinsed three times with ice-cold PBS, drained and mounted using 15 µl of DABCO/glycerol medium. p38α, p38γ, and TO-PRO-3 (binds dsDNA) were visualized using an LSM-510 confocal fluorescence microscope (Carl Zeiss, Oberkochen, Germany) as described previously [17], [18] and [19]. Control experiments were performed omitting the primary antibody.

2.6. Activation of p38

Purified GST-p38 isoforms (0.5 mg/ml) were activated by incubating in the presence of constitutively active His6-MKK6(EE) (0.16 mg/ml) in the presence of 1 mM ATP, 10 mM $MgCl_2$, 0.62 mM EGTA, 0.25 mM DTT, 1 mM Na_3VO_4, 10 µg/ml leupeptin, and 1 µM microcystin in PBS overnight at room temperature without mixing [20]. This procedure has been shown previously to give complete dual (TGY) phosphorylation of p38α [20]. To separate phosphorylated GST-p38 from His6-MKK6(EE), reaction mixtures were incubated with glutathione Sepharose beads for 2–3 h at 4 °C on a clinical rotor, centrifuged for 2 min at 5000 rpm and 4 °C, washed thrice with TBS containing 1 mM EDTA (TBSE), and bound GST-p38 eluted with reduced glutathione. Purified, activated p38 was then dialyzed against TBSE buffer followed by a storage buffer comprising 50% glycerol, 50 mM Tris (pH 7.5 at 5 °C), 150 mM NaCl, 0.1 mM EGTA, 0.03% Brij 35, 1 mM benzamidine, 0.2 mM PMSF, and 0.1% β-mercaptoethanol. Protein concentrations for each isoform were determined on 10–20% SDS-PAGE using BSA as a standard. Proteins were separated on gels and stained with Coomassie Brilliant Blue R250. Gels were scanned using a VersaDoc 4000 imaging system and p38 and BSA band densities determined using Quantity One software (Bio-Rad Laboratories, Inc). The specific activity of each phosphorylated p38 isoform was determined by incubating activated p38 (20 ng) with 0.33 mg/ml MBP, 100 µM [γ^{32}P]ATP (10 µCi), 1 mM EGTA, 10 mM $MgCl_2$, 10 mM DTT, 10 µg/ml leupeptin, 1 mM Na_3VO_4, and 1 µM microcystin LR at 30 °C for 2, 5, 8, and 10 min. Reactions were stopped with SDS-PAGE sample buffer and separated on 10–20% SDS-PAGE, stained with Coomassie blue, the MBP band excised from the gel, and ^{32}P incorporation in MBP measured by liquid scintillation counting.

2.7. Immunoblotting

SDS-PAGE and immunoblotting were performed as described previously [17]. Following the transfer, nitrocellulose membranes were rinsed in PBS and fixed by with glutaraldehyde [21].

2.8. Pressure-overload hypertrophy

Chronic pressure-overload was induced in male C57BL/6 mice (10 weeks old) by transverse aortic constriction (TAC) for 1, 3, 7, 14, and 28 days as described [21]. Sham mice underwent the same surgical procedure except the aortae were not constricted.

Animal handling followed the guidelines of the Canadian Council of Animal Care.

2.9. Miscellaneous methods

Protein concentrations were determined by the method of Bradford [22] using bovine serum albumin (BSA) as a standard.

3. Results

3.1. Expression of p38 isoforms in heart

Although the expression of p38α, p38β, and p38γ in heart has been shown previously [5], nothing is known about the expression of p38δ or the relative abundance of each isoform. To further our understanding of p38 signaling in heart we quantified the relative mRNA abundance for each p38 isoform using real time quantitative PCR. As the p38 isoforms show high degree of DNA sequence homology (> 60%), primers were directed towards regions of lower homology and on different exons. In addition, primers were designed to specifically amplify amplicons of similar size (p38α 271 bases, p38β 264 bases, p38γ 269 bases, and p38δ 202 bases). Equal amplicon size allowed us to better compare the relative expression levels. The specificity of each primer pair was verified both by melting curve and sequencing. Using these isoform specific primers (Table 1), the mRNA abundance was measured in mouse heart and expressed relative to the abundance of p38α mRNA. We detected mRNA for all four p38 isoforms with p38α and p38γ mRNAs being the most abundant followed by p38β (10.6%), and p38δ (0.08%) (Fig. 1A).

As it's the level of protein that is important with respect to function, we examined the expression of each p38 isoform by immunoblotting. At the amino acid level p38 isoform have more than 60% sequence homology [23], hence there is possibility that antibodies may cross react. We first used purified recombinant p38 isoforms (Fig. 1B) to assess the isoform-selectivity of each antibody. Different commercially available antibodies were screened against pure p38 isoforms and only those that were specific for the intended isoform were employed in subsequent studies (Fig. 1C). Using these isoform-specific antibodies, expression of each p38 isoform in hearts lysate was assessed by immunoblotting. All four p38 isoforms were detected (Fig. 1D). We then quantified the expression of p38 isoform expression by immunoblotting using purified GST-p38 isoforms as standards. Similar to mRNAs, p38α and p38γ were the most abundant isoforms at the protein level, followed by p38β (0.018%) and p38δ (0.016%) (Fig. 1E). In conclusion p38δ is expressed in heart and at a

level comparable to p38β. Furthermore, p38α and p38γ are expressed at similar levels, indicating that p38γ might also play an important role in regulating cardiac function.

3.2. p38 expression during chronic pressure overload

p38α/β dominant negative transgenic mice are resistant to cardiac fibrosis during pressure overload [10]. In addition, inhibition of p38α/β activity reduces apoptotic cell death in cultured myocytes and intact heart during pressure overload or ischemia/reperfusion [11] and [12]. However, although they are activated by similar upstream kinases, there is very little known about the function of p38γ and p38δ. Our results (Fig. 1A and E) showed p38γ is expressed at levels similar to p38α. Therefore, we examined the effect of chronic pressure overload on the expression of each p38 isoform to see if any particular isoform shows alterations in expression, as this would suggest potentially a more prominent role in cardiac pathophysiology. Chronic pressure overload was induced by transverse aorta constriction and mice were sacrificed after 1, 3, or 7 days. Total RNA was subsequently isolated and the relative mRNA abundance of each p38 isoform was quantified by qPCR. There was no change in the quantity of p38α mRNA. In contrast, p38β and p38δ mRNA increased within 1 day of pressure overload and remained elevated whereas p38γ mRNA showed an initial increase but had returned to basal levels by day 7 (Fig. 2A). However, although increases in mRNA abundance were observed for p38β, p38γ, and p38δ, the protein level of each isoform was unaltered within this time-frame (Fig. 2B).

Chronic pressure overload induces a hypertrophic response that is associated with both the re-expression of fetal genes and activation of the p38 MAPK pathway. To verify the establishment of a hypertrophic response, we assessed the levels of atrial natriuretic peptide (ANP) and β-myosin heavy chain (β-MHC) [24] mRNA in sham and banded hearts by qPCR. ANP and β-MHC mRNA was increased in TAC hearts on day 1 and gradually increased further through day 7 (Fig. 2D). The time-course for activation of p38 signaling was also examined. We examined the effect of pressure overload on the phosphorylation of p38 MAPK and its downstream effector hsp25 using phospho-specific antibodies to the T-G-Y motif in p38 and Ser-15 and Ser-82 in hsp25

(Fig. 2C). p38 phosphorylation was increased on day 1, peaked on day 3, and then declined but remained elevated, relative to sham animals, on day 7. The phospho-p38 antibody revealed a doublet on day 3, suggested at least 2 isoforms were activated. A similar time course was observed for phosphorylation of hsp25 (Fig. 2C). Hence, although chronic pressure overload include a sustained increase in ANP and β-MHC mRNA, high levels of p38 activation were not sustained.

Similar to ANP and β-MHC, the abundance of p38β and p38δ mRNA increased in response to pressure overload. ANP and β-MHC are fetally expressed genes that become re-expressed during pathological cardiac hypertrophy. We sought to determine the temporal expression of each p38 isoform in the ventricular myocardium during post-natal development. mRNA was isolated from neonatal, 7 day, 20 day, and adult (8 week) hearts. Analysis by qPCR showed that (relative to neonatal hearts) p38α mRNA was reduced by 2-fold at 7 and 20 days (Fig. 3A), p38β mRNA dropped 2-fold at 20 days (Fig. 3B), p38γ mRNA was reduced at 7 and 20 days (Fig. 3C), and p38δ mRNA dropped more than 3-fold within 7 days of birth (Fig. 3D). However, whereas the mRNA content for p38α, p38β, and p38γ had returned to levels comparable to those in the neonatal heart by 8 weeks, p38δ mRNA remained low in the adult heart.

3.3. Specific activity

The level of expression is only one determinant of the impact an enzyme may have on cellular function. Other factors include its subcellular localization, substrate specificity, activation, and turnover number. Therefore we examined the specific activity of each p38 isoform, following phosphorylation *in vitro* by His6-MKK6(EE) and repurification, towards MBP. The specific activity of p38α was 75.70 U/mg (Fig. 4A), p38β was 76.05 U/mg (Fig. 4B), p38γ was 96.13 U/mg (Fig. 4C), and p38δ was 190.9 U/mg (Fig. 4D). Hence, the specific activity of p38δ towards MBP was more than two fold higher than the other isoforms. However, this cannot compensate for the comparatively low levels of p38δ protein relative to p38α and p38γ, and suggesting p38α and p38γ may play more prominent roles in the heart.

3.4. Subcellular distribution of p38γ and p38α during pressure overload-induced hypertrophy

Although each p38 isoforms are activated, with variable efficiency, by similar upstream kinases MKK3, MKK4, and MKK6 [25], no study to date has described the effect of chronic pressure overload on the cellular localization of p38. Hence, we studied TAC induced pressure-overload in mice. Mice were sacrificed 7, 14, and 28 days after surgery, time-points where molecular and morphological changes associated with pathological hypertrophy were clearly apparent. These time points were chosen to examine localization once hypertrophy had been established rather than during the acute or early phases of the response to pressure overload [26]. Cryosections of the ventricles were prepared and immunostained with anti-p38α, anti-p38γ, or anti-phospho-p38 antibodies. As immunoblotting showed p38β and p38δ 1) were in far lower abundance and 2) their antibodies reveal non-specific bands, we did not determine the subcellular localization of these isoforms. p38α and p38γ localized to the cytoplasm and nucleus in sham hearts. However, increased nuclear localization of p38γ was observed in sections from TAC hearts at 7, 14, and 28 days (Left panel of Fig. 5A, B and C). In contrast, no nuclear accumulation of p38α was observed (Right panel of Fig. 5A, B and C). Reexpression of BNP and β-MHC confirmed a persistent hypertrophic response in these hearts (Fig. 5D). No differences between TAC and sham were observed with the anti-phospho-p38 antibody (results not shown), which is consistent with the low levels of phospho-p38 detected by immunoblot after day 3 (Fig. 2C). These results suggest that p38α and p38γ respond differently to chronic pressure overload in terms of their subcellular localization. These differences in localization would result in access to different substrates and hence distinct functional effects. Nuclear accumulation for p38γ and not p38α, as well as differential regulation at transcriptional level during heart development and hypertrophy strongly suggests non-redundant roles of p38α and p38γ in the heart as well as a potential role for p38γ in the maintenance and/or progression of pathological ventricular hypertrophy.

To understand the consequences of the nuclear localization of p38γ, we sought to identify substrates in cytosolic and nuclear fractions from rat heart specific to

phosphorylated, activated GST-p38α/β/γ/δ upon incubation in the presence of [γ^{32}P]ATP. However, no isoform-specific phosphorylation was observed in either subcellular fraction (results not shown). The failure to detect added incorporation of ^{32}P into proteins in the cytosolic and nuclear fractions might reflect low copy number or phosphorylation status of target proteins in these fractions or, perhaps, the absence of a suitable scaffolding protein.

4. Discussion

To date p38α, p38β, and p38γ have been reported in heart with p38α being considered to be the dominant isoform [3], [4] and [5]. We now show that p38δ is expressed in the mouse heart at protein levels that are comparable to p38β. In addition, at both the mRNA and protein levels, expression of p38α and p38γ are similar, suggesting that both play important roles in the heart. Finally, p38γ was shown to accumulate in the nucleus in hearts hypertrophying due to chronic pressure overload.

p38δ was detected in mouse heart by immunoblotting and found to be expressed at levels similar to p38β. There are numerous reports suggesting that, although expressed at levels much lower than p38α, p38β plays a distinct role in the heart. p38α and p38β are activated in the heart in response to ischemia and reperfusion [27] and pressure overload [26], as well as following the exposure of cardiac myocytes to cytokines [28], hypertrophic agonists [29] and mechanical stretch [30]. In simulated ischemia phosphorylation of p38α increases whereas that of p38β decreases [31]. Moreover inhibition of p38α during ischemia has a protective effect [31] and [32]. Similarly, $p38\alpha^{+/-}$ mice are resistant to infarction [33]. In contrast, during preconditioning, activation of p38α decreases and that of p38β increases [31], suggesting that p38β is protective whereas p38α is detrimental. Expression of constitutively active MKK6bE or MKK3bE along with wild-type or dominant negative p38α (DN-p38α) or p38β (DN-p38β) in neonatal myocytes indicates p38α mediates apoptosis whereas p38β is involved in the hypertrophic response [34]. Mice expressing a dominant-negative form of 14-3-3η (DN-14-3-3) are unable to compensate for pressure overload resulting in increased myocyte apoptosis and mortality. DN-14-3-3/DNp38β mice, and to a lesser extent DN-14-3-3/DN-p38α mice, show reduced mortality and cardiac myocyte apoptosis in response to pressure overload [35]. Taken together, these data indicate that, although expressed at lower levels than p38α or p38γ, p38β plays a distinct role in the heart. Hence, further study might also reveal a unique role for p38δ in the heart.

The anti-apoptotic role of p38α and p38β has been studied in pressure overload hypertrophy and ischemia/reperfusion [11] and [12]. However, little is known regarding

the roles of p38γ or p38δ. We therefore studied the effect of chronic pressure overload on the expression and subcellular localization of p38 isoforms in the mouse heart. No change in expression of p38α mRNA was observed in response to chronic pressure overload, whereas mRNA levels for p38β/γ/δ was increased. However, no corresponding change in expression was detected at protein level during the first 7 days following TAC. It has been shown in transfected HEK293T cells overexpressing p38α and p38γ that p38α activation reduces p38γ protein via activation of the c-jun-dependent ubiquitin–proteosome pathway [36]. However, in heart, although there was a peak of p38 phosphorylation at day 3 of TAC, p38γ protein levels were unaffected.

p38γ was detected in the cytoplasm and nucleus. Due to the -KETXL sequence in its C-terminus [15] p38γ is able to bind PDZ domains. As a result of this, p38γ binds to a number of PDZ-containing proteins such as α1-syntrophin, SAP90/PSD95, and SAP97/hDlg [15] and [37]. These proteins are scaffold proteins that are usually targeted to the cytoskeleton. Upon phosphorylation by p38γ, hDlg is released from the cytoskeleton [37]. Other substrates include the microtubule-associated protein tau [38] and CapZ-interacting protein [39]. Although p38γ was previously reported to be exclusively cytosolic in neonatal rat ventricular myocytes [3], in the present study, p38γ immunoreactivity accumulated in the nuclei during chronic pressure overload. Nuclear substrates for p38γ identified to date include transcription factors such as ATF2, AP-1, Elk-1, MEF2A, p53, SAP1 and SAP2 [40], [41] and [42]. MEF2 transcription factors are involved in the regulation of inducible gene expression during hypertrophy and MEF2 activity is increased during pressure or volume overload [43]. Activation of MEF2A and MEF2C is stimulated by p38; however, p38α may be more efficient than p38γ at activating MEF2 [44], [45] and [46]. Expression of an active variant of p38γ attenuates, whereas active p38α induces, expression of AP-1-driven reporter genes [42]. Furthermore, in the skeletal muscle cell line C2C12, over expression of p38γ leads to differentiation from myoblasts to myotubes whereas expression of dominant negative p38γ prevents this differentiation [16] and [47]. Given that p38γ is a prominent p38 isoform in heart and it accumulated in the nucleus during chronic pressure overload, it is

quite possible that p38γ plays a role in the changes in gene expression associated with pathological hypertrophy.

Nuclear translocation of p38γ but not p38α 7–28 days after the initiation of pressure overload may result from 1) the activation of TAB-1, which binds to and activates p38α independently of MKK3/6 but retains the activated p38α in the cytosol [48], 2) the sustained activation of a p38γ-specific MKK resulting in its nuclear translocation, 3) the interaction of p38γ with a PDZ-domain containing protein that shuttles p38γ into the nucleus, or 4) the interaction of activated p38γ with a nuclear PDZ-domain containing protein which retains p38γ within the nucleus. Similar to p38γ, YES kinase-associated protein (YAP) contains the PDZ-binding motif -FLTWL in its C-terminus that is essential for both translocation of YAP from the cytosol to the nucleus and its ability to promote apoptosis in response to low serum [49]. It is thought that one or more yet unidentified PDZ-domain containing proteins are responsible for the nucleocytoplasmic shuttling of YAP. In addition, PDZ-containing proteins including the Ca^{2+}/calmodulin-associated Ser/Thr kinase (CASK), l-periaxin, ZO-1, MAGI-1c, and LIM-kinase 1 contain nuclear localization signals and shuttle between the cytoplasm and the nucleus [50], [51], [52], [53], [54] and [55].

The small GTP-binding protein RhoA activates p38γ, but not p38α, through MKK3/6 [41]. Similarly, overexpression of the MEK kinase Cot in NIH3T3 cells activates cotransfected p38γ, but not p38α or p38δ [56]. MKK6 activates all p38 isoforms but the efficiency varies between isoforms and with the nature of the stimuli [57]. Remy et al. recently characterized the phosphorylation and activation of each p38 isoform in mouse embryonic fibroblasts (MEF) lacking MKK3 and/or MKK6 in response to hyperosmotic shock, ultraviolet (UV) radiation, anisomycin, and TNFα [25]. These authors showed that MKK3 and MKK6 are both essential for full activation of p38α, p38γ and p38β by environmental stress, whereas MKK6 is the major p38γ activator in response to TNFα. In contrast, MKK3 mediated p38δ activation in response to UV radiation, hyperosmotic shock, anisomycin or TNFα. In the absence of MKK3 and MKK6, MKK4 mediates the activation of p38α [58] but not p38β/δ/γ to UV radiation [25]. These authors concluded that the ability of MKK3 versus MKK6 to

activate an individual p38 isoform is dependent upon the nature and intensity of the stimulus as well cell-specific properties such as the expression level of MKK3, MKK6 and of the p38 isoforms. As the actual effect of activation of a given isoform would, then depend upon its subcellular localization and substrate specificity, p38 signaling may actually be spatially and temporally compartmentalized in physiological systems. Further study is required to understand role of p38γ in the myocyte nucleus during chronic pressure overload.

5. Conclusions

We have shown that p38α and p38γ are present at comparable protein levels in the mouse heart. In addition, 38δ is expressed at protein levels similar to p38β. Although the mRNA abundance for p38β, p38δ, and p38γ changed in response to chronic pressure overload, the corresponding protein levels remained unchanged. Furthermore, p38γ accumulated in nucleus in hypertrophying hearts whereas p38α did not, which might suggest a distinct role for p38γ during the maintenance or progression of ventricular hypertrophy in response to chronic pressure overload.

Abbreviations

DTT, dithiothreitol; ERK, extracellular signal-regulated kinase; GST, glutathione S-transferase; MAPK, mitogen-activated protein kinase; MBP, myelin basic protein; NES, nuclear export signal; PKI, cyclic AMP-dependent protein kinase inhibitory peptide; PAGE, polyacrylamide gel electrophoresis; PMSF, phenylmethylsulfonyl fluoride; TAC, transverse aortic constriction; TX-100, Triton X-100.

Acknowledgments

We thank Dr. Maya Khairallah for her thoughtful discussion and critical reading of the manuscript. This work was supported by grants from the Canadian Institutes of Health Research [MOP-77791] and the Fonds de l'Institut de Cardiologie de Montréal (FICM). BGA and CF were Senior Scholars of the Fondation de la Recherche en Santé du Québec (FRSQ).

The authors declare no conflicts of interest.

References

[1] Z. Chen, T.B. Gibson, F. Robinson, L. Silvestro, G. Pearson, B. Xu, A. Wright, C. Vanderbilt, M.H. Cobb, Chem. Rev. 101 (8) (2001) 2449.

[2] A. Clerk, P.H. Sugden, Circ. Res. 99 (5) (2006) 455.

[3]N.W. Court, C.G. dos Remedios, J. Cordell, M.A. Bogoyevitch, J. Mol. Cell. Cardiol. 3(2002) 413.

[4]K. Ono, J. Han, Cell. Signal. 12 (1) (2000) 1.

[5] K. Seta, J. Sadoshima, J. Mol. Cell. Cardiol. 34 (6) (2002) 597.

[6] B. Ge, H. Gram, F. di Padova, B. Huang, L. New, R.J. Ulevitch, Y. Luo, J. Han, Science 295 (2002) 1291.

[7] J.M. Salvador, P.R. Mittelstadt, T. Guszczynski, T.D. Copeland, H. Yamaguchi, E. Appella, A.J. Fornace Jr., J.D. Ashwell, Nat. Immunol. 6 (2005) 390.

[8] A. Ota, J. Zhang, P. Ping, J. Han, Y. Wang, Circ. Res. 106 (2010) 1404.

[9] N. Gerits, S. Kostenko, U. Moens, Transgenic Res. 16 (3) (2007) 281.

[10] S. Zhang, C. Weinheimer, M. Courtois, A. Kovacs, C.E. Zhang, A.M. Cheng, Y. Wang, A.J. Muslin, J. Clin. Invest. 111 (2003) 833.

[11] R. Kerkela, T. Force, J. Am. Coll. Cardiol. 48 (3) (2006) 556.

[12] C.P. Baines, J.D. Molkentin, J. Mol. Cell. Cardiol. 38 (1) (2005) 47.

[13] X.L. Ma, S. Kumar, F. Gao, C.S. Louden, B.L. Lopez, T.A. Christopher, C. Wang, J.C. Lee, G.Z. Feuerstein, T.L. Yue, Circulation 99 (13) (1999) 1685.

[14] J. Ren, S. Zhang, A. Kovacs, Y. Wang, A.J. Muslin, J. Mol. Cell. Cardiol. 38 (4) (2005) 617.

[15] M. Hasegawa, A. Cuenda, M.G. Spillantini, G.M. Thomas, V. Buee-Scherrer, P. Cohen, M. Goedert, J. Biol. Chem. 274 (18) (1999) 12626.

[16] C. Lechner, M.A. Zahalka, J.F. Giot, N.P. Moller, A. Ullrich, Proc. Natl. Acad. Sci. U. S. A. 93 (9) (1996) 4355.

[17] B. Boivin, D. Chevalier, L.R. Villeneuve, E. Rousseau, B.G. Allen, J. Biol. Chem. 278 (2003) 29153.

[18] B. Boivin, C. Lavoie, G. Vaniotis, A. Baragli, L.R. Villeneuve, N. Ethier, P. Trieu, B.G. Allen, T.E. Hébert, Cardiovasc. Res. 71 (1) (2006) 69.

[19] B. Boivin, L.R. Villeneuve, N. Farhat, D. Chevalier, B.G. Allen, J. Mol. Cell. Cardiol. 38 (2005) 665.

[20] G.A. Keesler, J. Bray, J. Hunt, D.A. Johnson, T. Gleason, Z. Yao, S.W. Wang, C. Parker, H. Yamane, C. Cole, H.S. Lichenstein, Protein Expr. Purif. 14 (2) (1998) 221.

[21] C.P. Connern, A.P. Halestrap, Biochemistry 35 (25) (1996) 8172.

[22] M.M. Bradford, Anal. Biochem. 72 (1976) 248.

[23] L. New, J. Han, Trends Cardiovasc. Med. 8 (5) (1998) 220.

[24] X.J. Du, Br. J. Pharmacol. 152 (2) (2007) 169.

[25] G. Remy, A.M. Risco, F.A. Inesta-Vaquera, B. Gonzalez-Teran, G. Sabio, R.J. Davis, A. Cuenda, Cell. Signal. 22 (2010) 660.

[26] G. Esposito, S.V.N. Prasad, A. Rapacciuolo, L. Mao, W.J. Koch, H.A. Rockman, Circulation 103 (2001) 1453.

[27] M.A. Bogoyevitch, J. Gillespie-Brown, A.J. Ketterman, S.J. Fuller, R. Ben-Levy, A.Ashworth, C.J. Marshall, P.H. Sugden, Circ. Res. 79 (1996) 162.

[28] A. Clerk, J.G. Harrison, C.S. Long, P.H. Sugden, J. Mol. Cell. Cardiol. 31 (12) (1999) 2087.

[29] A. Clerk, P.H. Sugden, Am. J. Cardiol. 83 (12A) (1999) 64H.

[30] S. Kudoh, I. Komuro, Y. Hiroi, Y. Zou, K. Harada, T. Sugaya, N. Takekoshi, K. Murakami, T. Kadowaki, Y. Yazaki, J. Biol. Chem. 273 (37) (1998) 24037.

[31] A.T. Saurin, J.L. Martin, R.J. Heads, C. Foley, J.W. Mockridge, M.J. Wright, Y. Wang, M.S. Marber, FASEB J. 14 (2000) 2237.

[32] S. Kumphune, R. Bassi, S. Jacquet, P. Sicard, J.E. Clark, S. Verma, M. Avkiran, S.J.O'Keefe, M.S. Marber, J. Biol. Chem. 285 (5) (2010) 2968.

[33] K. Otsu, N. Yamashita, K. Nishida, S. Hirotani, O. Yamaguchi, T. Watanabe, S. Hikoso, Y. Higuchi, Y. Matsumura, M. Maruyama, T. Sudo, H. Osada, M. Hori, Biochem. Biophys. Res. Commun. 302 (1) (2003) 56.

[34] Y. Wang, S. Huang, V.P. Sah, J. Ross Jr., J.H. Brown, J. Han, K.R. Chien, J. Biol. Chem. 273 (1998) 2161.

[35] S. Zhang, J. Ren, C.E. Zhang, I. Treskov, Y. Wang, A.J. Muslin, Circ. Res. 93 (11) (2003)1026.

[36] X. Qi, N.M. Pohl, M. Loesch, S. Hou, R. Li, J.Z. Qin, A. Cuenda, G. Chen, J. Biol. Chem. 282 (43) (2007) 31398.

[37] G. Sabio, J.S. Arthur, Y. Kuma, M. Peggie, J. Carr, V. Murray-Tait, F. Centeno, M. Goedert, N.A. Morrice, A. Cuenda, EMBO J. 24 (6) (2005) 1134.

[38] M. Goedert, M. Hasegawa, R. Jakes, S. Lawler, A. Cuenda, P. Cohen, FEBS Lett. 409 (1) (1997) 57.

[39] C.E. Eyers, H. McNeill, A. Knebel, N. Morrice, S.J. Arthur, A. Cuenda, P. Cohen, Biochem. J. 389 (Pt 1) (2005) 127.

[40] A. Cuenda, P. Cohen, V. Buee-Scherrer, M. Goedert, EMBO J. 16 (2) (1997) 295.

[41] M.J. Marinissen, M. Chiariello, J.S. Gutkind, Genes Dev. 15 (5) (2001) 535.

[42] N. Askari, R. Diskin, M. Avitzour, R. Capone, O. Livnah, D. Engelberg, J. Biol. Chem. 282 (1) (2007) 91.

[43] H. Akazawa, I. Komuro, Circ. Res. 92 (10) (2003) 1079.

[44] A. Zetser, E. Gredinger, E. Bengal, J. Biol. Chem. 274 (8) (1999) 5193.

[45] M. Zhao, L. New, V.V. Kravchenko, Y. Kato, H. Gram, F. di Padova, E.N. Olson, R.J.Ulevitch, J. Han, Mol. Cell. Biol. 19 (1) (1999) 21.

[46] B.W. Wang, H. Chang, P. Kuan, K.G. Shyu, J. Endocrinol. 197 (1) (2008) 85.

[47] E. Perdiguero, V. Ruiz-Bonilla, L. Gresh, L. Hui, E. Ballestar, P. Sousa-Victor, B. Baeza-Raja, M. Jardi, A. Bosch-Comas, M. Esteller, C. Caelles, A.L. Serrano, E.F. Wagner, P. Munoz-Canoves, EMBO J. 26 (5) (2007) 1245.

[48] G. Lu, Y.J. Kang, J. Han, H.R. Herschman, E. Stefani, Y. Wang, J. Biol. Chem. 281 (9) (2006) 6087.

[49] T. Oka, M. Sudol, Genes Cells 14 (5) (2009) 607.

[50] C.J. Gottardi, M. Arpin, A.S. Fanning, D. Louvard, Proc. Natl. Acad. Sci. U. S. A. 93 (20) (1996) 10779.

[51] I. Dobrosotskaya, R.K. Guy, G.L. James, J. Biol. Chem. 272 (50) (1997) 31589.

[52] N. Yang, K. Mizuno, Biochem. J. 338 (Pt 3) (1999) 793.

[53] D.L. Sherman, P.J. Brophy, J. Biol. Chem. 275 (7) (2000) 4537.

[54] A. Traweger, C. Lehner, A. Farkas, I.A. Krizbai, H. Tempfer, E. Klement, B. Guenther, H.C. Bauer, H. Bauer, Differentiation 76 (1) (2008) 99.

[55] N. Ojeh, V. Pekovic, C. Jahoda, A. Maatta, J. Cell Sci. 121 (Pt 16) (2008) 2705.

[56] M. Chiariello, M.J. Marinissen, J.S. Gutkind, Mol. Cell. Biol. 20 (5) (2000) 1747.

[57] G. Alonso, C. Ambrosino, M. Jones, A.R. Nebreda, J. Biol. Chem. 275 (51) (2000) 40641.

[58] D. Brancho, N. Tanaka, A. Jaeschke, J.J. Ventura, N. Kelkar, Y. Tanaka, M. Kyuuma, T.Takeshita, R.A. Flavell, R.J. Davis, Genes Dev. 17 (16) (2003) 1969.

Figure Legends

Fig. 1. Cardiac expression of p38 in murine heart. (A) The abundance of the mRNA for each p38 isoform was measured in murine heart total RNA by qPCR. Shown are the mean ± S.E. (n = 5). (B) Purified GST-p38 isoforms (2 μg) were separated on 10–20% acrylamide-gradient SDS-PAGE and visualized using Coomassie Brilliant Blue R250. (C) Isoform selectivity of p38 antibodies. Purified GST-p38 isoforms (5 ng) were separated on 10–20% acrylamide-gradient SDS-PAGE, transferred to nitrocellulose, and probed with the indicated p38 isoform-specific antibodies. (D) Detection of p38 isoforms in mouse heart lysates. Lysates (50 μg) from 2 separate hearts (a, b) were separated on 10–20% acrylamide-gradient SDS-PAGE, transferred to nitrocellulose and probed with the indicated p38 isoform-specific antibody. Detection conditions were separately optimized for each isoform. (E) Quantification of p38 isoforms in mouse heart lysates. Standard curves were constructed for each isoform using the purified recombinant p38 isoforms shown in Fig. 1B. Heart lysates (5 and 50 μg) and were resolved, together with a standard curve of the appropriate p38 isoform, on 10–20% acrylamide-gradient SDS-PAGE, transferred to nitrocellulose, and probed with an appropriate isoform specific antibody. The absolute amount of each isoform was calculated (in fmol), using the predicted molecular mass of the GST-p38 isoform, and expressed per microgram of heart lysate. Numbers at the left indicate the positions of the molecular mass marker proteins (kDa).

Fig. 2. Effect of pressure-overload hypertrophy on p38 expression. Mice were sacrificed 1, 3, and 7 days after constriction of the transverse aorta (TAC) and the hearts isolated. (A) mRNA for each p38 was quantified by qPCR and normalized to GAPDH expression. Shown are the relative abundance of p38α, p38β, p38γ, and p38δ mRNA. (B) To assess p38 expression at the protein level, 50 μg heart lysate were separated on 10–20% acrylamide-gradient SDS-PAGE, transferred to nitrocellulose and probed the indicated antibodies. Detection conditions were separately optimized for each isoform. (C) Phosphorylation of p38 and HSP25 was studied using phosphospecific antibodies. (D) Cardiac fetal gene expression. To confirm that TAC induced a hypertrophic response, in each heart atrial natriuretic peptide (ANP) and β-myosin heavy chain (β-

MHC) mRNA was quantified by qPCR. Shown are the mean ± S.E. (n = 6). ***, $p < 0.001$: **, $p < 0.01$: *, $p < 0.05$: one-way ANOVA with Newman–Keuls post-hoc analysis.

Fig. 3. Changes of p38 mRNA during post-natal heart development. The abundance mRNA each p38 isoform was determined during post-natal heart development. Total RNA was isolated from neonatal, 7 day, 20 day, and adult (8 weeks) hearts and the level of mRNA quantified by qPCR. ((A) p38α, (B) p38β, (C) p38γ, and (D) p38δ). Samples were normalized to GAPDH. Shown are the mean ± S.E. (n = 3). ***, $p < 0.001$: **, $p < 0.01$: *, $p < 0.05$: one-way ANOVA with Newman–Keuls post-hoc analysis.

Fig. 4. Specific activity of p38 isoforms. An aliquot (20 ng) of each activated p38 isoform was incubated with MBP (0.33 mg/ml) and [γ^{32}P]ATP. Reactions were terminated after 2, 5, 8, or 10 min by addition of SDS-PAGE sample buffer. Proteins were separated on 10–20% SDS-PAGE, stained with Coomassie blue, the MBP band excised and ^{32}P incorporation in MBP determined by scintillation counting. ^{32}P incorporation was plotted against time for (A) p38α, (B) p38β, (C) p38γ, and (D) p38δ. Shown are the mean ± S.E. (n = 2).

Fig. 5. Subcellular localization of p38α and p38γ during chronic pressure overload. Mice were sacrificed after 1, 2, or 4 weeks of TAC and 14 μm sections prepared. After fixation and blocking, sections were probed with anti-p38α, anti-p38γ or anti-phospho-p38 (not shown) antibodies and visualized using an ALEXA fluor 448-coupled secondary (anti-rabbit) antibody followed by confocal microscopy. Immunolocalization of p38α and p38γ after (A) 7 days, (B) 14 days, and (C) 28 days of TAC. Nuclei were visualized by staining with TO-PRO 3 iodide. In 14-d samples, actin distribution was also revealed using phalloidin. Shown are the representative images of n = 3 and 3 sections per heart. (D) To confirm that TAC induced a hypertrophic response, sections from each heart were also assessed for expression of B-type natriuretic peptide (BNP) and β-myosin heavy chain (β-MHC). Shown are the mean ± S.E. (n = 3). ***, $p < 0.001$: **, $p < 0.01$: *, $p < 0.05$: one-way ANOVA with Newman–Keuls post-hoc analysis.

Figure 1

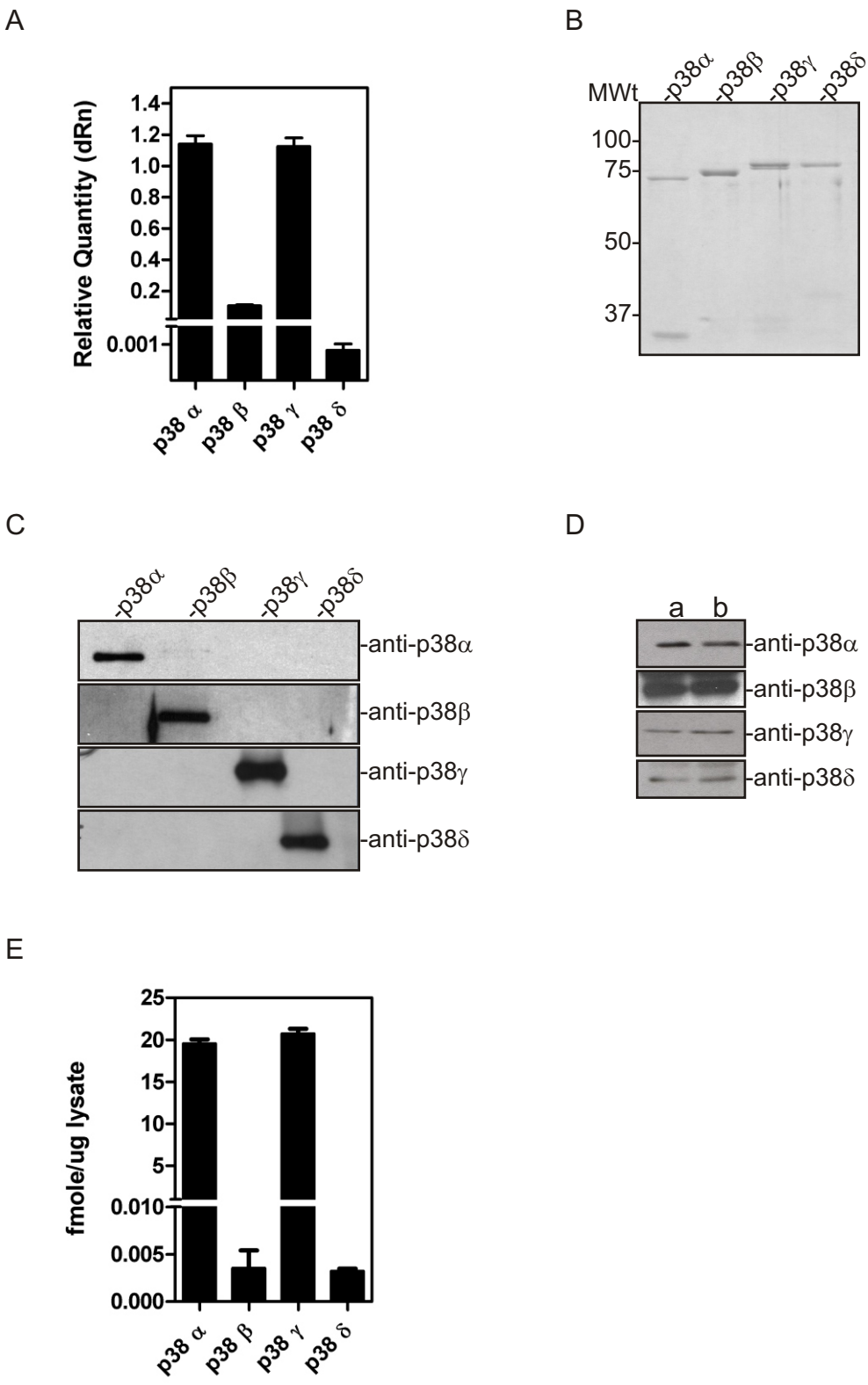
A
Relative Quantity (dRn)
1.4
1.2
1.0
0.8
0.6
0.4
0.2
0.001
p38 α
p38 β
p38 γ
p38 δ
B
MWt
-p38α
-p38β
-p38γ
-p38δ
100
75
50
37
C
-p38α
-p38β
-p38γ
-p38δ
-anti-p38α
-anti-p38β
-anti-p38γ
-anti-p38δ
D
a
b
-anti-p38α
-anti-p38β
-anti-p38γ
-anti-p38δ
E
fmole/ug lysate
25
20
15
10
5
0.010
0.005
0.000
p38 α
p38 β
p38 γ
p38 δ

Figure 2

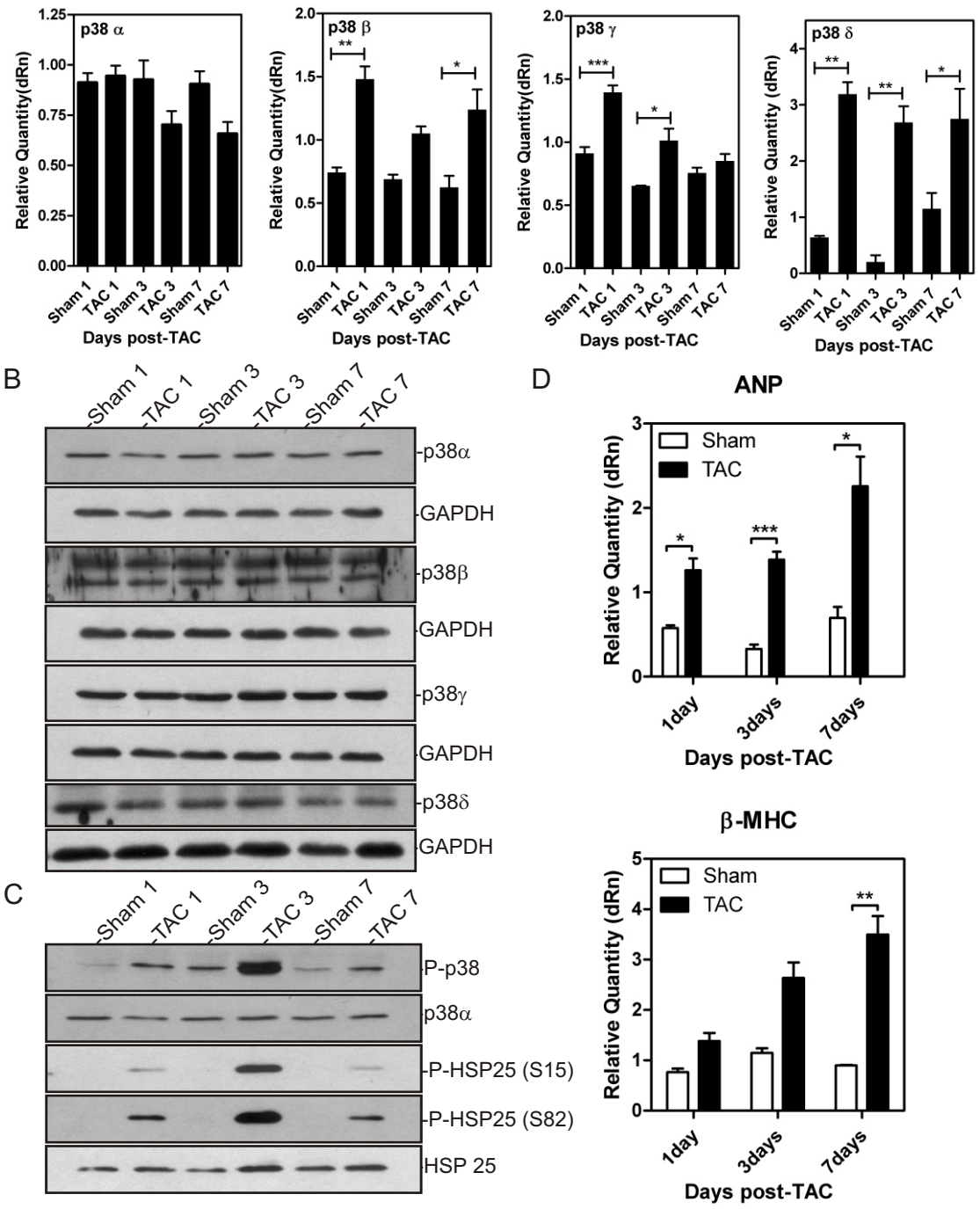
A
p38 α
p38 β
p38 γ
p38 δ
Relative Quantity(dRn)
Relative Quantity (dRn)
Sham 1
TAC 1
Sham 3
TAC 3
Sham 7
TAC 7
Days post-TAC
B
p38α
GAPDH
p38β
GAPDH
p38γ
GAPDH
p38δ
GAPDH
C
P-p38
p38α
P-HSP25 (S15)
P-HSP25 (S82)
HSP 25
D
ANP
Sham
TAC
Relative Quantity (dRn)
1day
3days
7days
Days post-TAC
β-MHC
Sham
TAC
Relative Quantity (dRn)
1day
3days
7days
Days post-TAC

Figure 3

A

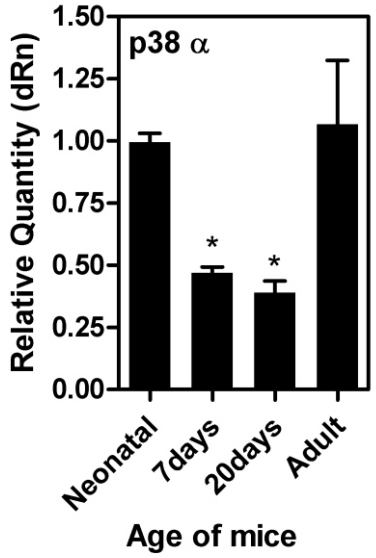

B

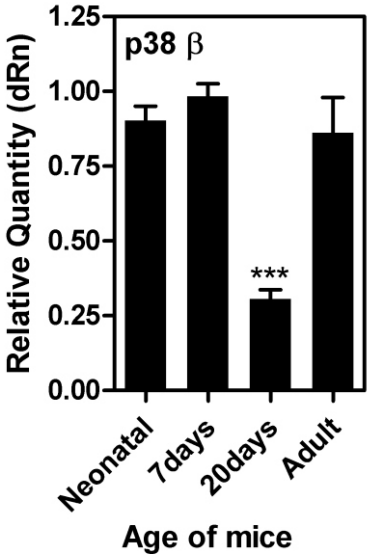

C

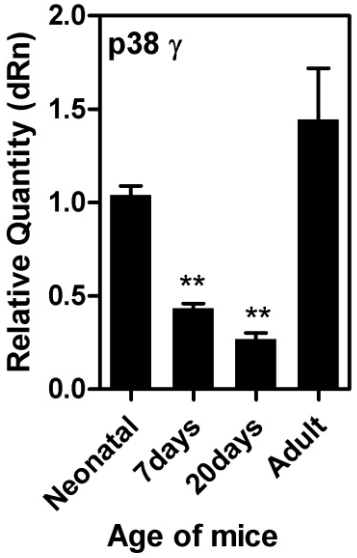

D

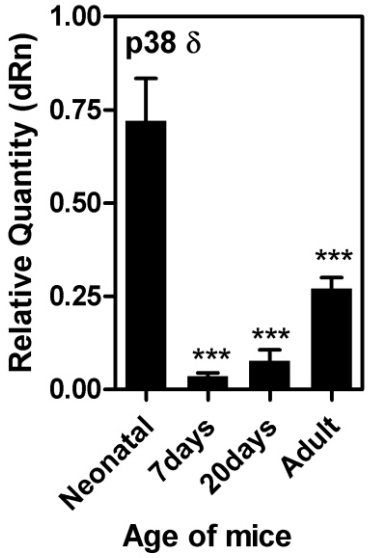

Figure 4

A

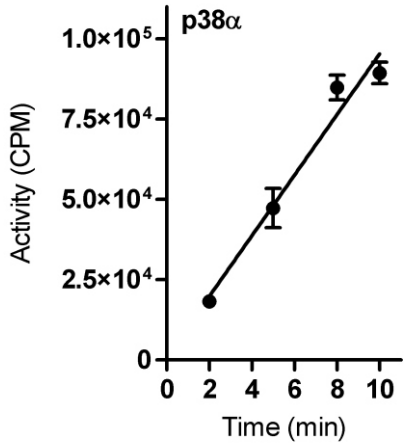

B

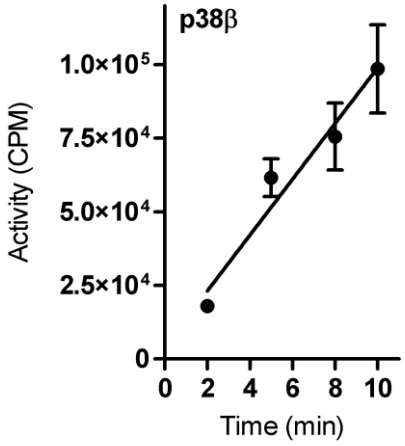

C

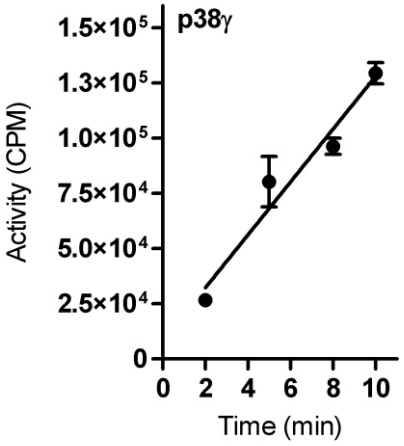

D

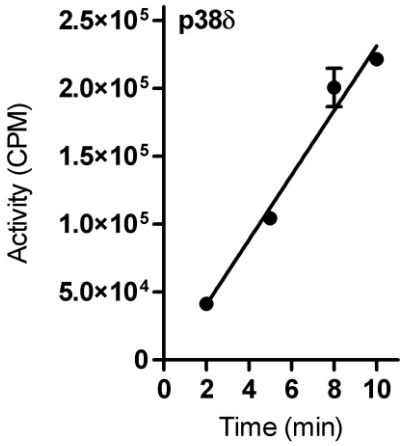

Figure 5A,B

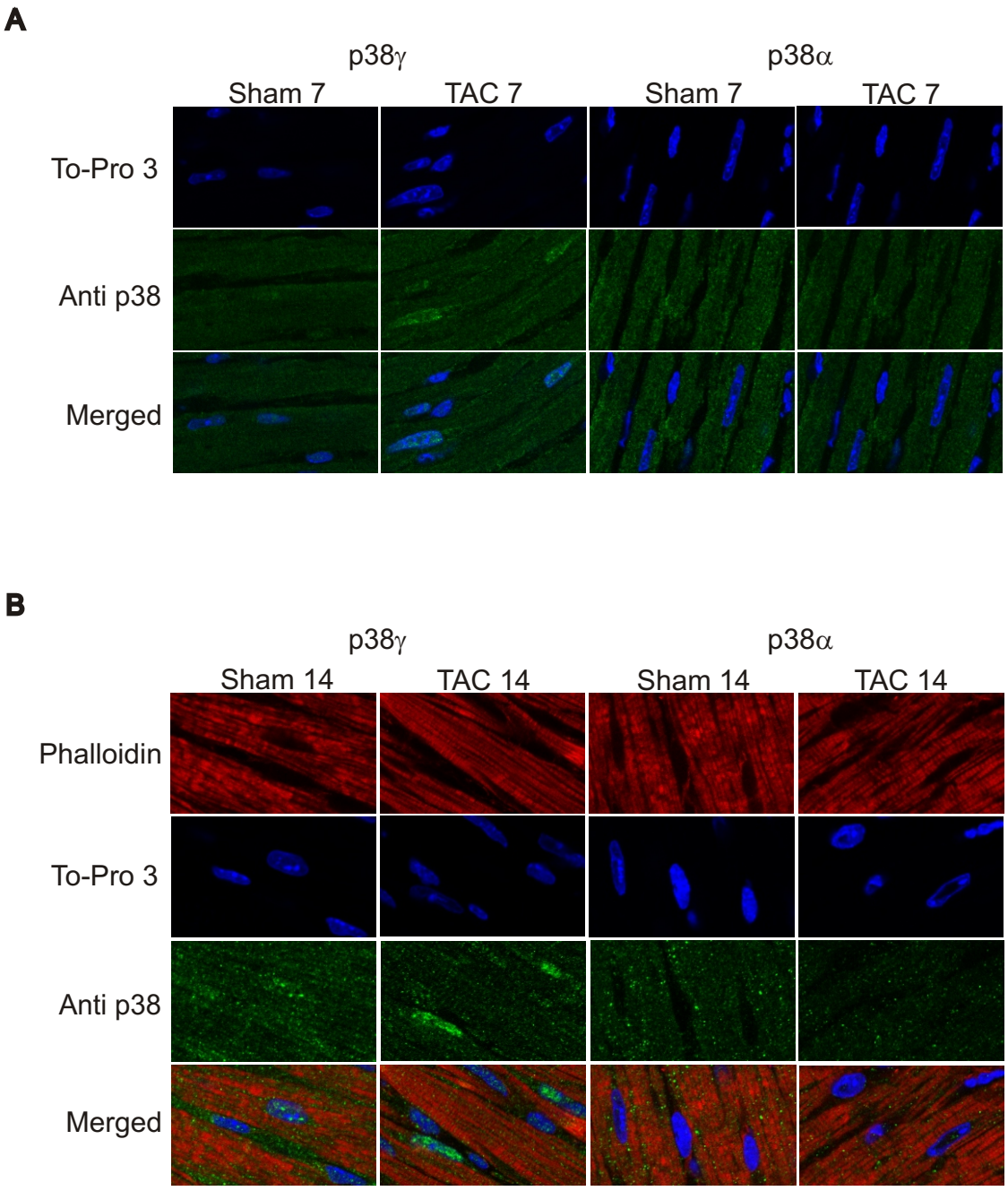
A
p38γ
p38α
Sham 7
TAC 7
Sham 7
TAC 7
To-Pro 3
Anti p38
Merged
B
p38γ
p38α
Sham 14
TAC 14
Sham 14
TAC 14
Phalloidin
To-Pro 3
Anti p38
Merged

Figure 5C,D

C

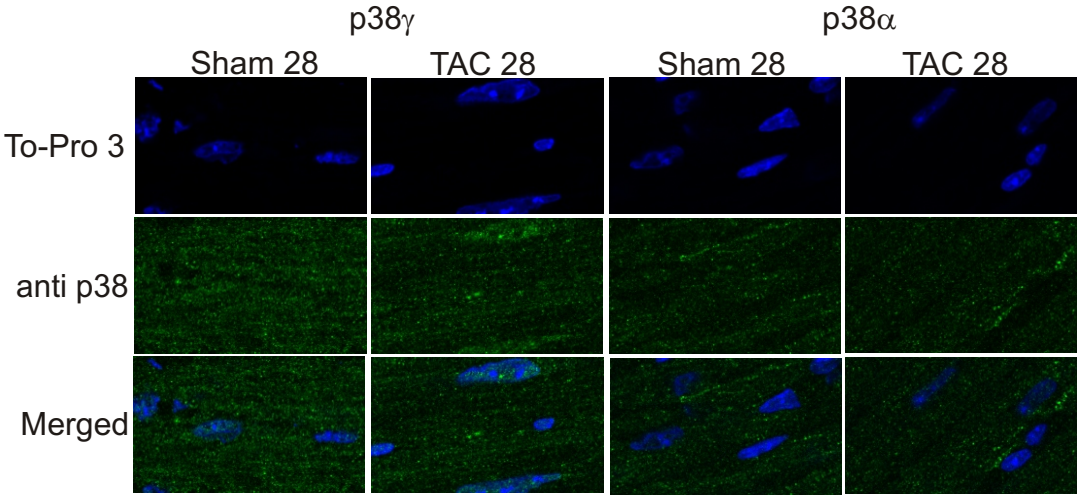

D

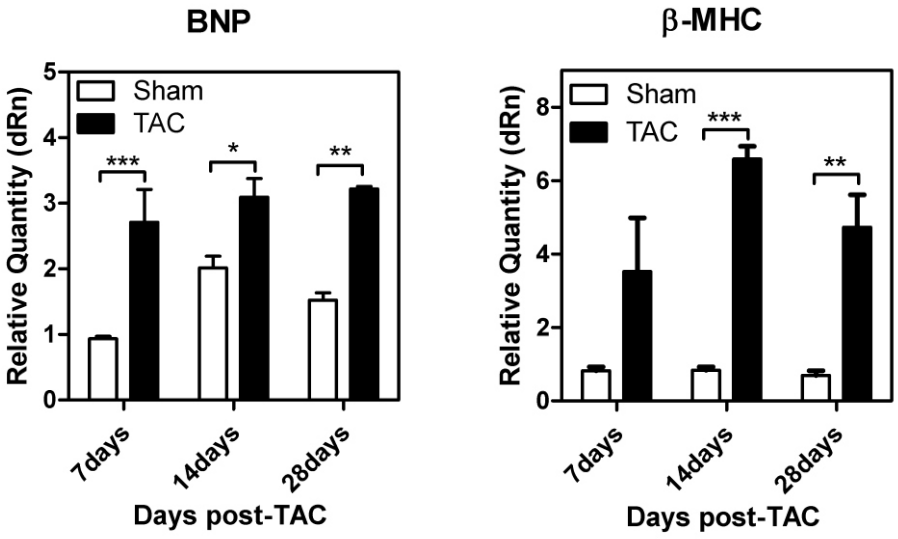

Tables

Table 1**.** Primers used during real-time QPCR.

Target	**Primers**
p38α S	5’- AAT CTC CTC AGA GTC TGC AAG -3’
p38α AS	5’- GCT CTT CCA CTC ATC TAT GAG AAG G -3’
p38β S	5’- GAC CTC AGC AGT GTC TTC CAT -3’
p38β AS	5’- GAG CTG TGA GGG TTC CAG G -3’
p38γ S	5’- TTT GCC TCT GTC CTG ACC AAC -3’
p38γ AS	5’- GGA ACT CTG GCT CCT AGC TGC -3’
p38δ S	5’- GAT TTC ACA CAG CTC TTT CCA CGC -3’
p38δ AS	5’- CCA CAC TGA GTT TCT CAT GTT CT -3’
ANP S	5’-GTG CGG TGT CCA ACA CAG A-3’
ANP AS	5’-TTC TAC CGG CAT CTT CTC CTC-3’
BNP S	5’- GTT TGG GCT GTA ACG CAC TGA-3’
BNP AS	5’-GAA AGA GAC CCA GGC AGA GTC A-3’
β-MHC S	5’-AGG GTG GCA AAG TCA CTG CT-3’
β-MHC AS	5’-CAT CAC CTG GTC CTC CTT CA-3’
GAPDH S	5’-CTG CAC CAC CAA CTG CTT AGC-3’
GAPDH AS	5’-ACT GTG GTC ATG AGC CCT TCC A-3’

S, sense; AS, anti-sense; GAPDH, Glyceraldehyde 3-phosphate dehydrogenase; QPCR, quantitative polymer chain reaction; ANP, atrial natriuretic peptide; BNP, B-type natriuretic peptide; β-MHC, β-myosin heavy chain.

ARTICLE-3

Dingar D, Shi Y, Gillis MA, Meloch S, Gaestel M, Tardif JC, and Allen BG. “ERK3-MK5 regulates interstitial fibrosis in mouse heart during chronic pressure-overload.” In preparation.

ERK3-MK5 regulates interstitial fibrosis in mouse heart during chronic pressure-overload

Dharmendra Dingar[1,2], Yanfen Shi[1], Marc-Antoine Gillis[1], Sylvain Meloche[3], Matthias Gaestel[4], Jean-Claude Tardif [1,5], and Bruce G. Allen[1,2,5,6*]

[1] Montreal Heart Institute, 5000 Belanger St., Montréal, Québec, Canada, H1T 1C8.

[2] Department of Biochemistry, Université de Montréal, Montréal, Québec, Canada, H3C 3J7.

[3] Institute de Recherche en Immunologie et Cancerologie, and Department of Pharmacology and Molecular Biology, Université de Montréal, Montréal, Québec, Canada, H3C 3J7.

[4] Institute of Biochemistry, Hannover Medical School, Carle-Neuberg-strasse 1, 30625 Hannover, Germany.

[5] Department of Medicine, Université de Montréal, Montréal, Québec, Canada, H3C 3J7.

[6] Department of Pharmacology and Therapeutics, McGill University, Montréal, Québec, Canada H3G 1Y6.

* Address for Correspondence: Montreal Heart Institute, 5000 Belanger St., Montréal, Québec, Canada, H1T 1C8. Telephone: (514) 376-3330 (3591). FAX: (514) 376-1355.

Keywords: MK5/PRAK, ERK3, ERK4, Fibrosis, p38 MAP kinase, left ventricular hypertrophy, Chronic pressure overload, Diastolic function

ABSTRACT

Chronic pressure overload induces cardiac left ventricular hypertrophy, fibrosis, and contractile dysfunction, resulting in impaired cardiac function. p38 MAPK is activated during pressure overload and has been implicated in cardiac fibrosis. MK5 is activated by p38 and highly expressed in the heart, but its physiological role remains unknown. This study was to determine if MK5 mediates any of the detrimental effects induced by chronic pressure overload. We studied the effect of transverse aortic constriction (TAC)-induced pressure overload in mice heterozygous for a functional knockout of MK5 ($MK5^{+/-}$) and their wild-type ($MK5^{+/+}$) littermates. Following 2 wks of TAC, heart weight/body weight ratios were significantly and similarly increased in both $MK5^{+/-}$ and $MK5^{+/+}$ hearts. Transthoracic echocardiography revealed TAC impaired left ventricular diastolic and systolic function in $MK5^{+/+}$, but not in $MK5^{+/-}$ hearts. Interestingly, regional differences were observed: MK5 haploinsufficiency was more protective in the basal septum than in the LV basal lateral wall segment. Interstitial fibrosis was not observed in $MK5^{+/-}$ hearts 2 or 3 wks post-TAC. Furthermore, TAC-induced increases in collagen alpha 1 type 1 (COL1A1) mRNA levels were significantly lower in $MK5^{+/-}$ hearts. MK5 is also activated by the atypical MAPKs, ERK3 and ERK4. In both sham and 3 wk TAC hearts, MK5 immunoprecipitates contained ERK3, but not ERK4 or p38α. In $ERK3^{+/-}$ mice, pressure overload failed to induce fibrosis and the induction of COL1A1 expression was attenuated. $MK5^{+/-}$ or $ERK3^{+/-}$ haploinsufficiency did not attenuate the increase in TGFβ1 mRNA induced by pressure overload. Our results demonstrate that ERK3-MK5 signaling plays a role in cardiac fibrosis during pressure overload.

1. Introduction

Cardiac hypertrophy in which individual myocytes grow in length (sarcomeres added in series) and/or width (sarcomeres added in parallel) occurs as a way of decreasing ventricular wall tension and increasing cardiac pump function. It occurs when the myocyte is continuously exposed to increased external stimuli such as stretch, hemodynamic overload and/or an increase in neurohormonal factors. Cardiac hypertrophy is an adaptive response for maintaining cardiac output in response to stress. However, in the long term, hypertrophy predisposes individuals to arrhythmia, heart failure, and sudden death. Hypertrophic stimuli activate a wide variety of signaling pathways in cardiac tissues, such as the mitogen activated protein kinase (MAPK) pathways, calcineurin-nuclear factor of activated T cells (NFAT), and the phosphatidylinositol 3-kinase (PI3K)/protein kinase B (PKB) pathway [1]. Five distinct MAPK pathways have been identified in mammals: extracellular signal-regulated kinases (ERKs) 1/2, ERK3/4, ERK5, c-jun amino-terminal kinases (JNKs) (1-3), and p38 MAPKs (α, β, γ, and δ) [2]. Each pathway displays a characteristic hierarchical organization wherein MAPK kinase kinases (MAPKKK) phosphorylate and activate MAPK kinases (MAPKK), which in turn activate their respective MAPKs. Downstream of certain MAPKs lies an additional level of protein kinases, the MAP kinase-activated protein kinases (MAPKAPKs): these include MK2, MK3 and MK5 (also known as PRAK) [3].

Increased wall stress, due to pressure overload leads to the release of local ligands such as angiotensin II and endothelin-1[4, 5], as well as activation of intrinsic stretch receptors in cardiomyocytes, which includes the integrin family of transmembrane proteins [6, 7]. Furthermore, cultured cardiomyocytes subjected to mechanical stress leads to the activation of extracellular signal regulated kinases (ERK1/2), c-jun N-terminal kinase (JNK), and p38 MAPK, while stress induced release of angiotensin II and endothelin-1 activates ERKs [5, 8], while stretch, independent of angiotensin II release, strongly activates JNK [9], suggesting that JNK might be directly activated by stretch. In the heart, ERK1/2 regulates hypertrophy and also reduces contractility, while p38 MAPK regulates fibrosis, and JNK regulates both fibrosis and hypertrophy [10].

Fibrosis reduces three-dimensional organizations in heart muscle and increases stiffness of myocardium, which causes diastolic dysfunction [11, 12]. Additionally, mice expressing a constitutively active form of MEK5, which activates ERK5, show eccentric cardiac hypertrophy associated with the addition of sarcomeres within individual cardiomyocytes [13]. Finally, atypical MAPKs ERK3 and ERK4 are known to be expressed in the heart but their physiological role remains unknown [14, 15]

MK5 originally classified as a p38 Regulated/Activated Protein Kinase (PRAK) [16, 17], mediates senescence upon activation by p38 in response to induction of oncogenic *ras* [18]. MK5 has 5 splice variants which are regulated during hypertrophy and postnatal heart development [14] and can also be phosphorylated by atypical MAPKs ERK3 and ERK4 [15, 19, 20]. ERK3 and ERK4 show 50% homology with ERK1/2 within the kinase domain but have an S-E-G rather than a T-E-Y motif within the activation loop, contain a unique C-terminal extension and are exclusively found in vertebrates [21]. ERK3 expression is regulated both during transcription [22, 23] and at the protein level via the ubiquitin-proteosome pathway [24, 25]. However, ERK4 is found to be a far more stable protein [15, 26]. In intact cells, ERK3/ERK4 serine is phosphorylated in the S-E-G motif and is required for a stable interaction with, enzymatic activation, and subcellular relocalization of MK5. Once activated, MK5 phosphorylates Ser-386 in both ERK3/ERK4 [27]. ERK3 knock-out mice die within a day after birth from acute respiratory failure, have lower heart, lung, liver, and body weight, and lower insulin-like growth factor (IGF)-2 serum levels [28]. We have previously shown that MK5-ERK3 are in complex, that neither exist alone and that the complex is unaltered during pressure overload, where p38 MAPK is activated [14]. This observation may shed some light on the lack of stable endogenous ERK3 in a MK5 depleted background [20]. Furthermore, $MK5^{-/-}$ mice are viable and show no change in tissue morphology and behavior [29]. Despite having knockout mice the physiological roles of MK5 and ERK3 remain unknown. Although we thought that MK5 may be involved in mediating some of the detrimental effects of p38 activation, given the phosphorylation of MK5 by ERK3/4, we would not be able to exclusively attribute any effects observed in the $MK5^{+/-}$ mice to its activation by p38. As we have show

previously that ERK3, but not ERK4 or p38α, co-immunoprecipitate from heart lysates with MK5 [14] the effects of chronic pressure overload was examined in both MK5 and ERK3 haploinsufficient mice. Here we show that $MK5^{+/-}$ or $ERK3^{+/-}$ mice were resistant to pressure overload-induced cardiac interstitial fibrosis.

2. Materials and methods

2.1. Materials

Membrane grade (reduced) Triton X-100, leupeptin, and PMSF were from Roche Molecular Biochemicals, SDS-polyacrylamide gel electrophoresis reagents, nitrocellulose, and Bradford protein assay reagents were from Bio-Rad. All other reagents were of analytical grade or best grade available.

2.2. *Knockout mice*

MK5 [29] and ERK3 [28] knock-out mice have been described previously. MK5 knockout mice were rederived and backcrossed twice onto a C57BL/6 background. Twelve- to 13-wk old male wild type and knockout mice were used in these studies. $MK5^{-/-}$ mice show embryonic lethality with incomplete penetrance resulting in only about 50% of the expected number of $MK5^{-/-}$ embryos detectable after day E12. Surviving $MK5^{-/-}$ mice fail to reproduce. $MK5^{+/-}$ mice are healthy. $ERK3^{-/-}$ mice do not show embryonic lethality but die within 24 hours of birth. Heterozygous mice were compared with wild-type littermates in the experiments described herein.

All animal experiments were approved by the local ethics committee and performed according to the guidelines of the Canadian Council on Animal Care.

2.3. Transverse aortic constriction

Baseline assessments of cardiac structure and function were performed by transthoracic echocardiography (see below). The following day, transverse aortic constriction was done in adult (12-13 wks) male mice sedated with isofluorane gas as described [30]. Sham animals underwent the identical surgical procedure but the aorta was not constricted. The surgeon was blinded to the genotype of the mice. Two- or 3-weeks after surgery, assessment by transthoracic echocardiography was repeated. The next day, mice were anesthetized with pentobarbital and *in vivo* cardiac function was assessed using a Millar Micro-Tip catheter. Mice were then sacrificed, the hearts removed and heart weighed, snap-frozen in liquid nitrogen-chilled 2-methyl butane, and

stored at -80°C. The surgeon was blinded with respect to the transgenic status of the mice.

2.4. Transthoracic Echocardiography and Calculations

Transthoracic echocardiography was performed on mice, mildly sedated with isofluorane, 1 day before TAC and 1 day before sacrifice using a Vivid 7 Dimension ultrasound system (GE Healthcare Ultrasound, Horten, Norway) and i13L probe (10-14 MHz). Ascending aortae were visualized in a modified parasternal long axis view to assess flow at the site of constriction: peak velocity, peak and mean gradient were measured using sample volume enlarged pulsed wave Doppler (PW). Left ventricular (LV) M-mode spectrum was obtained in parasternal short axis view at the level of papillary muscle. LV dimensions at both end cardiac diastole (LVDd) and systole (LVDs) were measured, the thickness of LV anterior wall (LVAW) and that of LV posterior wall (LVPW) at end cardiac diastole were also measured at this view; LV mass was calculated by $(((LVDd + LVAW + LVPW)^3 - LVDd^3) \times 1.04) \times 0.8 + 0.14$ [31] corrected by LVDd, and body weight (BW). LV fractional shortening (FS) was calculated by (LVDd – LVDs) / LVDd x 100%. LV basal lateral and septal peak systolic velocities (Sm) were derived by tissue Doppler imaging (TDI) to study LV regional contractility. To study LV diastolic properties: pulsed wave Doppler was used to evaluate transmitral flow in apical 4-chamber view, peak velocities in early filling (E), atrial filling (A) were measured. Mitral annulus movement was recorded by TDI, velocities during early filling Em, and atrial filling Am were measured for both lateral and septal annulus, lateral and septal E/Em were calculated. LV isovolumic relaxation time (IVRT) was measured using sample volume enlarged PW at the conjunction of LV inflow and outflow in apical 5-chamber view, and was corrected by the square root of R-R interval [IVRT/(RR)1/2] on simultaneously recorded ECG. The time intervals from the end of Am to the beginning of Em (b), and from the beginning to the end of Sm (a) were measured in both lateral and septal TDI, LV regional myocardial performance index (MPI) was calculated by (b-a)/a x 100% for both basal lateral and basal septal wall.The average of three consecutive cardiac cycles was used for each measurement.

Special care was taken to obtain similar imaging planes during pre-operative and pre-sacrifice assessments for each animal. The echocardiographer was blinded to the genotype of the mice.

2.5. Histological analysis

Hearts were embedded in Tissue-Tek O.C.T. compound (Sakura Finetek USA, inc.) and longitudinal cryosections (8 μm) of the ventricles were prepared and stained with Masson trichrome. Images were taken at 10X.

2.6. Quantitative real time-PCR

Total cellular RNA was isolated from longitudinal cryosections (14 μm) of murine ventricular myocardium using RNeasy® Micro kits (Qiagen Inc.) with minor modifications. Total RNA was extracted by vortexing tissue section in 300 μl TRIzol reagent (Sigma) for 30 s. After incubating at ambient temperature for 5 min, 60 μl chloroform was added, samples were again vortexed, and maintained at ambient temperature for an additional 2-3 min. After centrifugation for 15 min at 18,300 x g and 4°C, the upper aqueous phase was collected, diluted with an equal volume of 70% ethanol, and total RNA purified on Qiagen columns according to the manufacturers instructions. Finally total RNA was eluted with 14 μl of distilled, RNAse-free water. As the quantity of RNA recovered was too small to permit quantification of total RNA, cDNA synthesis was performed with 11 μl of the isolated total RNA in 20 μl reaction volume as described previously [14]. The primers used are shown in Supplemental Table 1.

2.7. Immunoblotting

SDS-PAGE and immunoblotting were performed as described previously [32]. Following the transfer, nitrocellulose membranes were rinsed in PBS and fixed with glutaraldehyde [33] prior to blocking.

2.8. Statistical Analysis

Quantitative analysis for qPCR was performed by single observer in a blinded manner. One-way ANOVA followed by Newman-Keuls test was performed for the statistical comparisons. Values were shown mean and SEM, ***, $p < 0.001$: **, $p < 0.01$: *, $p < 0.05$.

3. Results

Chronic pressure overload induces cardiac hypertrophy, reexpression of fetal genes, interstitial fibrosis, and activation of MAPKs, including p38 [34]. Chronic activation of p38 induces interstitial fibrosis, but not hypertrophy [35]. In contrast, acute activation of p38 results in the rapid induction of a severe cardiomyopathy that includes myocyte hypertrophy, interstitial fibrosis, and contractile dysfunction [36]. MK5 is a downstream effector of p38 [3, 17, 37] that is expressed in the heart yet has, as of yet, no identified physiological or pathophysiological function. The objective of the present study was to determine if MK5 plays a role in pathological cardiac remodeling induced by chronic pressure overload. We employed mice heterozygous for a functional knockout of MK5 ($MK5^{+/-}$) and their wild-type ($MK5^{+/+}$) litter mates. These mice have been described elsewhere [29].

3.1. Transthoracic echocardiographic characterization of MK5 haploinsufficient mice.

Echocardiographic examination of 12-wk old male $MK5^{+/+}$ and $MK5^{+/-}$ mice revealed no significant differences in cardiac structure, systolic, or diastolic function (Supplemental Table 2).

3.2. Effect of MK5 haploinsufficiency on pressure overload-induced hypertrophy

$MK5^{+/+}$ and $MK5^{+/-}$ mice underwent transverse aortic constriction (TAC) and were sacrificed 2 wks post-surgery. All mice were assessed by transthoracic echocardiography 1 day before surgery and 1 day prior to sacrifice. Direct hemodynamic assessment using a Millar Micro-Tip catheter showed that TAC induced comparable increases in systolic and mean arterial pressure (Table 1) as well as peak left ventricular pressure in $MK5^{+/+}$ and $MK5^{+/-}$ mice (Fig. 1A). Echocardiographic imaging of the ascending aorta was performed to assess cross-TAC aortic flow and revealed comparable changes in hemodynamics (Table 2). Following TAC, heart weight to body weight ratios (HW/BW) were increased by 32% in $MK5^{+/+}$ (from 4.9±0.4 mg/g to 6.5±0.4 mg/g, $p<0.01$) and by 42% in $MK5^{+/-}$ (4.5±0.1 mg/g to 6.4±0.3 mg/g, $p<0.01$)

(Fig. 1B). The increased HW/BW ratio in $MK5^{+/+}$ and $MK5^{+/-}$ indicated the development of similar levels of hypertrophy in both groups. Echocardiographic analysis of LV mass/body weight ratio (LVM/BW) confirmed similar levels hypertrophy in $MK5^{+/+}$ and $MK5^{+/-}$ hearts post-TAC (Table 2). In $MK5^{+/+}$ mice the LVM/BW ratio increased by 29% after TAC (from 7.8±0.4 mg/g to 10.1±0.3 mg/g, $p>0.05$), and in $MK5^{+/-}$ by 23% (from 8.0±0.2 mg/g to 9.8±0.5 mg/g, $p<0.05$). Hence, MK5 haploinsufficiency did not alter left ventricular hypertrophy in response to pressure overload.

3.3. Gene expression in $MK5^{+/-}$ mice following TAC

Pathological LV hypertrophy is associated with the re-expression of cardiac fetal genes atrial and B-type natriuretic peptides (ANP, BNP) and beta-myosin heavy chain (β-MHC) [38]. Hence ANP, BNP, and β-MHC mRNA levels were quantified by qPCR. Pressure-overload increased β-MHC, ANP, and BNP mRNA levels in $MK5^{+/+}$ and $MK5^{+/-}$ hearts; however, the increase in BNP mRNA was less pronounced in $MK5^{+/-}$ hearts and the increase in ANP mRNA failed to reach significance (Fig. 2). There was no significant difference in ANP, BNP, and β-MHC mRNA levels between $MK5^{+/-}$ and $MK5^{+/+}$ in sham-operated hearts. In summary, MK5-deficiency did not prevent molecular remodeling in response to pressure overload: however, the increases in ANP and BNP mRNA abundance were attenuated.

3.4. Echocardiographic characterization of $MK5^{+/-}$ mice following TAC

Ventricular function was assessed by echocardiography. LV Fractional shortening (FS) and ejection fraction (EF) were similarly reduced in $MK5^{+/+}$ and $MK5^{+/-}$ mice following 2 wk of pressure overload (Table 2). In response to TAC, early transmitral flow velocity (E) was significantly increased ($p<0.05$) in $MK5^{+/-}$ mice whereas in $MK5^{+/+}$ mice the increase in E wave velocity did not reach significance. Tissue Doppler imaging was employed to assess systolic (Sm) and early diastolic (Em) myocardial velocities of the basal segments of interventricular septum and basal lateral

LV wall. Lateral-Sm was reduced by pressure overload in both $MK5^{+/+}$ and $MK5^{+/-}$ hearts whereas septal-Sm was reduced in $MK5^{+/+}$ but not $MK5^{+/-}$ hearts. Lateral-Em was unaffected by pressure overload in $MK5^{+/+}$ mice whereas septal-Em was actually higher in $MK5^{+/-}$ hearts following pressure overload. The ratio of early transmitral flow velocity to diastolic myocardial velocity (E/Em), an index of LV filling pressure, was significantly higher in banded $MK5^{+/+}$ mice than in both sham mice and band $MK5^{+/-}$ mice. Furthermore, isovolumetric relaxation time (IVRT, IVRTc) and myocardial performance index (MPI) were elevated in banded $MK5^{+/+}$ but not $MK5^{+/-}$ hearts. Hence, MK5 haploinsufficiency had a beneficial effect on myocardial tissue velocities during chronic pressure overload that was more pronounced in the basal septal than the basal lateral LV segment. Furthermore, hearts from $MK5^{+/-}$ mice showed improved diastolic function during chronic pressure-overload in comparison with $MK5^{+/+}$ hearts.

3.5. $MK5^{+/-}$ hearts are resistant to fibrosis

In addition to LV hypertrophy and molecular remodeling, pressure overload induces interstitial fibrosis, resulting in increased myocardial stiffness. Hence, collagen accumulation was examined in cryosections of the ventricular myocardium by Masson trichrome staining. Pressure overload resulted in increased collagen deposition (stained blue) in $MK5^{+/+}$ hearts but not in $MK5^{+/-}$ hearts (Fig. 3A,B). No genotype-dependent differences in collagen deposition were observed in sham hearts. Collagen type 1 accounts for approximately 85% of the total collagen content of the heart. Consequently, collagen alpha 1 type 1 (COL1A1) mRNA levels were measured by qPCR and found to increase as a result of pressure overload (Fig. 3C). This increase, however, was reduced by 50% in $MK5^{+/-}$ hearts compared with $MK5^{+/+}$ hearts. No significant difference was observed in COL1A1 mRNA levels between sham $MK5^{+/+}$ and $MK5^{+/-}$ hearts, suggesting that formation of a normal extracellular matrix was not adversely affected in $MK5^{+/-}$ mice.

To determine if the effect of MK5 haploinsufficiency was preventing or merely delaying interstitial fibrosis, a separate group of mice underwent TAC and were sacrificed 3 wk post-surgery. Unexpectedly, although direct assessment of

hemodynamic function indicated TAC induced similar increases in peak aortic BP and peak LVP (supplemental Fig 1A, Supplemental Table 3) in $MK5^{+/+}$ and $MK5^{+/-}$ mice, HW/BW increased by 64% in $MK5^{+/+}$ mice (from 4.4±0.2 mg/g to 7.3±0.4 mg/g, $p<0.001$) following 3 wk of pressure overload, whereas $MK5^{+/-}$ hearts showed only a 27% increase (from 4.5±0.2 mg/g to 5.8±0.6 mg/g) (Supplemental Fig. 1B). MK5 haploinsufficiency did not alter body weight (data not shown). Three weeks of pressure-overload increased β-MHC, ANP, and BNP mRNA levels in $MK5^{+/+}$ and $MK5^{+/-}$ hearts (Supplemental Fig. 1C,D,E). As observed following 2 wk of pressure overload, Masson trichrome staining revealed increased collagen deposition in $MK5^{+/+}$ but not $MK5^{+/-}$ hearts 3 wk post-TAC (Fig. 3B). Similarly, the increase in COL1A1 mRNA induced by pressure overload was significantly reduced in $MK5^{+/-}$ hearts (Fig. 3C). These results suggest that MK5 activation is involved in cardiac interstitial fibrosis in response to pressure-overload.

3.6. MK5-ERK3 signaling in the heart

Atypical MAPKs ERK3 and ERK4 are known bind to and regulate the activation of MK5, and it is currently controversial whether MK5 is regulated by p38 and/or ERK3/4 *in vivo*. In lysates prepared from control, sham-operated, or 3-d post-TAC mouse hearts, ERK3, but not ERK4 or p38α, co-immunoprecipitated with MK5 [14]. Given the involvement of MK5 activity in reactive fibrosis, we sought to determine if chronic exposure to pressure overload altered the composition of MK5 complexes in mouse heart. To this end, we assessed if ERK3, ERK4, or p38α co-immunoprecipitated with MK5 in lysates from sham and TAC hearts 3-wks post-surgery. In each case, ERK3 co-immunoprecipitated with MK5 whereas p38α and ERK4 immunoreactivity was not detected (Fig. 4A). Immunoblotting using an anti-phospho-p38 antibody confirmed activation of the p38 pathway in banded hearts. ERK3, ERK4 and p38α protein levels were unaffected by pressure overload (Fig. 4B). Thus, MK5 is in a complex with, and regulated by, ERK3 in the mouse heart during pressure overload. Hence we sought to determine if ERK3 also plays a role in reactive fibrosis.

3.7. Transthoracic echocardiographic characterization of ERK3 haploinsufficient mice.

Conventional echocardiographic examination of 12-wk old male $ERK3^{+/+}$ and $ERK3^{+/-}$ mice revealed no significant differences in left ventricular diameter, wall thickness, MPI, as well or transmitral flow velocities (Table 3). Tissue Doppler imaging revealed no change in basal lateral LV or basal septal Sm velocities but a reduction in both basal septal and basal lateral LV segment Em, indicating that LV compliance was reduced in $ERK3^{+/-}$ compared to $ERK3^{+/+}$ mice.

3.8. Hypertrophic response in ERK3 haploinsufficient mice following TAC

$ERK3^{+/+}$ and $ERK3^{+/-}$ mice [28] underwent TAC and were sacrificed 3 wk post-surgery. Direct assessment of hemodynamic function using a Millar catheter revealed that systolic and mean aortic BP as well as peak LV pressure increased similarly in banded $ERK3^{+/+}$ and $ERK3^{+/-}$ mice (Fig. 5A, Table 4). Following TAC, HW/BW increased by 44% (from 4.7±0.1 mg/gm to 6.7±0.4 mg/gm, $p<0.001$) in $ERK3^{+/+}$ mice and by 34% (from 4.6±0.1 mg/g to 6.2±0.2 mg/g, $p<0.001$) in $ERK3^{+/-}$ mice (Fig. 5B). Hence, pressure overload induced LV hypertrophy in both $ERK3^{+/+}$ and $ERK3^{+/-}$ mice. Moreover, the HW/BW was the same in both sham-operated groups. Newborn $ERK3^{-/-}$ and $ERK3^{+/-}$ mice have significantly lower body weight as compared to their wild type littermates. Newborn $ERK3^{-/-}$ mice also exhibit a reduction in absolute heart weight in comparison with $ERK3^{+/+}$ litter mates [28]. Adult (12-13 wks) $ERK3^{+/+}$ and $ERK3^{+/-}$ mice did not differ in heart or body weight (Fig. 5C,D). Hence, the effects of ERK3 haploinsufficiency on growth normalized with age. Furthermore, ANP, BNP, and β-MHC mRNA levels were assessed in RNA isolated from $ERK3^{+/+}$ and $ERK3^{+/-}$ hearts. Following TAC, BNP and β-MHC mRNA levels increased significantly in $ERK3^{+/+}$ and $ERK3^{+/-}$ hearts. Interestingly, while ANP increased significantly in $ERK3^{+/+}$ hearts, pressure overload did not induce an increase in ANP mRNA in $ERK3^{+/-}$ hearts (Fig. 5E). In conclusion, ERK3 haploinsufficiency did not prevent the development of left ventricular hypertrophy or the increase in BNP and β-MHC mRNA in response to chronic pressure-overload.

3.9. Echocardiographic assessment of ERK3$^{+/-}$ mice after 3 weeks of pressure overload

Echocardiographic imaging of the ascending aorta was performed to assess cross-TAC aortic flow and revealed comparable changes in hemodynamics although the cross-TAC peak velocity and peak gradients were lower in banded ERK3$^{+/-}$ than ERK3$^{+/+}$ mice. Echocardiography confirmed that both ERK3$^{+/+}$ and ERK$^{+/-}$ hearts hypertrophied in response to pressure overload. However, surprisingly, although pressure overload induced hypertrophy in both ERK3$^{+/+}$ and ERK3$^{+/-}$ mice, none of the functional parameters assessed by echo were altered (Table 5). As the MK5 and ERK3 mice were in different background strain, this strain difference might underlie that ability of TAC to alter cardiac function in the MK5 mice but not the ERK3 mice. A comparison of these 2 strains by echocardiography revealed numerous differences (Supplemental Table 4).

3.10. ERK3$^{+/-}$ hearts are resistant to fibrosis following TAC

Masson trichrome staining revealed that pressure overload increased collagen deposition (stained blue) in ERK3$^{+/+}$ hearts but not in ERK3$^{+/-}$ hearts (Figure 6A). No collagen deposition was observed in sham hearts. Similarly, COL1A1 mRNA levels were significantly increased in ERK3$^{+/+}$, but not ERK3$^{+/-}$ hearts, in response to TAC (Fig. 6B). These results suggest a role for ERK3 in the development of cardiac fibrosis in response to chronic pressure-overload.

3.11. Assessment of TGF-β expression in ERK3 and MK5 mice post-TAC

TGF-β1 controls the development of cardiac fibrosis through the activation of its receptor (TGF-β receptor type 1 and type 2), which phosphorylates Smads 2 and 3 (reviewed in [39]). Therefore, we assessed TGF-β1 and TGF-β3 mRNA levels by qPCR in total RNA from sham and banded hearts. TGF-β1 and TGF-β3 mRNA levels were increased significantly in both MK5$^{+/+}$ and MK5$^{+/-}$ hearts both 2- and 3-wks post-TAC (Fig. 7A). Similarly, pressure overload increased TGF-β1 mRNA levels both ERK3$^{+/+}$

and ERK3$^{+/-}$ hearts (Fig. 7B). In contrast, whereas TGF-β3 mRNA content was significantly increased in ERK3$^{+/+}$ hearts in response to TAC, the increase observed in ERK3$^{+/-}$ hearts did not reach significance. Interestingly, the relative abundance of both TGF-β1 and TGF-β3 mRNA was lower in ERK3$^{+/-}$ hearts than in there respective ERK3$^{+/+}$ counterparts. In summary, MK5 and ERK3 haploinsufficiency did not prevent the pressure-overload-induced increase in TGFβ1 mRNA.

4. Discussion

The physiological function of MK5 and atypical MAPKs ERK3/ERK4 are currently unknown. We show that, in response to chronic pressure overload, hearts from $MK5^{+/-}$ mice reexpressed fetal genes (e.g., ANP, BNP, β-MHC) and hypertrophied but were resistant to myocardial interstitial fibrosis. Although MK5 has been shown to be activated both by p38α/β [17] and ERK3/4 [15, 19, 20, 27], in the mouse heart, MK5 is bound to ERK3 but not ERK4 or p38α [14]. In addition, although pressure overload elevated phospho p38 levels in comparison to sham-operated mice, MK5 immune complexes contained ERK3, but not p38α or ERK4 immunoreactivity. Similar to $MK5^{+/-}$ hearts, $ERK3^{+/-}$ hearts underwent molecular remodeling and hypertrophied in response the pressure overload, but fibrosis was not detected. These results imply a role for ERK3-MK5 signalling in pressure overload-induced myocardial interstitial fibrosis.

Pressure overload induced activation of p38α and p38β and translocation of p38 into the nucleus [40, 41]. Transfecting neonatal myocytes with activated mutants of MAP kinase kinase 6b (MKK6b) or MKK3b, upstream activators of p38β and p38α, evokes changes characteristic of the hypertrophic phenotype and apoptosis, respectively [40]. In the intact heart, the situation appears more complicated. Chronic inhibition of p38 signaling, using cardiac-directed expression of DN-p38α, DN-p38β, DN-MKK3, or DN-MKK6, facilitates cardiac hypertrophy, expression of fetal genes (ANP and BNP), but not fibrosis, in response to pressure overload [35, 42] or infusion of Ang II, isoproterenol, or phenylephrine (PE) [42]. In addition, cardiac-specific expression of constitutively active MKK3bE or MKK6bE results in cardiac fibrosis and systolic and diastolic dysfunction, but not hypertrophy [43] in some cases, but hypertrophy in others [44]. Expression of an activated form of TAK1, an MKKK, in heart resulted in p38 activation associated with hypertrophy [45]. Cardiac-specific $p38\alpha^{-/-}$ mice exhibit hypertrophy in response to aortic banding, but also show cardiac dysfunction and dilation accompanied by massive fibrosis and myocyte apoptosis [46]. One explanation for the differences observed using *in vivo* models is that the chronic nature of the modification in p38 signaling employed in these models may interfere with other aspects of intracellular signalling or induce compensatory mechanisms. The role of p38 in

hypertrophy may depend upon the nature and duration of the hypertrophic stimulus [46-48] as the nature and intensity of the stimuli can alter which p38 isoforms become activated [49]. In fact, mice having life-long changes in p38 signaling may have developed compensatory mechanism. Consistent with this, a recent report showed that the acute activation of p38α, induced by the conditional and myocyte-specific expression of MKK3bE, in the adult mouse heart resulted in the rapid onset of a severe cardiomyopathy involving impaired cardiac function, hypertrophy, and interstitial fibrosis [36]. Hence, it would appear that inhibition of p38 would be a desirable pharmacological intervention in the treatment of cardiovascular disease. However, no inhibitors have progressed to phase III clinical trials due, in part, to adverse effects including hepatotoxicity, skin rash, and dizziness [50]. In addition, as the means whereby p38 mediates deleterious effects upon cardiac structure and function remains unknown, a better understanding of the roles and regulation of downstream targets of p38 is important. *In vitro* and *in vivo* studies have suggested the involvement of MK5 downstream of p38 MAPK [16-18, 37, 51]. The biological role of MK5 remains unknown; however, $MK5^{+/-}$ mice underwent hypertrophy and molecular remodeling in response to chronic pressure overload, they were resistant to cardiac interstitial fibrosis. These results suggest that MK5 may mediate the pro-fibrotic effects of p38 activation in the heart. However, MK5 is also regulated by atypical MAPKs ERK3/ERK4 [15, 19, 20] and in the heart MK5 appears to associate with ERK3, but not ERK4 or p38α [14]. Similarly, following 3 wks of pressure overload ERK3, but not p38 or ERK4, co-immunoprecipitated with MK5. In fact, it has been controversial whether or not MK5 and p38 for a complex *in vivo*. Tandem affinity purification studies did not detect p38α-MK5 complexes in HEK293 cells [29] whereas MK5 and p38 co-immunoprecipitate when over expressed in NIH3T3 cells [52, 53]. Alternatively, activation of p38 causes relocalization of MK5 from the nucleus to the cytosol and this relocalization is blocked upon mutating the putative p38-docking motif in MK5 [14, 37, 51, 52]. Consistent with a functional role for ERK3-MK5 signalling in the myocardium, $ERK3^{+/-}$ mice underwent hypertrophy and molecular remodeling, but not fibrosis, in response to chronic pressure overload, in a manner similar to $MK5^{+/-}$ mice. Taken together, these

results indicate that the increased myocardial interstitial fibrosis induced by pressure overload involves ERK3-MK5 signalling.

Chronic pressure overload induces cardiac fibroblast proliferation, increased interstitial fibrosis, and remodeling of the extracellular matrix. Cardiac interstitial fibrosis can result from either enhanced collagen deposition or reduced degradation. Collagen type I and type III are the major components of the cardiac ECM with collagen type 1 comprising approximately 85% of total collagen in the heart and hence representing a major determinant for myocardial stiffness [54, 55]. In both $MK5^{+/-}$ and $ERK3^{+/-}$ hearts, pressure overload failed to induce a noticeable increase in collagen accumulation within 3 weeks. This was accompanied by a significant reduction in the ability of pressure overload to increase COL1α1 mRNA synthesis and/or stability. TGFβ is a growth factor expressed in both myocytes and fibroblasts that acts upon receptors that are also expressed in both cell types. In ventricular myocytes TGFβ induces molecular remodeling and hypertrophy [56] whereas in fibroblasts, it induces proliferation, differentiation to myofibroblasts, and production of ECM proteins including collagen, fibronectin, and proteoglycans [39]. TGFβ also reduces ECM breakdown by both inhibiting matrix metalloproteinase (MMP) expression and by inducing the synthesis of MMP inhibitors, such as plasminogen activator inhibitor-1 (PAI-1) and tissue inhibitors of metalloproteinases (TIMPs) [57]. As shown previously [58, 59], pressure overload increased myocardial TGFβ1 and TGFβ3 mRNA and this increase was unaffected by MK5 haploinsufficiency. A similar expression pattern for TGFβ1 was observed in $ERK3^{+/-}$ hearts. In contrast, pressure overload failed to induce an increase in TGFβ3 mRNA in $ERK3^{+/-}$ hearts. Very little is curently know regarding the role of TGFβ3 in cardiac remodeling; however, a polymorphism of TGFβ3 is associated with changes in LV geometry in hypertensive patients [60]. β-AR signaling has been implicated downstream of TGFβ1 and the catalytic subunit of protein kinase A (PKA) was recently shown to phosphorylate MK5, resulting in its activation and translocation out of the nucleus [61, 62]. However, as β_1-AR blockade in mice overexpressing TGFβ1 is antihypertrophic but not antifibrotic [63] whereas MK5 haploinsufficiency prevented fibrosis, it is unlikely that MK5 haploinsufficiency is

preventing fibrosis by attenuating TGFβ1/βAR signalling in the heart. In summary, $MK5^{+/-}$ or $ERK3^{+/-}$ prevented pressure-overload induced fibrosis and attenuated increases in COL1α1 expression without blocking increased TGFβ expression or preventing LV hypertrophy, implicating MK5-ERK3 post-TGFβ receptor signalling in cardiac fibroblasts.

Although $MK5^{+/-}$ and $ERK3^{+/-}$ mice showed similar reductions in the ability of pressure overload to induce myocardial interstitial fibrosis, MK5- and ERK3-deficient mice show markedly different phenotypes. In fact, $MK5^{-/-}$ mice either show no obvious phenotype or embryonic lethality with incomplete penetrance, resulting in 50% of the predicted $MK5^{-/-}$ offspring, depending upon the genetic background of the mice [64]. $ERK3^{-/-}$ mice do not show embryonic lethality but die within 24 hours of birth [28]. Around 40% of $ERK3^{-/-}$ neonates show severe respiratory distress and die within 15 min of delivery. In addition, ERK3-deficient mice show evidence of intrauterine growth restriction (IUGR) [28]. Heart, lung and liver weights are 25-40% lower in E18.5 $ERK3^{-/-}$ embryos than their $ERK3^{+/+}$ litter mates. At birth, $ERK3^{-/-}$ and $ERK3^{+/-}$ mice are of significantly lower body weight than wild type mice [28]. In humans, IUGR affects 5-10% of all newborns and is defined as having a birth weight below the 10^{th} percentile for gestational age [65]. Fetal growth restriction (birth weight adjusted for gestational age) is associated with an increased incidence of hypertension, diabetes mellitus, and cardiovascular mortality in adulthood [66, 67]. Crispi et al recently demonstrated that IUGR induced adaptive cardiovascular changes that persist in childhood [68]. Specifically, children having undergone IUGR have hearts that are larger in diameter, with normal wall thickness, resulting in dilated ventricular chambers. Reduced stroke volume was compensated for by increased heart rate and vascular assessment revealed increased systolic and diastolic blood pressure. Although ejection fraction remained unchanged, assessment of cardiac function by echocardiography revealed significant reduction in both septal and lateral S and E velocities, indicating changes in both systolic and diastolic function. Follow studies also revealed the children with IUGR remained of lower body weight and size in comparison with control children (age range 2-6 yr). In contrast, by the age of 15 weeks, $ERK3^{+/-}$ mice did not differ significantly

from wild type in terms of body weight, heart weight or LV diameter. Hence these mice had recovered from IUGR in terms of growth and the shape of the heart remained unaffected. Whereas early S wave velocity was reduced in IUGR children, in ERK3$^{+/-}$ mice systolic function was unaffected. However, in both IUGR children and ERK3$^{+/-}$ mice septal and LV lateral E wave velocity was reduced, resulting in an elevation in E/Em ratios. In contrast, MK5$^{+/-}$ mice showed normal cardiac structure and function at a comparable age. Hence, ERK3$^{+/-}$ mice recapitulated some but not all of the effects of IUGR observed in humans, which may be attributed to differences in age or species differences in the response to fetal growth restriction.

Study Limitations

We were unable to determine if ERK3$^{+/-}$ altered the changes in cardiac functional evoked by pressure overload as in this particular strain of mice 3 weeks of pressure overload evoked morphological and molecular changes but no functional changes.

The mouse models employed herein were not equivalent. In the case of the MK5$^{+/-}$ mouse, the mice express one wild-type copy of MK5 and one copy that is non-functional due to a deletion within the catalytic domain. In contrast, the ERK3$^{+/-}$ mice contain one null allel and hence express half the normal amount of ERK3 protein. Hence, if ERK3 plays a structural role in addition to is role as a protein kinase, functions related to this interaction will also be affected.

5. Conclusions

MK5 and ERK3 form a complex in the mouse heart. In the present study, we shown that although $MK5^{+/-}$ and $ERK3^{+/-}$ hearts hypertrophied in response to chronic pressure overload they were resistant to fibrosis and less prone to diastolic dysfunction. Furthermore, MK5 and ERK3 remained associated after 3 wks of pressure overload. The lack of collagen accumulation in response to pressure-overload in $ERK3^{+/-}$ or $MK5^{+/-}$ hearts was not the result of reduced TGF-β synthesis. Here, for the first time we show a role for MK5/ERK3 during the pathological cardiac remodeling induced by pressure-overload. Further studies will address the mechanism by which MK5/ERK3 signaling regulates fibrosis.

Abbreviations

The abbreviations used are: ANP, atrial natriuretic peptide; BNP, B-type natriuretic peptides; β-MHC, β-myosin heavy chain; TGF-β1, transforming growth factor beta 1; TGF-β3, transforming growth factor beta 3; COL1α1, collagen type 1 alpha 1; DMSO, dimethylsulfoxide; DTT, dithiothreitol; MAP kinase, mitogen-activated protein kinase; MK2, MAP kinase-activated protein kinase-2; MK3, MAP kinase-activated protein kinase-3; MK5, MAP kinase-activated protein kinase-5; ERK3, extra-cellular regulated kinase 3; ERK4, extra-cellular regulated kinase 4; IGF-2, insulin like growth factor-2; PAGE, polyacrylamide gel electrophoresis; PMSF, phenylmethylsulfonyl fluoride; TX-100, Triton X-100.

Acknowledgments

We thank Ms. Karine Bouthillier and Ms. Kim Levesque for animal care and breeding, and Mr. George Vaniotis for critical reading of the manuscript. This work was supported by grants from the Canadian Institutes of Health Research (MOP-77791) and the Fonds de l'Institut de Cardiologie de Montréal (FICM). BGA was a New Investigator of the Heart and Stroke Foundation of Canada and Senior Scholar of the Fondation de la Recherche en Santé du Québec (FRSQ).

The authors declare no conflicts of interest.

References

[1] Heineke J, Molkentin JD. Regulation of cardiac hypertrophy by intracellular signalling pathways. Nat Rev Mol Cell Biol. 2006; 7(8): 589-600.

[2] Chen Z, Gibson TB, Robinson F, Silvestro L, Pearson G, Xu B, et al. MAP kinases. Chem Rev. 2001; 101(8): 2449-76.

[3] Roux PP, Blenis J. ERK and p38 MAPK-activated protein kinases: a family of protein kinases with diverse biological functions. Microbiol Mol Biol Rev. 2004 Jun; 68(2): 320-44.

[4] Sadoshima J, Izumo S. The cellular and molecular response of cardiac myocytes to mechanical stress. Annu Rev Physiol. 1997; 59: 551-71.

[5] Sadoshima J, Izumo S. Molecular characterization of angiotensin II--induced hypertrophy of cardiac myocytes and hyperplasia of cardiac fibroblasts. Critical role of the AT1 receptor subtype. Circ Res. 1993; 73(3): 413-23.

[6] Taylor JM, Rovin JD, Parsons JT. A role for focal adhesion kinase in phenylephrine-induced hypertrophy of rat ventricular cardiomyocytes. J Biol Chem. 2000; 275(25): 19250-7.

[7] Aikawa R, Nagai T, Kudoh S, Zou Y, Tanaka M, Tamura M, et al. Integrins play a critical role in mechanical stress-induced p38 MAPK activation. Hypertension. 2002 Feb; 39(2): 233-8.

[8] Yamazaki T, Komuro I, Kudoh S, Zou Y, Shiojima I, Mizuno T, et al. Angiotensin II partly mediates mechanical stress-induced cardiac hypertrophy. Circ Res. 1995; 77(2): 258-65.

[9] Komuro I, Kudo S, Yamazaki T, Zou Y, Shiojima I, Yazaki Y. Mechanical stretch activates the stress-activated protein kinases in cardiac myocytes. FASEB J. 1996; 10(5): 631-6.

[10] Wakatsuki T, Schlessinger J, Elson EL. The biochemical response of the heart to hypertension and exercise. Trends Biochem Sci. 2004; 29(11): 609-17.

[11] Kuwahara F, Kai H, Tokuda K, Kai M, Takeshita A, Egashira K, et al. Transforming growth factor-beta function blocking prevents myocardial fibrosis and diastolic dysfunction in pressure-overloaded rats. Circulation. 2002; 106(1): 130-5.

[12] Matsubara LS, Matsubara BB, Okoshi MP, Cicogna AC, Janicki JS. Alterations in myocardial collagen content affect rat papillary muscle function. Am J Physiol Heart Circ Physiol. 2000; 279(4): H1534-H9.

[13] Nicol RL, Frey N, Pearson G, Cobb M, Richardson J, Olson EN. Activated MEK5 induces serial assembly of sarcomeres and eccentric cardiac hypertrophy. EMBO J. 2001 Jun 1; 20(11): 2757-67.

[14] Dingar D, Benoit MJ, Mamarbachi AM, Villeneuve LR, Gillis MA, Grandy S, et al. Characterization of the expression and regulation of MK5 in the murine ventricular myocardium. Cell Signal. 2010 Jul; 22(7): 1063-75.

[15] Kant S, Schumacher S, Singh MK, Kispert A, Kotlyarov A, Gaestel M. Characterization of the atypical MAPK ERK4 and its activation of the MAPK-activated protein kinase MK5. J Biol Chem. 2006; 281(46): 35511-9.

[16] Ni H, Wang XS, Diener K, Yao Z. MAPKAPK5, a novel mitogen-activated protein kinase (MAPK)-activated protein kinase, is a substrate of the extracellular-regulated kinase (ERK) and p38 kinase. Biochem Biophys Res Commun. 1998; 243(2): 492-6.

[17] New L, Jiang Y, Zhao M, Liu K, Zhu W, Flood LJ, et al. PRAK, a novel protein kinase regulated by the p38 MAP kinase. EMBO J. 1998; 17(12): 3372-84.

[18] Sun P, Yoshizuka N, New L, Moser BA, Li Y, Liao R, et al. PRAK is essential for ras-induced senescence and tumor suppression. Cell. 2007; 128(2): 295-308.

[19] Schumacher S, Laass K, Kant S, Shi Y, Visel A, Gruber AD, et al. Scaffolding by ERK3 regulates MK5 in development. EMBO J. 2004; 23(24): 4770-9.

[20] Seternes OM, Mikalsen T, Johansen B, Michaelsen E, Armstrong CG, Morrice NA, et al. Activation of MK5/PRAK by the atypical MAP kinase ERK3 defines a novel signal transduction pathway. EMBO J. 2004; 23(24): 4780-91.

[21] Coulombe P, Meloche S. Atypical mitogen-activated protein kinases: structure, regulation and functions. Biochim Biophys Acta. 2007; 1773(8): 1376-87.

[22] Zimmermann J, Lamerant N, Grossenbacher R, Furst P. Proteasome- and p38-dependent regulation of ERK3 expression. J Biol Chem. 2001; 276(14): 10759-66.

[23] Hoeflich KP, Eby MT, Forrest WF, Gray DC, Tien JY, Stern HM, et al. Regulation of ERK3/MAPK6 expression by BRAF. Int J Oncol. 2006; 29(4): 839-49.

[24] Coulombe P, Rodier G, Pelletier S, Pellerin J, Meloche S. Rapid turnover of extracellular signal-regulated kinase 3 by the ubiquitin-proteasome pathway defines a novel paradigm of mitogen-activated protein kinase regulation during cellular differentiation. Mol Cell Biol. 2003; 23(13): 4542-58.

[25] Coulombe P, Rodier G, Bonneil E, Thibault P, Meloche S. N-Terminal ubiquitination of extracellular signal-regulated kinase 3 and p21 directs their degradation by the proteasome. Mol Cell Biol. 2004; 24(14): 6140-50.

[26] Aberg E, Perander M, Johansen B, Julien C, Meloche S, Keyse SM, et al. Regulation of MAPK-activated protein kinase 5 activity and subcellular localization by the atypical MAPK ERK4/MAPK4. J Biol Chem. 2006; 281(46): 35499-510.

[27] Deleris P, Rousseau J, Coulombe P, Rodier G, Tanguay PL, Meloche S. Activation loop phosphorylation of the atypical MAP kinases ERK3 and ERK4 is required for binding, activation and cytoplasmic relocalization of MK5. J Cell Physiol. 2008; 217(3): 778-88.

[28] Klinger S, Turgeon B, Levesque K, Wood GA, Aagaard-Tillery KM, Meloche S. Loss of Erk3 function in mice leads to intrauterine growth restriction, pulmonary immaturity, and neonatal lethality. Proc Natl Acad Sci U S A. 2009; 106(39): 16710-5.

[29] Shi Y, Kotlyarov A, Laabeta K, Gruber AD, Butt E, Marcus K, et al. Elimination of protein kinase MK5/PRAK activity by targeted homologous recombination. Mol Cell Biol. 2003; 23(21): 7732-41.

[30] Rockman HA, Ross RS, Harris AN, Knowlton KU, Steinhelper ME, Field LJ, et al. Segregation of atrial-specific and inducible expression of an atrial natriuretic factor transgene in an in vivo murine model of cardiac hypertrophy. Proc Natl Acad Sci U S A. 1991; 88(18): 8277-81.

[31] Reffelmann T, Kloner RA. Transthoracic echocardiography in rats. Evalution of commonly used indices of left ventricular dimensions, contractile performance, and hypertrophy in a genetic model of hypertrophic heart failure (SHHF-Mcc-facp-Rats) in comparison with Wistar rats during aging. Basic Res Cardiol. 2003 Sep; 98(5): 275-84.

[32] Boivin B, Chevalier D, Villeneuve LR, Rousseau E, Allen BG. Functional endothelin receptors are present on nuclei in cardiac ventricular myocytes. J Biol Chem. 2003; 278(31): 29153-63.

[33] Connern CP, Halestrap AP. Chaotropic agents and increased matrix volume enhance binding of mitochondrial cyclophilin to the inner mitochondrial membrane and sensitize the mitochondrial permeability transition to [Ca2+]. Biochemistry. 1996; 35(25): 8172-80.

[34] Esposito G, Prasad SV, Rapacciuolo A, Mao L, Koch WJ, Rockman HA. Cardiac overexpression of a G(q) inhibitor blocks induction of extracellular signal-regulated kinase and c-Jun NH(2)-terminal kinase activity in in vivo pressure overload. Circulation. 2001 Mar 13; 103(10): 1453-8.

[35] Zhang S, Weinheimer C, Courtois M, Kovacs A, Zhang CE, Cheng AM, et al. The role of the Grb2-p38 MAPK signaling pathway in cardiac hypertrophy and fibrosis. J Clin Invest. 2003; 111(6): 833-41.

[36] Streicher JM, Ren S, Herschman H, Wang Y. MAPK-activated protein kinase-2 in cardiac hypertrophy and cyclooxygenase-2 regulation in heart. Circ Res. 2010 Apr 30; 106(8): 1434-43.

[37] Seternes OM, Johansen B, Hegge B, Johannessen M, Keyse SM, Moens U. Both binding and activation of p38 mitogen-activated protein kinase (MAPK) play essential roles in regulation of the nucleocytoplasmic distribution of MAPK-activated protein kinase 5 by cellular stress. Mol Cell Biol. 2002; 22(20): 6931-45.

[38] Akashi YJ, Springer J, Lainscak M, Anker SD. Atrial natriuretic peptide and related peptides. Clin Chem Lab Med. 2007; 45(10): 1259-67.

[39] Rosenkranz S. TGF-beta1 and angiotensin networking in cardiac remodeling. Cardiovasc Res. 2004; 63(3): 423-32.

[40] Wang Y, Huang S, Sah VP, Ross J, Jr., Brown JH, Han J, et al. Cardiac muscle cell hypertrophy and apoptosis induced by distinct members of the p38 mitogen-activated protein kinase family. J Biol Chem. 1998 Jan 23; 273(4): 2161-8.

[41] Dingar D, Merlen C, Grandy S, Gillis MA, Villeneuve LR, Mamarbachi AM, et al. Effect of pressure overload-induced hypertrophy on the expression and localization

of p38 MAP kinase isoforms in the mouse heart. Cell Signal. 2010 Nov; 22(11): 1634-44.

[42] Braz JC, Bueno OF, Liang Q, Wilkins BJ, Dai YS, Parsons S, et al. Targeted inhibition of p38 MAPK promotes hypertrophic cardiomyopathy through upregulation of calcineurin-NFAT signaling. J Clin Invest. 2003 May; 111(10): 1475-86.

[43] Liao P, Georgakopoulos D, Kovacs A, Zheng M, Lerner D, Pu H, et al. The in vivo role of p38 MAP kinases in cardiac remodeling and restrictive cardiomyopathy. Proc Natl Acad Sci U S A. 2001; 98(21): 12283-8.

[44] Fernando P, Deng W, Pekalska B, DeRepentigny Y, Kothary R, Kelly JF, et al. Active kinase proteome screening reveals novel signal complexity in cardiomyopathy. Mol Cell Proteomics. 2005; 4(5): 673-82.

[45] Zhang D, Gaussin V, Taffet GE, Belaguli NS, Yamada M, Schwartz RJ, et al. TAK1 is activated in the myocardium after pressure overload and is sufficient to provoke heart failure in transgenic mice. Nat Med. 2000; 6(5): 556-63.

[46] Nishida K, Yamaguchi O, Hirotani S, Hikoso S, Higuchi Y, Watanabe T, et al. p38alpha mitogen-activated protein kinase plays a critical role in cardiomyocyte survival but not in cardiac hypertrophic growth in response to pressure overload. Mol Cell Biol. 2004; 24(24): 10611-20.

[47] Liang Q, Molkentin JD. Redefining the roles of p38 and JNK signaling in cardiac hypertrophy: dichotomy between cultured myocytes and animal models. J Mol Cell Cardiol. 2003; 35(12): 1385-94.

[48] Petrich BG, Wang Y. Stress-activated MAP kinases in cardiac remodeling and heart failure; new insights from transgenic studies. Trends CardiovascMed. 2004; 14(2): 50-5.

[49] Remy G, Risco AM, Inesta-Vaquera FA, Gonzalez-Teran B, Sabio G, Davis RJ, et al. Differential activation of p38MAPK isoforms by MKK6 and MKK3. Cell Signal. 2010 Apr; 22(4): 660-7.

[50] Hammaker D, Firestein GS. "Go upstream, young man": lessons learned from the p38 saga. Ann Rheum Dis. 2010 Jan; 69 Suppl 1: i77-82.

[51] New L, Jiang Y, Han J. Regulation of PRAK subcellular location by p38 MAP kinases. Mol Biol Cell. 2003; 14(6): 2603-16.

[52] Li Q, Zhang N, Zhang D, Wang Y, Lin T, Zhou H, et al. Determinants that control the distinct subcellular localization of p38alpha-PRAK and p38beta-PRAK complexes. J Biol Chem. 2008 Apr 18; 283(16): 11014-23.

[53] Tanoue T, Maeda R, Adachi M, Nishida E. Identification of a docking groove on ERK and p38 MAP kinases that regulates the specificity of docking interactions. EMBO J. 2001 Feb 1; 20(3): 466-79.

[54] Heeneman S, Cleutjens JP, Faber BC, Creemers EE, van Suylen RJ, Lutgens E, et al. The dynamic extracellular matrix: intervention strategies during heart failure and atherosclerosis. J Pathol. 2003 Jul; 200(4): 516-25.

[55] Berg TJ, Snorgaard O, Faber J, Torjesen PA, Hildebrandt P, Mehlsen J, et al. Serum levels of advanced glycation end products are associated with left ventricular diastolic function in patients with type 1 diabetes. Diabetes Care. 1999 Jul; 22(7): 1186-90.

[56] Rosenkranz S, Flesch M, Amann K, Haeuseler C, Kilter H, Seeland U, et al. Alterations of beta-adrenergic signaling and cardiac hypertrophy in transgenic mice overexpressing TGF-beta(1). Am J Physiol Heart Circ Physiol. 2002 Sep; 283(3): H1253-62.

[57] Schiller M, Javelaud D, Mauviel A. TGF-beta-induced SMAD signaling and gene regulation: consequences for extracellular matrix remodeling and wound healing. J Dermatol Sci. 2004; 35(2): 83-92.

[58] Villarreal FJ, Dillmann WH. Cardiac hypertrophy-induced changes in mRNA levels for TGF-beta 1, fibronectin, and collagen. Am J Physiol. 1992 Jun; 262(6 Pt 2): H1861-6.

[59] Li JM, Brooks G. Differential protein expression and subcellular distribution of TGFbeta1, beta2 and beta3 in cardiomyocytes during pressure overload-induced hypertrophy. J Mol Cell Cardiol. 1997 Aug; 29(8): 2213-24.

[60] Hu BC, Li L, Sun RH, Gao PJ, Zhu DL, Wang JG, et al. The association between transforming growth factor beta3 polymorphisms and left ventricular structure in hypertensive subjects. Clin Chim Acta. 2010 Apr 2; 411(7-8): 558-62.

[61] Kostenko S, Shiryaev A, Gerits N, Dumitriu G, Klenow H, Johannessen M, et al. Serine residue 115 of MAPK-activated protein kinase MK5 is crucial for its PKA-regulated nuclear export and biological function. Cell Mol Life Sci. 2010 Aug 25.

[62] Gerits N, Mikalsen T, Kostenko S, Shiryaev A, Johannessen M, Moens U. Modulation of F-actin Rearrangement by the Cyclic AMP/cAMP-dependent Protein Kinase (PKA) Pathway Is Mediated by MAPK-activated Protein Kinase 5 and Requires PKA-induced Nuclear Export of MK5. J Biol Chem. 2007; 282(51): 37232-43.

[63] Seeland U, Schaffer A, Selejan S, Hohl M, Reil JC, Muller P, et al. Effects of AT1- and beta-adrenergic receptor antagonists on TGF-beta1-induced fibrosis in transgenic mice. Eur J Clin Invest. 2009 Oct; 39(10): 851-9.

[64] Gaestel M. MAPKAP kinases - MKs - two's company, three's a crowd. Nat Rev Mol Cell Biol. 2006; 7(2): 120-30.

[65] Figueras F, Eixarch E, Gratacos E, Gardosi J. Predictiveness of antenatal umbilical artery Doppler for adverse pregnancy outcome in small-for-gestational-age babies according to customised birthweight centiles: population-based study. BJOG. 2008 Apr; 115(5): 590-4.

[66] Palinski W, Napoli C. Impaired fetal growth, cardiovascular disease, and the need to move on. Circulation. 2008 Jan 22; 117(3): 341-3.

[67] Kaijser M, Bonamy AK, Akre O, Cnattingius S, Granath F, Norman M, et al. Perinatal risk factors for ischemic heart disease: disentangling the roles of birth weight and preterm birth. Circulation. 2008 Jan 22; 117(3): 405-10.

[68] Crispi F, Bijnens B, Figueras F, Bartrons J, Eixarch E, Le Noble F, et al. Fetal growth restriction results in remodeled and less efficient hearts in children. Circulation. 2010 Jun 8; 121(22): 2427-36.

Figure Legends

Figure 1. **Hypertrophic response of MK5$^{+/-}$ hearts to pressure overload.** Pressure overload was induced in MK5$^{+/-}$ and wild type litter mate controls (MK5$^{+/+}$) mice by transverse aortic constriction (TAC) and mice were sacrificed 2 wks post-surgery. Sham animals underwent the identical surgical procedure, however the aorta was not constricted. (**A**) Left ventricular maximum developed pressure was measured using by a Millar micro-tip catheter pressure transducer. (**B**) Mice were sacrificed, heart weight/body weight ratio of MK5$^{+/-}$ and MK5$^{+/+}$ measured. **(C)** HW/BW ratio versus left ventricular maximum developed pressure. Shown are the mean ± S.E. (n= 6-9). ***, $p <$ 0.001: **, $p < 0.01$: *, $p < 0.05$: one-way ANOVA with Newman-Keuls post-hoc analysis.

Figure 2. **Expression of molecular markers of hypertrophy in the ventricular myocardium of MK5$^{+/+}$ and MK5$^{+/-}$ mice after 2 weeks of pressure overload.** Total RNA was isolated from 14 μm transverse cryosections of the ventricular myocardium. mRNA levels were quantified by qPCR. The relative abundance of (**A**) atrial natriuretic peptide (ANP)**,** (**B**) B-type natriuretic peptide (BNP)**,** (**C**) and beta-myosin heavy chain (β-MHC) was normalized to GAPDH mRNA levels. Shown are the mean ± S.E. (n= 6-9). ***, $p < 0.001$: **, $p < 0.01$: *, $p < 0.05$: one-way ANOVA with Newman-Keuls post-hoc analysis.

Figure 3. **Assessment of cardiac fibrosis in MK5$^{+/+}$ and MK5$^{+/-}$ mice after pressure overload.** Transverse cryocections (8 μm) of the ventricular myocardium were stained with Masson's trichrome (**A**) 2 wks and (**C**) 3 wks post-TAC. Note the increased extracellular matrix content (stained blue). 3 sections for each heart were stained and shown are the representative images. The original magnification was 10X. Total RNA was isolated from 14 μm transverse cryosections of the ventricular myocardium. Collagen alpha 1 type 1 (COL1A1) mRNA levels were measured in MK5$^{+/+}$ and MK5$^{+/-}$ 2 (**B**) and 3 wks (**D**) post-TAC by qPCR and were normalized to the amount of GAPDH mRNA. Shown are the mean ± S.E. (n= 6-9). ***, $p < 0.001$: **, $p < 0.01$: *, $p < 0.05$: one-way ANOVA with Newman-Keuls post-hoc analysis.

Figure 4. **ERK3 co-immunoprecipitates with MK5.** (**A**) Mice were sacrificed after 3 wk of pressure overload, the ventricular myocardium isolated, lysates prepared, and MK5 immunoprecipitated with ab anti-MK5 antibody. Purified rabbit IgG was employed in control immunoprecipitations. Immunoprecipitate were separated on SDS-PAGE and transferred to nitrocellulose membrane. Co-immunoprecipitated ERK3, ERK4, p38α, phospho p38, and GAPDH were detected by immunoblotting. Aliquots (50 μg) of lysate from TAC and sham hearts were included as controls (Input). Results shown are representative of 3 animals in each group. (**B**) Lysates (50 μg) from 3 TAC and sham hearts were analyzed by SDS-PAGE and immunoblotting using an anti-ERK3, anti-p38, or anti-ERK4 antibodies. Shown are the mean ± S.E. (n=3).

Figure 5. **Hypertrophic response of ERK3$^{+/-}$ mice to pressure overload.** Pressure overload was induced in ERK3$^{+/-}$ and wild type litter mate controls (ERK3$^{+/+}$) mice by transverse aortic constriction (TAC) and mice were sacrificed 3 wks post-surgery. Sham animals underwent the identical surgical procedure, however the aorta was not constricted. (**A**) Left ventricular maximum developed pressure was measured using by a Millar micro-tip catheter pressure transducer. (**B**) Mice were sacrificed and heart weight/body weight ratio measured. **(C)** HW/BW ratio versus left ventricular maximum developed pressure. (**D**) Body weight (n=17) of ERK3$^{+/+}$ and ERK3$^{+/-}$ mice. (**E**) Heart weight (n=7) of ERK3$^{+/+}$ and ERK3$^{+/-}$ mice. (**F**) Total RNA was isolated from 14 μm transverse cryosections of the ventricular myocardium. mRNA levels were quantified by qPCR. The relative abundance of atrial natriuretic peptide (ANP)**,** B-type natriuretic peptide (BNP)**,** and beta-myosin heavy chain (β-MHC) was normalized to the amount of GAPDH mRNA. (n= 7-8). Shown are the mean ± S.E. ***, $p < 0.001$: **, $p < 0.01$: *, $p < 0.05$: one-way ANOVA with Newman-Keuls post-hoc analysis except for (C-D) where Students t-Test was performed.

Figure 6. **Assessment of cardiac fibrosis in ERK3$^{+/+}$ and ERK3$^{+/-}$ mice after 3 weeks of pressure overload.** (**A**) Transverse cryocections (8 μm) of the ventricular myocardium were stained with Masson's trichrome in ERK3$^{+/+}$ and ERK3$^{+/-}$ hearts 3 wks post-TAC. Note the increased extracellular matrix content (stained blue). For each heart, 3 sections were stained: and representative images are shown. The original

magnification was 10X. (**B**) Total RNA was isolated from 14 μm transverse cryosections of the ventricular myocardium. Collagen alpha 1 type 1 (COL1A1) mRNA levels were measured by qPCR and normalized to the amount of GAPDH mRNA. Shown are the mean ± S.E. (n= 7-8). ***, $p < 0.001$: **, $p < 0.01$: *, $p < 0.05$: one-way ANOVA with Newman-Keuls post-hoc analysis.

Figure 7. **Quantification of TGFβ1 and TGFβ3 mRNA.** Total RNA was isolated from 14 μm transverse cryosections of the ventricular myocardium. Transforming growth factor-beta 1 (TGF-β1) and transforming growth factor-beta 3 (TGF-β3) mRNA was quantified by qPCR and normalized to the amount of GAPDH mRNA in: (**A**) $MK5^{+/+}$ and $MK5^{+/-}$ hearts 2 and 3 wks post TAC hearts and (**B**) $ERK3^{+/+}$ and $ERK3^{+/-}$ hearts 3 wks post-TAC. Shown are the mean ± S.E. (n= 6-9). ***, $p < 0.001$: **, $p < 0.01$: *, $p < 0.05$: one-way ANOVA with Newman-Keuls post-hoc analysis.

Supplementary Figure 1. **Response of $MK5^{+/-}$ hearts to 3 weeks of pressure overload.** Pressure overload was induced in $MK5^{+/-}$ and wild type litter mate controls ($MK5^{+/+}$) mice by transverse aortic constriction (TAC) for 3 wks. Sham animals underwent the identical surgical procedure, however the aorta was not constricted. (**A**) 2 wk post-surgery, left ventricular maximum pressure was measured following catheter insertion in LV. (**B**) Mice were sacrificed, heart weight/body weight ratio of $MK5^{+/-}$ and $MK5^{+/+}$ measured. Total RNA was isolated from 14 μm ventricle sections. The relative abundance of (**C**) atrial natriuretic peptide (ANP)**,** (**D**) B-type natriuretic peptide (BNP)**,** (**E**) and b-myosin heavy chain (β-MHC) was quantified by qPCR and normalized to GAPDH mRNA levels. Shown are the mean ± S.E. (n= 6-9). ***, $p < 0.001$: **, $p < 0.01$: *, $p < 0.05$: one-way ANOVA with Newman-Keuls post-hoc analysis.

Figure 1

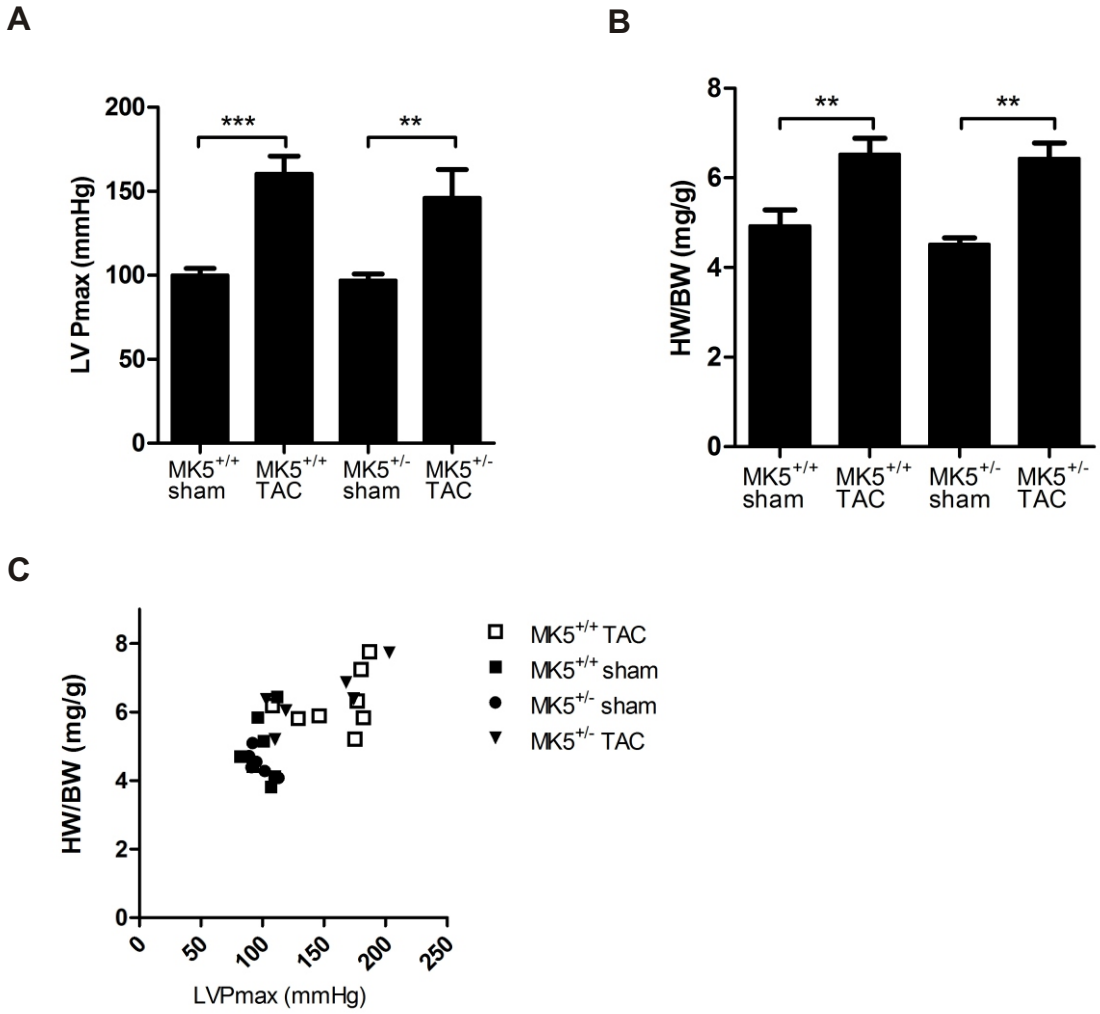
A
LV Pmax (mmHg)
200
150
100
50
0
***
**
MK5+/+ sham
MK5+/+ TAC
MK5+/- sham
MK5+/- TAC
B
HW/BW (mg/g)
8
6
4
2
0
**
**
MK5+/+ sham
MK5+/+ TAC
MK5+/- sham
MK5+/- TAC
C
HW/BW (mg/g)
8
6
4
2
0
0
50
100
150
200
250
LVPmax (mmHg)
MK5+/+ TAC
MK5+/+ sham
MK5+/- sham
MK5+/- TAC

Figure 2

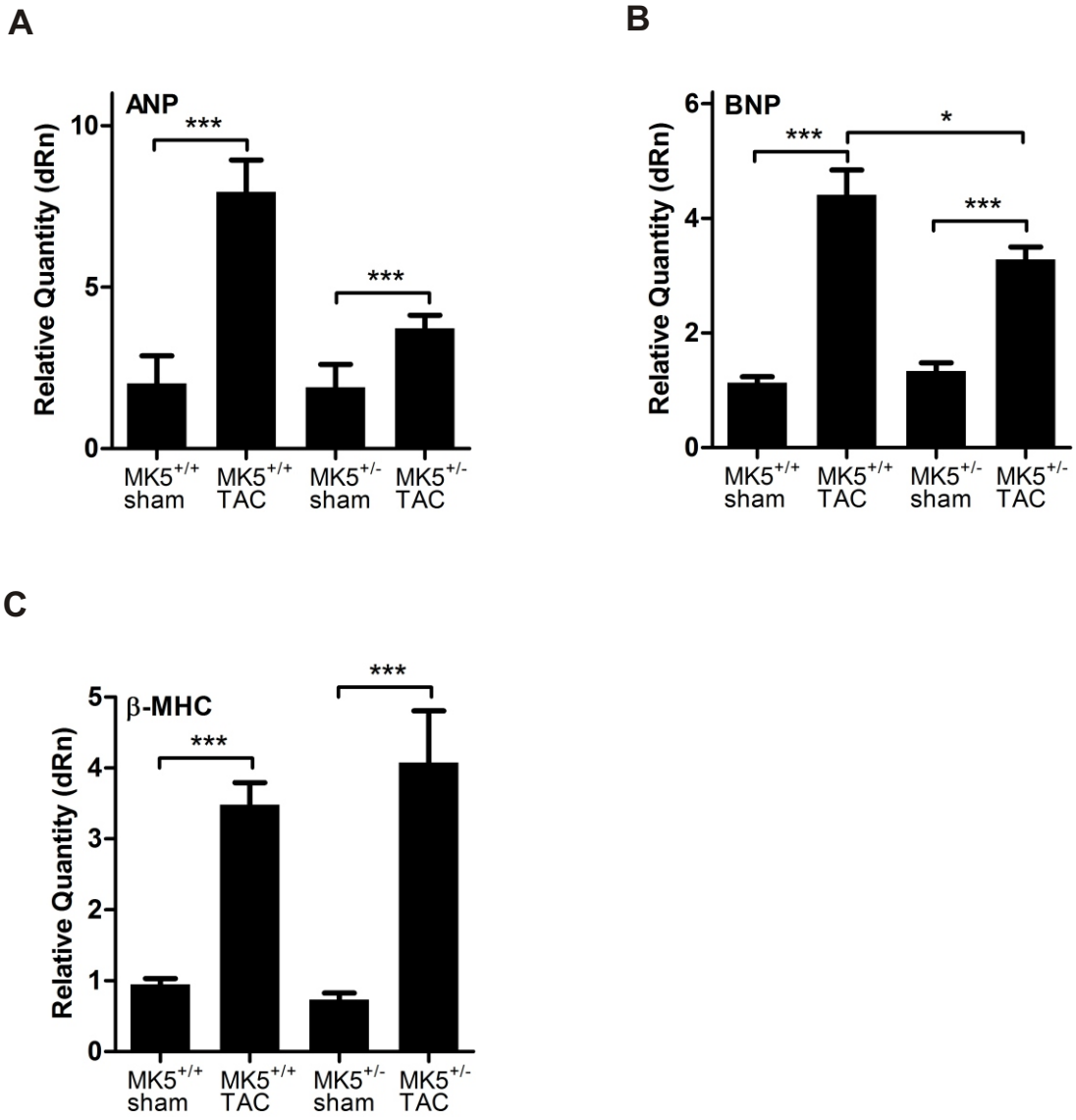
A
ANP
Relative Quantity (dRn)
10
5
0
***
***
MK5+/+ sham
MK5+/+ TAC
MK5+/- sham
MK5+/- TAC
B
BNP
Relative Quantity (dRn)
6
4
2
0
***
*
***
MK5+/+ sham
MK5+/+ TAC
MK5+/- sham
MK5+/- TAC
C
β-MHC
Relative Quantity (dRn)
5
4
3
2
1
0
***
***
MK5+/+ sham
MK5+/+ TAC
MK5+/- sham
MK5+/- TAC

Figure 3

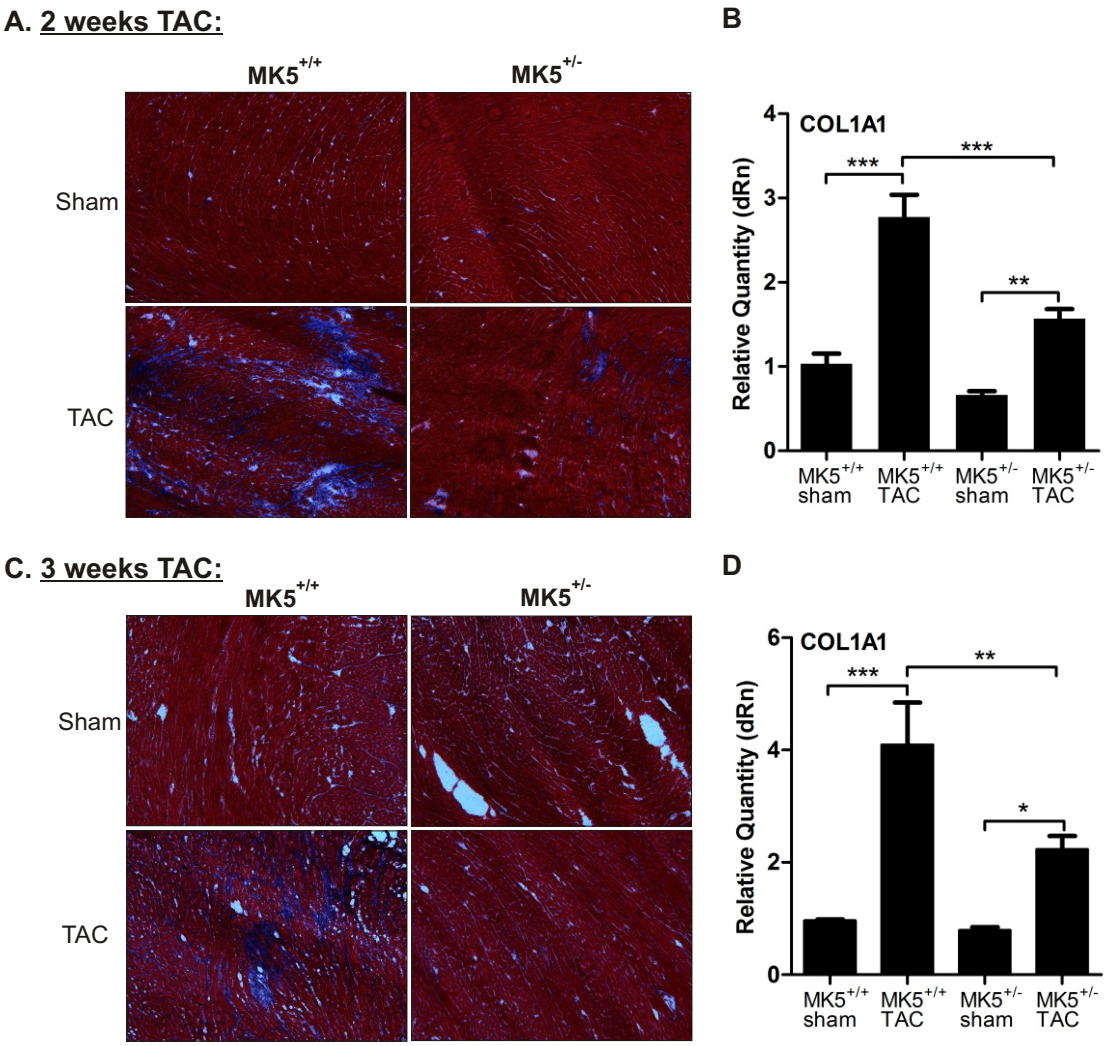
A. 2 weeks TAC:
MK5+/+
MK5+/-
Sham
TAC
B
COL1A1
Relative Quantity (dRn)
***
***
**
MK5+/+ sham
MK5+/+ TAC
MK5+/- sham
MK5+/- TAC
C. 3 weeks TAC:
MK5+/+
MK5+/-
Sham
TAC
D
COL1A1
Relative Quantity (dRn)
***
**
*
MK5+/+ sham
MK5+/+ TAC
MK5+/- sham
MK5+/- TAC

Figure 4

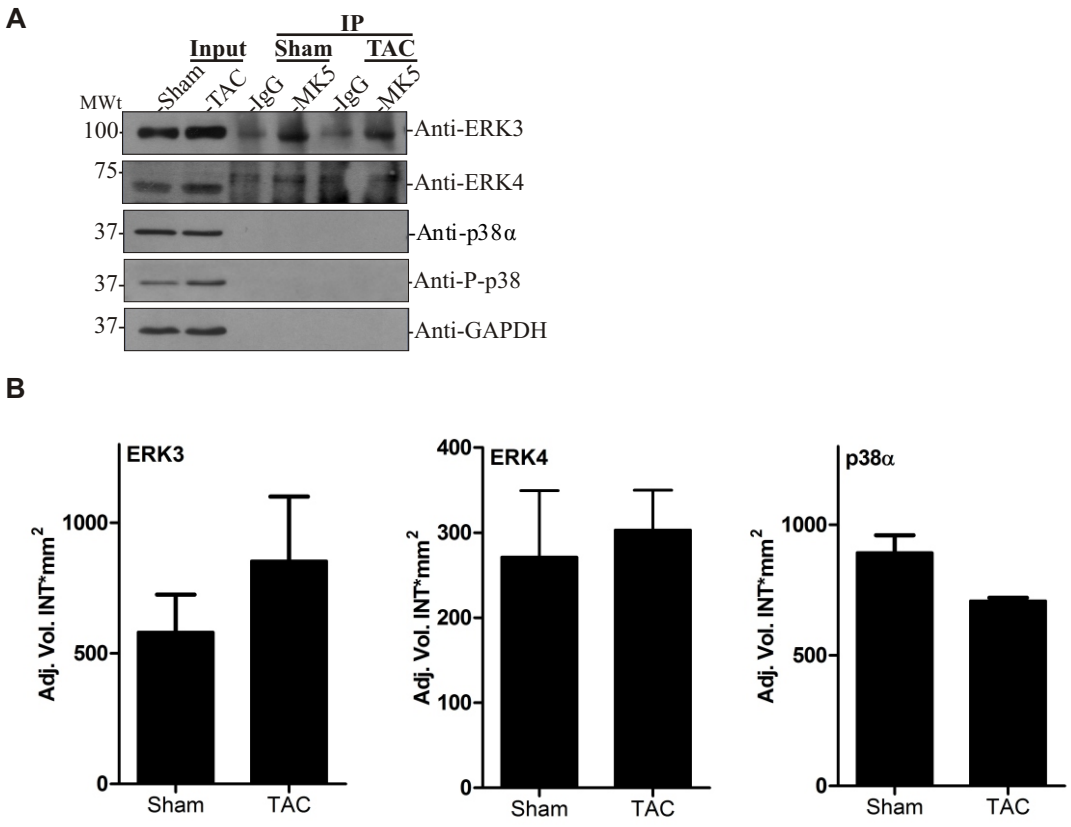
A
IP
Input
Sham
TAC
Sham
TAC
IgG
MK5
IgG
MK5
MWt
100
75
37
37
37
Anti-ERK3
Anti-ERK4
Anti-p38α
Anti-P-p38
Anti-GAPDH
B
ERK3
ERK4
p38α
Adj. Vol. INT*mm2
0
500
1000
100
200
300
400
Sham
TAC

Figure 5

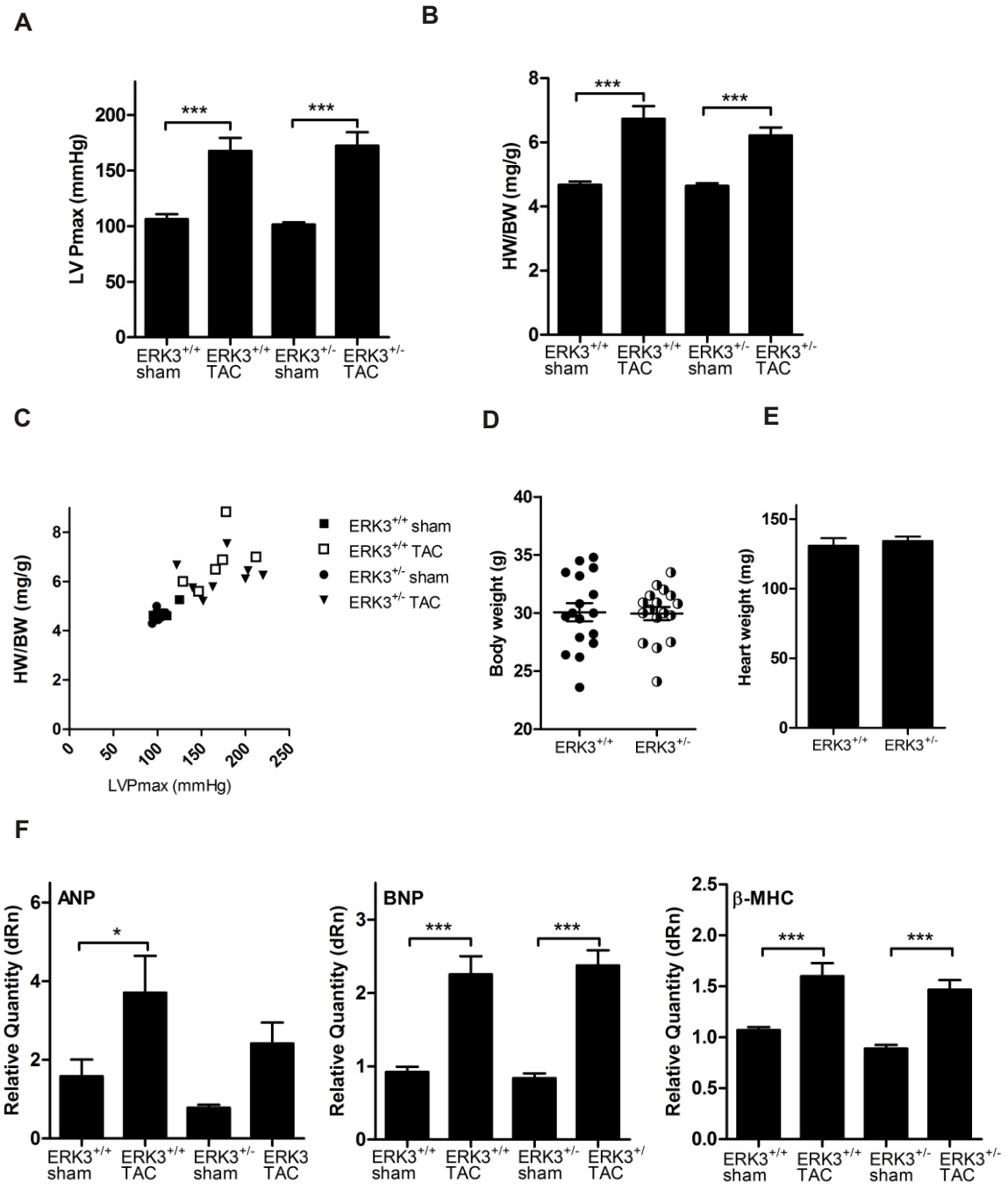
A
LV Pmax (mmHg)
***
***
ERK3+/+ sham
ERK3+/+ TAC
ERK3+/- sham
ERK3+/- TAC
B
HW/BW (mg/g)
C
HW/BW (mg/g)
LVPmax (mmHg)
ERK3+/+ sham
ERK3+/+ TAC
ERK3+/- sham
ERK3+/- TAC
D
Body weight (g)
E
Heart weight (mg)
F
ANP
BNP
β-MHC
Relative Quantity (dRn)
*

Figure 6

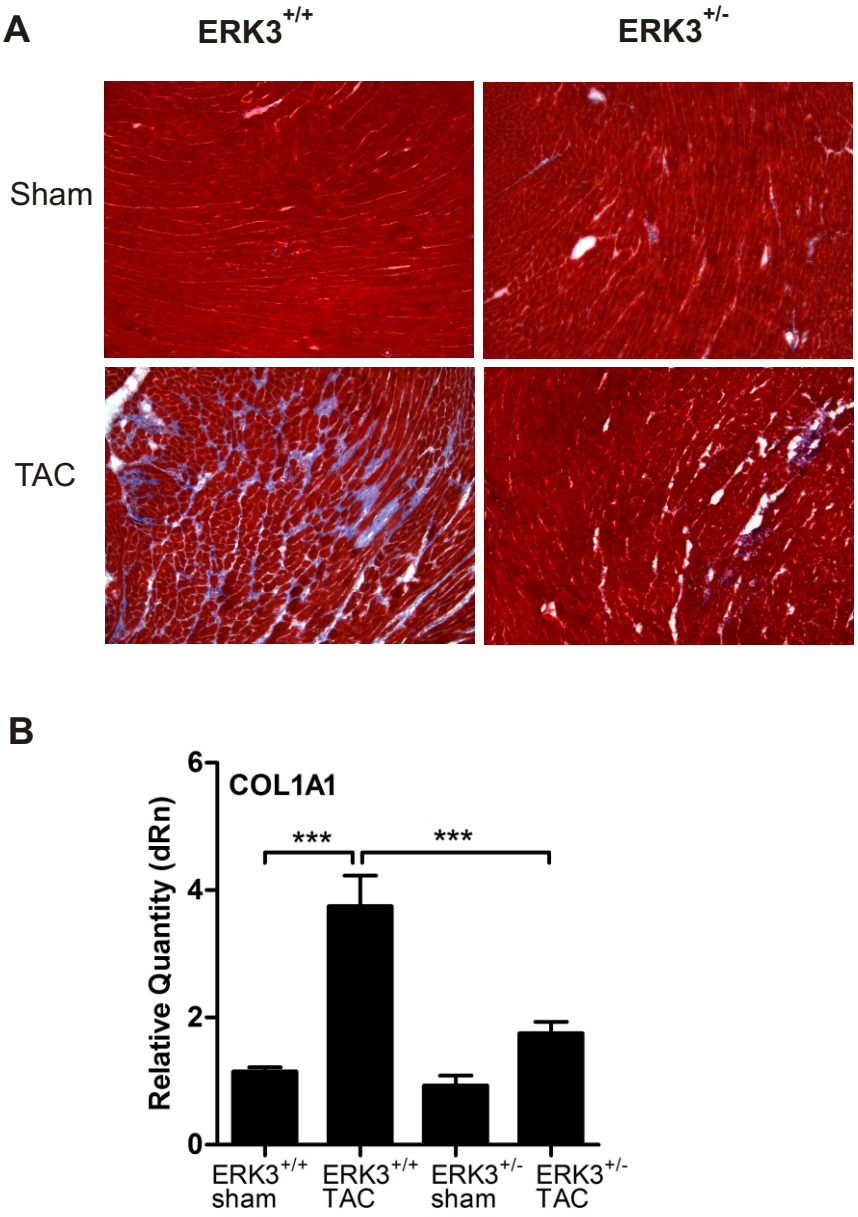
A
ERK3+/+
ERK3+/-
Sham
TAC
B
COL1A1
Relative Quantity (dRn)
6
4
2
0
***
***
ERK3+/+ sham
ERK3+/+ TAC
ERK3+/- sham
ERK3+/- TAC

Figure 7

A MK5:

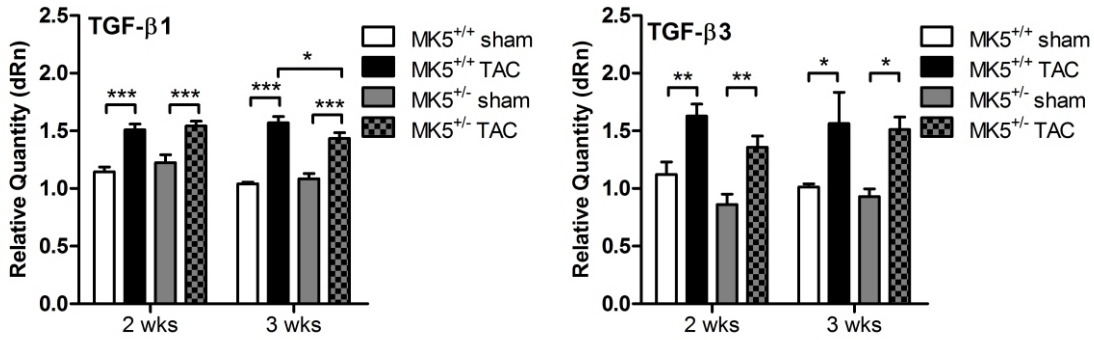

B ERK3:

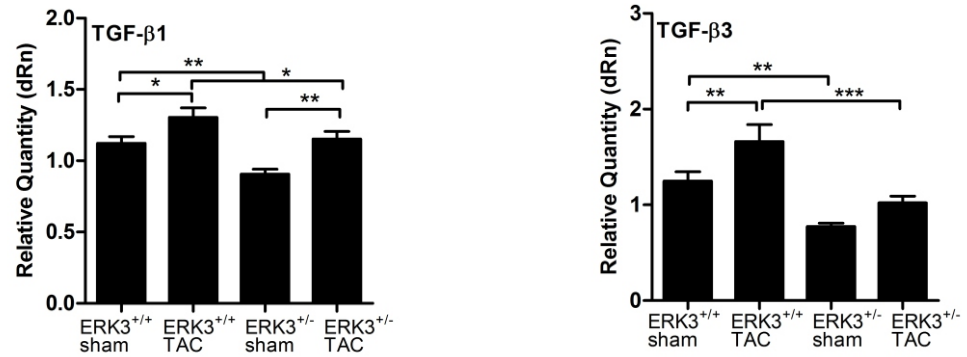

Sup. figure 1

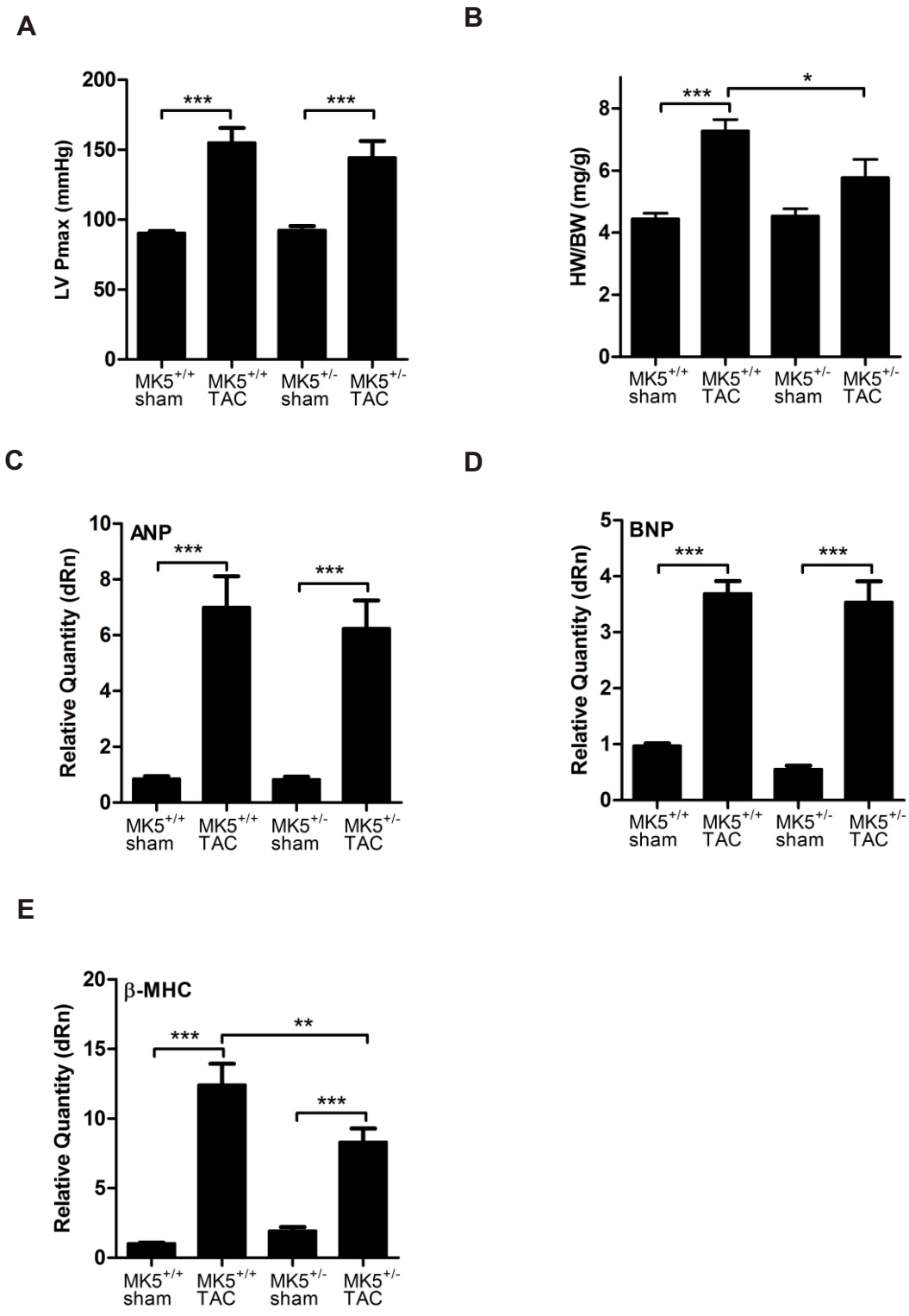
A
LV Pmax (mmHg)
200
150
100
50
0
***
***
MK5+/+ sham
MK5+/+ TAC
MK5+/- sham
MK5+/- TAC
B
HW/BW (mg/g)
8
6
4
2
0
***
*
C
ANP
Relative Quantity (dRn)
10
8
6
4
2
0
D
BNP
5
4
3
2
1
E
β-MHC
20
15
10
5
**

Tables

Table 1. Hemodynamic parameters for $MK5^{+/+}$ and $MK5^{+/-}$ mice after 2 wk of pressure overload.

	Sham		**TAC**	
	$MK5^{+/+}$ (n=7)	**$MK5^{+/-}$ (n=6)**	**$MK5^{+/+}$ (n=9)**	**$MK5^{+/-}$ (n=6)**
P max (mmHg)	99.6±3.5	94.8±4.3	144.8±9.8ξ	130.7±15.2
P min (mmHg)	64.0±2.8	61.5±3.0	65.3±4.9	67.1±5.1
P mean (mmHg)	75.8±2.9	72.6±3.2	91.8±5.1	88.3±7.5
LVP max (mmHg)	100±4.1	97.0±3.7	160.5±10.3ξ	146.2±16.7ξ
LVP min (mmHg)	1.8±1.2	2.6±0.6	1.3±0.9	2.1±1.2
LVP dPmax (mmHg/s)	6598±540.0	6145±382.0	5993±792.4	5982±515.7
LVP dPmin (mmHg/s)	-5774±437.1	-5586±407.8	-6269±822.7	-6545±648.1
Ped (mmHg)	8.4±1.4	8.3±1.2	8.3±1.9	9.4±2.7
CT (msec)	13.4±0.6	13.2±0.4	15.4±3.1	13.8±0.5
RT (msec)	46.7±0.9	45.8±1.1	41.7±5.2	47.3±1.5
Tau (msec)	9.1±0.4	8.9±0.5	8.2±0.9	9.2±0.5
HR (bpm)	354.0±17.9	356.3±19.3	304.8±40.5	333.5±17.9

Data reported as mean ± SEM. For statistical comparisons One-way ANOVA followed by Newman-Keuls test was performed. Shown are the values of mean and SEM. ξ: $p<0.05$ vs Sham; †: $p<0.05$ for $MK5^{+/-}$ vs $MK5^{+/+}$.

Table 2. Echocardiographic parameters of $MK5^{+/+}$ and $MK5^{+/-}$ mice after 2 wk of pressure overload.

	Sham		**TAC**	
	$MK5^{+/+}$ (n=6)	**$MK5^{+/-}$ (n=7)**	**$MK5^{+/+}$ (n=6)**	**$MK5^{+/-}$ (n=8)**
Aortic Peak Velocity (cm/s)	119.1±11.2	117.3±4.3	381.5±36.58ξ	332.2±63.7ξ
R-R interval (msec)	136.8±6.7	136.0±5.1	164.2±10.5ξ	148.0±11.0
Left ventricular dimensions and mass				
LVAWd (mm)	0.8±0.02	0.8±0.03	1.0±0.08ξ	0.9±0.06
LVPWd (mm)	0.7±0.03	0.8±0.04	0.9±0.05ξ	0.8±0.05
LVEDD (mm)	4.3±0.1	4.1±0.1	4.2±0.1	4.2±0.2
LVESD (mm)	2.5±0.1	2.3±0.1	2.8±0.2	2.8±0.2ξ
LV mass (mg)	233.4±6.2	236.4±8.0	267.7±12.5ξ	250.8±6.0
LV mass / LVDd (mg/mm)	54.5±0.8	57.5±0.9†	63.7±2.7ξ	59.8±2.5
LV mass/BW (mg/g)	7.8±0.4	8.0±0.2	10.1±0.3ξ	9.8±0.5ξ
Systolic Function				
FS (%)	40.5±2.0	43.0±1.4	32.5±2.7ξ	34.5±1.2ξ
LVEF (%)	77.3±2.2	80.1±1.4	66.9±3.6ξ	70.2±1.6ξ
Lateral Sm (cm/s)	2.9±0.1	3.0±0.2	2.0±0.2ξ	2.5±0.1ξ

Septal Sm (cm/s)	3.2±0.4	2.6±0.2	1.9±0.1ξ	3.1±0.4†
Diastolic function				
E velocity (cm/s)	72.1±5.1	63.9±5.9	82.6±5.5	87.0±8.7ξ
E DT (msec)	37.4±4.2	42.4±4.5	38.7±5.1	36.6±3.1
E D rate (m/s^2)	20.2±2.0	15.3±0.7†	25.0±4.8	24.3±2.5ξ
Septal Em	3.0±0.2	2.7±0.2	2.9±0.2	3.9±0.4ξ†
Septal E/Em	24.7±2.7	24.1±1.7	28.7±1.4	23.1±2.0†
Lateral Em	2.9±0.1	3.0±0.3	2.8±0.3	3.4±0.1†
Lateral E/Em	24.8±1.8	21.8±2.4	30.7±2.1ξ	25.2±2.3
LV isovolumetric relaxation time				
IVRT (msec)	13.8±1.0	13.2±1.3	22.5±2.7ξ	15.1±1.8†
IVRTc	1.18±0.1	1.13±0.1	1.74±0.2ξ	1.23±0.1†
Myocardial performance index				
Septal MPI (%)	82.7±8.8	84.4±10.0	111.5±14.0*	68.3±10.5†
Lateral MPI (%)	81.2±6.7	96.1±5.9	112.8±14.5ξ	76.1±13.7†
Global MPI (%)	22.4±2.4	31.4±6.7	53.1±4.6ξ	31.1±3.2†

LVAWd, LV anterior wall end-diastolic thickness; LVPWd, LV posterior wall end-diastolic thickness; LVEDD, Left ventricular end-diastolic diameter; LVESD, Left ventricular end-systolic diameter; FS, Fractional shortening, LVEF, Left ventricular ejection fraction; E, early diastolic transmitral filling velocity; IVRT, isovolumic

relaxation time; IVRTc, rate-corrected isovolumic relaxation time; EDT, early diastolic transmitral filling deceleration time; ED rate, early diastolic transmitral filling deceleration rate; Em, peak early diastolic tissue velocity; Sm, peak systolic tissue velocity.

Data reported as mean ± SEM. ξ: $p<0.05$ vs Sham; †: $p<0.05$ for $MK5^{+/-}$ vs $MK5^{+/+}$.

Table 3. Structural and functional assessment of $ERK3^{+/+}$ and $ERK3^{+/-}$ mice by echocardiography.

	$ERK3^{+/+}$ (n=14)	**$ERK3^{+/-}$ (n=15)**
Aortic Peak Velocity (cm/s)	58.4±2.5	63.4±2.4
Aortic Peak Gradient (mmHg)	1.4±0.1	1.7±0.1
Aortic Mean Gradient (mmHg)	0.7±0.1	0.9±0.1†
R-R interval (msec)	181.5±8.5	198.9±10.3
Left ventricular dimensions and mass		
LVAWd (mm)	0.8±0.02	0.8±0.01
LVPWd (mm)	0.8±0.03	0.8±0.01
LVEDD (mm)	4.2±0.1	4.2±0.1
LVESD (mm)	2.9±0.1	2.9±0.1
LV mass (mg)	238.6±5.9	237.6±3.7
LV mass / LVDd (mg/mm)	57.4±0.9	57.0±0.4
LV mass/BW (mg/g)	8.0±0.2	8.0±0.2
Systolic Function		
FS (%)	31.1±1.3	31.3±1.5
LVEF (%)	65.3±1.8	65.4±2.4
Lateral Sm (cm/s)	2.0±0.1	1.9±0.1

Septal Sm (cm/s)	2.1±0.1	2.1±0.1
Diastolic function		
E velocity (cm/s)	87.4±4.3	82.3±5.4
E DT (msec)	49.3±3.0	43.7±3.1
E D rate (m/s^2)	19.0±1.9	20.0±1.8
Septal Em	4.2±0.3	2.9±0.3†
Septal E/Em	21.5±0.8	29.4±1.8†
Lateral Em	3.7±0.3	2.6±0.3†
Lateral E/Em	24.7±1.6	34.1±2.2†
Left ventricular isovolumetric relaxation time		
IVRT (msec)	21.6±2.0	23.9±3.2
IVRTc	1.6±0.1	1.7±0.2
Myocardial performance index		
Septal MPI (%)	59.2±2.3	62.8±2.6
Lateral MPI (%)	62.6±1.7	64.2±2.0
Global MPI (%)	44.0±3.9	44.6±4.5

LVAWd, LV anterior wall end-diastolic thickness; LVPWd, LV posterior wall end-diastolic thickness; LVEDD, Left ventricular end-diastolic diameter; LVESD, Left ventricular end-systolic diameter; FS, Fractional shortening, LVEF, Left ventricular ejection fraction; E, early diastolic transmitral filling velocity; IVRT, isovolumic relaxation time; IVRTc, rate-corrected isovolumic relaxation time; EDT, early diastolic

transmitral filling deceleration time; ED rate, early diastolic transmitral filling deceleration rate; Em, peak early diastolic tissue velocity; Sm, peak systolic tissue velocity.

Data reported as mean ± SEM. †, $p < 0.05$ versus $ERK3^{+/+}$.

Table 4. Hemodynamic parameters for ERK3$^{+/+}$ and ERK3$^{+/-}$ mice after 3 wk of pressure overload.

	Sham		**TAC**	
	ERK3$^{+/+}$ (n=6)	**ERK3$^{+/-}$ (n=7)**	**ERK3$^{+/+}$ (n=6)**	**ERK3$^{+/-}$ (n=8)**
P max (mmHg)	106.0±4.6	101.0±1.4	156.2±10.7 ξ	155.0±7.4 ξ
P min (mmHg)	74.4±3.6	71.4±1.2	75.2±4.4	80.3±2.8
P mean	85.0±3.8	74.5±7.0	102.2±6.3ξ	105.2±3.7 ξ
LVP max (mmHg)	106.3±4.4	101.4±2.0	167.7±11.6ξ	172.4±12.0 ξ
LVP min (mmHg)	4.0±1.6	1.2±0.6	5.4±1.0	3.2±1.3
LVP dPmax (mmHg/s)	6480±361.9	6515±360.6	6882±529.2	8110±616.2
LVP dPmin (mmHg/s)	-5831±446.7	-5833±338.7	-7035±324.6	-8273±671.7 ξ
Ped (mmHg)	8.7±1.8	5.2±0.9	9.6±1.6	7.7±2.0
CT (msec)	14.3±0.6	15.1±0.5	14.5±0.7	14.2±0.9
RT (msec)	48.4±1.9	48.7±1.4	47.7±1.0	45.4±1.3
Tau (msec)	3.3±2.0	3.1±1.7	0.1±0.1	2.4±1.4
HR (bpm)	345.8±19.0	344.0±21.0	346.7±12.1	388.9±9.9

Data reported as mean ± SEM. For statistical comparisons One-way ANOVA followed by Newman-Keuls test was performed. Shown are the values of mean and SEM. ξ: $p<0.05$ vs Sham; †: $p<0.05$ for ERK3$^{+/-}$ vs ERK3$^{+/+}$.

Table 5. Echocardiographic paramerters of ERK3$^{+/+}$ and ERK3$^{+/-}$ mice after 3 wk of pressure overload.

	Sham		**TAC**	
	ERK3$^{+/+}$ (n=7)	**ERK3$^{+/-}$ (n=7)**	**ERK3$^{+/+}$ (n=7)**	**ERK3$^{+/-}$ (n=8)**
Aortic Peak Velocity (cm/s)	73.7±8.5	78.5±5.4	287.7±15.7ξ	235.3±13.1ξ†
R-R interval (msec)	164.5±7.2	188.0±6.1†	158.9±9.9	192.7±9.8†
Left ventricular dimensions and mass				
LVAWd (mm)	0.82±0.01	0.8±0.02	1.1±0.04ξ	1.0±0.02ξ†
LVPWd (mm)	0.8±0.04	0.7±0.02	1.0±0.04ξ	0.9±0.04ξ
LVEDD (mm)	4.0±0.1	4.0±0.1	4.4±0.1ξ	4.2±0.1
LVESD (mm)	2.5±0.1	2.6±0.1	3.0±0.2ξ	2.7±0.2
LV mass (mg)	234.3±3.8	231.0±3.6	298.7±13.2ξ	261.6±6.0ξ†
LV mass / LVDd (mg/mm)	59.2±0.9	57.4±0.9	67.7±1.7ξ	63.1±1.5ξ
LV mass/BW (mg/g)	8.4±0.3	8.0±0.2	9.7±0.4ξ	9.3±0.2ξ
Systolic Function				
FS (%)	37.5±1.9	34.5±1.5	32.5±2.9	35.4±2.7
LVEF (%)	73.9±2.3	70.2±1.9	66.6±4.8	70.5±3.6
Lateral Sm (cm/s)	2.2±0.1	2.1±0.1	2.1±0.3	2.0±0.1

Septal Sm (cm/s)	2.5±0.1	2.5±0.1	2.6±0.2	2.7±0.1
Diastolic function				
E velocity (cm/s)	85.2±4.4	79.9±2.5	92.2±6.0	90.6±5.5
E DT (msec)	34.6±2.1	41.3±1.2†	34.8±3.0	38.8±3.0
E D rate (m/s^2)	25.1±2.0	19.5±1.1†	28.3±3.8	24.5±2.7
Septal Em	Nd	nd	nd	nd
Septal E/Em	Nd	nd	nd	nd
Lateral Em	Nd	nd	nd	nd
Lateral E/Em	Nd	nd	nd	nd
LV isovolumetric relaxation time				
IVRT (msec)	19.8±1.4	22.6±1.1	21.4±1.7	22.7±2.0
IVRTc	1.55±0.1	1.65±0.1	1.69±0.1	1.63±0.1
Myocardial performance index				
Septal MPI (%)	63.7±4.7	71.3±4.6	64.0±6.6	61.6±2.4
Lateral MPI (%)	68.3±3.5	76.2±2.7	70.4±4.2	64.2±2.4ξ
Global MPI (%)	42.0±3.8	51.2±3.6	48.7±2.8	41.0±4.3

LVAWd, LV anterior wall end-diastolic thickness; LVPWd, LV posterior wall end-diastolic thickness; LVEDD, Left ventricular end-diastolic diameter; LVESD, Left ventricular end-systolic diameter; FS, Fractional shortening, LVEF, Left ventricular ejection fraction; E, early diastolic transmitral filling velocity; IVRT, isovolumic

relaxation time; IVRTc, rate-corrected isovolumic relaxation time; EDT, early diastolic transmitral filling deceleration time; ED rate, early diastolic transmitral filling deceleration rate; Em, peak early diastolic tissue velocity; Sm, peak systolic tissue velocity.

Data reported as mean ± SEM. ξ: $p<0.05$ vs Sham; †: $p<0.05$ for $ERK3^{+/-}$ vs $ERK3^{+/+}$.
nd, not determined

Supplemental Table 1. The primers used for qPCR

Target	Primers
ANP S	5'-GTG CGG TGT CCA ACA CAG A-3'
ANP AS	5'-TTC TAC CGG CAT CTT CTC CTC-3'
BNP S	5'-GTT TGG GCT GTA ACG CAC TGA-3'
BNP AS	5'-GAA AGA GAC CCA GGC AGA GTC A-3'
β-MHC S	5'-AGG GTG GCA AAG TCA CTG CT-3'
β-MHC AS	5'-CAT CAC CTG GTC CTC CTT CA-3'
TGF-β1 S	5'-TGC TAA TGG TGG ACC GCA A-3'
TGF-β1 AS	5'-AGA TGT CTT TGG TTT TCT CAT AGA TGG-3'
TGF-β3 S	5'-AGA GAT CCA TAA ATT CGA CAT-3'
TGF-β3 AS	5'-ACA CAT TGA AAC GAA AAA CCT-3'
COL1α1 S	5'-CTG ACG CAT GGC CAA GAA GAC A-3'
COL1α1 AS	5'- CGT GCC ATT GTG GCA GAT ACA GAT -3'
GAPDH S	5'-CTG CAC CAC CAA CTG CTT AGC-3'
GAPDH AS	5'-ACT GTG GTC ATG AGC CCT TCC A-3'

S, sense; AS, anti-sense; GAPDH, glyceraldehyde 3-phosphate dehydrogenase; qPCR, quantitative polymerase chain reaction; ANP, atrial natriuretic peptide; BNP, B-type natriuretic peptides; β-MHC, β-myosin heavy chain; TGF-β1, transforming growth factor beta 1; TGF-β3, transforming growth factor beta 3; COL1α1, collagen type 1 alpha 1.

Supplemental Table 2. Structural and functional assessment of $MK5^{+/+}$ and $MK5^{+/-}$ mice by echocardiography.

	$MK5^{+/+}$ (n=13)	**$MK5^{+/-}$ (n=12)**
Aortic Peak Velocity (cm/s)	87.2±8.4	94.6±6.7
Aortic Peak Gradient (mmHg)	3.4±0.6	3.7±0.5
Aortic Mean Gradient (mmHg)	1.9±0.4	2.1±0.3
R-R interval (msec)	147.5±5.5	150.3±5.4
Left ventricular dimensions and mass		
LVAWd (mm)	0.7±0.02	0.7±0.04
LVPWd (mm)	0.7±0.02	0.6±0.03
LVEDD (mm)	4.1±0.1	4.1+0.2
LVESD (mm)	2.6±0.2	2.5±0.2
LV mass (mg)	217.1±4.1	211.5±7.8
LV mass / LVDd (mg/mm)	53.5±1.1	52.3±1.3
LV mass/BW (mg/g)	8.5±0.5	8.0±0.3
Systolic Function		
FS (%)	38.3±2.3	38.4±2.3
LVEF (%)	74.1±2.6	74.5±2.6
Lateral Sm (cm/s)	3.0±0.1	2.9±0.2

Septal Sm (cm/s)	2.9±0.2	2.9±0.2
Diastolic function		
E velocity (cm/s)	60.0±3.7	62.2±2.5
E DT (msec)	40.0±2.6	40.8±2.7
E D rate (m/s^2)	15.7±1.3	15.8±1.3
Septal Em	3.3±0.2	3.4±0.2
Septal E/Em	18.2±1.0	18.8±1.0
Lateral Em	3.0±0.3	3.3±0.2
Lateral E/Em	15.6±1.6	19.2±1.3
Left ventricular isovolumetric relaxation time		
IVRT (msec)	15.2±1.6	15.6±1.6
IVRTc	1.2±0.1	1.3±0.1
Myocardial performance index		
Septal MPI (%)	79.2±8.4	69.9±7.6
Lateral MPI (%)	81.0±6.1	91.7±12.6
Global MPI (%)	36.8±5.0	46.3±5.5

LVAWd, LV anterior wall end-diastolic thickness; LVPWd, LV posterior wall end-diastolic thickness; LVEDD, Left ventricular end-diastolic diameter; LVESD, Left ventricular end-systolic diameter; FS, Fractional shortening, LVEF, Left ventricular ejection fraction; E, early diastolic transmitral filling velocity; IVRT, isovolumic relaxation time; IVRTc, rate-corrected isovolumic relaxation time; EDT, early diastolic

transmitral filling deceleration time; ED rate, early diastolic transmitral filling deceleration rate; Em, peak early diastolic tissue velocity; Sm, peak systolic tissue velocity.

Data reported as mean ± SEM. †, $p < 0.05$ versus $ERK3^{+/+}$.

Supplemental Table 3. Hemodynamic parameters for $MK5^{+/+}$ and $MK5^{+/-}$ mice after 3 wk of pressure overload.

	Sham		**TAC**	
	$MK5^{+/+}$ (n=9)	**$MK5^{+/-}$ (n=8)**	**$MK5^{+/+}$ (n=8)**	**$MK5^{+/-}$ (n=8)**
P max (mmHg)	89.9±2.0	89.9±3.1	143.7±5.6 ξ	142.3±10.8 ξ
P min (mmHg)	57.4±2.6	58.7±3.1	64.8±2.9	65.1±3.6
P mean	69.7±2.7	71.3±3.3	90.7±2.9ξ	93.9±6.1ξ
LVP max (mmHg)	90.6±1.3	92.6±2.7	155.1±10.4 ξ	144.4±11.8 ξ
LVP min (mmHg)	2.3±1.0	3.3±1.5	2.7±0.5	8.0±2.7
LVP dPmax (mmHg/s)	4872±145.1	5176±234.7	6308±630.6 ξ	5047±362.8
LVP dPmin (mmHg/s)	-4794±216.7	-4865±168.3	-6542±567.1 ξ	-5589±417.9
Ped (mmHg)	6.9±1.2	7.6±2.3	6.33±0.3	16.6±3.1 ξ†
CT (msec)	14.3±0.5	14.0±0.5	15.1±0.6	13.7±0.6
RT (msec)	48.4±0.8	49.0±1.4	46.7±1.6	47.7±0.6
Tau (msec)	9.4±0.5	9.3±0.4	8.7±0.5	9.4±0.5
HR (bpm)	327.4±15.1	329.8±15.4	387.7±20.2	328.5±15.9

Data reported as mean ± SEM. For statistical comparisons One-way ANOVA followed by Newman-Keuls test was performed. Shown are the values of mean and SEM. ξ: $p<0.05$ vs Sham; †: $p<0.05$ for $MK5^{+/-}$ vs $MK5^{+/+}$.

Supplemental Table 4. Structural and functional assessment of ERK3 and MK5 mice by echocardiography.

	ERK3$^{+/+}$ (n=14)	**MK5$^{+/+}$ (n=13)**
Aortic Peak Velocity (cm/s)	58.4±2.5*	87.2±8.4
Aortic Peak Gradient (mmHg)	1.4±0.1*	3.4±0.6
Aortic Mean Gradient (mmHg)	0.7±0.1*	1.9±0.4
R-R interval (msec)	181.5±8.5*	147.5±5.5
Left ventricular dimensions and mass		
LVAWd (mm)	0.8±0.02*	0.7±0.02
LVPWd (mm)	0.8±0.03*	0.7±0.02
LVEDD (mm)	4.2±0.1	4.1±0.1
LVESD (mm)	2.9±0.1	2.6±0.2
LV mass (mg)	238.6±5.9*	217.1±4.1
LV mass / LVDd (mg/mm)	57.4±0.9*	53.5±1.1
LV mass/BW (mg/g)	8.0±0.2	8.5±0.5
BW (g)	29.8±0.8*	26.2±1.3
Systolic Function		
FS (%)	31.1±1.3*	38.3±2.3
LVEF (%)	65.3±1.8*	74.1±2.6

Lateral Sm (cm/s)	2.0±0.1*	3.0±0.1
Septal Sm (cm/s)	2.1±0.1*	2.9±0.2
Diastolic function		
E velocity (cm/s)	87.4±4.3*	60.0±3.7
E DT (msec)	49.3±3.0*	40.0±2.6
E D rate (m/s^2)	19.0±1.9	15.7±1.3
Septal Em	4.2±0.3*	3.3±0.2
Septal E/Em	21.5±0.8*	18.2±1.0
Lateral Em	3.7±0.3	3.0±0.3
Lateral E/Em	24.7±1.6	21.9±2.1
Left ventricular isovolumetric relaxation time		
IVRT (msec)	21.6±2.0*	15.2±1.6
IVRTc	1.6±0.1*	1.2±0.1
Myocardial performance index		
Septal MPI (%)	59.2±2.3*	79.2±8.4
Lateral MPI (%)	62.6±1.7*	81.0±6.1
Global MPI (%)	44.0±3.9	36.8±5.0

LVAWd, LV anterior wall end-diastolic thickness; LVPWd, LV posterior wall end-diastolic thickness; LVEDD, Left ventricular end-diastolic diameter; LVESD, Left ventricular end-systolic diameter; FS, Fractional shortening, LVEF, Left ventricular

ejection fraction; E, early diastolic transmitral filling velocity; IVRT, isovolumic relaxation time; IVRTc, rate-corrected isovolumic relaxation time; EDT, early diastolic transmitral filling deceleration time; ED rate, early diastolic transmitral filling deceleration rate; Em, peak early diastolic tissue velocity; Sm, peak systolic tissue velocity.

Data reported as mean ± SEM. *, $p < 0.05$ versus $MK5^{+/+}$.

UNPUBLISHED RESULTS

Screening for MK5 substrates in the heart

There is still a lack of knowledge about the upstream signaling and regulatory inputs that control the expression and/or activity of ERK3 and ERK4. In fact, MK5 is currently the only known target downstream of ERK3/ERK4 [63, 107, 108]. *In vitro*, MK5 phosphorylates Hsp27, however studies in MK5 knock-out MEFs raised serious concerns about *in vivo* HSP25 (mouse homologue of HSP27) as a substrate of MK5 [106]. Therefore, given the involvement of MK5 in pathological fibrosis and to gain a further understanding of MK5 downstream signaling, we sought to identify its substrates in the heart. Rat heart cytosol was incubated with activated GST-MK5 (phosphorylated in vitro with p38α) in the presence of [γ^{32}P]ATP and protein phosphorylation was assessed by autoradiography following SDS-PAGE (1D) or IPG-PAGE (2D). Two low molecular weight proteins were labeled with $^{32}PO_4$ in 1D as well as 2D gels (Fig. 7A). In both cases, regions of the gel containing the phosphorylated protein were excised and the protein was identified by liquid chromatography-tandem mass spectrometry (LC-MSMS). The high molecular weight band corresponded to Hsp25 and the lower MWt band corresponded to alpha-B crystalline (αBC). We confirmed these observations by showing that activated GST-MK5 was able to phosphorylate purified recombinant His-HSP27 and bovine αBC. Activated GST-MK2 was employed as a positive control. GST-MK5 incorporated more phosphate in Hsp27 than GST-MK2, but in the case of αBC both enzymes incorporated same amount of phosphate (Fig. 7B). MK2 is known to phosphorylate HSP27 and αBC *in vitro* and *in vivo* [161]. Phosphorylation of cytosolic and purified bovine αBC by activated GST-MK5 may indicate αBC as a novel substrate for MK5, although phosphorylation of αBC *in vivo* by MK5 remains to be determined.

Figure 7

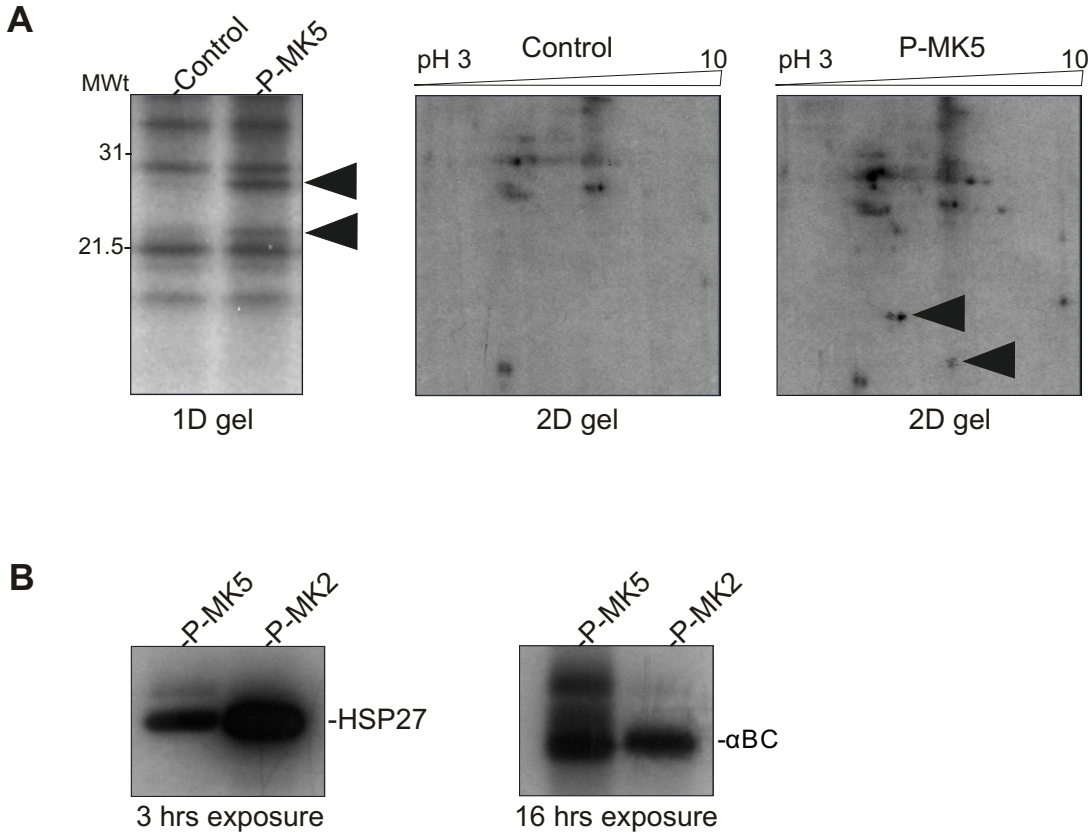

Fig. 7. Screening for MK5 substrates in heart (**A**) GST-MK5 (1 mU) was incubated with 50 µg cytosol and 10 µM [γ^{32}P]ATP (10 µCi) for 60 min at 30°C. Reactions were terminated using 4x SDS-PAGE sample buffer. Proteins were separated on 10-20% SDS-PAGE. Gels were stained with Coomassie blue, dried and exposed to x-ray film. For 2D gels, reactions were stopped by addition of TCA, the protein pellet dissolved in rehydration buffer, and protein resolved on 7 cm pH 3-10 IPG strips. For the second dimension, proteins were resolved on 10-20% SDS page as discussed above. Shown are representative images of two independent experiments. (**B**) 0.1 µg of phosphorylated GST-MK5 or GST-MK2 was incubated with 1.0 µg of purified recombinant His_6-Hsp27 (left) or bovine αB-crystallin (right) and 10 µM [γ^{32}P]ATP (1 µCi). Solid arrow shows point of $^{32}PO_4$ incorporation in 1D and 2D gel.

DISCUSSION

MK5 is phosphorylated both by p38 and atypical MAPKs, ERK3 and ERK4. Recently PKA has also been shown to be involved. Despite this, the physiological role of MK5 and ERK3/ERK4 remain unknown. Moreover, p38α is considered to be the dominant p38 isoform in heart. Little is known about p38γ and p38δ. Here we show that following 2- and 3-wks of pressure overload, hearts from $MK5^{+/-}$ mice developed hypertrophy but were resistant to myocardial interstitial fibrosis. In lysates prepared from normal hearts, where p38 would not be activated, ERK3, but not ERK4 or p38α, co-immunoprecipitated with MK5. After acute or chronic pressure overload, MK5 remained bound to ERK3 while no interaction with ERK4 or p38α was detected. Similar to $MK5^{+/-}$ hearts, following 3 wks of pressure overload, $ERK3^{+/-}$ mice developed hypertrophy whereas cardiac interstitial fibrosis was not detected. Thus ERK3-MK5 signaling plays a role in pressure overload-induced myocardial interstitial fibrosis. Furthermore, in the heart, mRNA for 5 splice variants of MK5 (MK5.1-5.5) including the original form (MK5: referred to herein as MK5.1), was detected. One of the variant (MK5.3) lacked binding sites for ERK3/ERK4, while two others (MK5.4-5.5) lacked part of kinase domain and hence were catalytically inactive. The relative abundance of variant mRNA was changed in response to chronic pressure overload and during postnatal heart development. Hence, distinct effects may be mediated by these MK5 variants which would increase the functional diversity of ERK3-MK5 signaling. To date all p38 isoforms except p38δ have been reported in the heart. p38α is considered to be the dominant isoform. Here we show that p38δ is expressed in the mouse heart at protein levels which are comparable to p38β, and at both mRNA and protein levels p38α and p38γ expressions levels were similar. Moreover, p38γ but not p38α accumulated in the nucleus in hearts in response to chronic pressure overload, which suggests that p38γ may play a distinct role during pressure overload-induced cardiac remodelling. In summary, we have now shown 1) ERK3-MK5 signaling plays an important role in pressure overload-induced cardiac interstitial fibrosis and 2) p38γ may play an important role in the heart.

Due to the availability of pharmacological inhibitors, such as SB203580, p38α and p38β have been studied extensively in the heart, and have been shown to be activated in response to various stimuli such as ischemia and reperfusion, pressure overload, pro-hypertrophic agonists, and mechanical stretch [162-165]. During ischemia, inhibition of p38α is protective and $p38\alpha^{+/-}$ mice are resistant to infarction [166-168]. In neonatal myocytes, p38β has been shown to be involved in the MKK6-mediated hypertrophic response and p38α in the MKK3-mediated apoptosis [33]. Our results showed that p38δ was expressed at protein levels similar to p38β, and its mRNA levels increased in the hypertrophying mouse heart. Despite lower expression of p38β relative to p38α/γ, it has been shown to mediate specific signaling in the heart [33]. Therefore, further study may also reveal a unique role for p38δ in the heart.

Until now p38α has been considered to be the predominant isoform in the heart: however, this has not been studied systematically. We therefore studied the p38 isoform expression profile and subcellular distribution in both the normal mouse heart as well as those subjected to pressure overload. p38γ mRNA and protein was expressed at levels similar to p38α. Moreover, in response to pressure overload, p38β/γ/δ mRNA levels were increased. However, no corresponding changes were observed at the protein level. In response to pressure overload, p38γ, but not p38α, accumulated in the nucleus. p38γ is the only member of the p38 family to have a KETXL sequence in its C-terminus. This sequence can interact with PDZ domains [169], which may allow p38γ to diversify its signaling. One would ask, why p38γ and not p38α accumulates in nucleus following pressure overload. The answer could be in p38γ's ability to interact with proteins containing a PDZ domain. For example, the PDZ-binding motif FLTWL in YES kinase-associated protein (YAP) is essential for its nuclear import and ability to promotes apoptosis in HEK293 cells in response to low serum [170]. p38γ has been shown to interact with number of PDZ-containing proteins such as α1-syntrophin, SAP90/PSD95, and SAP97/hDlg [169, 171] as well as several transcription factors, including MEF2A, AP-1, p53, ATF2, Elk-1, SAP1, and SAP2 [172-174]. Under pathological conditions, p38α has been shown to regulate myocardial fibrosis and apoptosis [33, 51, 175]. As p38γ was expressed at protein equivalent levels to p38α, and accumulates in the nucleus

when the heart is chronically exposed to pressure overload, it is highly likely that p38γ plays a role in the changes in gene expression associated with cardiac remodeling. In order to begin to understand the consequences of the nuclear localization of p38γ, we sought to identify proteins in cytosolic and nuclear fractions isolated from rat heart that became phosphorylated while incubated in the presence of [γ^{32}P]ATP plus phosphorylated, activated GST-p38α, GST-p38β, GST-p38γ, or GST-p38δ. However, no p38-specific phosphorylation was observed in either subcellular fraction. The failure to detect p38-dependent incorporation of ^{32}P into proteins in the cytosolic or nuclear fraction may reflect low copy number or phosphorylation status of target proteins in these fractions or localization or, perhaps, the absence of a suitable scaffolding protein.

MK2, MK3, and MK5 lie downstream of p38. The physiological roles of MK3 and MK5 remain unknown. Herein we determined if MK5 is involved in pathological remodeling of the heart. In response to chronic pressure overloads, mice heterozygous for a functional knockout of MK5 underwent molecular remodeling and hypertrophy but were resistant to fibrosis in response to chronic pressure overload induced by TAC. *In vitro* and in cells studies have shown the involvement of MK5 downstream of p38 and atypical MAPKs ERK3 and ERK4 [63, 87-90, 94, 108]. Of the four p38 isoforms, MK5 is regulated by p38α and p38β. In HeLa cells, in response to stress or constitutively activated form of MKK6, p38α and p38β activate MK5 [88]. Additinally, *in vitro* kinetic studies also demonstrate MK5 to be a better substrate for p38α and p38β than p38γ and p38δ [176]. MK5 interacts physically with all of its known upstream kinases. MK5 and p38 co-immunoprecipitate when over expressed in NIH3T3 cells [91, 177]. Over-expressed ERK4 forms a complex with ERK3 and in HEK cells, endogenous (i.e., not heterologously expressed) ERK3 and ERK4 both interact with MK5. Moreover, deletion of either ERK3 or ERK4 does not affect the ability of the other ERK to interact with MK5: in an ERK3-deficient background ERK4 is still able to interact with MK5 and vice versa [62, 63]. This suggests that the interaction of MK5 with ERK4 or ERK3 is independent of the presence of the other atypical MAPK. Similarly, at endogenous levels, both ERK3 and ERK4 are physiological regulators of MK5 activity. MK5 activity is reduced by 50% in ERK3$^{-/-}$ cells or following siRNA-mediated knock down

of either ERK3 or ERK4. Combined siRNA mediated knock down of ERK3 plus ERK4 reduces MK5 activity by 80% [63, 108]. Therefore, in the heart we sought to determine which of these kinases (e.g., p38α, p38β, ERK3, ERK4) interact with MK5. Immunoprecipitation of MK5 from whole mouse heart lysates resulted in co-immunoprecipitation of ERK3 but not ERK4 or p38α. Under these conditions p38 activity was minimal. We then determined if MK5 interacts with p38α under conditions where the p38 pathway was activated. We have shown a peak in phospho p38 levels occurs 3 d post-TAC. In hearts exposed to either acute (3 days) or chronic (3 weeks) pressure overload, immunoprecipitation of MK5 resulted in co-immunoprecipitation of ERK3, but not ERK4 or p38α. Hence, in the heart, activation of the p38 pathway does not appear to induce the formation of a stable p38-MK5 complex or alter the stability of MK5-ERK3 complexes. These observations suggesting that the pro-fibrotic signaling of MK5 is regulated by ERK3. Consistently, similar to $MK5^{+/-}$ mice, $ERK3^{+/-}$ mice underwent hypertrophy and molecular remodeling, but not fibrosis in response to 3 weeks of pressure overload. Taken together, these results show that MK5-ERK3 signaling plays an important role in remodeling of the myocardial extracellular matrix and resulting increase in wall stress induced by chronic pressure overload.

During fibrosis, both the synthesis and degradation of collagen are altered, the net result of with is collagen accumulation. Collagen type I and type III are the major components of the cardiac ECM. Approximately 85% of total collagen in the heart is collagen type 1, and hence it is a major determinant of myocardial stiffness [178, 179]. In both $MK5^{+/-}$ and $ERK3^{+/-}$ hearts, TAC induced less collagen accumulation, as detected by Masson trichrome staining, and this reduction appears to be a consequence of hampered COL1α1 mRNA synthesis and/or stability. In both $MK5^{+/-}$ and $ERK3^{+/-}$ hearts, the ability of pressure overload to induce an increase in COL1α1 mRNA levels was reduced compared to wild type littermates. In the heart, TGF-β1 is a locally generated cytokine that induces fibroblast proliferation, fibroblast differentiation into myofibroblasts, and increased production of ECM proteins, including collagens, fibronectin, and proteoglycans [141]. On the other hand, to maintain the increase in fibrosis, TGF-β also reduces the degradation of ECM by inhibiting the expression of

matrix metalloproteinases (MMP), and by inducing the expression of protease inhibitors, such as plasminogen activator inhibitor-1 (PAI-1) and tissue inhibitors of metalloproteinases (TIMPs) [142]. There was no difference in TGF-β1 and TGF-β3 mRNA levels in $MK5^{+/-}$ hearts following 2 and 3 wks TAC compared to hearts from wild type littermates. A similar TGF-β1 pattern was observed in $ERK3^{+/-}$ TAC hearts. In conclusion, although chronic pressure overload failed to induce fibrosis in $MK5^{+/-}$ and $ERK3^{+/-}$ hearts, the increase in TGFβ mRNA, was maintained, suggesting the involvement of ERK3-MK5 in the fibrotic response to pressure overload lies downstream of TGFβ transcription.

The results presented herein indicate that MK5 and ERK3 are involved in the increase in interstitial fibrosis induced by chronic pressure overload, the main determinant of diastolic dysfunction in heart disease. These results may be interpreted as suggesting that MK5 or ERK3 activities may represent potential targets for the treatment of fibrosis induced by pressure overload. However, this study was based on genetic models wherein the actual level of expression of MK5 or ERK3 was reduced. It remains to be determined if the antifibrotic effects were due to the reduction in MK5 or ERK3 activity or due to a decrease in the cellular content of these proteins. Both MK5 and ERK can physically interact with other proteins within the cell and it may be the loss of these physical interactions, rather than a reduction in kinase activity, that has resulted in reduced fibrosis. For example, in the absence of a binding partner such as MK5, ERK3 is rapidly broken down. Hence, reductions in MK5 expression results in reduced in ERK3 content as well and thus the protective effects observed in the $MK5^{+/-}$ mouse may have resulted from a reduction in ERK3 protein levels or activity. Future studies will be required to address the involvement of the catalytic activity of MK5 and ERK3 in the development of interstitial fibrosis using mice engineered to express inactive mutants of MK5 or ERK3 in order to resolve this issue.

An analysis of cDNA prepared from the mouse ventricular myocardium demonstrated 5 splice variants of MK5 (MK5.1-5), including the originally published form (MK5.1). The putative amino acid sequences indicated that all variants retain the activating phosphorylation site (Thr-182) plus both the NES and NLS within the C-

terminus. MK5.2 lacks 2 amino acids, MK5.3 lacks C-terminal amino acids 370 through 473, and MK5.4 and MK5.5 lack kinase subdomains I-VIb. In full-length MK5, C-terminal amino acid residues 383-393 and 460-465 are required for its interaction with ERK3/ERK4 [110]. Hence, with the exception of MK5.3, all other variants retain the binding sites for ERK3/ERK4. Moreover, the relative abundance of MK5.3 mRNA was reduced following 1 wk of pressure overload. At this point, the role played by each variant in MK5 mediated myocardial fibrosis remains unclear, as the deletion of exon 6 in the MK5 knockout mice used in this study [106] affects all 5 variants. In the future, gain of function studies wherein the introduction of MK5.1-3 variant into isolated $MK5^{-/-}$ cardiac fibroblast or loss of function studies wherein the introduction of MK5.4-5 in to wild type cardiac fibroblast, should reveal if these variants play a similar role in the regulation of collagen expression.

MK5 is located within the nucleus when inactive and translocates to the cytosol upon over-expression or activation of p38 [89-91]. Similarly, in HEK293 cells, exogenously expressed MK5.1-V5, MK5.2-V5 or MK5.3-V5 localized to the nucleus. Incubation with anisomycin, which activates p38, resulted in the translocation of all 3 variants to the cytosol. The nuclear export was blocked by SB203580, an inhibitor of p38α/β activity. Therefore, the lack of 2 amino acid residues on MK5.2 and 103 amino acid residues in the C-terminal of MK5.3 had no effect on p38-mediated subcellular relocalization. Surprisingly, exogenously expressed MK5.4-V5 and MK5.5-V5 localized to the cytoplasm and p38 activation induced a small increase in immunocytofluorescence within the nucleus. The nuclear import of MK5.4 and MK5.5 was not blocked by SB203580. Hence, the absence of kinase subdomains I-VIb in MK5.4 and MK5.5 affected its ability to translocate into, or be retained within, the nucleus. One possible explanation for the small amount of MK5.4 and MK5.5 in nucleus following p38 activation is that it interacts with p38 within the cytosol and enters the nucleus as heterodimer with activated p38.

In MK5 signaling, the regulation of its activity by upstream kinases and its downstream effectors are currently controversial. The activation and subcellular localization of MK5 is regulated by both p38 and ERK3/ERK4. Recently, PKA was also

shown to be involved. When originally identified, MK5 was described as a p38 substrate, as its activation and cellular localization depended on p38 activity [88]. Additionally, in the cellular localization of MK5 was altered by just over-expression of kinase-dead p38α or p38β as well as non-activatable p38α [89, 90], suggesting that the binding of p38 to MK5 may be sufficient to induce translocation. However, these studies may also reflect an inappropriate localization or translocation of p38 when overexpressed. More recent studies suggest that the regulation of MK5 activity may be more complicated. While both the stability of p38α and stress induced Hsp25 (mouse homologue of Hsp27) phosphorylation are reduced in cells isolated from MK2-deficient mice, no such effects are observed in cells from MK5-deficient mice [106, 132]. These observations raised serious concerns about the role of MK5 as an Hsp25-kinase and substrate for p38 *in vivo*. On the other hand, in a different line of MK5 knockout mice, MK5 has been shown to mediate senescence in response to the induction of oncogenic *ras* through activation of p38 [94]. These differences in *in vivo* observations remain unexplained. Both lines of mice are in a similar genetic background: however, one line expressed non-functional MK5 [106] whereas the other does not express MK5 [94]. It is possible that deletion of the kinase domain within MK5 might not be enough to eliminate all of MK5's functions: MK5 may also serve as a scaffold to recruit other proteins.

Atypical MAPKs ERK3 and ERK4 regulate both the activity and cellular localization of MK5 [63, 108]. Although inactive MK5 primarily located within the nucleus, it constantly shuttles between nucleus and cytoplasm [90]. Over-expressing ERK3 retains MK5 in the cytoplasm [107]. The phosphorylation of ERK3 and ERK4 within the activating S-E-G motif does not change in response extracellular mitogenic or stress stimuli [65, 109]. However, both ERK3 and ERK4 directly phosphorylate MK5 and phosphorylation of ERK3 and ERK4 within their S-E-G motif is indispensable for their ability to form a stable interaction with MK5 and thus regulate its activation and subcellular localization [65]. During embryogenesis ERK3 and MK5 mRNA expression peaks at day E11 [107]. ERK3 accumulates during cell differentiation, inducing G1 arrest, and thus inhibiting cell proliferation [59]. Hence, it is conceivable that both

ERK3/ERK4 and p38 regulate MK5 activity and cellular localization, depending upon the differentiation status and nature of the cell system being studied. Given the p38's ability to regulates ERK3 transcription and translation [61], and the dependence of MK5 activation and interactions on ERK3/ERK4 phosphorylation [65], it is also possible that a kinase that phosphorylates ERK3/ERK4 is under indirect control of p38 activity. In the heart, MK5 co-immunoprecipitated ERK3 but not ERK4 or p38α, and this ERK3-MK5 complex was stable irrespective of p38 activity. Moreover, exogenously added GST-MK5 in the heart lysate was able to pull down ERK4 and p38 immunoreactivity but not ERK3. These observations suggest that there is no free ERK3 in the heart: all the ERK3 is bound to the endogenous proteins, including, but not limited to, MK5. Conversely, exogenously added GST-ERK3 or GST-p38α were not able to pull down endogenous MK5 from mouse heart lysates. These results suggest that although MK5 can interact with p38 and ERK4 in cultured cells at the levels expressed in the heart, MK5 and ERK3 are in complexes and neither is in an unbound form. These results do not, however, indicate 1) if MK5 and ERK3 are present only as an ERK3-MK5 complex versus complexes with other endogenous proteins, and 2) if ERK3-MK5 complexes also include other proteins.

Little is known about the substrate specificity of MK5. *In vitro,* MK5 phosphorylates Hsp27, but studies in MK5 knockout MEF cell raised some concerns about Hsp25 being a MK5 substrate *in vivo* [106]. In our *in vitro* kinase assay screening for MK5 substrates, activated GST-MK5 incorporated $^{32}PO_4$ into αB-crystallin. αB-crystallin belongs to the family of small heat shock proteins (sHsps) and is phosphorylated at three serine sites corresponding to residues 19, 45, and 59. Serine 59 gets phosphorylated by MK2, serine 45 appears under the control of p42/p44 MAPK, and the kinase responsible for the phosphorylation of ser 19 remains unknown [161]. In U373 MG human glioma cells, Kato *et al.* showed that these three serine residues are phosphorylated by three different protein kinases, and the kinase responsible for phosphorylating ser 19 eluted from a Superdex 200 gel filtration column with an apparent molecular mass of around 60 kDa: however, they were not able to identify the kinase. Moreover, mitotic cells and cells treated with phorbol 12-myristate 13-acetate

(PMA) increased the phosphorylation at ser 19 [180]. The molecular mass of MK5 is 54 kDa, close to the unidentified 60 kDa kinase that phosphorylated αBC on ser 19. Additionally, in the isolated perfused heart, ischemic stress induces αB-crystallin translocation from a diffuse, cytosolic localization to the sarcomeres [181]. This translocation was shown to be temporally coordinated with increased αB-crystallin phosphorylation, although the identities of the phosphorylated residues have yet to be established [182]. Moreover, in PC12 cells PKA activated MK5, which was required for PKA induced microfilament rearrangement [98]. Altogether it appears that αB-crystallin may be a novel MK5 substrate, however this requires further characterization.

CONCLUSIONS

This study shows a novel role for ERK3-MK5 in the heart during pathological remodelling induced by pressure overload. We have shown that $MK5^{+/-}$ and $ERK3^{+/-}$ hearts hypertrophy but are resistant to fibrosis and show preserved diastolic function following pressure overload. The reduced collagen expression in $MK5^{+/-}$ or $ERK3^{+/-}$ was not due to reduction in TGFβ mRNA synthesis. Additionally, $ERK3^{+/-}$ hearts showed diastolic dysfunction. Moreover, MK5 and ERK3 are in a complex in control hearts, and the stability of this complex was not altered by 3-d or 3-wk of pressure overload. No unbound MK5 or ERK3 was detected in heart lysates.

We also have shown the existence of 5 splice variants (MK5.1-5.5) of MK5. One of the variant (MK5.3) lacked binding sites for ERK3/ERK4, while two others (MK5.4-5.5) lacked a complete kinase domain and hence were catalytically inactive. The relative abundance of variant mRNA was changed both in response to pressure overload and during postnatal heart development. Hence, distinct effects may be mediated by these MK5 variants which would increase the functional diversity of ERK3-MK5 signaling.

Furthermore, we have shown that p38δ is expressed in the mouse heart at protein levels which were comparable to p38β, and at both mRNA and protein levels p38α and p38γ expression levels were similar. Moreover, p38γ but not p38α accumulated in the nucleus in response to chronic pressure overload, which may suggest distinct role played by p38γ during hypertrophy.

ORIGINAL CONTRIBUTION TO THE LITERATURE

1. MK5 is involved in cardiac interstitial fibrosis induced by chronic pressure overload.
2. MK5 forms complex with ERK3 and not with ERK4 and/or p38 in control and hypertrophic heart, and the pro-fibrotic signaling mediated by MK5 may involve ERK3 activation.
3. In heart, both MK5 and ERK3 are bound to each other, or other proteins, hence there is no pool of uncomplexed MK5 or ERK3.
4. Like MK5, ERK3 is involved in cardiac interstitial fibrosis induced by chronic pressure overload.
5. A deficiency in ERK3 in heart results in diastolic dysfunction.
6. Demonstration of 5 splice variants of MK5 in the heart and its expression is regulated during post-natal heart development and pressure-overload induced hypertrophy.
7. The abundance of p38γ is equal to that of p38α at both mRNA and protein levels. It was previously thought that p38α was the dominant isoform in the heart.
8. Demonstrated the presence of p38δ in the heart at mRNA and protein levels, and its increase in mRNA levels with hypertrophy.
9. Following exposure to chronic pressure overload, p38γ accumulates in nucleus, suggesting p38γ may be involved in regulating in gene expression during pathologic remodelling of the heart.

REFERENCES

[1] Heineke J, Molkentin JD. Regulation of cardiac hypertrophy by intracellular signalling pathways. Nat Rev Mol Cell Biol. 2006; 7(8): 589-600.

[2] Katz AM. Physiology of the heart. 4th ed. Philadelphia: Lippincott Williams & Wilkins; 2006.

[3] Sadoshima J, Izumo S. The cellular and molecular response of cardiac myocytes to mechanical stress. Annu Rev Physiol. 1997; 59: 551-71.

[4] McMullen JR, Jennings GL. Differences between pathological and physiological cardiac hypertrophy: novel therapeutic strategies to treat heart failure. Clin Exp Pharmacol Physiol. 2007 Apr; 34(4): 255-62.

[5] Dorn GW, 2nd. The fuzzy logic of physiological cardiac hypertrophy. Hypertension. 2007 May; 49(5): 962-70.

[6] Berk BC, Fujiwara K, Lehoux S. ECM remodeling in hypertensive heart disease. J Clin Invest. 2007 Mar; 117(3): 568-75.

[7] Kinugawa K, Yonekura K, Ribeiro RC, Eto Y, Aoyagi T, Baxter JD, et al. Regulation of thyroid hormone receptor isoforms in physiological and pathological cardiac hypertrophy. Circ Res. 2001 Sep 28; 89(7): 591-8.

[8] Wakatsuki T, Schlessinger J, Elson EL. The biochemical response of the heart to hypertension and exercise. Trends Biochem Sci. 2004; 29(11): 609-17.

[9] Spinale FG. Myocardial matrix remodeling and the matrix metalloproteinases: influence on cardiac form and function. Physiol Rev. 2007 Oct; 87(4): 1285-342.

[10] Brown RD, Ambler SK, Mitchell MD, Long CS. The cardiac fibroblast: therapeutic target in myocardial remodeling and failure. Annu Rev Pharmacol Toxicol. 2005; 45: 657-87.

[11] Brancaccio M, Fratta L, Notte A, Hirsch E, Poulet R, Guazzone S, et al. Melusin, a muscle-specific integrin beta1-interacting protein, is required to prevent cardiac failure in response to chronic pressure overload. Nat Med. 2003 Jan; 9(1): 68-75.

[12] Peng X, Kraus MS, Wei H, Shen TL, Pariaut R, Alcaraz A, et al. Inactivation of focal adhesion kinase in cardiomyocytes promotes eccentric cardiac hypertrophy and fibrosis in mice. J Clin Invest. 2006 Jan; 116(1): 217-27.

[13] Knoll R, Hoshijima M, Hoffman HM, Person V, Lorenzen-Schmidt I, Bang ML, et al. The cardiac mechanical stretch sensor machinery involves a Z disc complex that is defective in a subset of human dilated cardiomyopathy. Cell. 2002 Dec 27; 111(7): 943-55.

[14] Heineke J, Ruetten H, Willenbockel C, Gross SC, Naguib M, Schaefer A, et al. Attenuation of cardiac remodeling after myocardial infarction by muscle LIM protein-calcineurin signaling at the sarcomeric Z-disc. Proc Natl Acad Sci U S A. 2005 Feb 1; 102(5): 1655-60.

[15] Zou Y, Akazawa H, Qin Y, Sano M, Takano H, Minamino T, et al. Mechanical stress activates angiotensin II type 1 receptor without the involvement of angiotensin II. Nat Cell Biol. 2004 Jun; 6(6): 499-506.

[16] Rakesh K, Yoo B, Kim IM, Salazar N, Kim KS, Rockman HA. beta-Arrestin-biased agonism of the angiotensin receptor induced by mechanical stress. Sci Signal. 2010; 3(125): ra46.

[17] Alberts B. Molecular biology of the cell. 3rd ed. New York: Garland Pub.; 1994.

[18] Kang M, Chung KY, Walker JW. G-protein coupled receptor signaling in myocardium: not for the faint of heart. Physiology (Bethesda). 2007 Jun; 22: 174-84.

[19] Wettschureck N, Rutten H, Zywietz A, Gehring D, Wilkie TM, Chen J, et al. Absence of pressure overload induced myocardial hypertrophy after conditional inactivation of Galphaq/Galpha11 in cardiomyocytes. Nat Med. 2001 Nov; 7(11): 1236-40.

[20] Adams JW, Sakata Y, Davis MG, Sah VP, Wang Y, Liggett SB, et al. Enhanced Galphaq signaling: a common pathway mediates cardiac hypertrophy and apoptotic heart failure. Proc Natl Acad Sci U S A. 1998 Aug 18; 95(17): 10140-5.

[21] D'Angelo DD, Sakata Y, Lorenz JN, Boivin GP, Walsh RA, Liggett SB, et al. Transgenic Galphaq overexpression induces cardiac contractile failure in mice. Proc Natl Acad Sci U S A. 1997 Jul 22; 94(15): 8121-6.

[22] Chen Z, Gibson TB, Robinson F, Silvestro L, Pearson G, Xu B, et al. MAP kinases. Chem Rev. 2001; 101(8): 2449-76.

[23] Roux PP, Blenis J. ERK and p38 MAPK-activated protein kinases: a family of protein kinases with diverse biological functions. Microbiol Mol Biol Rev. 2004; 68(2): 320-44.

[24] Bueno OF, De Windt LJ, Tymitz KM, Witt SA, Kimball TR, Klevitsky R, et al. The MEK1-ERK1/2 signaling pathway promotes compensated cardiac hypertrophy in transgenic mice. EMBO J. 2000 Dec 1; 19(23): 6341-50.

[25] Hunter JJ, Tanaka N, Rockman HA, Ross J, Jr., Chien KR. Ventricular expression of a MLC-2v-ras fusion gene induces cardiac hypertrophy and selective diastolic dysfunction in transgenic mice. J Biol Chem. 1995 Sep 29; 270(39): 23173-8.

[26] Harris IS, Zhang S, Treskov I, Kovacs A, Weinheimer C, Muslin AJ. Raf-1 kinase is required for cardiac hypertrophy and cardiomyocyte survival in response to pressure overload. Circulation. 2004 Aug 10; 110(6): 718-23.

[27] Kehat I, Davis J, Tiburcy M, Accornero F, Saba-El-Leil MK, Maillet M, et al. Extracellular signal-regulated kinases 1 and 2 regulate the balance between eccentric and concentric cardiac growth. Circ Res. 2011 Jan 21; 108(2): 176-83.

[28] Ono K, Han J. The p38 signal transduction pathway: activation and function. Cell Signal. 2000; 12(1): 1-13.

[29] Court NW, dos Remedios CG, Cordell J, Bogoyevitch MA. Cardiac expression and subcellular localization of the p38 mitogen-activated protein kinase member, stress-activated protein kinase-3 (SAPK3). J Mol Cell Cardiol. 2002; 34(4): 413-26.

[30] Seta K, Sadoshima J. What is the unique function of SAPK3/p38gamma in cardiac myocytes? J Mol Cell Cardiol. 2002; 34(6): 597-600.

[31] Gerits N, Kostenko S, Moens U. In vivo functions of mitogen-activated protein kinases: conclusions from knock-in and knock-out mice. Transgenic Res. 2007; 16(3): 281-314.

[32] Zhang S, Weinheimer C, Courtois M, Kovacs A, Zhang CE, Cheng AM, et al. The role of the Grb2-p38 MAPK signaling pathway in cardiac hypertrophy and fibrosis. J Clin Invest. 2003; 111(6): 833-41.

[33] Wang Y, Huang S, Sah VP, Ross J, Brown JH, Han J, et al. Cardiac Muscle Cell Hypertrophy and Apoptosis Induced by Distinct Members of the p38 Mitogen-activated Protein Kinase Family. Journal of Biological Chemistry. 1998 January 23, 1998; 273(4): 2161-8.

[34] Liao P, Georgakopoulos D, Kovacs A, Zheng M, Lerner D, Pu H, et al. The in vivo role of p38 MAP kinases in cardiac remodeling and restrictive cardiomyopathy. Proc Natl Acad Sci U S A. 2001; 98(21): 12283-8.

[35] Braz JC, Bueno OF, Liang Q, Wilkins BJ, Dai YS, Parsons S, et al. Targeted inhibition of p38 MAPK promotes hypertrophic cardiomyopathy through upregulation of calcineurin-NFAT signaling. J Clin Invest. 2003 May; 111(10): 1475-86.

[36] Nishida K, Yamaguchi O, Hirotani S, Hikoso S, Higuchi Y, Watanabe T, et al. p38alpha mitogen-activated protein kinase plays a critical role in cardiomyocyte survival but not in cardiac hypertrophic growth in response to pressure overload. Mol Cell Biol. 2004; 24(24): 10611-20.

[37] Streicher JM, Ren S, Herschman H, Wang Y. MAPK-activated protein kinase-2 in cardiac hypertrophy and cyclooxygenase-2 regulation in heart. Circ Res. 2010 Apr 30; 106(8): 1434-43.

[38] Kerkela R, Force T. p38 mitogen-activated protein kinase: a future target for heart failure therapy? J Am Coll Cardiol. 2006; 48(3): 556-8.

[39] Baines CP, Molkentin JD. STRESS signaling pathways that modulate cardiac myocyte apoptosis. J Mol Cell Cardiol. 2005; 38(1): 47-62.

[40] Ren J, Zhang S, Kovacs A, Wang Y, Muslin AJ. Role of p38alpha MAPK in cardiac apoptosis and remodeling after myocardial infarction. J Mol Cell Cardiol. 2005; 38(4): 617-23.

[41] Ma XL, Kumar S, Gao F, Louden CS, Lopez BL, Christopher TA, et al. Inhibition of p38 mitogen-activated protein kinase decreases cardiomyocyte apoptosis and improves cardiac function after myocardial ischemia and reperfusion. Circulation. 1999; 99(13): 1685-91.

[42] Moriguchi T, Kuroyanagi N, Yamaguchi K, Gotoh Y, Irie K, Kano T, et al. A novel kinase cascade mediated by mitogen-activated protein kinase kinase 6 and MKK3. J Biol Chem. 1996 Jun 7; 271(23): 13675-9.

[43] Watkins SJ, Jonker L, Arthur HM. A direct interaction between TGFbeta activated kinase 1 and the TGFbeta type II receptor: implications for TGFbeta signalling and cardiac hypertrophy. Cardiovasc Res. 2006 Feb 1; 69(2): 432-9.

[44] Ninomiya-Tsuji J, Kishimoto K, Hiyama A, Inoue J, Cao Z, Matsumoto K. The kinase TAK1 can activate the NIK-I kappaB as well as the MAP kinase cascade in the IL-1 signalling pathway. Nature. 1999 Mar 18; 398(6724): 252-6.

[45] Zhang D, Gaussin V, Taffet GE, Belaguli NS, Yamada M, Schwartz RJ, et al. TAK1 is activated in the myocardium after pressure overload and is sufficient to provoke heart failure in transgenic mice. Nat Med. 2000 May; 6(5): 556-63.

[46] Lee MR, Dominguez C. MAP kinase p38 inhibitors: clinical results and an intimate look at their interactions with p38alpha protein. Curr Med Chem. 2005; 12(25): 2979-94.

[47] Ge B, Gram H, Di Padova F, Huang B, New L, Ulevitch RJ, et al. MAPKK-independent activation of p38alpha mediated by TAB1-dependent autophosphorylation of p38alpha. Science. 2002 Feb 15; 295(5558): 1291-4.

[48] Tanno M, Bassi R, Gorog DA, Saurin AT, Jiang J, Heads RJ, et al. Diverse mechanisms of myocardial p38 mitogen-activated protein kinase activation: evidence for MKK-independent activation by a TAB1-associated mechanism contributing to injury during myocardial ischemia. Circ Res. 2003 Aug 8; 93(3): 254-61.

[49] Li J, Miller EJ, Ninomiya-Tsuji J, Russell RR, 3rd, Young LH. AMP-activated protein kinase activates p38 mitogen-activated protein kinase by increasing recruitment of p38 MAPK to TAB1 in the ischemic heart. Circ Res. 2005 Oct 28; 97(9): 872-9.

[50] Salvador JM, Mittelstadt PR, Guszczynski T, Copeland TD, Yamaguchi H, Appella E, et al. Alternative p38 activation pathway mediated by T cell receptor-proximal tyrosine kinases. Nat Immunol. 2005 Apr; 6(4): 390-5.

[51] Ota A, Zhang J, Ping P, Han J, Wang Y. Specific regulation of noncanonical p38alpha activation by Hsp90-Cdc37 chaperone complex in cardiomyocyte. Circ Res. 2010 Apr 30; 106(8): 1404-12.

[52] Cheung PC, Campbell DG, Nebreda AR, Cohen P. Feedback control of the protein kinase TAK1 by SAPK2a/p38alpha. EMBO J. 2003 Nov 3; 22(21): 5793-805.

[53] Takekawa M, Maeda T, Saito H. Protein phosphatase 2Calpha inhibits the human stress-responsive p38 and JNK MAPK pathways. EMBO J. 1998 Aug 17; 17(16): 4744-52.

[54] Patterson KI, Brummer T, O'Brien PM, Daly RJ. Dual-specificity phosphatases: critical regulators with diverse cellular targets. Biochem J. 2009 Mar 15; 418(3): 475-89.

[55] Oka T, Xu J, Molkentin JD. Re-employment of developmental transcription factors in adult heart disease. Semin Cell Dev Biol. 2007 Feb; 18(1): 117-31.

[56] Liang Q, Wiese RJ, Bueno OF, Dai YS, Markham BE, Molkentin JD. The transcription factor GATA4 is activated by extracellular signal-regulated kinase 1- and 2-mediated phosphorylation of serine 105 in cardiomyocytes. Mol Cell Biol. 2001 Nov; 21(21): 7460-9.

[57] Charron F, Tsimiklis G, Arcand M, Robitaille L, Liang Q, Molkentin JD, et al. Tissue-specific GATA factors are transcriptional effectors of the small GTPase RhoA. Genes Dev. 2001 Oct 15; 15(20): 2702-19.

[58] Coulombe P, Meloche S. Atypical mitogen-activated protein kinases: structure, regulation and functions. Biochim Biophys Acta. 2007; 1773(8): 1376-87.

[59] Coulombe P, Rodier G, Pelletier S, Pellerin J, Meloche S. Rapid turnover of extracellular signal-regulated kinase 3 by the ubiquitin-proteasome pathway defines a novel paradigm of mitogen-activated protein kinase regulation during cellular differentiation. Mol Cell Biol. 2003; 23(13): 4542-58.

[60] Coulombe P, Rodier G, Bonneil E, Thibault P, Meloche S. N-Terminal ubiquitination of extracellular signal-regulated kinase 3 and p21 directs their degradation by the proteasome. Mol Cell Biol. 2004; 24(14): 6140-50.

[61] Zimmermann J, Lamerant N, Grossenbacher R, Furst P. Proteasome- and p38-dependent regulation of ERK3 expression. J Biol Chem. 2001; 276(14): 10759-66.

[62] Aberg E, Perander M, Johansen B, Julien C, Meloche S, Keyse SM, et al. Regulation of MAPK-activated protein kinase 5 activity and subcellular localization by the atypical MAPK ERK4/MAPK4. J Biol Chem. 2006; 281(46): 35499-510.

[63] Kant S, Schumacher S, Singh MK, Kispert A, Kotlyarov A, Gaestel M. Characterization of the atypical MAPK ERK4 and its activation of the MAPK-activated protein kinase MK5. J Biol Chem. 2006; 281(46): 35511-9.

[64] Anhe GF, Torrao AS, Nogueira TC, Caperuto LC, Amaral ME, Medina MC, et al. ERK3 associates with MAP2 and is involved in glucose-induced insulin secretion. Mol Cell Endocrinol. 2006; 251(1-2): 33-41.

[65] Deleris P, Rousseau J, Coulombe P, Rodier G, Tanguay PL, Meloche S. Activation loop phosphorylation of the atypical MAP kinases ERK3 and ERK4 is required for binding, activation and cytoplasmic relocalization of MK5. J Cell Physiol. 2008; 217(3): 778-88.

[66] Tanguay PL, Rodier G, Meloche S. C-terminal domain phosphorylation of ERK3 controlled by Cdk1 and Cdc14 regulates its stability in mitosis. Biochem J. 2010; 428(1): 103-11.

[67] Rai R, Mahale A, Saranath D. Molecular cloning, isolation and characterisation of ERK3 gene from chewing-tobacco induced oral squamous cell carcinoma. Oral Oncol. 2004; 40(7): 705-12.

[68] Merkerova M, Bruchova H, Brdicka R. Expression analysis of PCNA gene in chronic myelogenous leukemia--combined application of siRNA silencing and expression arrays. Leuk Res. 2007; 31(5): 661-72.

[69] Crowe DL. Induction of p97MAPK expression regulates collagen mediated inhibition of proliferation and migration in human squamous cell carcinoma lines. Int J Oncol. 2004; 24(5): 1159-63.

[70] Julien C, Coulombe P, Meloche S. Nuclear export of ERK3 by a CRM1-dependent mechanism regulates its inhibitory action on cell cycle progression. J Biol Chem. 2003; 278(43): 42615-24.

[71] Hansen CA, Bartek J, Jensen S. A functional link between the human cell cycle-regulatory phosphatase Cdc14A and the atypical mitogen-activated kinase Erk3. Cell Cycle. 2008; 7(3): 325-34.

[72] Nigg EA. Mitotic kinases as regulators of cell division and its checkpoints. Nat Rev Mol Cell Biol. 2001 Jan; 2(1): 21-32.

[73] Stegmeier F, Amon A. Closing mitosis: the functions of the Cdc14 phosphatase and its regulation. Annu Rev Genet. 2004; 38: 203-32.

[74] Klinger S, Turgeon B, Levesque K, Wood GA, Aagaard-Tillery KM, Meloche S. Loss of Erk3 function in mice leads to intrauterine growth restriction, pulmonary immaturity, and neonatal lethality. Proc Natl Acad Sci U S A. 2009; 106(39): 16710-5.

[75] DeChiara TM, Efstratiadis A, Robertson EJ. A growth-deficiency phenotype in heterozygous mice carrying an insulin-like growth factor II gene disrupted by targeting. Nature. 1990 May 3; 345(6270): 78-80.

[76] Kuan CY, Yang DD, Samanta Roy DR, Davis RJ, Rakic P, Flavell RA. The Jnk1 and Jnk2 protein kinases are required for regional specific apoptosis during early brain development. Neuron. 1999 Apr; 22(4): 667-76.

[77] Kaiser RA, Liang Q, Bueno O, Huang Y, Lackey T, Klevitsky R, et al. Genetic inhibition or activation of JNK1/2 protects the myocardium from ischemia-reperfusion-induced cell death in vivo. J Biol Chem. 2005 Sep 23; 280(38): 32602-8.

[78] Tachibana H, Perrino C, Takaoka H, Davis RJ, Naga Prasad SV, Rockman HA. JNK1 is required to preserve cardiac function in the early response to pressure overload. Biochem Biophys Res Commun. 2006 May 19; 343(4): 1060-6.

[79] Sadoshima J, Montagne O, Wang Q, Yang G, Warden J, Liu J, et al. The MEKK1-JNK pathway plays a protective role in pressure overload but does not mediate cardiac hypertrophy. J Clin Invest. 2002 Jul; 110(2): 271-9.

[80] Crabtree GR. Generic signals and specific outcomes: signaling through Ca2+, calcineurin, and NF-AT. Cell. 1999 Mar 5; 96(5): 611-4.

[81] Liang Q, Bueno OF, Wilkins BJ, Kuan CY, Xia Y, Molkentin JD. c-Jun N-terminal kinases (JNK) antagonize cardiac growth through cross-talk with calcineurin-NFAT signaling. EMBO J. 2003 Oct 1; 22(19): 5079-89.

[82] Regan CP, Li W, Boucher DM, Spatz S, Su MS, Kuida K. Erk5 null mice display multiple extraembryonic vascular and embryonic cardiovascular defects. Proc Natl Acad Sci U S A. 2002 Jul 9; 99(14): 9248-53.

[83] Wang X, Merritt AJ, Seyfried J, Guo C, Papadakis ES, Finegan KG, et al. Targeted deletion of mek5 causes early embryonic death and defects in the extracellular signal-regulated kinase 5/myocyte enhancer factor 2 cell survival pathway. Mol Cell Biol. 2005 Jan; 25(1): 336-45.

[84] Kondoh K, Terasawa K, Morimoto H, Nishida E. Regulation of nuclear translocation of extracellular signal-regulated kinase 5 by active nuclear import and export mechanisms. Mol Cell Biol. 2006 Mar; 26(5): 1679-90.

[85] Hayashi M, Kim SW, Imanaka-Yoshida K, Yoshida T, Abel ED, Eliceiri B, et al. Targeted deletion of BMK1/ERK5 in adult mice perturbs vascular integrity and leads to endothelial failure. J Clin Invest. 2004 Apr; 113(8): 1138-48.

[86] Kimura TE, Jin J, Zi M, Prehar S, Liu W, Oceandy D, et al. Targeted deletion of the extracellular signal-regulated protein kinase 5 attenuates hypertrophic response and promotes pressure overload-induced apoptosis in the heart. Circ Res. 2010 Mar 19; 106(5): 961-70.

[87] Ni H, Wang XS, Diener K, Yao Z. MAPKAPK5, a novel mitogen-activated protein kinase (MAPK)-activated protein kinase, is a substrate of the extracellular-regulated kinase (ERK) and p38 kinase. Biochem Biophys Res Commun. 1998; 243(2): 492-6.

[88] New L, Jiang Y, Zhao M, Liu K, Zhu W, Flood LJ, et al. PRAK, a novel protein kinase regulated by the p38 MAP kinase. EMBO J. 1998; 17(12): 3372-84.

[89] Seternes OM, Johansen B, Hegge B, Johannessen M, Keyse SM, Moens U. Both binding and activation of p38 mitogen-activated protein kinase (MAPK) play essential roles in regulation of the nucleocytoplasmic distribution of MAPK-activated protein kinase 5 by cellular stress. Mol Cell Biol. 2002; 22(20): 6931-45.

[90] New L, Jiang Y, Han J. Regulation of PRAK subcellular location by p38 MAP kinases. Mol Biol Cell. 2003; 14(6): 2603-16.

[91] Li Q, Zhang N, Zhang D, Wang Y, Lin T, Zhou H, et al. Determinants that control the distinct subcellular localization of p38alpha-PRAK and p38beta-PRAK complexes. J Biol Chem. 2008 Apr 18; 283(16): 11014-23.

[92] ter Haar E, Prabhakar P, Liu X, Lepre C. Crystal structure of the p38 alpha-MAPKAP kinase 2 heterodimer. J Biol Chem. 2007 Mar 30; 282(13): 9733-9.

[93] White A, Pargellis CA, Studts JM, Werneburg BG, Farmer BT, 2nd. Molecular basis of MAPK-activated protein kinase 2:p38 assembly. Proc Natl Acad Sci U S A. 2007 Apr 10; 104(15): 6353-8.

[94] Sun P, Yoshizuka N, New L, Moser BA, Li Y, Liao R, et al. PRAK is essential for ras-induced senescence and tumor suppression. Cell. 2007; 128(2): 295-308.

[95] Collado M, Gil J, Efeyan A, Guerra C, Schuhmacher AJ, Barradas M, et al. Tumour biology: senescence in premalignant tumours. Nature. 2005 Aug 4; 436(7051): 642.

[96] Marasa BS, Srikantan S, Masuda K, Abdelmohsen K, Kuwano Y, Yang X, et al. Increased MKK4 abundance with replicative senescence is linked to the joint reduction of multiple microRNAs. Sci Signal. 2009; 2(94): ra69.

[97] Skalhegg BS, Tasken K. Specificity in the cAMP/PKA signaling pathway. Differential expression,regulation, and subcellular localization of subunits of PKA. Front Biosci. 2000 Aug 1; 5: D678-93.

[98] Gerits N, Mikalsen T, Kostenko S, Shiryaev A, Johannessen M, Moens U. Modulation of F-actin Rearrangement by the Cyclic AMP/cAMP-dependent Protein Kinase (PKA) Pathway Is Mediated by MAPK-activated Protein Kinase 5 and Requires PKA-induced Nuclear Export of MK5. J Biol Chem. 2007; 282(51): 37232-43.

[99] Laurenza A, Sutkowski EM, Seamon KB. Forskolin: a specific stimulator of adenylyl cyclase or a diterpene with multiple sites of action? Trends Pharmacol Sci. 1989 Nov; 10(11): 442-7.

[100] Kostenko S, Johannessen M, Moens U. PKA-induced F-actin rearrangement requires phosphorylation of Hsp27 by the MAPKAP kinase MK5. Cell Signal. 2009.

[101] Pichon S, Bryckaert M, Berrou E. Control of actin dynamics by p38 MAP kinase - Hsp27 distribution in the lamellipodium of smooth muscle cells. J Cell Sci. 2004 May 15; 117(Pt 12): 2569-77.

[102] Gaestel M. MAPKAP kinases - MKs - two's company, three's a crowd. Nat Rev Mol Cell Biol. 2006; 7(2): 120-30.

[103] Kostenko S, Shiryaev A, Gerits N, Dumitriu G, Klenow H, Johannessen M, et al. Serine residue 115 of MAPK-activated protein kinase MK5 is crucial for its PKA-regulated nuclear export and biological function. Cell Mol Life Sci. 2010 Aug 25.

[104] Tak H, Jang E, Kim SB, Park J, Suk J, Yoon YS, et al. 14-3-3epsilon inhibits MK5-mediated cell migration by disrupting F-actin polymerization. Cell Signal. 2007; 19(11): 2379-87.

[105] Gerits N, Shiryaev A, Kostenko S, Klenow H, Shiryaeva O, Johannessen M, et al. The transcriptional regulation and cell-specific expression of the MAPK-activated protein kinase MK5. Cell Mol Biol Lett. 2009; 14(4): 548-74.

[106] Shi Y, Kotlyarov A, Laabeta K, Gruber AD, Butt E, Marcus K, et al. Elimination of protein kinase MK5/PRAK activity by targeted homologous recombination. Mol Cell Biol. 2003; 23(21): 7732-41.

[107] Schumacher S, Laass K, Kant S, Shi Y, Visel A, Gruber AD, et al. Scaffolding by ERK3 regulates MK5 in development. EMBO J. 2004; 23(24): 4770-9.

[108] Seternes OM, Mikalsen T, Johansen B, Michaelsen E, Armstrong CG, Morrice NA, et al. Activation of MK5/PRAK by the atypical MAP kinase ERK3 defines a novel signal transduction pathway. EMBO J. 2004; 23(24): 4780-91.

[109] Perander M, Aberg E, Johansen B, Dreyer B, Guldvik IJ, Outzen H, et al. The Ser(186) phospho-acceptor site within ERK4 is essential for its ability to interact with and activate PRAK/MK5. Biochem J. 2008; 411(3): 613-22.

[110] Aberg E, Torgersen KM, Johansen B, Keyse SM, Perander M, Seternes OM. Docking of PRAK/MK5 to the atypical MAP kinases ERK3 and ERK4 defines a novel MAP kinase interaction motif. J Biol Chem. 2009.

[111] Canagarajah BJ, Khokhlatchev A, Cobb MH, Goldsmith EJ. Activation mechanism of the MAP kinase ERK2 by dual phosphorylation. Cell. 1997 Sep 5; 90(5): 859-69.

[112] Diskin R, Lebendiker M, Engelberg D, Livnah O. Structures of p38alpha active mutants reveal conformational changes in L16 loop that induce autophosphorylation and activation. J Mol Biol. 2007 Jan 5; 365(1): 66-76.

[113] Kaiser BK, Zimmerman ZA, Charbonneau H, Jackson PK. Disruption of centrosome structure, chromosome segregation, and cytokinesis by misexpression of human Cdc14A phosphatase. Mol Biol Cell. 2002 Jul; 13(7): 2289-300.

[114] Kostenko S, Khan MT, Sylte I, Moens U. The diterpenoid alkaloid noroxoaconitine is a Mapkap kinase 5 (MK5/PRAK) inhibitor. Cell Mol Life Sci. 2010 Jul 17.

[115] Folmer F, Blasius R, Morceau F, Tabudravu J, Dicato M, Jaspars M, et al. Inhibition of TNFalpha-induced activation of nuclear factor kappaB by kava (Piper methysticum) derivatives. Biochem Pharmacol. 2006; 71(8): 1206-18.

[116] Bain J, McLauchlan H, Elliott M, Cohen P. The specificities of protein kinase inhibitors: an update. Biochem J. 2003 Apr 1; 371(Pt 1): 199-204.

[117] Anderson DR, Meyers MJ, Vernier WF, Mahoney MW, Kurumbail RG, Caspers N, et al. Pyrrolopyridine inhibitors of mitogen-activated protein kinase-activated protein kinase 2 (MK-2). J Med Chem. 2007 May 31; 50(11): 2647-54.

[118] Mourey RJ, Burnette BL, Brustkern SJ, Daniels JS, Hirsch JL, Hood WF, et al. A benzothiophene inhibitor of mitogen-activated protein kinase-activated protein kinase 2 inhibits tumor necrosis factor alpha production and has oral anti-inflammatory efficacy in acute and chronic models of inflammation. J Pharmacol Exp Ther. 2010 Jun; 333(3): 797-807.

[119] Kotlyarov A, Neininger A, Schubert C, Eckert R, Birchmeier C, Volk HD, et al. MAPKAP kinase 2 is essential for LPS-induced TNF-alpha biosynthesis. Nat Cell Biol. 1999 Jun; 1(2): 94-7.

[120] Neininger A, Kontoyiannis D, Kotlyarov A, Winzen R, Eckert R, Volk HD, et al. MK2 targets AU-rich elements and regulates biosynthesis of tumor necrosis factor and

interleukin-6 independently at different post-transcriptional levels. J Biol Chem. 2002 Feb 1; 277(5): 3065-8.

[121] Lasa M, Mahtani KR, Finch A, Brewer G, Saklatvala J, Clark AR. Regulation of cyclooxygenase 2 mRNA stability by the mitogen-activated protein kinase p38 signaling cascade. Mol Cell Biol. 2000 Jun; 20(12): 4265-74.

[122] Han Q, Leng J, Bian D, Mahanivong C, Carpenter KA, Pan ZK, et al. Rac1-MKK3-p38-MAPKAPK2 pathway promotes urokinase plasminogen activator mRNA stability in invasive breast cancer cells. J Biol Chem. 2002 Dec 13; 277(50): 48379-85.

[123] Heidenreich O, Neininger A, Schratt G, Zinck R, Cahill MA, Engel K, et al. MAPKAP kinase 2 phosphorylates serum response factor in vitro and in vivo. J Biol Chem. 1999 May 14; 274(20): 14434-43.

[124] Treisman R. Journey to the surface of the cell: Fos regulation and the SRE. EMBO J. 1995 Oct 16; 14(20): 4905-13.

[125] Miranti CK, Ginty DD, Huang G, Chatila T, Greenberg ME. Calcium activates serum response factor-dependent transcription by a Ras- and Elk-1-independent mechanism that involves a Ca2+/calmodulin-dependent kinase. Mol Cell Biol. 1995 Jul; 15(7): 3672-84.

[126] Rivera VM, Miranti CK, Misra RP, Ginty DD, Chen RH, Blenis J, et al. A growth factor-induced kinase phosphorylates the serum response factor at a site that regulates its DNA-binding activity. Mol Cell Biol. 1993 Oct; 13(10): 6260-73.

[127] Tan Y, Rouse J, Zhang A, Cariati S, Cohen P, Comb MJ. FGF and stress regulate CREB and ATF-1 via a pathway involving p38 MAP kinase and MAPKAP kinase-2. EMBO J. 1996 Sep 2; 15(17): 4629-42.

[128] Kotlyarov A, Yannoni Y, Fritz S, Laass K, Telliez JB, Pitman D, et al. Distinct cellular functions of MK2. Mol Cell Biol. 2002 Jul; 22(13): 4827-35.

[129] Sudo T, Kawai K, Matsuzaki H, Osada H. p38 mitogen-activated protein kinase plays a key role in regulating MAPKAPK2 expression. Biochem Biophys Res Commun. 2005 Nov 18; 337(2): 415-21.

[130] Shiroto K, Otani H, Yamamoto F, Huang CK, Maulik N, Das DK. MK2-/- gene knockout mouse hearts carry anti-apoptotic signal and are resistant to ischemia reperfusion injury. J Mol Cell Cardiol. 2005 Jan; 38(1): 93-7.

[131] Ronkina N, Kotlyarov A, Dittrich-Breiholz O, Kracht M, Hitti E, Milarski K, et al. The mitogen-activated protein kinase (MAPK)-activated protein kinases MK2 and MK3 cooperate in stimulation of tumor necrosis factor biosynthesis and stabilization of p38 MAPK. Mol Cell Biol. 2007 Jan; 27(1): 170-81.

[132] Kotlyarov A, Neininger A, Schubert C, Eckert R, Birchmeier C, Volk HD, et al. MAPKAP kinase 2 is essential for LPS-induced TNF-alpha biosynthesis. Nat Cell Biol. 1999; 1(2): 94-7.

[133] Ronkina N, Kotlyarov A, ttrich-Breiholz O, Kracht M, Hitti E, Milarski K, et al. The mitogen-activated protein kinase (MAPK)-activated protein kinases MK2 and MK3 cooperate in stimulation of tumor necrosis factor biosynthesis and stabilization of p38 MAPK. Mol Cell Biol. 2007; 27(1): 170-81.

[134] Ronkina N, Kotlyarov A, Gaestel M. MK2 and MK3--a pair of isoenzymes? Front Biosci. 2008; 13: 5511-21.

[135] Nicoletti A, Michel JB. Cardiac fibrosis and inflammation: interaction with hemodynamic and hormonal factors. Cardiovasc Res. 1999; 41(3): 532-43.

[136] Bujak M, Frangogiannis NG. The role of TGF-beta signaling in myocardial infarction and cardiac remodeling. Cardiovasc Res. 2007 May 1; 74(2): 184-95.

[137] Jalil JE, Doering CW, Janicki JS, Pick R, Shroff SG, Weber KT. Fibrillar collagen and myocardial stiffness in the intact hypertrophied rat left ventricle. Circ Res. 1989 Jun; 64(6): 1041-50.

[138] Mukherjee D, Sen S. Collagen phenotypes during development and regression of myocardial hypertrophy in spontaneously hypertensive rats. Circ Res. 1990 Dec; 67(6): 1474-80.

[139] Shirwany A, Weber KT. Extracellular matrix remodeling in hypertensive heart disease. J Am Coll Cardiol. 2006 Jul 4; 48(1): 97-8.

[140] Norton GR, Tsotetsi J, Trifunovic B, Hartford C, Candy GP, Woodiwiss AJ. Myocardial stiffness is attributed to alterations in cross-linked collagen rather than total

collagen or phenotypes in spontaneously hypertensive rats. Circulation. 1997 Sep 16; 96(6): 1991-8.

[141] Border WA, Noble NA. Transforming growth factor beta in tissue fibrosis. N Engl J Med. 1994 Nov 10; 331(19): 1286-92.

[142] Schiller M, Javelaud D, Mauviel A. TGF-beta-induced SMAD signaling and gene regulation: consequences for extracellular matrix remodeling and wound healing. J Dermatol Sci. 2004; 35(2): 83-92.

[143] Crawford SE, Stellmach V, Murphy-Ullrich JE, Ribeiro SM, Lawler J, Hynes RO, et al. Thrombospondin-1 is a major activator of TGF-beta1 in vivo. Cell. 1998 Jun 26; 93(7): 1159-70.

[144] Lyons RM, Gentry LE, Purchio AF, Moses HL. Mechanism of activation of latent recombinant transforming growth factor beta 1 by plasmin. J Cell Biol. 1990 Apr; 110(4): 1361-7.

[145] Rosenkranz S. TGF-beta1 and angiotensin networking in cardiac remodeling. Cardiovasc Res. 2004; 63(3): 423-32.

[146] Leask A. TGFbeta, cardiac fibroblasts, and the fibrotic response. Cardiovasc Res. 2007 May 1; 74(2): 207-12.

[147] Oga T, Matsuoka T, Yao C, Nonomura K, Kitaoka S, Sakata D, et al. Prostaglandin F(2alpha) receptor signaling facilitates bleomycin-induced pulmonary fibrosis independently of transforming growth factor-beta. Nat Med. 2009 Dec; 15(12): 1426-30.

[148] Olman MA. Beyond TGF-beta: a prostaglandin promotes fibrosis. Nat Med. 2009 Dec; 15(12): 1360-1.

[149] Nagase H, Visse R, Murphy G. Structure and function of matrix metalloproteinases and TIMPs. Cardiovasc Res. 2006 Feb 15; 69(3): 562-73.

[150] Laviades C, Varo N, Fernandez J, Mayor G, Gil MJ, Monreal I, et al. Abnormalities of the extracellular degradation of collagen type I in essential hypertension. Circulation. 1998 Aug 11; 98(6): 535-40.

[151] Lopez B, Gonzalez A, Querejeta R, Larman M, Diez J. Alterations in the pattern of collagen deposition may contribute to the deterioration of systolic function in hypertensive patients with heart failure. J Am Coll Cardiol. 2006 Jul 4; 48(1): 89-96.

[152] Landgraf P, Rusu M, Sheridan R, Sewer A, Iovino N, Aravin A, et al. A mammalian microRNA expression atlas based on small RNA library sequencing. Cell. 2007 Jun 29; 129(7): 1401-14.

[153] Thum T, Gross C, Fiedler J, Fischer T, Kissler S, Bussen M, et al. MicroRNA-21 contributes to myocardial disease by stimulating MAP kinase signalling in fibroblasts. Nature. 2008 Dec 18; 456(7224): 980-4.

[154] Duisters RF, Tijsen AJ, Schroen B, Leenders JJ, Lentink V, van der Made I, et al. miR-133 and miR-30 regulate connective tissue growth factor: implications for a role of microRNAs in myocardial matrix remodeling. Circ Res. 2009 Jan 30; 104(2): 170-8, 6p following 8.

[155] van Rooij E, Sutherland LB, Thatcher JE, DiMaio JM, Naseem RH, Marshall WS, et al. Dysregulation of microRNAs after myocardial infarction reveals a role of miR-29 in cardiac fibrosis. Proc Natl Acad Sci U S A. 2008 Sep 2; 105(35): 13027-32.

[156] Larsen JK, Gerthoffer WT, Hickey E, Weber LA. Cloning and sequencing of a cDNA encoding the canine HSP27 protein. Gene. 1995; 161(2): 305-6.

[157] Coulombe P, Meloche S. Dual-tag prokaryotic vectors for enhanced expression of full-length recombinant proteins. Anal Biochem. 2002 Nov 15; 310(2): 219-22.

[158] Keesler GA, Bray J, Hunt J, Johnson DA, Gleason T, Yao Z, et al. Purification and activation of recombinant p38 isoforms alpha, beta, gamma, and delta. Protein Expr Purif. 1998; 14(2): 221-8.

[159] Boivin B, Chevalier D, Villeneuve LR, Rousseau E, Allen BG. Functional endothelin receptors are present on nuclei in cardiac ventricular myocytes. J Biol Chem. 2003; 278(31): 29153-63.

[160] Connern CP, Halestrap AP. Chaotropic agents and increased matrix volume enhance binding of mitochondrial cyclophilin to the inner mitochondrial membrane and sensitize the mitochondrial permeability transition to [Ca2+]. Biochemistry. 1996; 35(25): 8172-80.

[161] Arrigo AP, Simon S, Gibert B, Kretz-Remy C, Nivon M, Czekalla A, et al. Hsp27 (HspB1) and alphaB-crystallin (HspB5) as therapeutic targets. FEBS Lett. 2007 Jul 31; 581(19): 3665-74.

[162] Esposito G, Prasad SV, Rapacciuolo A, Mao L, Koch WJ, Rockman HA. Cardiac overexpression of a G(q) inhibitor blocks induction of extracellular signal-regulated kinase and c-Jun NH(2)-terminal kinase activity in in vivo pressure overload. Circulation. 2001 Mar 13; 103(10): 1453-8.

[163] Bogoyevitch MA, Gillespie-Brown J, Ketterman AJ, Fuller SJ, Ben-Levy R, Ashworth A, et al. Stimulation of the stress-activated mitogen-activated protein kinase subfamilies in perfused heart. p38/RK mitogen-activated protein kinases and c-Jun N-terminal kinases are activated by ischemia/reperfusion. Circ Res. 1996 Aug; 79(2): 162-73.

[164] Clerk A, Sugden PH. Activation of protein kinase cascades in the heart by hypertrophic G protein-coupled receptor agonists. Am J Cardiol. 1999 Jun 17; 83(12A): 64H-9H.

[165] Kudoh S, Komuro I, Hiroi Y, Zou Y, Harada K, Sugaya T, et al. Mechanical stretch induces hypertrophic responses in cardiac myocytes of angiotensin II type 1a receptor knockout mice. J Biol Chem. 1998 Sep 11; 273(37): 24037-43.

[166] Saurin AT, Martin JL, Heads RJ, Foley C, Mockridge JW, Wright MJ, et al. The role of differential activation of p38-mitogen-activated protein kinase in preconditioned ventricular myocytes. FASEB J. 2000 Nov; 14(14): 2237-46.

[167] Kumphune S, Bassi R, Jacquet S, Sicard P, Clark JE, Verma S, et al. A chemical genetic approach reveals that p38alpha MAPK activation by diphosphorylation aggravates myocardial infarction and is prevented by the direct binding of SB203580. J Biol Chem. 2010 Jan 29; 285(5): 2968-75.

[168] Otsu K, Yamashita N, Nishida K, Hirotani S, Yamaguchi O, Watanabe T, et al. Disruption of a single copy of the p38alpha MAP kinase gene leads to cardioprotection against ischemia-reperfusion. Biochem Biophys Res Commun. 2003 Feb 28; 302(1): 56-60.

[169] Hasegawa M, Cuenda A, Spillantini MG, Thomas GM, Buee-Scherrer V, Cohen P, et al. Stress-activated protein kinase-3 interacts with the PDZ domain of alpha1-syntrophin. A mechanism for specific substrate recognition. J Biol Chem. 1999; 274(18): 12626-31.

[170] Oka T, Sudol M. Nuclear localization and pro-apoptotic signaling of YAP2 require intact PDZ-binding motif. Genes Cells. 2009 May; 14(5): 607-15.

[171] Sabio G, Arthur JS, Kuma Y, Peggie M, Carr J, Murray-Tait V, et al. p38gamma regulates the localisation of SAP97 in the cytoskeleton by modulating its interaction with GKAP. EMBO J. 2005; 24(6): 1134-45.

[172] Cuenda A, Cohen P, Buee-Scherrer V, Goedert M. Activation of stress-activated protein kinase-3 (SAPK3) by cytokines and cellular stresses is mediated via SAPKK3 (MKK6); comparison of the specificities of SAPK3 and SAPK2 (RK/p38). EMBO J. 1997 Jan 15; 16(2): 295-305.

[173] Marinissen MJ, Chiariello M, Gutkind JS. Regulation of gene expression by the small GTPase Rho through the ERK6 (p38 gamma) MAP kinase pathway. Genes Dev. 2001; 15(5): 535-53.

[174] Askari N, Diskin R, Avitzour M, Capone R, Livnah O, Engelberg D. Hyperactive variants of p38alpha induce, whereas hyperactive variants of p38gamma suppress, activating protein 1-mediated transcription. J Biol Chem. 2007 Jan 5; 282(1): 91-9.

[175] Zhang S, Ren J, Zhang CE, Treskov I, Wang Y, Muslin AJ. Role of 14-3-3-mediated p38 mitogen-activated protein kinase inhibition in cardiac myocyte survival. Circ Res. 2003; 93(11): 1026-8.

[176] Moise N, Dingar D, Mamarbachi AM, Villeneuve LR, Farhat N, Gaestel M, et al. Characterization of a novel MK3 splice variant from murine ventricular myocardium. Cell Signal. 2010 Oct; 22(10): 1502-12.

[177] Tanoue T, Maeda R, Adachi M, Nishida E. Identification of a docking groove on ERK and p38 MAP kinases that regulates the specificity of docking interactions. EMBO J. 2001; 20(3): 466-79.

[178] Heeneman S, Cleutjens JP, Faber BC, Creemers EE, van Suylen RJ, Lutgens E, et al. The dynamic extracellular matrix: intervention strategies during heart failure and atherosclerosis. J Pathol. 2003 Jul; 200(4): 516-25.

[179] Berg TJ, Snorgaard O, Faber J, Torjesen PA, Hildebrandt P, Mehlsen J, et al. Serum levels of advanced glycation end products are associated with left ventricular diastolic function in patients with type 1 diabetes. Diabetes Care. 1999 Jul; 22(7): 1186-90.

[180] Kato K, Ito H, Kamei K, Inaguma Y, Iwamoto I, Saga S. Phosphorylation of alphaB-crystallin in mitotic cells and identification of enzymatic activities responsible for phosphorylation. J Biol Chem. 1998 Oct 23; 273(43): 28346-54.

[181] Golenhofen N, Ness W, Koob R, Htun P, Schaper W, Drenckhahn D. Ischemia-induced phosphorylation and translocation of stress protein alpha B-crystallin to Z lines of myocardium. Am J Physiol. 1998 May; 274(5 Pt 2): H1457-64.

[182] Golenhofen N, Htun P, Ness W, Koob R, Schaper W, Drenckhahn D. Binding of the stress protein alpha B-crystallin to cardiac myofibrils correlates with the degree of myocardial damage during ischemia/reperfusion in vivo. J Mol Cell Cardiol. 1999 Mar; 31(3): 569-80.